Tesis Doctoral

Deciphering the Contribution of MicroRNAs to Human Cardiac Aging: Therapeutic Insights

Autora
Natalia Hernández Bellido

Directores
Laura Ordovás Vidal
Ralf Köhler

Tutor
Ángel Luis García Otín

Universidad de Zaragoza
Instituto de Investigación en Ingeniería de Aragón (I3A)

2026

A los míos.

Agradecimientos

No es ningún secreto que soy una chica de muchas palabras, pero no precisamente cuando se trata de ponerme sentimental. Esta vez, sin embargo, la ocasión lo merece.

Para empezar, quiero expresar mi más sincero agradecimiento a mis directores y tutor de tesis, Laura, Ralf y Ángel Luis, por su orientación y apoyo a lo largo de todo este trabajo. En particular, a mi directora, por tu implicación, dedicación y, sobre todo, por la confianza depositada en mí desde el inicio de este largo camino, allá por el verano de 2018, cuando todavía no sabía ni utilizar una pipeta ni hacer una dilución. Gracias por todo lo aprendido y por haber sido un apoyo constante durante estos años.

Igualmente, me gustaría dar las gracias a la familia BSICoS, por su paciencia y sus ánimos incondicionales a lo largo de esta auténtica montaña rusa de emociones. En especial, a mis compañeros de interminables horas de trabajo (y también de cervezas, ¡cómo no!): Marcos, Carol, Marina, Laura Paz, Aida, Alba, Cristina y Elisa. También, al resto de personas con las que he colaborado más estrechamente durante este camino: Alejandro, Silvia, David, Adrián, Nuria, Ester…

Me gustaría hacer una mención especial a dos personas muy importantes durante este camino: Laura G, por acompañarme desde mis inicios hasta el final y ser una parte fundamental de esta tesis, y Hazel, por ser mi luz y el mejor refugio cuando todo se volvía oscuro. Sin vosotras esta tesis no habría sido lo mismo.

Por otro lado, quiero agradecer a Myriam, por brindarme su mano para llevar a cabo mi estancia predoctoral en Baltimore y confiar en mí desde el principio, y a Krystyna, por todo su trabajo y ayuda en cualquier momento, siempre dispuesta a ello. También al resto del laboratorio LGG, por acogerme como a una más, y hacer de esta etapa una experiencia enormemente enriquecedora, tanto a nivel personal como profesional.

En especial, gracias a Carlos Anerillas, por convertirte en mi familia aquellos meses en el “culo del mundo” y, a día de hoy, afortunadamente, seguir siéndolo en nuestra tierra. Gracias por todo lo que has hecho y sigues haciendo por mí, y por abrirme las puertas de tu nuevo laboratorio; espero que por muchos años más (si tu paciencia lo permite).

Finalmente, gracias a la familia SenHomE, y en especial a Aida, por convertirte en mi gran apoyo estos últimos meses, haciendo este final mucho más dulce, y espero que así siga.

Más allá de lo académico y del laboratorio, no podría haber llegado hasta aquí sin el apoyo de mi familia. Por eso, solo puedo dedicaros estas palabras de agradecimiento, que, aunque se quedan cortas, salen desde lo más profundo.

A mi madre, Mila, por ser el pilar fundamental de todo lo que soy y de todo lo que he logrado. Gracias por tu esfuerzo constante y por enseñarme a no rendirme nunca, incluso cuando el camino se hacía cuesta arriba. Gracias por creer en mí incluso cuando yo dudaba, por estar siempre, en cada paso, y por ser mi mayor ejemplo. Gracias también por todas las broncas y por bajarme siempre los pies al suelo. Y también a ti, Emiliano, por tu apoyo constante y tu comprensión durante este camino.

A mi padre, Ramón, por tu apoyo incondicional, tu paciencia y tu confianza plena en mí, no solo durante este proceso, sino a lo largo de toda mi vida. Gracias por darme la tranquilidad de saber que siempre puedo contar contigo.

A mis hermanos, por acompañarme (y aguantarme) en cada etapa de mi vida y darme fuerzas, incluso sin darse cuenta, cuando más lo necesitaba. Gracias por estar siempre ahí, por hacerme desconectar en los momentos más difíciles y por llenar de ligereza incluso los días más complicados. Gracias a los tres, de corazón, por hacerme la hermana mayor más afortunada del mundo.

Gracias, Diego, por tus consejos y tus palabras de aliento en cada momento, por saber escuchar y ayudarme a ver las cosas desde otra perspectiva.

Gracias, Dani, por tu alegría y tu sonrisa tan enérgica, capaces de sacarme una sonrisa incluso en los días más grises.

Gracias, Daniela, por tu cariño y admiración desde el día que naciste, y por la forma tan especial que tienes de alegrar todo a tu alrededor.

Al resto de mi familia —abuelos, abuelas, tíos, tías, primos y primas —, gracias por vuestro cariño y por estar siempre presentes, de una forma u otra, a lo largo de este camino. Por interesaros, por preguntar y por celebrar conmigo cada pequeño logro, y ojalá así siga siendo muchos años más.

Especial mención a mi yaya Aurora, por su amor constante e incondicional, por su cuidado (incluyendo sus caracoles y su lomo con bechamel) y por todos esos besos y abrazos tan alentadores que siempre llegaban en el momento justo.

También a los que ya no están —Urbano, Ernesto, Rosa y Pitusa—, pero siguen muy presentes en mi recuerdo y en mi corazón. Me gusta pensar que, de alguna manera, me

han acompañado hasta aquí y me seguirán acompañando siempre, de eso no tengo dudas. Esto también es por vosotros.

A mis amigos y amigas, a los Uteberos, a los Novalleros y a los Zaragozanos, gracias por las risas que llegaron cuando más falta hacían, por los abrazos cuando más los necesitaba y por estar siempre sumando, cada uno a vuestra manera. Por todos esos momentos que me han ayudado a desconectar de todo, a relativizar los problemas y a seguir adelante cuando más lo necesitaba. Gracias a todos y todas por hacerme sentir tan afortunada de teneros. Es un auténtico orgullo tener amigos y amigas como vosotros, y ojalá que así siga al menos 100 años más.

En especial:

Carlos, gracias por tu valentía y tu coraje.

Cris, gracias por tu generosidad al ayudar.

María, gracias por tu calma en los momentos de caos.

Maru, gracias por tu alegría contagiosa.

Andrea, gracias por tu capacidad de hacer reír a los demás.

Laura, gracias por tu optimismo contagioso.

Ale, gracias por tu cariño.

Carla, gracias por tu espíritu positivo.

Lorena, gracias por tu autenticidad y lealtad.

Mara, gracias por tu madurez y tranquilidad.

Nerea, gracias por estar siempre dispuesta a dar sin esperar nada a cambio.

Teresa, gracias por tu forma de cuidar a los demás.

Janire, gracias por tu bondad.

Alicia, gracias por tu serenidad.

Solo me queda agradecer a una persona que, sin querer, apareció en el momento que menos esperaba, pero sin saber, más necesitaba. Poco a poco ha ido ocupando un lugar muy importante, siempre con palabras de apoyo y admiración, y ojalá todo esto sea solo el principio y siga así por mucho mucho tiempo más. Gracias por hacerlo todo más fácil, Jose.

También quiero agradecer a todas aquellas personas que, aunque solo hayan formado parte de una etapa de este recorrido, han dejado su huella en mí y me han enseñado muchas cosas que me llevo conmigo para siempre.

Finalmente, agradecer de nuevo a todas las personas que han contribuido, directa o indirectamente, a lo largo de este camino. Gracias por hacerme sentir tan orgullosa de la gente que me rodea. Este logro también es vuestro, porque sin vosotros nada de esto habría sido posible.

Os quiero mucho.

Funding

This thesis has been developed in the frame of the following scientific projects:

- Gobierno de Aragón PROY_B08_24
- Ministerio de Ciencia e Innovación PID2022-139859OB-I00
- Reference Group BSICoS T39_23R
- Gobierno de Aragón LMP128_21
- Ministerio de Ciencia e Innovación PID2019-105674RB-100

I was supported by a PhD fellowship from the Departamento de Ciencia, Universidad y Sociedad del Conocimiento from the Gobierno de Aragón 2020-2024. The Gobierno de Aragón also supported my research stay in the National Institute on Aging (NIA) in Baltimore, Maryland, the United States (MVB_03_23).

Abstract

Cardiovascular diseases remain the leading cause of death worldwide, with aging representing one of the most significant predisposing risk factors. As the heart ages, it undergoes structural and functional remodeling driven by cellular and molecular alterations, including changes in gene expression regulated by microRNAs. These small non-coding RNAs have emerged as promising cardiac therapeutics due to their pivotal role in the regulation of the heart pathophysiology. However, despite their potential, most studies investigating cardiac microRNAs in aging have been conducted in animal models, given the inherent challenges associated with human research.

Cardiac aging is commonly evaluated in relation to chronological age, which fails to account for the cumulative influence of genetic and environmental factors acting together over time. In contrast, biological age reflects a more accurate representation of the physiological state of an individual or an organ. Advancing the understanding of the molecular mechanisms underlying cardiac biological aging while identifying novel therapeutic targets and biomarkers for its monitoring could facilitate the development of effective biotechnological strategies to promote healthy cardiac aging and to enable the early detection of accelerated aging or the monitoring of intervention effects, respectively. This could ultimately contribute to reduce the socioeconomic burden of cardiovascular disease.

This thesis investigates the role of microRNAs in human cardiac biological aging, explores the potential of cardiac microRNA-based therapies, and examines their technological challenges and translational perspectives. It also demonstrates the use of DNA nanotechnology as a non-viral platform to modulate age-dysregulated microRNAs in human cardiac cells, and proposes a minimally-invasive individual biomarker of aging as an indicator of cardiovascular health-related biological age.

Chapter 2 describes the identification of miR-24-2 as a genetically conserved microRNA in humans, monkeys and mice, which is consistently upregulated in the heart tissue of all of these species in association with the cardiac biological age marker SenesAge. Gain-of-function studies in human cardiomyocytes derived from induced pluripotent stem cells describe its regulatory action controlling processes related to aging hallmarks such as proteostasis or telomere maintenance, and to cardiac aging such as altered cardiac contraction and development and disrupted electrophysiological activity. These findings corroborate the relationship of miR-24-2 with the mechanisms of aging, while other

altered processes describe the functional impact of the microRNA, underscoring the potential effects of therapies designed to modulate its action.

Chapter 3 carries out a comprehensive review of the state of the art in cardiac microRNA-based therapeutics, highlighting both recent advances and persisting limitations, particularly regarding targeted delivery systems. This chapter identifies a major bottleneck in late-stage preclinical studies due to inefficient delivery. However, it shows that heart-targeted nanocarriers, especially those functionalized with cardiac-specific ligands, can overcome these barriers and enhance therapeutic efficacy, thereby showing their capacity to unlock the clinical potential of microRNA therapies.

Chapter 4 presents the development of a biocompatible anti-miR-24-2 therapy employing DNA nanotechnology. The *in vitro* characterization demonstrates that the engineered nanocarriers efficiently deliver functional anti-miR-24-2 molecules in a cellular model and in human cardiomyocytes derived from induced pluripotent stem cells. Specifically, the anti-microRNA nanotherapy is able to release the inhibitory pressure on validated target genes. This work provides proof of concept for the modulation of age-dysregulated microRNAs in human cardiac cells, offering therapeutic potential to counteract age-associated cardiac dysfunction.

Chapter 5 introduces the design and validation of an individual-specific biological age index and evaluates a cardiac-enriched and age-related microRNA, miR-490-3p, as indicators of cardiac biological age. The study describes the development of GamC, a blood-based gene expression biomarker that correlates with chronological age across independent populations and demonstrates moderate responsiveness to healthy-aging interventions in centenarians. In contrast, plasma levels of miR-490-3p show moderate to low correlation with chronological age or GamC, respectively. However, they are too low for reliable quantification, thereby excluding its value as a heart-specific biomarker of aging. Altogether, this chapter provides a clinically translatable and individualized tool, GamC, with potential for real-time monitoring of cardiovascular health-related biological age.

In conclusion, this thesis advances the understanding of the molecular mechanisms driving human cardiac aging regulated by core microRNAs and demonstrates the feasibility of targeting an age-dysregulated microRNA using DNA nanotechnology. It also contributes a novel framework for assessing cardiac biological age through blood-based biomarkers, bridging molecular insights with clinical applications. Collectively, these findings lay the groundwork for future strategies aimed at promoting healthy cardiac aging and reducing the burden of cardiovascular disease in aging populations.

Resumen

Las enfermedades cardiovasculares siguen siendo la principal causa de muerte a nivel mundial, y el envejecimiento representa uno de los factores de riesgo predisponentes más importantes. A medida que el corazón envejece, sufre una remodelación estructural y funcional impulsada por alteraciones celulares y moleculares, incluidos cambios en la expresión génica regulada por microARNs. Estos pequeños ARN no codificantes se han convertido en herramientas terapéuticas cardiacas prometedoras debido a su papel fundamental en la regulación de la fisiopatología del corazón. Sin embargo, a pesar de su potencial, la mayoría de los estudios que investigan los microARN cardíacos en el envejecimiento se han realizado en modelos animales, dados los retos inherentes asociados a la investigación en humanos.

El envejecimiento cardíaco se evalúa comúnmente en relación con la edad cronológica, lo que no tiene en cuenta la influencia acumulativa de los factores genéticos y ambientales que actúan conjuntamente a lo largo del tiempo. Por el contrario, la edad biológica refleja una representación más precisa del estado fisiológico de un individuo o un órgano. Avanzar en la comprensión de los mecanismos moleculares que subyacen al envejecimiento biológico cardíaco al tiempo que se identifican nuevos objetivos terapéuticos y biomarcadores para su seguimiento, podría facilitar el desarrollo de estrategias biotecnológicas eficaces para promover un envejecimiento cardíaco saludable y para la detección precoz del envejecimiento acelerado o la monitorización del efecto de la intervención, respectivamente. En última instancia, esto podría contribuir a reducir la carga socioeconómica de las enfermedades cardiovasculares

Esta tesis investiga el papel de los microARN en el envejecimiento biológico cardíaco humano, explora el potencial de las terapias basadas en microARN cardíacos y examina sus retos tecnológicos y perspectivas traslacionales. También demuestra el uso de la nanotecnología del ADN como plataforma no viral para modular los microARN desregulados por la edad en células cardíacas humanas, y propone un biomarcador de envejecimiento del individuo mínimamente invasivo como indicador de la edad biológica relacionada con la salud cardiovascular.

El *Capítulo 2* describe la identificación del miR-24-2 como un microRNA conservado genéticamente en humanos, monos y ratones, que está consistentemente sobreexpresado en el tejido cardíaco de todas especies en asociación con el marcador

de edad biológica cardíaca SenesAge. Los estudios de ganancia de función en cardiomiocitos humanos derivados de células madre pluripotentes inducidas describen su acción reguladora que controla procesos relacionados con los pilares del envejecimiento, como la proteostasis o el mantenimiento de los telómeros, y con el envejecimiento cardíaco, como la alteración de la contracción y el desarrollo cardíacos y la disrupción de la actividad electrofisiológica. Estos hallazgos corroboran la relación del miR-24-2 con los mecanismos del envejecimiento, mientras que otros procesos alterados describen el impacto funcional del microARN, lo que subraya los posibles efectos de las terapias diseñadas para modular su acción.

El *Capítulo 3* realiza una revisión exhaustiva del estado actual de las terapias cardíacas basadas en microARNs, destacando tanto los avances recientes como las limitaciones persistentes, en particular en lo que respecta a los sistemas de administración dirigida. Este capítulo identifica un importante obstáculo en los estudios preclínicos en fase avanzada debido a la ineficiencia de la administración. Sin embargo, esto muestra que los sistemas de nanotransportadores dirigidos al corazón, especialmente los funcionalizados con ligandos específicos cardiacos, pueden superar estas barreras y mejorar la eficacia terapéutica, mostrando así su capacidad de desbloquear el potencial clínico de las terapias con microARN.

El *Capítulo 4* presenta el desarrollo de una terapia biocompatible contra el miR-24-2 que emplea nanotecnología de ADN. La caracterización *in vitro* demuestra que el nanotransportador anti-microARN diseñado libera eficazmente moléculas funcionales anti-miR-24-2 en modelos celulares y en cardiomiocitos humanos derivados de células madre inducibles pluripotentes. En concreto, la nanoterapia anti-microARN es capaz de liberar la presión inhibitoria sobre genes diana validados. Este trabajo proporciona una prueba de concepto para la modulación de microARN desregulados por la edad en células cardíacas humanas, lo que ofrece un potencial terapéutico para contrarrestar la disfunción cardíaca asociada al envejecimiento.

El *Capítulo 5* presenta el diseño y la validación de un índice de edad biológica específico para cada individuo y evalúa un microARN enriquecido en el corazón y relacionado con la edad, miR-490-3p, como indicadores del envejecimiento biológico cardíaco. El estudio describe el desarrollo de GamC, un biomarcador de expresión génica basado en la sangre que se correlaciona con la edad cronológica en poblaciones independientes y demuestra una respuesta moderada a las intervenciones de envejecimiento saludable en centenarios. Por el contrario, los niveles plasmáticos de miR-490-3p muestran una asociación de moderada a baja con la edad cronológica o GamC, respectivamente. Sin

embargo, sus niveles de expresión son demasiado bajos para una cuantificación fiable, lo que excluye su valor como biomarcador específico del envejecimiento cardíaco. En conjunto, este capítulo proporciona una herramienta clínicamente aplicable e individualizada, GamC, con potencial para la monitorización en tiempo real de la edad biológica relacionada con la salud cardiovascular.

En conclusión, esta tesis avanza en la comprensión de los mecanismos moleculares que impulsan el envejecimiento cardíaco humano regulado por microARN y demuestra la viabilidad de modular un microARN desregulado con la edad utilizando nanotecnología de ADN. También contribuye con un marco novedoso para evaluar la edad biológica cardíaca a través de biomarcadores basados en sangre, tendiendo un puente entre los conocimientos moleculares y las aplicaciones clínicas. En conjunto, estos hallazgos sientan las bases para futuras estrategias destinadas a promover un envejecimiento cardíaco saludable y reducir la carga de las enfermedades cardiovasculares en las poblaciones que envejecen.

Contents

Abstract XVII

Resumen XXI

List of figures XXIX

List of tables XXXI

List of acronyms XXXIII

Chapter 1. Introduction

1.1 Aging and cardiovascular diseases 3

1.2 Gene regulation by ncRNAs: miR biology 5

1.2.1 MiR biogenesis 7

1.2.2 Mechanism of action of miRs 8

1.3 The role of miRs in cardiac pathophysiology and aging 9

1.4 MiR as therapeutics and biomarkers 10

1.5 Biological aging 11

1.6 Translational models of research in HD and aging 13

1.7 Hypothesis and goals 15

1.8 Structure of the thesis 17

Chapter 2. Uncovering miR-24-2 key role in human cardiac biological aging

2.1 Introduction 25

2.2 Materials and methods 26

2.2.1 Animal models of natural aging 26

2.2.2 Quantification of gene and miR expression levels 27

2.2.3 Generation of mir-24-2^{+} and mir-24-2^{-} inducible hiPSC lines 27

2.2.4 Directed differentiation of hiPSCs to iCMs 28

2.2.5 Identification of human miR orthologue genes 29

2.2.6 Flow cytometry 29

2.2.7 Mass spectrometry, proteomics and Western Blot 29

2.2.8 Transcriptomics and bioinformatic analysis 30

2.2.9 Statistical Analysis 31

2.3 Results 32

2.3.1 SenesAge explains cardiac biological aging in naturally aged animals 32

2.3.2 The expression profiles of upregulated human BIO-AGEmiRs are generally maintained with age across species 34

2.3.3 Mir-24-2 upregulation perturbs the proteome affecting metabolism, cardiac function and development and aging hallmarks 38

2.3.4 Transcriptome profiling identifies cardiac contractility and tissue structure and development regulated by mir-24-2 in human iCMs 43
2.4 Discussion 46
2.5 Conclusions 49

Chapter 3. Cardiac miRNA therapies: challenges and opportunities

3.1 Introduction 53
3.2 Current development status of cardiac miR therapies 55
3.2.1 Effective miR therapies in late preclinical research 56
3.2.2 MiR therapies in clinical trials suitable for cardiac therapy 60
3.3 The challenge of *in vivo* miR delivery 64
3.3.1 Polymeric NCs 64
3.3.2 Lipid-based NCs 65
3.3.3 Inorganic NCs 66
3.3.4 Hydrogels 67
3.3.5 EVs 67
3.4 The challenge of targeted delivery to the heart 73
3.4.1 Non-cardiac specific targeting 73
3.4.2 Cardiac specific targeting 74
3.5 Conclusions 76

Chapter 4. Development of anti-miRNA nanotherapies to modulate miR-24-2

4.1 Introduction 81
4.2 Materials and methods 83
4.2.1 DNCs development and structural characterization 83
4.2.2 Characterization of DNCs bioactivity 84
4.2.3 Statistical Analysis 88
4.3 Results 88
4.3.1 DNCs correctly self-assemble into stable biodegradable structures carrying anti-miR-24-2 88
4.3.2 DNCs specifically capture miR-24-2 91
4.3.3 DNCs appropriately internalize in HEK293 cells showing biocompatibility 93
4.3.4 SERCA2 levels are effectively restored by N_B in a cellular model system 95
4.3.5 N_B functionality is verified in human iCMs 96
4.4 Discussion 97
4.5 Conclusions 98

Chapter 5. Definition of biomarkers descriptive of cardiovascular health-related biological age

5.1 Introduction ... 103

5.2 Materials and methods ... 104

5.2.1 Identification of consistently dysregulated age-related genes in blood for GamC building ... 104

5.2.2 Donors and samples of the study cohort ... 105

5.2.3 Gene and miR expression analysis by qPCR and generation of GamC ... 105

5.2.4 Validation cohorts and transcriptomic analysis ... 106

5.2.5 ECG data recording and HRV analysis ... 107

5.2.6 Accelerometer data recording and analysis ... 109

5.2.7 Exercise intervention ... 110

5.2.8 Statistical Analysis ... 111

5.3 Results ... 112

5.3.1 GamC is associated with CA ... 112

5.3.2 GamC association with age is maintained across independent study cohorts and at the transcriptome-wide level ... 114

5.3.3 GamC marginally describes age-related changes in the ANS function ... 118

5.3.4 GamC is associated with PA levels and responds modestly to a healthy-aging exercise intervention in centenarians ... 119

5.3.5 Cardiac-enriched miR-490-3p is not suitable for cardiac BA monitoring in human plasma ... 122

5.4 Discussion ... 122

5.5 Conclusions ... 125

General conclusions/Conclusiones generales

General conclusions ... 129

Conclusiones generales ... 132

Study limitations, future work, scientific production and academic activities

Study limitations and future work ... 139

Scientific production and academic activities ... 140

Publications in peer-reviewed journals derived from the thesis ... 140

Conference proceedings derived from collaborations during the thesis ... 140

Congresses and conferences derived from collaborations during the thesis ... 141

Teaching collaboration and bachelor thesis supervision ... 143

Courses ... 143

Annexes ... 145

Bibliography ... 157

List of figures

Figure 1. Hallmarks of aging 3
Figure 2. Cardiac aging hallmarks 4
Figure 3. Biogenesis of miRs, mechanism of action and passive and active transport into extracellular space and body fluids 7
Figure 4. Overview of the role of miRs in cardiac disease and aging 10
Figure 5. Types of miR therapies 11
Figure 6. RMCE constructs for the generation of the mir-24-2^{+} and mir-24-2^{-} 28
Figure 7. Experiment workflow from hiPSC lines to induced iCM 29
Figure 8. Evaluation of the cardiac BA-indicator SenesAge in the heart tissue of naturally aged animal models and human 32
Figure 9. Association analysis between cardiac function-related genes and CA or SenesAge in mouse, monkey and human cardiac tissue 33
Figure 10. Analysis of the expression levels of BIO-AGEmiRs at the pri-miR and mature miR stages 36
Figure 11. Assessment of the mir-24-2 induction levels 39
Figure 12. Profiling of the proteomic changes in response to mir-24-2 overexpression in iCMs 39
Figure 13. Functional annotation of the total proteome with the overexpression of mir-24-2 40
Figure 14. Workflow of the identification of putative targets of mir-24-2 41
Figure 15. Profiling of the transcriptomic changes in response to mir-24-2 overexpression in iCMs 44
Figure 16. Functional annotation of the transcriptome with the overexpression of mir-24-2 45
Figure 17. Analysis of the protein and mRNA perturbation coherence in response to mir-24-2 overexpression 46
Figure 18. Challenges of cardiac miR therapies 53
Figure 19. Representation of the course of miR-related research in HD and its progress into clinical investigations 55
Figure 20. pmiRGLO-SERCA2 vector map 87
Figure 21. DNCs assembly in their two configurations (N_A and N_B) 89
Figure 22. Characterization of the DNCs 90
Figure 23. Assessment of capture capacity and specificity of miR-24-2 by DNCs 92
Figure 24. Cellular viability, kinetic of cellular uptake, intracellular stability of anti-miR fragments of DNCs in HEK293 cells 93
Figure 25. Subcellular location of DNCs in HEK293 94
Figure 26. Functional assay of miR-24-2 inhibition by luciferase reporter assay 95
Figure 27. Functional evaluation of N_B in iCMs 97
Figure 28. Workflow for the description and characterization of GamC 104
Figure 29. Evaluation of the relation with age of the candidate genes, GamC and AR 114

Figure 30. Normalized and standardized expression values of *ABLIM1*, *CCR7* and *LEF1* in blood samples of the individuals of the three independent validation cohorts 115
Figure 31. Validation of GamC and aging rate in independent cohorts 116
Figure 32. Evaluation of Gamc biological relevance at the molecular level in independent cohorts 117
Figure 33. Independent association analysis between accelerometer metrics and HRV parameters in the study cohort 118
Figure 34. Evaluation of the association of age with HRV parameters 119
Figure 35. Evaluation of the association of age with parameters of PA 120
Figure 36. Evaluation of healthy-aging intervention study in centenarians 121
Figure 37. Evaluation of the relation with age and with GamC of the cardiac-enriched miR ... 122

Figure A1. Vector sequence used for hiPSC recombinant line to overexpress mir-24-2-tdT ...147

List of tables

Table 1. Monkey animals 27
Table 2. Association analyses of cardiac function- and age-related genes with CA and SenesAge in animal models and in humans 34
Table 3. List of human BIO-AGEmiRs genes and their orthologous in animal species 35
Table 4. Association of BIO-AGEmiRs and mature miRs with SenesAge in animal models (mouse and monkey) and in humans 37
Table 5. Putative cardiac targets of mir-24-2 downregulated at the protein level 42
Table 6. Preclinical efficacy evaluation of miR therapies in large animal models 59
Table 7. miR therapies in clinical trials with potential application in cardiac pathologies 63
Table 8. NCs for miR delivery for cardiac therapeutic purposes 69
Table 9. Individuals in the study cohort 105
Table 10. Description of the validation cohorts A, B and C 107
Table 11. Studies reporting age-related changes in the blood transcriptome found in the identification phase of the workflow.....113
Table 12. Analysis of the relationship of *ABLIM1*, *CCR7* and *LEF1* expression levels with CA and gender 115

Table A1. Method details for RNA processing and gene expression analysis..... 148
Table A2. PCR primers used in the thesis..... 149
Table A3. Sequences of DNA oligonucleotides used to prepare DNCs..... 152
Table A4. Data related to the study cohort..... 153

List of acronyms

AA	Average Acceleration
AAV	Adeno-Associated Virus
AF	Atrial Fibrillation
AMI	Acute Myocardial Infarction
ANS	Autonomous Nervous System
A-TP	Atrial Tachypacing
BA	Biological age
BOA	Biomarker of Aging
bp	Base pair
CA	Chronological age
CEM	Cardiomyocyte expansion media
CME	Coronary Microembolization
CMM	Cardiomyocyte Maintenance Media
CMs	Cardiomyocytes
CPP	Cell Penetrating Peptide
CTP	Cardiac Targeting Peptide
CV	Cardiovascular
CVD	Cardiovascular disease
d	Day
DEG	Differentially Expressed Gene
DEP	Differentially Expressed Protein
DFA	Detrended Fluctuation Analysis
DGL	Dendrigraft poly-L-lysine
DLBCL	Diffuse large B-cell lymphoma
DNC	DNA nanocarrier
DSPE-PEG	Distearoylphosphosphatidyl-ethanolamine
EAM	Experimental Autoimmune Myocarditis
ECG	Electrocardiogram
EV	Extracellular vesicle
FDR	Adjusted p-value
GO	Gene Ontology
h	Hour
HCM	Hypertrophic Cardiomyopathy
HD	Heart disease
HF	Heart failure
HG	Host Gene
hiPSCs	Human Inducible Pluripotent Stem Cells
HRV	Heart rate variability
I/R	Ischemia/Reperfusion
IC	Intracoronary
iCMs	Cardiomyocytes derived from hiPSC
ID	Intradermal
IG	Intensity gradient
IM	Intramyocardial
IMTP	Ischemic Myocardial Targeting Peptide
IP	Intraperitoneal
IQR	Interquartile range
IT	Inactive time
IV	Intravenous
LAD	Left anterior descending artery
LDL	Low density lipoprotein
LMW	Low molecular weight
LNA	Locked Nucleic Acid
LNC	Lipid-based nanocarrier

lncRNA	Long non-coding RNA
LPA	Light physical activity
LV	Left Ventricle
LVEF	Left Ventricle Ejection Fraction
MFI	Median fluorescence intensity
MHR	Mean Heart Rate
MI	Myocardial infarction
min	Minutes
miR	MicroRNA
MPA	Moderate Physical Activity
mRNA	Messenger RNA
ms	Milliseconds
MSC	Mesenchymal stem cells
MSN	Mesoporous silica nanocarrier
MVPA	Moderate to vigorous Physical Activity
ncRNA	Non-coding RNA
NCs	Nanocarriers
P	P-value
PA	Physical activity
PBMC	Peripheral Blood Mononuclear Cell
PCM	Primary-cardiomyocyte peptide
PEG	Polyethylene glycol
PEI	Polyethylene imine
PGEA	Ethanolamine-aminated polyglycidyl methacrylate
PK/PD	Pharmacokinetics/pharmacodynamics
PLA	Polylactic acid
PLGA	Poly(lactic-co-glycolic) acid
PLN	Phospholamban
PNS	Parasympathetic Nervous System
Pre-miR	Pre-microRNA
Pri-miR	Primary microRNA
pTAC	Percutaneous transverse aortic constriction
R	Correlation coefficient
RGD	Arginine-glycine-aspartic acid tripeptide
ROS	Reactive Oxygen Species
s	Second
SC	Subcutaneous
TAC	Transversal aortic constriction
VPA	Vigorous Physical Activity
w	Week

Chapter 1

Introduction

1.1 Aging and cardiovascular diseases

Aging is a natural and unavoidable process. It is defined as the progressive and cumulative decline of the normal physiological functions of cells, tissues, and organs over time [1]. This decline originates at the molecular level. Age-related functional deterioration is associated with several hallmarks, such as genomic instability, telomere attrition, epigenetic alterations, loss of proteostasis, impaired autophagy, mitochondrial dysfunction, cellular senescence, altered intercellular communication and chronic inflammation **(Figure 1)** [1].

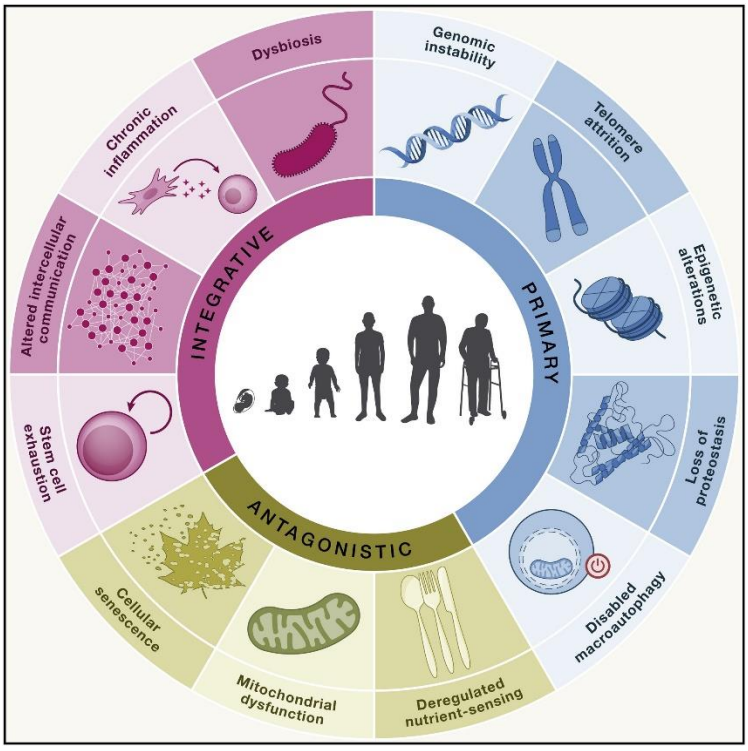


Figure 1. Hallmarks of aging. Figure extracted from [1].

Cardiovascular disease (CVD) is the leading cause of death worldwide, accounting for 17.9 million deaths per year [2]. Over four out of five CVD-related deaths are due to heart attacks and strokes. Two-thirds of them occur in individuals over the age of 70 [2]. Furthermore, more than 50% of individuals aged 65 and older suffer from some form of CVD [3]. Age is a major risk factor for CVD [4] and, consequently, the increase in life expectancy correlates with the prevalence of CVD [3]. It is estimated that the increase in life expectancy will double the population aged 60 and older, growing from 1 billion in 2017 to 2.1 billion in 2050 [5]. The aging of the population, coupled with the prevalence of comorbidities, is expected to further consolidate and potentially exacerbate the CVD epidemiological burden [6,7].

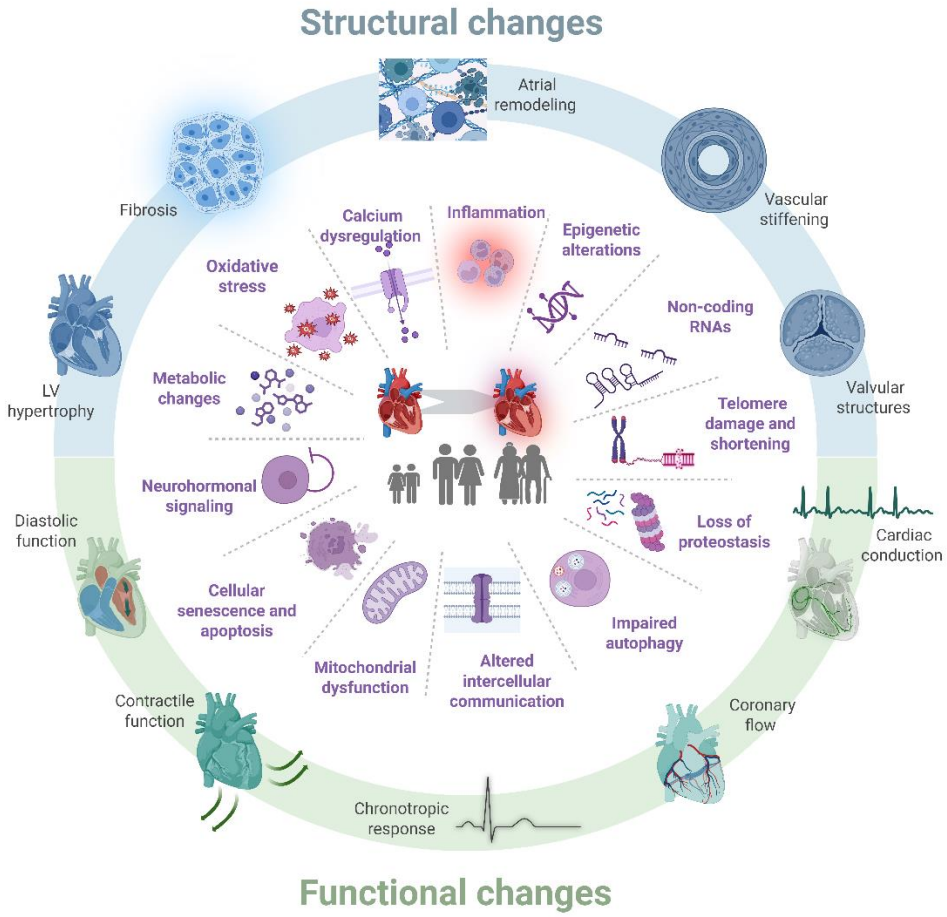


Figure 2. Cardiac aging hallmarks. The outer rim depicts the structural and functional changes of the aged heart. The inner circle shows the cellular and molecular mechanisms that cause these changes. Figure created with BioRender.

With age, the heart undergoes pathophysiological alterations within the cardiovascular (CV) system. These alterations become more pronounced as the heart's reparative mechanisms become less effective over time. The aging heart exhibits structural changes, including concentric hypertrophy of the left ventricle (LV), interstitial and perivascular fibrosis, atrial remodeling, vascular stiffening and changes in valvular structures. At the cardiac functional level, these alterations manifest as diastolic dysfunction, reduced contractile function and chronotropic reserve, impaired coronary flow regulation, and altered cardiac conduction, resulting in a higher propensity for arrhythmias, particularly atrial fibrillation (AF). At the cellular level, there is a cardiomyocyte (CM) loss by apoptosis and necroptosis, and CMs undergo hypertrophy. Fibroblast activation promotes excessive extracellular matrix deposition, which contributes to fibrosis. Endothelial cell senescence and dysfunction reduce nitric oxide bioavailability and angiogenic capacity, further compromising cellular homeostasis. Impaired autophagy and mitochondrial dysfunction also compromise cellular

homeostasis. The underlying cardiac molecular hallmarks of these age-related alterations include the accumulation of reactive oxygen species (ROS), DNA damage and telomere damage and shortening, epigenetic alterations, loss of proteostasis, defects in calcium handling, inflammation, metabolic dysfunctions (such as those related to oxidative phosphorylation, the tricarboxylic acid cycle, β-oxidation, glycolysis and nucleotide repair pathways), chronic activation of neurohormonal signaling, altered intercellular communication and dysregulated gene expression **(Figure 2)** [8–12]**.** Gene expression can be modulated at multiple levels and through different mechanisms, including the contribution of non-coding RNAs (ncRNAs) [13]. These molecular mechanisms, particularly those related to ncRNAs, are still poorly characterized in humans compared with the functional and structural changes.

The steadily increasing elderly population puts enormous pressure is placed on the scientific community and healthcare systems to develop new solutions that reduce the socioeconomic burden of CVD. A deeper understanding of the physiological and pathological processes associated with aging in the CV system could lead to new interventions that promote healthy CV aging and thereby reduce CVD-related mortality. Specifically, an understanding of novel layers of cardiac gene expression regulation during aging could advance this field through the development of new therapies or biomarkers.

1.2 Gene regulation by ncRNAs: miR biology

Traditionally, non-coding DNA was referred to as “junk DNA” and was considered non-functional. More recently, it has begun to be referred to as the “dark genome,” in recognition of its proven, yet largely unknown functionality. For example, bioinformatic studies of epigenetics predict that loci associated with AF reside within DNA regulatory regions [14,15]. However, the dark genome contains many more functional elements than just regulatory DNA. In fact, next-generation RNA sequencing techniques have revealed that approximately 75% of the human genome is transcribed, yet less than 2% is translated into proteins [16]. In other words, the vast majority of the human genome’s transcription of the human genome, virtually ubiquitous, produces ncRNAs. This strongly contradicts the traditional status as genetic “junk” and instead suggests that it plays a major role in all biological processes.

The two main families of ncRNAs are long non-coding RNAs (lncRNAs) and microRNAs (miRs). These ncRNAs regulate gene expression and protein function, and there is ample evidence that they play a key role in cardiac physiology and the pathophysiology

of CVD [17]. Interest in these molecules as new therapeutic targets and therapies is therefore growing rapidly [18]. LncRNAs are RNAs that are more than 200 nucleotides long and are transcribed by RNA polymerase II. They exert their regulatory effects at multiple levels (epigenetic, transcriptional, post-transcriptional, translational, and post-translational) by interacting with DNA, RNA, or proteins. Combining genome-wide association studies (GWAS) and tissue transcriptomics, it has been shown that lncRNAs are associated with complex human diseases, including coronary artery disease [19].

MiRs are single-stranded RNA molecules of 22-24 nucleotides in length that mainly regulate gene expression at the post-transcriptional level [3,20]. They typically inhibit the expression of their targets post-transcriptionally, but they can also regulate it at the transcriptional level [21,22]. The mammalian genome is estimated to contain over 2000 miRs, and approximately 60% of protein-coding genes are regulated by them [23]. Each miR can modulate the expression of hundreds of messenger RNAs (mRNAs), highlighting its pleiotropic effect [24], but each mRNA can also be regulated by more than one miR. For example, *MIR15AHG* directly or indirectly regulates approximately 14% of the entire leukemia cells transcriptome [25]. The complex regulatory capacity of miRs explains their involvement in a wide range of biological processes in living organisms, including development, physiology, and disease. This broad regulatory potential stimulates their study as therapeutic targets and therapies as they can potentially control multiple targets of a pathogenic molecular cascade [18,26,27].

In addition to their therapeutic potential, miRs have potential as biomarkers. They can be secreted into body fluids to facilitate intercellular communication via autocrine, paracrine, and/or endocrine mechanisms [28]. They can be actively secreted into blood, saliva or urine, through extracellular vesicles (EVs), originating from endosomes or from plasma membrane budding, or loaded into RNA-binding proteins, such as Argonaute (AGO) or lipoproteins; or passively released after tissue damage [29,30] **(Figure 3)**. This enables their use as biomarkers of physiological or pathological states [31]. Indeed, miRs have been extensively investigated for this purpose in a variety of diseases (reviewed in [32]).

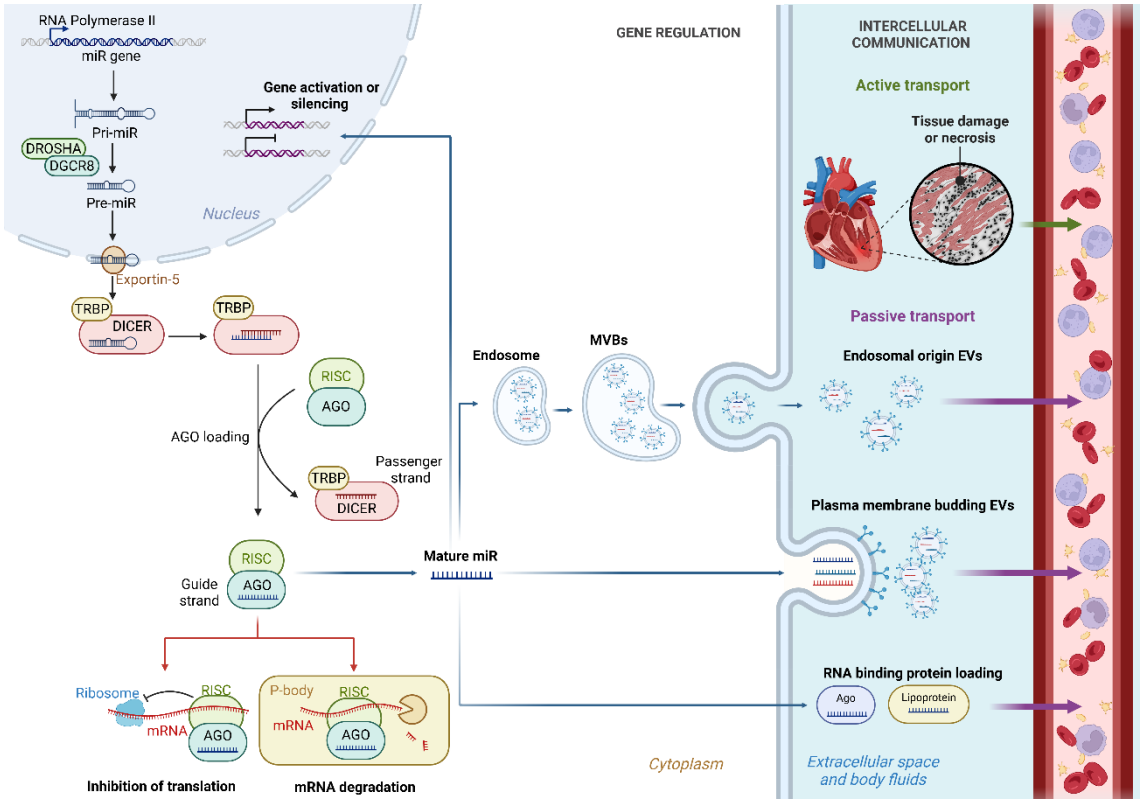


Figure 3. Biogenesis of miRs, mechanism of action and passive and active transport into extracellular space and body fluids. Figure adapted from [30] with BioRender.

1.2.1 MiR biogenesis

MiRs are synthesized from a primary miR (pri-miR) that is typically canonically transcribed in the nucleus by RNA polymerase II **(Figure 3)**. Pri-miRs contain a 5' cap and do not necessarily contain a poly(A) tail [33]. They are mainly expressed from introns and/or exons (70%) or intergenic regions (30%) [34,35].

In the nucleus, pri-miRs form hairpin structures that are cleaved into pre-miRs by the ribonuclease III DROSHA, which forms a complex with the RNA-binding protein DGCR8. This complex protects the miR from degradation and is exported to the cytoplasm, where it binds to a protein complex formed by the RNase III endonuclease enzyme DICER and the transactivation response RNA-binding protein (TRBP). The hairpin loop of the pre-miRs is then cleaved, resulting in a miR duplex of approximately 22-27 nucleotides with a 2-nucleotide overhang at the 3' end [33]. The miR duplex interacts with the RNA-induced silencing complex (RISC), which contains AGO2. AGO2's endonucleolytic cleavage activity destabilizes the miR duplex by nicking it. Then, RNA helicases unwrap the miR duplex, producing the guide strand, which is typically considered the active miR. The other strand, known as the passenger strand, is often degraded by a RISC

component with endoribonuclease activity, but in some cases this strand can also be active [36,37].

The miR guide strand can be derived from either the 5´ end (5p) or the 3´ end (3p) of the duplex. The “miR arm switching”, the differential loading of a miR strand into RISC, is usually determined by the identity of the first 5´ end nucleotide of each strand or the thermodynamic stability of the two ends of the duplex [38], although in some cases it is not determined by strand selection *per se*, and is influenced by target abundance [39]. Although the miR guide strand is usually more highly expressed than its passenger strand, the expression levels of each strand and “arm switching” have demonstrated cell/tissue- and species-specificity [40]. According to the Human Genome Nomenclature Committee [41], mature miRs are termed miR-X, while pri-miRs and pre-miRs are designated as MIRX and mir-X, respectively.

The expression levels of mature miRs can be regulated at multiple stages of their biogenesis. This evidence comes from different observations. For instance, both the precursor and mature forms exhibit tissue- and cell-specific expression patterns. However, this specificity is not always conserved between the precursor and mature forms of a given miR. The processing of mature miRs derived from polycistronic pri-miRs and pre-miRs has shown high variability in individual mature miR processing [42,43]. Additionally, competitive biogenesis between pri-miRs due to microprocessor encumbrance has also been demonstrated [44].

These facts all highlight the precise regulation of miR biogenesis, although further studies are required to elucidate all the mechanisms that mediate and regulate miR maturation.

1.2.2 Mechanism of action of miRs

The miRISC complex, which is formed by RISC and AGO2 and loaded with the active miR strand, typically exerts its post-transcriptional regulatory function in the cytoplasm **(Figure 3)**. The seed region, consisting of nucleotides 2-8 at the 5' end of the miR, is generally essential for binding specificity to its targets, although it has been reported that the 3´ end or other regions of the miR (non-seed sequence) also play a role in target recognition [45]. Depending on the degree of complementarity with the target mRNA, miRs induce translational repression with partial complementarity [3,46], or mRNA degradation with full complementarity [47]. Most miRs interact with their target mRNA at the 3' untranslated region (UTR) [48], though they have also been reported to interact

with other regions, including the 5' UTR or coding regions [3,20]. Additionally, miRs targeting the 5´ or 3´ UTR have also been shown to positively regulate gene expression by stabilizing mRNA or activating translation [49].

In addition to the canonical mechanism of action, the guide miR strand can also be transported to the nucleus, where it exerts transcriptional regulation through gene silencing or gene activation. These nuclear miRs can interact with promoter regions, promoter-associated RNAs, enhancer regions, ncRNAs, induce epigenetic modifications or recruit transcriptional activators to gene promoters, leading to transcriptional silencing or activation [50].

1.3 The role of miRs in cardiac pathophysiology and aging

MiRs play a fundamental role in many biological processes, including development, physiology, disease and aging. Dysregulated miRs in mouse, non-human primate and human tissues have been reported. For example, downregulated genes encoding proteins involved in mitochondrial function in aged mouse liver tissue are predicted targets of the upregulated miR-93, miR-214 and miR-709 [51]. Aging in murine skeletal muscle and brain tissue, among others, has also been associated with changes in miR expression profiles [52]. Similar observations have been reported in non-human primates and humans. For example, in the skeletal muscle of aged rhesus monkeys [53] or in the brain of rhesus monkeys, chimpanzees and humans [54]. The expression patterns of miRs during aging appear to be tissue-specific [52], consistent with the observation that aging involves organ-specific proteins and molecular pathways [55,56].

At the cardiac level, miRs have been shown to be dysregulated in processes associated with heart disease (HD) or aging [57], and to play a role in cardiac regeneration [58]. This underscores their significance in preserving the proper cardiac structure and function [3]. Specifically, preclinical *in vitro* and *in vivo* research has demonstrated the contribution of specific miRs to cardiac hypertrophy, fibrosis, apoptosis or proliferation, among other pathological processes and in the context of cardiac disease, regeneration or aging. *Ex vivo,* several dysregulated miRs have also been reported in diseased or aged human cardiac tissue **(Figure 4)**. In humans, examples include the upregulation of miR-34a with age [59], miR-132 with heart failure (HF) [60], and miR-328, miR-24-2 and miR-206 with AF [61–63]; and the downregulation of miR-125-5p in the infarcted heart [64]. Additionally, bulk transcriptomics of the human LV has identified 20 pri-miRs dysregulated with biological age (BA), denominated BIO-AGEmiRs [12].

Overall, although a link has been established between miRs and the aging heart, further studies are needed to understand how they contribute to govern human cardiac aging, as well as their future therapeutic prospects.

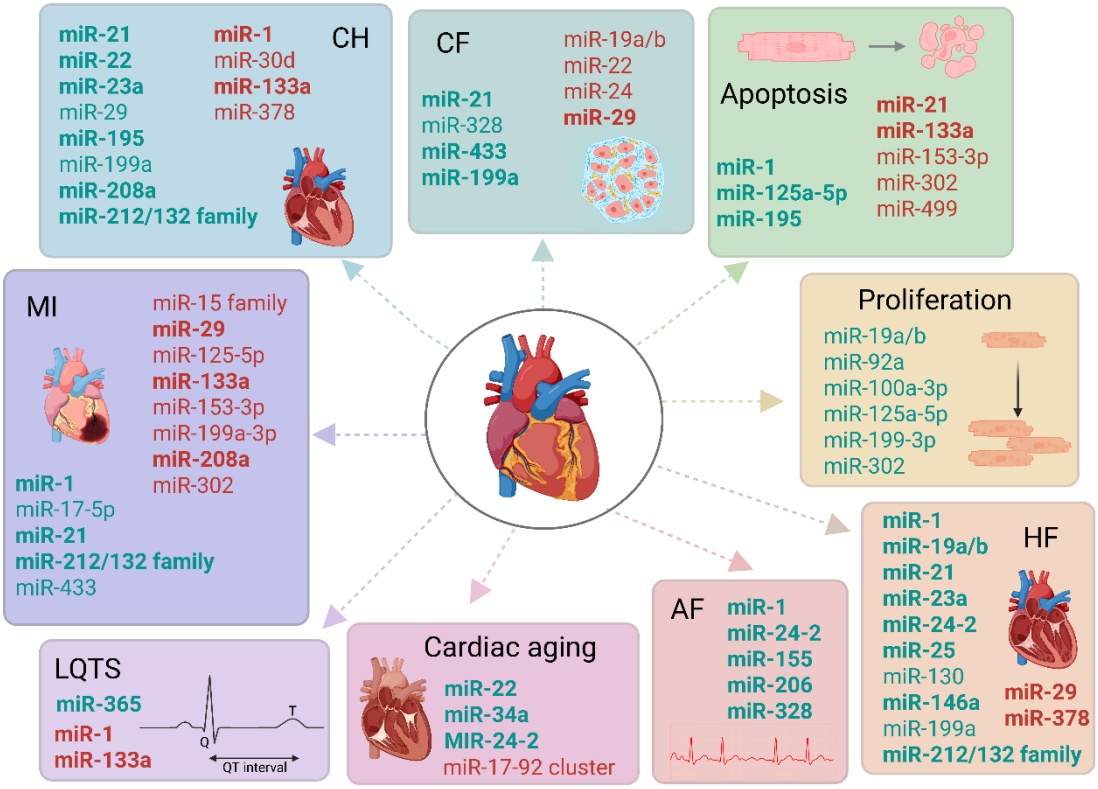


Figure 4. Overview of the role of miRs in cardiac disease and aging. miRs involved in pathological processes, diseases, and in cardiac aging in animal models and in humans. Upregulated and downregulated miRs are color coded in green and red letters, respectively. Bold letters represent those dysregulated in human tissue. Figure created with BioRender (AF: Atrial fibrillation, CH: cardiac hypertrophy, CF: cardiac fibrosis, HF: Heart failure, LQTS: Long-QT syndrome, MI: Myocardial infarction)

1.4 MiR as therapeutics and biomarkers

Since their description, Interest in the therapeutic potential of miRs has grown substantially because they offer a completely new spectrum of therapeutic possibilities for treating diseases with unmet medical needs. According to their canonical regulatory mechanism, there are two types of miR therapies: miR suppression, which uses anti-miR sequences to inhibit a given miR, and miR replacement, which uses miR mimic sequences, to increase its levels **(Figure 5).**

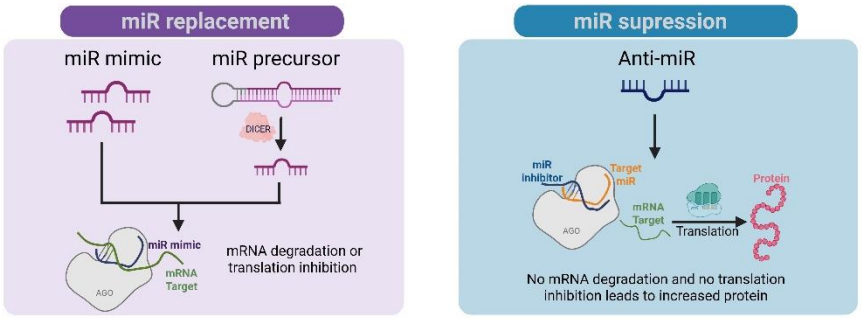


Figure 5. Types of miR therapies. miR replacement (left) and miR suppression therapies (right). Figure created with BioRender.

Abundant preclinical research supports the therapeutic effect of miRs in cardiac and non-cardiac diseases [26]. However, different hurdles related to their intrinsic molecular nature and their mechanisms of action have limited their progress into clinical applications. Ensuring the stability of miR therapies *in vivo* and delivering them not only to a given organ but also to a specific cell type of interest are major challenges in the field. Exploring and further developing recent advances in targeted drug delivery will likely provide key opportunities to overcome these obstacles and unlock the full therapeutic potential of miR treatments. A more detailed review of this scenario is provided in Chapter 3.

The ability to detect miRs in a variety of biological fluids [28] also highlights their potential as biomarkers. A substantial number of miR-based biomarkers associated with HD and CVD have been described [65,66]. Additionally, some circulating miRs have been identified to be dysregulated in elder compared to younger donors [67,68], although without studying their tissue/organ origin and specificity [69]. Our group identified two cardiac BIO-AGEmiRs, MIR4461 and MIR490, that were enriched in the human heart compared to other human tissues [12]. Their value as cardiac-specific indicators of BA is now explored in Chapter 5.

1.5 Biological aging

The molecular, cellular and physiological changes that occur with age are not uniform within and between individuals or populations [70]. Aging is a much more complex biological process than just the chronological age (CA). BA, the age of the individual defined by the extent of age-dependent biological changes [70], captures the effects of genetic and environmental factors acting over time. This effect is expressed in the individual's aging rate, which is the difference between BA and CA. Individuals who age

quickly or slowly, with early or late functional decline, respectively, have different disease susceptibility and mortality risks [71]. Promoting healthy aging aims to achieve slow aging rates. Therefore, determining BA is crucial for gaining insight into the role of specific mechanisms involved in the aging process, to predict the age-related disease and mortality risk in individuals and, given its environmentally modifiable nature [72,73], to guide personalized preventive measures and potential therapeutic interventions that promote healthy aging, but, more importantly, to objectively evaluate their efficacy. Additionally, since aging can be organ-specific due to physiological differences between organs [56,74], determining the organ-specific BA in an individual can provide further insight into an individual's age-related conditions. Consistent with this idea, our group reported cardiac BA indicators based on gene expression, namely *CDKN2A* (a cell senescence marker, now termed SenesAge) and AppAge (a composite index of nearly 3000 age-related genes. These indicators can better describe age-related transcriptomic and structural phenotypes in the human heart than CA [12], however they are invasive. Overall, there is a growing interest in the field of geroscience, particularly in describing minimally or non-invasive biomarkers of aging (BOA) that can estimate BA at the individual or organ level.

At the individual level, many age prediction methods, clocks and predictors, have been reported to explore the association between age and age-related biological markers (reviewed extensively in [75]). However, the terms “clock” and “predictor” are used ambiguously and/or include mixed concepts that are difficult to distinguish. For instance, their accuracy is often judged by their ability to approximate CA, being actually CA predictors, or their biological relevance is usually determined by their ability to predict mortality or disease, making them more appropriate as death or disease timers rather than current BA indicators [76]. In other cases, some methods even include CA as an age-related marker [71,77,78], so they are not strictly speaking aging clocks. Ideally, an aging clock should be an age-related index based on biological data, a BOA, related to an individual’s current age-related health status, their BA. An aging clock can be a predictive biomarker of disease/mortality risk and, ideally, a response biomarker that can monitor changes in BA induced by healthy-aging interventions. Conversely, an age predictor attempts to accurately estimate CA using biological data, somehow losing its ability to capture the variance in health status of individuals, making it more useful for other purposes such as forensics.

At the organ level, determining BA ideally requires describing of BOAs that can be detected in body fluids and are based on organ-enriched biomolecules. Several organ-specific BOAs have been reported, such as the kidneys [79], lungs [80], skeletal muscle

[81], brain [82], skin [83,84] and blood [83], as well as cell-specific BOAs for example in neurons and hepatocytes [85]. Specifically, some BOAs have been developed for the heart, such as those based on epigenetics [86], images from CV magnetic resonance [87] and other imaging technics [11]. However, so far cardiac miR-based BOAs have not been described.

Different types of biological data have been used to estimate BA (reviewed in [70,76]). These include, for example, clocks based on epigenetics [77,78] or biomarkers, such as metabolites, proteins, genomics and clinical measures. Among these, BA indices based on gene and/or protein expression markers may be more sensitive to detect changes in the aging rate than, for example, clinical or physiological features, due to the rapidity of such changes and the sensitivity of the techniques used to quantify them [56]. Both protein- and RNA-based indices have been successfully used to estimate BA [56,88,89]. Machine learning techniques and molecular omics data have also emerged as popular options for developing age predictors and aging clocks, as they offer a wide range of applications even across different tissues, organs and systems [74,76]. However, these techniques are highly complex and costly tools, which may limit their clinical translation. Furthermore, comparisons of BA estimators within the same [90–92] or independent study populations [70] have shown variability in the predictive power and biological information explained by each BA estimator. This underscores the complementary nature of BA estimators and the need for validation in independent populations. This is concerning because differences in age range, gender, ethnicity, sample size, and the data analysis strategy chosen, can significantly affect the predictions and estimates of model performance [93,94]. Nevertheless, blood-based biomarkers offer significant advantages over current methods in terms of simplicity, cost-effectiveness and scalability for clinical translation [95,96].

1.6 Translational models of research in HD and aging

Animal models are commonly used in preclinical research and, although they are unable to represent human genetic variability, especially small animals, they provide an opportunity to study specific mechanisms within a whole-body system. Large animal models more closely resemble human cardiac physiology, function and structure, but the small animals are widely used due to their ease of handling and housing, as well as their cost-effectiveness. Consequently, large animals have mainly been employed to validate and translate the findings obtained from small animals.

For the study of miR biology in animal models, in addition to interspecies differences in physiology, longevity, organism size or genomic homogeneity, it is also necessary to consider the evolutionary conservation of miRs and their target sequences. Although miR genes are generally conserved across species, sequence variations occur in the terminal stem-loop and in the 5′ and 3′ ends of the precursors, and the genomic location of human orthologous miR genes varies across species. Mature miR sequences, especially the seed regions, are the most conserved across species [97–100]. Also, the target sites of mature miRs, are highly conserved across species especially between closely related species [23,101], though some studies have demonstrated species specificity [102].

Many studies in small animal models have revealed the important contribution of miRs to HD and aging **(Figure 4)**. However, the number of studies validating animal findings in human samples or cellular models is quite limited. This is mainly explained by the scarcity of human cardiac tissue samples, whether from post-mortem donors, rejected transplants or small biopsies taken from living donors, or to the impossibility of conducting longitudinal studies, particularly in the case of aging. To fill this gap, different human-based models have been developed. Cellular systems including human inducible pluripotent stem cells (hiPSC)-derived cardiomyocytes (iCMs) serve as valuable models due to their closer resemblance to human cardiac pathophysiological and developmental processes [103]. iCMs have been used to demonstrate the role of miRs in HD. For example, the role of miR-19b in HF and arrhythmias previously demonstrated in mice [104,105], as well as the roles of miR-208a-3p, miR-23a-3p and miR-22-3p in cardiac hypertrophy also demonstrated in animal models [106–110]. Contradictory outcomes have also been reported. For instance, the expression of hsa-miR-1-2 was increased in endothelin-1–induced hypertrophic model of iCMs, whereas Ikeda and colleagues reported a decrease in the expression of miR-1 in rodent models of cardiac hypertrophy and demonstrated that the overexpression of miR-1 mitigates hypertrophy [111,112]. These discrepancies likely reflect differences in species, hypertrophic stimulus, cell maturity or experimental timing, and illustrate the need for careful cross-model validation in translationally relevant models, such as iCMs. In this sense, advances in tissue engineering with hiPSC-derived cells [113] can provide more biomimetic human-based 3D systems to investigate the miR contribution to cardiac physiology and pathology.

Ex vivo models also exist. They are based on living tissues maintained in an artificial environment through perfusion that closely mimic *in vivo* conditions, such as myocardial tissue wedges and *ex vivo* perfused hearts (extensively reviewed in [113]). However,

given the scarcity of human heart tissue, *ex vivo* models of animal origin are used, which also face the interspecies limitations described earlier.

In silico models are also relevant tools (extensively reviewed in [113]). Computational modeling is a powerful approach that contributes to the myriad of preclinical research. This approach uses experimental data to mimic key features of the heart, integrating processes that occur over multiple timescales and from subcellular components to the whole heart, allowing the study of dynamic interactions and the prediction of system-wide effects. They are human-based, cost-effective, reproducible, and adaptable to research needs, allowing the simulation of physiological and pathological conditions. However, their accuracy is highly dependent on real human data, and they still require validation through *in vivo* studies to ensure their efficacy. These models are being used to study genetic mutations, drug effects and cardiac pathology, and to link molecular findings to clinical outcomes. However, advances in data quality and model accuracy are still needed [114].

1.7 Hypothesis and goals

The **hypothesis** of this thesis is that miRs are key regulators of cardiac aging and their investigation can generate new fundamental knowledge capable of supporting therapeutic insights directed towards promoting healthy cardiac aging. Therefore, **the aim of this thesis** is to gain insight into the contribution of miRs to human cardiac biological aging in order to support the development of therapeutic advances with potential to promote healthy cardiac aging and tools that enable the real-time monitoring of CV health-related BA.

The specific goals are:

1. *To identify key miRs with contribution to human cardiac biological aging.*

MiRs play important roles in all types of biological processes. This chapter aims to identify central miRs in human cardiac biological aging using a cross-species approach. In addition, to profile the landscape of molecular perturbations derived from altered miR expression in human cardiac cells with the goal of corroborating their contribution to human cardiac aging and, in addition, understand the potential molecular impact derived from their therapeutic modulation.

2. *To describe the state of the art of cardiac miR therapies, focusing on the challenges faced to understand their future prospects.*

Several intrinsic properties of miRs impede the development of effective cardiac miR therapies, challenging their cardiac penetration and, therefore efficacy. This chapter aims to describe the current state of development of cardiac miR therapies, focusing on the challenges faced and the advances achieved in overcoming them by exploiting the use of nanocarriers and cardiac-specific ligands for targeted delivery to the heart. Following a comprehensive review, this chapter summarizes the progress that can unlock the therapeutic potential of cardiac miR therapies and exposes the future perspectives.

3. *To develop advanced miR therapies capable of modulating age-related effects in human cardiac cells.*

Exploiting the therapeutic potential of miRs to modulate the harmful effects of aging could be a new biotechnological approach to promoting healthy cardiac aging. This chapter aims to advance this therapeutic option. Leveraging DNA nanotechnology and relevant human-based cellular models, the ultimate goal of this chapter is to demonstrate the *in vitro* efficacy of newly developed treatments to modulate the levels of key age-related miRs and their targets in human cardiac cells.

4. *To develop tools for minimally invasive monitoring of CV health-related BA.*

Current BOAs are often too complex to be translated into clinical practice and/or are not real-time indicators of BA capable of monitoring healthy aging interventions. The aim of this chapter is to develop simple and minimally invasive BOAs, both at the individual level and specifically for the heart with these capacities. Using the expression of age-related genes consistently dysregulated with age in blood, as well as the plasma levels of cardiac enriched BIO-AGEmiRs, respectively, this chapter pursues to create such tools and preliminary evaluate their monitoring capacity.

1.8 Structure of the thesis

The thesis is organized as follows:

- **Chapter 2** describes the work carried out to identify miR-24-2 as a genetically conserved and consistently upregulated miR across species in relation to BA. In addition, mir-24-2 gain-of-function studies were performed to profile the regulatory role of the miR in human iCMs. Specifically, proteomic and transcriptomic data describe the regulatory action of the miR in this cell type demonstrating perturbations in biological process related to aging, among others, subsequently supporting its therapeutic value in promoting healthy cardiac aging.

The research described in this chapter generated the following communications to congresses:

Hernández-Bellido N., Köhler R., Ordovás L. “MicroRNAs in human cardiac aging: therapeutics targets and biomarkers”. “III Ciclo de Seminarios Biomédicos ipIBA”. Instituto de Investigación Sanitaria de Aragón (IIS Aragón), Zaragoza (Spain). 2024. Oral communication.

Hernández-Bellido N., Ramos-Marquès E., Hernández-Vicente A., García-Mendívil L., Santander-Badules H., Mercanti G., Garrido-Huéscar E., Garatachea N., Köhler R., Pueyo E., Ordovás L. “microRNAs en envejecimiento cardiaco humano: dianas terapéuticas y biomarcadores”. IV Jornada del I3A - XII Jornada de Jóvenes Investigadores, Instituto de Investigación en Ingeniería de Aragón (I3A), Zaragoza (Spain). 2023. https://doi.org/10.26754/jjii3a.20239029. Poster and congress proceeding.

Hernández-Bellido N., Ramos-Marquès E., Hernández-Vicente A., García-Mendívil L., Santander-Badules H., Mercanti G., Garrido-Huéscar E., Garatachea N., Köhler R., Pueyo E., Ordovás L. “microRNAs in human cardiac aging: therapeutic targets and biomarkers”. Seminarios ipIBA day. Instituto de Investigación Sanitaria de Aragón (IIS Aragón), Zaragoza (Spain). 2023. Poster.

Hernández-Bellido N., Ramos-Marquès E., Hernández-Vicente A., García-Mendívil L., Santander-Badules H., Mercanti G., Garrido-Huéscar E., Garatachea N., Köhler R., Pueyo E., Ordovás L. “microRNAs in human cardiac aging: therapeutic targets and biomarkers”. Iberus Connect PhD Student Congress (CEDIC), Zaragoza (Spain). 2023. Poster.

- **Chapter 3** provides a comprehensive review of the state of the art of the development of cardiac miR therapies, highlighting the challenges that hinder progress and the potential momentum generated by breakthroughs in targeted delivery to the heart using nanocarriers (NCs). Specifically, the chapter reveals a bottleneck in the late preclinical efficacy trials, primarily due to delivery limitations of naked therapies. However, it further demonstrates how targeted delivery of miR therapeutics with NCs

can enhance efficacy by overcoming these limitations. Thus, this work testifies to the promise of unlocking the full clinical value of cardiac miR therapies.

The bibliographic revision conducted in this chapter has been published in a manuscript:

Hernández-Bellido N.✉, Hernández-Ainsa S., Köhler R., Ordovás L.✉ (2026). Nanotechnology-driven heart targeting to fulfil the potential of cardiac miRs therapies". *International Journal of Pharmaceutics.* https://doi.org/10.1016/j.ijpharm.2026.126643 (✉Corresponding author)

- **Chapter 4** describes the development of an anti-miR-24-2 therapy based on DNA nanotechnology. This work was carried out in collaboration with the team of Dr. Silvia Hernandez Ainsa from the Institute of Nanoscience and Materials of Aragon (INMA). Specifically, I carried out the *in vitro* functional characterization of the therapy *in vitro* to demonstrate that the generated anti-miR NC can (i) deliver functional anti-miR-24-2 sequences in a cellular model system restoring the levels of SERCA2 (a miR-24-2 target) and (ii) modulate predicted target genes in human iCMs. Therefore, this chapter provides *in vitro* proof-of-concept for the ability of the developed treatment to module an age-dysregulated miR in human cardiac cells.

The research described in this chapter generated the following publication and communications to congresses as first or presenting author:

Postigo A.*, **Hernández-Bellido N.***, Sánchez-Barat M., García-Mendívil L., Pueyo E., del Barrio J., Hernández-Ainsa S.✉, Ordovás L.✉ (2024). DNA-Based Nanocarriers to Sequester Altered microRNAs in Cardiac Dysfunction. *Advanced Therapeutics,* 2400247. https://doi: 10.1002/adtp.202400247 (*Equal contribution, ✉Corresponding author)

Postigo A.*, **Hernández-Bellido N.*,** Sánchez-Barat M., García-Mendívil L., Leo-Escartín L., Ripalda-Paredes M., del Barrio J., Ordovás L., Hernández-Ainsa S. "Designer DNA-based nanocarriers for the delivery of microRNA therapies against cardiac dysfunction". 6th Functional DNA Nanotechnology Workshop", Munich (Germany). 2024. Poster. (*Equal contribution)

Postigo A.*, **Hernández-Bellido N.*,** Sánchez Barat M., Orrite C., Garrido-Huéscar E., García-Mendívil L., Pueyo E., Ordovás L., Hernández-Ainsa S. "Design of DNA-based nanocarriers for the delivery of microRNA therapies against cardiac dysfunction ". Cellular Biology of the Heart & Myocardial Function (CBFH) Biennial meeting, Naples (Italy). 2023. Poster. (*Equal contribution)

Hernández-Bellido N., Postigo A., Orrite C., Garrido-Huéscar E., García-Mendívil L., Pueyo E., Hernández-Ainsa S., Ordovás L. "Non-viral delivery of microRNA therapies for cardiac dysfunction using DNA nanostructures". 12th Biennial Congress of the Spanish Society in Gene and Cellular Therapy (SETGYC), Pamplona (Spain). 2023. Oral communication.

Hernández-Bellido N., Postigo A., Orrite C., Garrido-Huéscar E., García-Mendívil L., Pueyo E., Hernández-Ainsa S., Ordovás L. "Terapias cardiacas avanzadas con microRNAs basadas en nanoestructuras de DNA". III Jornadas del I3A - XI Jornada de Jóvenes Investigadores. Instituto de Investigación en Ingeniería de Aragón (I3A), Zaragoza (Spain). 2022. https://doi.org/10.26754/jjii3a.20227026. Poster and congress proceeding.

Hernández-Bellido N., Postigo A., Orrite C., Garrido-Huéscar E., García-Mendívil L., Pueyo E., Hernández-Ainsa S., Ordovás L. "Terapias cardiacas avanzadas con microRNAs basadas en nanoestructuras de DNAs". Seminarios ipIBA day, Zaragoza (Spain). 2022. Poster.

Hernández-Bellido N., Postigo A., Orrite C., Garrido-Huéscar E., García-Mendívil L., Pueyo E., Hernández-Ainsa S., Ordovás L. "Towards advanced cardiac miRNA therapies through DNA-based nanostructures". Frontiers in CardioVascular Biomedicine, Budapest (Hungary). 2022. https://doi: 10.1093/cvr/cvac066.087. Poster and congress proceeding.

- **Chapter 5** presents the generation and evaluation of a simple blood-based BOA, denominated GamC, and the assessment of the potential of circulating cardio-enriched BIO-AGEmiRs as minimally invasive indicators of human cardiac BA. Specifically, this chapter shows the value of GamC as indicator of the synchronous CV health-related BA of individuals and its potential monitoring capacity in a short-term intervention study carried out in centenarians, but rules out the BOA capacity of the cardio-enriched miR-490-3p. Thus, this chapter proposes a simple and clinically translatable BOA for real-time monitoring of CV health-related BA.

The research described in this chapter generated the following publication and communications to conferences and congresses:

Hernández-Bellido, N.✉, Hernández-Vicente, A., García-Mendívil, L., Ramos-Marquès, E., Hernando, D., Cebollada, A., Köhler, R., Garatachea, N., Pueyo, E., Ordovás, L.✉(2025). A simple blood biomarker based on gene expression describes cardiovascular health-related biological age. *Geroscience.* https://doi.org/10.1007/s11357-025-01784-6. (✉Corresponding author)

Hernández-Bellido N., Ramos-Marquès E., Hernández-Vicente A., García-Mendívil L., Santander-Badules H., Garrido-Huéscar E., Sánchez-Barat M., Garatachea N., Köhler R., Pueyo E., Ordovás L. "Identification of biological age indicators as potential predictors of physical and cardiac-related conditions ". Cellular Biology of the Heart & Myocardial Function (CBFH) Biennial meeting, Naples (Italy). 2023. Poster.

Hernández-Bellido N., Köhler R., Ordovás L. "MicroRNAs in human cardiac aging: therapeutics targets and biomarkers". "III Ciclo de Seminarios Biomédicos ipIBA", Instituto de Investigación Sanitaria de Aragón (IIS Aragón), Zaragoza (Spain). 2024. Oral communication.

Hernández-Bellido N., Ramos-Marquès E., Hernández-Vicente A., García-Mendívil L., Santander-Badules H., Mercanti G., Garrido-Huéscar E., Garatachea N., Köhler R., Pueyo E., Ordovás L. “microRNAs en envejecimiento cardiaco humano: dianas terapéuticas y biomarcadores”. IV Jornada del I3A - XII Jornada de Jóvenes Investigadores, Instituto de Investigación en Ingeniería de Aragón (I3A), Zaragoza (Spain). 2023. https://doi.org/10.26754/jjii3a.20239029. Poster and congress proceeding.

Hernández-Bellido N., Ramos-Marquès E., Hernández-Vicente A., García-Mendívil L., Santander-Badules H., Mercanti G., Garrido-Huéscar E., Garatachea N., Köhler R., Pueyo E., Ordovás L. “microRNAs in human cardiac aging: therapeutic targets and biomarkers”. Seminarios ipIBA day, Zaragoza (Spain). 2023. Poster.

Hernández-Bellido N., Ramos-Marquès E., Hernández-Vicente A., García-Mendívil L., Santander-Badules H., Mercanti G., Garrido-Huéscar E., Garatachea N., Köhler R., Pueyo E., Ordovás L. “microRNAs in human cardiac aging: therapeutic targets and biomarkers”. Iberus Connect PhD student Congress (CEDIC), Zaragoza (Spain). 2023. Poster.

Hernández-Bellido N., Köhler R., Ordovás L. “microRNAs cardiacos en envejecimiento cardiaco: dianas terapéuticas y biomarcadores”. “Seminarios ipIBA day”, Zaragoza (Spain). 2022. Oral communication.

Chapter 2

Uncovering miR-24-2 key role in human cardiac biological aging

This work was partially conducted in collaboration with the laboratory of Dr. Myriam Gorospe at the National Institute on Aging (NIA) in Baltimore, USA, where I completed a research stay, and with the laboratory of Prof. Mindaugas Valius at Vilnius University in Lithuania.

2.1 Introduction

Different pathophysiological changes occur with age, and these can vary considerably between individuals of comparable CA based on their individual aging rate. However, although inter-individual differences exist, the hallmarks underlying the aging processes are well defined both at the general [1] and cardiac levels (Chapter 1). This suggests that core mechanisms orchestrate the process of individual and heart aging from the molecular level all the way up to the tissue and organ function. The organ-specific program is consistent with the existence of tissue-specific molecular pathways during aging [55,56]. Some of these molecular mechanisms are known to be conserved between species, but the identification of species-specific age-related pathways emphasizes the importance of human studies for devising optimal therapeutic strategies to modulate the aging rate [115].

Given that miRs regulate all classes of pathological and biological processes including cardiac aging [13], it is highly likely they also contribute to govern the cardiac aging process and that core miR-based mechanisms are maintained across species. To improve the knowledge of the contribution of miR to human cardiac aging, our group analyzed the miR expression profile in human heart tissue during biological aging in a cross-sectional transcriptomic study [12]. A total of 20 BIO-AGEmiRs were identified, although their relevance, especially at the mature level, was not established.

As introduced in Chapter 1, miRs can simultaneously regulate a large number of targets [24] potentially affecting multiple molecular pathways. Although miRs act preferentially through inhibition of protein translation, their effect on the transcriptome is notable [116,117]. At the individual gene level, the effect of miR-mediated regulation is subtle, but globally, these changes may translate into shifts of molecular pathways that explain changes in full biological processes [118,119] with consequences at the cellular and tissue levels. Understanding the downstream molecular regulatory network of a miR potentially involved in a pathophysiological process with known phenotypes across species, i.e., cardiac aging, can contribute to confirm its role in such process as well as to understand the expected species-specific molecular impact derived from its therapeutic modulation. The most highly expressed miRs in a given tissue are proposed as the ones that significantly regulate gene expression in this particular context [120]. Therefore, profiling the proteomic and transcriptomic effect of a miR regulation in the main cell type of the studied tissue constitutes a complementary approach to define the miR regulatory network that, as just mentioned, will confirm its biological role in such process and determine the impact of its modulation. This is of particular interest in human cardiac cells.

Hypothesizing that hallmark mechanisms of cardiac aging involve miRs and that those with an essential role are preserved across species, we used a cross-species strategy to uncover the most relevant miRs in cardiac aging. The expression levels of the orthologous human BIO-AGEmiRs were assessed in the heart tissue of two naturally aged animal models, mice and monkeys, at both the pri-miR and mature miR levels. This identified miR-24-2 as a commonly dysregulated age-related miR which is, in addition, highly expressed in these tissues and in human iCMs. To define the regulatory network of miR-24-2 in human cardiac tissue, we profiled the proteomic and transcriptomic changes induced by mir-24-2 overexpression in human iCMs. The detection of disturbed processes defined as general and heart-specific aging hallmarks, such as metabolism and proteostasis, and cardiac contraction and electrophysiological processes, among other functions, substantiates the role of miR-24-2 in human cardiac BA. But the results also define the extent of molecular cascades that could be affected by its therapeutic modulation.

2.2 Materials and methods

2.2.1 Animal models of natural aging

The import, housing, experimental procedures, and euthanasia of mice (*Mus musculus*) were approved by the Animal Care and Use Committee (ACUC) of the National Institute on Aging (NIA). C57BL/6JN male mice were maintained under controlled conditions (12–hours light/dark cycle and food and water were supplied *ad libitum*). LV tissue from young (3 months, n=6) and elder (24 months, n=6) mice were collected, flash-frozen in liquid nitrogen and stored at -80 ºC until assayed.

Rhesus monkeys (*Macaca mulatta*) were housed at the NIH Animal Centre in Poolesville, Maryland. The animal center is fully accredited by the American Association for Accreditation of Laboratory Animal Care, and all of the procedures were approved by the Animal Care and Use Committee of the NIA Intramural Program. Animals were maintained individually in standard primate caging in a controlled environment (12–hours light/dark cycle and adequate room temperature and humidity). All monkeys were given standard chow diets (TestDiet® #5038 Purina Mills, Richmond, IN or NIA-1–87, Purina Animal Nutrition LLC, Minneapolis, Minnesota) and were fed ad libitum. LV tissues (n=12 were obtained from male animals over the course of natural aging without selection based on health status, with ages ranging from 5.8 to 27.94 years old **(Table 1)**, that had been part of NIA studies. Animals were euthanized at NIH Animal Centre and perfused

with ice cold ringers. Tissues were flash-frozen in liquid nitrogen and stored at -80 ºC until required.

Table 1. Monkey animals: sample code, sex (M: male) and age (y.o.: years old)

Sample code	Sex	Age (y.o.)
M1333	M	27.84
PH0476	M	26.62
RQ6710	M	25.11
AK9J	M	23.87
9SM	M	23.61
M1385	M	22.73
M1382	M	22.71
ZJ29	M	19.93
M1497	M	18.96
RQ6783	M	15.87
M1473	M	15.52
CW8M	M	12.78
M1500	M	10.14
DGEL	M	5.8

2.2.2 Quantification of gene and miR expression levels

RNA was extracted, retrotranscribed and amplified by quantitative PCR (qPCR)**,** according to the methods displayed in **Table A1** and using primers listed in **Table A2.** Gene expression was normalized with the reference genes indicated in **Table A1** and expression calculated as either relative ($2^{-\Delta\Delta Ct}$ method) or absolute ($2^{-\Delta Ct}$) **(Table A1)**.

Normalized gene expression values of the human LV were obtained from bulk tissue RNA-seq data (containing gene and polyadenylated pri-miRs) from previous work of the group [12]. The quantification of pri-miRs was done using primers flanking the stem loop. In case of the polycistronic pri-miRs, where a single precursor contained multiple miRs, primers were designed in the most 3'-end stem loop of the pri-miR.

2.2.3 Generation of mir-24-2^{+} and mir-24-2^{-} inducible hiPSC lines

The master cell line (MCL), hiPSC-FRT3, kindly provided by Prof. Verfaillie (Katholieke Universiteit Leuven, Belgium) [121], was routinely maintained on vitronectin- (Gibco) coated dishes in Essential 8 (E8) medium (Thermo Fisher). This human iPSC line that contained flippase recognition target (FRT) sequences in the *AAVS1 locus,* was used to generate two inducible cell lines expressing tdT-mir-24-2 (line mir-24-2^{+}) or only tdT (line

mir-24-2$^-$), by flippase recombinase-mediated cassette exchange (RMCE), as previously described [121]. The RMCE donor vector for the inducible expression of mir-24-2 was created by cloning the DNA sequence corresponding to the human miR-24-2 stem loop sequence flanked by ~200 base pairs (bp) (using primers listed in **Table A2**) downstream of tdTomato (tdT) of the pZ: F3-P (Chs4) X4 TetOn-3F-tdT-F vector. The obtained constructs are represented below **(Figure 6).**

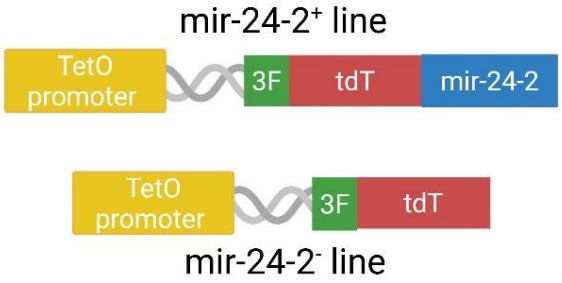


Figure 6. RMCE constructs for the generation of the mir-24-2$^+$ and mir-24-2$^-$ hiPSC lines (3F: 3Flag sequence). The pZ:F3- pZ:F3-P (cHS4)X4 tdT-F was kindly provided by Prof. Verfaillie (Stem Cell Institute Leuven, KU Leuven, Leuven, Belgium) [121], and contains cHS4 insulator sequences that were kindly provided by Prof. Brindley (George Washington University, Washington DC, USA) [122]. Figure created with BioRender. The sequence of the miR-24-2-expressing construct is provided in **Figure A1**.

2.2.4 Directed differentiation of hiPSCs to iCMs

For differentiation, hiPSCs were passaged with EDTA 0.5 mM (Gibco) and plated at 10^5 cells/cm^2 on hESC-qualified Matrigel (Falcon) coated plates with E8 medium supplemented with 5 µM Rock Inhibitor. After 48 hours (h), hiPSCs were differentiated into iCMs as previously described [123]. From day 10 of differentiation, a CM enrichment and expansion protocol was applied [124,125]. For each induction experiment, iCMs in expansion were detached using TrypLE Select (10x), seeded at 4-5x10^5 cells/cm^2. At this point, the culture was checked for iCMs purity by estimating the proportion of Cardiac Troponin T2/Myosin Light Chain 2 (TNNT2$^+$/MYL2$^+$) double positive cells by flow cytometry (see section 2.2.6). Cultures with more than 95% of TNNT2$^+$/MYL2$^+$ were only used. The iCMs were expanded for 3 more days (until reaching 85-90% confluence) and transferred to CM maintenance medium (CMM) for 4 days before starting the induction with 2 µg/ml of doxycycline for 14 days. At the endpoint, the induced iCMs were harvested for RNA and protein extraction and evaluation of the degree of induction reported by tdT by flow cytometry. Only cultures with induction levels above 50% of tdT$^+$ cells were used **(Figure 7)**.

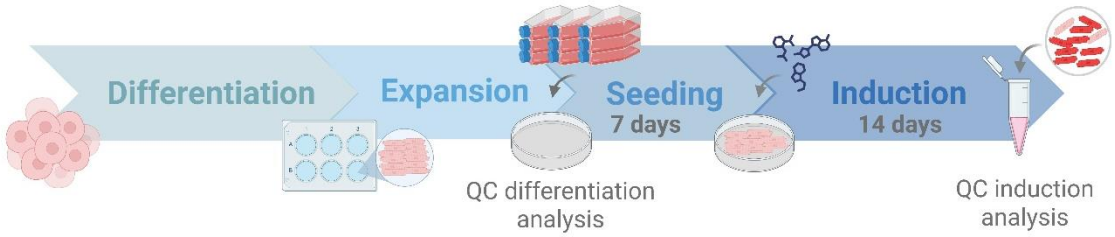


Figure 7. Experiment workflow from hiPSC lines to induced iCM (QC: quality control). Figure created with BioRender.

2.2.5 Identification of human miR orthologue genes

The murine or monkey gene sequences orthologous to the human BIO-AGEmiRs genes were obtained from the NCBI Gene database. For non-annotated genes, the human pre-miR sequences were used to conduct a sequence homology search against the mouse or monkey genomes using the NCBI Blast alignment tool.

2.2.6 Flow cytometry

Determination of the purity of the iCMs progenies was done by fixing the cells with 2% paraformaldehyde (PFA) for 15 minutes (min) at 4 ºC, blocking with PBS, 10% donkey serum and 0.1% saponin at room temperature for 15 min and then, incubating them in blocking buffer for 15 min with primary antibodies BV421-conjugated mouse anti-TNNT2 (BD Biosciences, 565618) at 1 µg/ml and the rabbit anti-MYL2 (Abcam, ab48003) conjugated to Cy5 (Abcam, ab188288) at 6 µg/ml. The levels of doxycycline induction (tdT reporter) was analyzed in live cells. Gallios 10 cytometer (Beckman Coulter) was used to record at least 10000 events and FlowJo was used for analysis.

2.2.7 Mass spectrometry, proteomics and Western Blot

Washed pellets of mir-24-2^{+} and mir-24-2^{-} induced iCMs were lysed in 7 M urea, 2 M thiourea and 4% CHAPS buffer supplemented with protease and phosphatase inhibitor cocktail (Thermo Fisher) at room temperature and sonicated. After debris removal, protein concentration was determined using the Pierce Coomassie (Bradford) kit following the manufacturer´s instructions. Then, the protein lysates were supplemented with 40 mM of DTT.

Filter aided sample preparation (FASP) method [126] was used for protein digestion prior to mass spectrometry analyses. Liquid chromatographic (LC) analysis was performed in

a Waters Acquity ultra performance LC system (Waters Corporation, Wilmslow, UK) and peptide separation was performed on an ACQUITY UPLC HSS T3 250 mm analytical column. Data were acquired using Synapt G2 mass spectrometer and MassLynx 4.1 software (Waters Corporation) in positive ion mode using data-independent acquisition (UDMSE) [127]. Raw data files were processed and searched using Progenesis QI for proteomics 2.0.55 (Waters Corporation, UK). Data was analyzed using trypsin as the cleavage protease, one missed cleavage was allowed, and fixed modification was set to carbamidomethylation of cysteines, variable modification was set to oxidation of methionine. Minimum identification criteria included 1 fragment ions per peptide, 3 fragment ions and one peptide per protein. UniprotKB/SwissProt database was used for protein identification.

The differential expression analysis of the identified proteins was carried out using a standard workflow established in the R package DEP, version 1.28.0 [128]. Only proteins detected in at least two out of three replicates in at least one experimental condition were included for analysis. Data were normalized using the variance stabilization normalization (VSN) method with the function "normalize_vsn," and the differential protein expression analysis was performed via the function "test_diff" in the DEP package. Normalized counts of mir-24-2^{+} iCMs were relativized to the mir-24-2^{-} iCMs. Functional annotation of the proteomic perturbation induced by mir-24-2, including Gene Ontology (GO), was conducted with all the identified proteins by using SRplot [129]. Obtained significant GO biological processes (FDR ≤ 0.05) were manually classified in broader functional categories.

Western Blot was used to verify the induction levels of the transgene in both mir-24-2^{+} and mir-24-2^{-} lines through FLAG expression and to quantify the expression levels of SERCA2. GAPDH antibody (1:10000, Santa Cruz Biotechnology, sc-47724), FLAG antibody (1:500, Sigma-Aldrich, F-104) and SERCA2 antibody (1:500, Abcam, ab2817) were used as primary antibodies and Alexa Fluor 790 donkey anti-mouse (1:10000, Thermo Fisher, A11371) was used as secondary. The blots were developed in Odyssey CLx-1189 (LI-COR) and analyzed by Image Studio Software.

2.2.8 Transcriptomics and bioinformatic analysis

Total RNA was extracted from mir-24-2^{+} and mir-24-2^{-} induced iCMs according to the methods displayed in **Table A1**. A specialized service conducted the RNA-sequencing. Briefly, polyadenylated transcripts were captured using the ABclonal Poly (A) mRNA Capture Module, and strand-specific libraries were prepared using the Fast RNA-seq

Library Prep Kit V2 according to the manufacturer's instructions. Library quality was verified by qPCR and Agilent TapeStation, and sequencing was performed on an Illumina NovaSeq X Plus platform using paired-end 150 bp reads.

The FASTQ files from sequencing were trimmed for adapter sequences using BBDuk from BBMap (v39.12) and mapped to the human reference genome hg38 (Ensembl v104) with STAR aligner (v2.7.10b_0328). Then, the reads were summarized and quantified using featureCounts in R package Subread (v2.20.0) to create gene counts. Then, normalization of counts and differential expression analysis was performed with DESeq2 package v1.46.0. For differential expression analysis, normalized counts of mir-24-2^{+} iCMs were relativized to the mir-24-2^{-} iCMs. Functional annotation on the transcriptome and Gene Set Enrichment Analysis (GSEA) was conducted using all the RNAs with p-value (P) ≤ 0.05 by using SRplot [129]. Obtained significant GO biological processes (FDR ≤ 0.05) were classified in broader categories as in the proteomic analysis. Validation of transcriptomic results was conducted according to the methods displayed in **Table A1**.

The "multiMiR" R package [130] was used to identify the validated and predicted targets of the 5p and 3p strands of miR-24-2. The predicted targets were filtered by the prediction confidence score of each database, namely scores ≥ 0.8, ≥ 80, ≤ -1 and ≤ -0.2 for DIANA-microT, miRDB, miRanda and TargetScan, respectively. From this genome-wide predicted targetome, the cardiac-specific one was obtained by gene lists cross-comparison with the 50% top expressed genes in the human LV [12].

2.2.9 Statistical Analysis

All statistical analyses were conducted in GraphPad Prism 8. Spearman and Pearson correlations were carried out for non-linear and linear association analysis, respectively. Mann-Whitney U test was carried out for comparisons between groups. Bars represent median and interquartile range (IQR). All experiments were repeated a minimum of three independent times, unless indicated otherwise in the figure captions. Statistical threshold was established at P ≤ 0.1 for qPCR in animal models and in iCMs. For the rest of analyses, the statistical threshold was established at P ≤ 0.05 or FDR ≤ 0.05 and FDR ≤ 0.1 where indicated.

2.3 Results

2.3.1 SenesAge explains cardiac biological aging in naturally aged animals

First, to compare animal and human BA-related data, the ability of the human cardiac BA-indicator SenesAge [12] to describe the cardiac BA in the models of natural aging was assessed. For that, its relationship with CA and the expression profiles of senescence-associated and cardiac function-related genes in the heart tissue of aging animals compared to human data were studied [12] **(Figures 8 and 9 and Table 2)**.

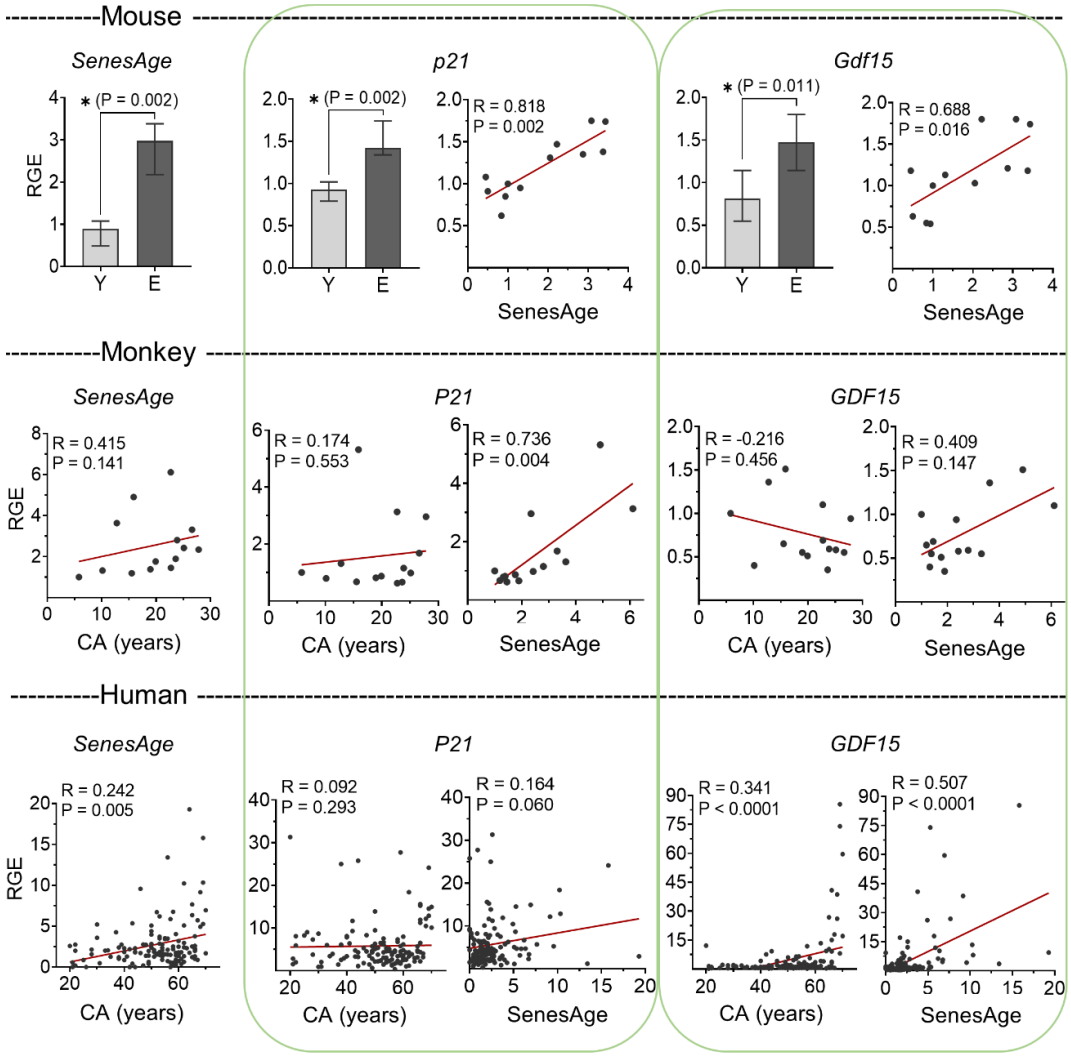


Figure 8. Evaluation of the cardiac BA-indicator SenesAge in the heart tissue of naturally aged animal models and human. Analysis of the relation between the expression of SenesAge (relative gene expression -RGE- to an arbitrary young individual) and CA (left panels) by qPCR (animal models) or RNA-seq (human). Correlation analysis of *P21* (middle panels) and *GDF15* expression (right panels) with CA or SenesAge in mice, monkey and human cardiac tissue from young (Y) to elder (E). (R: Spearman's correlation coefficient, P: p-value, linear regression shown as red line).

SenesAge significantly increased 3.4-fold (P = 0.002) in the heart of aged mice and was associated with CA in the heart of monkeys (R = 0.415) approaching significance (P = 0.141), in agreement with human data (R = 0.242, P = 0.005) [12]. The senescence markers *p21* and *Gdf15* were significantly upregulated in relation to CA in mice and did not significantly change in monkeys. In chronologically aged humans, *GDF15* significantly increased (R = 0.341, P ≤ 0.0001), but *P21* was unchanged. However, both genes maintained (mice) or increased (monkey) their association with SenesAge, showing medium to high correlation coefficients (R from 0.409 to 0.818), that was significant for all but for the monkey's *GDF15* (P=0.147). In humans, *GDF15* increased significantly its correlation with SenesAge (R = 0.507, P ≤ 0.0001), while *P21* increased as compared to CA, but without being a relevant association (R = 0.164, P = 0.060) **(Figure 8)**.

As compared to humans, a large proportion of the human orthologous age-associated and cardiac function-related genes maintained their gene downregulated expression profile in the naturally aged animals. Specifically, 50.0% and 72.2% of the mouse and monkey orthologous genes, respectively, reduced their expression levels with CA. Mimicking the changes that occur in the human profile, the observed downregulation strengthened with SenesAge in both species, despite the smaller sample size compared to the human study. Specifically, the murine downregulated orthologues raised up to 66.7%, with 50.0% of them decreasing their correlation value as compared to CA, whereas the percentage of downregulated monkey orthologues stayed at 72.2%, but 61.5% of them decreased their correlation value as compared to CA **(Figure 9 and Table 2)**.

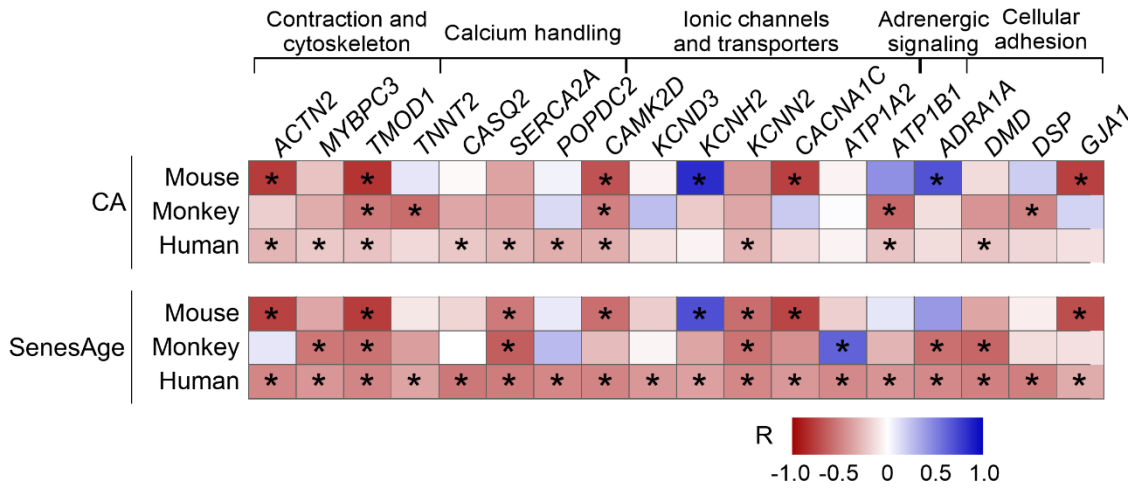


Figure 9. Association analysis between cardiac function-related genes and CA or SenesAge in mouse, monkey and human cardiac tissue (R: Spearman´s correlation coefficient).

Table 2. Association analyses of cardiac function- and age-related genes with CA and SenesAge in animal models and in humans. (R: Spearman´s correlation coefficient, P: p-value, N/A: not-applicable, Green cells: R<0.1, Yellow cells: P ≤ 0.05/0.1).

Functional categories	Gene name	Mouse qPCR data (n=12)				Monkey qPCR data (n=14)				Human RNA-seq data GTEX (n=132)			
		CA		SenesAge		CA		SenesAge		CA		SenesAge	
		R	P	R	P	R	P	R	P	R	P	R	P
Contraction and cytoskeleton	*ACTN2*	-0.773	0.009	-0.748	0.007	-0.194	0.504	0.097	0.741	-0.292	0.001	-0.477	<0.0001
	MYBPC3	-0.241	0.485	-0.350	0.266	-0.328	0.253	-0.534	0.052	-0.213	0.014	-0.414	<0.0001
	TMOD1	-0.799	0.007	-0.761	0.005	-0.524	0.057	-0.551	0.044	-0.237	0.006	-0.479	<0.0001
	TNNT2	0.097	0.788	-0.095	0.770	-0.577	0.033	-0.383	0.176	-0.149	0.088	-0.359	<0.0001
Calcium handling	*CASQ2*	-0.024	0.974	-0.165	0.538	-0.350	0.221	0.000	1.000	-0.217	0.012	-0.533	<0.0001
	SERCA2	-0.363	0.260	-0.523	0.084	-0.379	0.181	-0.634	0.017	-0.279	0.001	-0.514	<0.0001
	POPDC2	0.048	0.937	0.084	0.800	0.143	0.623	0.268	0.351	-0.321	0.0002	-0.472	<0.0001
	CAMK2D	-0.676	0.026	-0.566	0.059	-0.501	0.070	-0.268	0.350	-0.321	0.0002	-0.484	<0.0001
Ion channels and transporters	*KCND3*	-0.048	0.937	-0.203	0.528	0.255	0.376	-0.044	0.883	-0.111	0.204	-0.407	<0.0001
	KCNH2	0.824	0.004	0.688	0.016	-0.209	0.470	-0.356	0.210	-0.048	0.589	-0.375	<0.0001
	KCNN2	-0.411	0.195	-0.571	0.056	-0.350	0.221	-0.547	0.046	-0.291	0.001	-0.471	<0.0001
	CACNA1C	-0.752	0.011	-0.731	0.009	0.208	0.474	-0.437	0.119	-0.146	0.095	-0.407	<0.0001
	ATP1A2	-0.048	0.937	-0.189	0.558	0.011	0.976	0.613	0.022	-0.047	0.590	-0.466	<0.0001
	ATP1B1	0.436	0.162	0.095	0.770	-0.598	0.027	-0.298	0.299	-0.235	0.007	-0.422	<0.0001
Adrenergic signaling	*ADRA1A*	0.677	0.022	0.403	0.194	-0.132	0.651	-0.563	0.039	-0.140	0.110	-0.465	<0.0001
Cellular adhesion	*DMD*	-0.145	0.699	-0.357	0.256	-0.420	0.136	-0.601	0.026	-0.230	0.008	-0.498	<0.0001
	DSP	0.194	0.563	-0.074	0.821	-0.485	0.081	-0.137	0.639	-0.161	0.066	-0.504	<0.0001
	GJA1	-0.752	0.011	-0.696	0.015	0.172	0.553	-0.124	0.672	-0.124	0.158	-0.330	<0.0001
Senescence markers	*GDF15*	0.751	0.011	0.688	0.016	-0.216	0.456	0.409	0.147	0.341	<0.0001	0.507	<0.0001
	P21	0.870	0.002	0.818	0.002	0.174	0.553	0.736	0.004	0.092	0.293	0.164	0.060
SenesAge	*CDKN2A*	0.869	0.002	N/A		0.415	0.141	N/A		0.242	0.005	N/A	

% downregulated R ≤ 0.1 (green)	**50.0**		**66.7**		**72.2**		**72.2**	
% downregulated P ≤ 0.1 (green+yelow)	**55.6**		**50.0**		**30.8**		**38.5**	
% downregulated in SenesAge that strengthened R from CA (green+red)			**50.0**				**61.5**	

Overall, as in human data, SenesAge accentuated the expression profiles observed with CA in both models of natural aging and greatly described the gene expression profile associated with age in humans, being this relation apparently stronger for the monkeys than for mice. Thus, SenesAge is used hereafter as the age parameter for all the species.

2.3.2 The expression profiles of upregulated human BIO-AGEmiRs are generally maintained with age across species

The murine and monkey orthologous genes of the human cardiac BIO-AGEmiRs were identified using gene databases or a homology sequence search with the human pre-miR sequences. We found 50% and 85% of the 20 human miR genes in the murine and

monkey genomes, respectively **(Table 3).** Two of these were non-conserved in both species, *MIR3648-2* and *MIR4461,* being *MIR4461* one of the cardio-enriched miRs previously described as suitable for its evaluation as BOA (Chapter 1).

Table 3. List of human BIO-AGEmiRs genes and their orthologous in animal species. (Chr: chromosome, DNA sense strand: (+), DNA antisense strand: (-), N/A: not applicable).

Human					Mouse		Monkey	
Dysregulation with SenesAge	**BIO-AGEmiR**	**ENSEMBL ID**	**miRBase (Acc. nº Stem loop)**	**Genome location**	**miRBase (Acc. nº Stem loop)**	**Genome location**	**miRBase (Acc. nº Stem loop)**	**Genome location**
Upregulated	*MIR1304*	ENSG00000284458	MI0006371	chr11(-)	N/A	Not conserved	MI0020887	chr14(-)
	MIR155HG	ENSG00000234883	MI0000681	chr21(+)	MI0000177	chr16(+)	MI0007645	chr3(-)
	MIR210HG	ENSG00000199038	MI0000286	chr11(-)	MI0000286	chr7(-)	MI0007670	chr14(-)
	MIR24-2	ENSG00000284387	MI0000081	chr19(-)	MI0000572	chr8(+)	MI0003053	chr19(-)
	MIR296	ENSG00000284040	MI0000747	chr20(-)	MI0000394	chr2(-)	MI0007681	chr10(+)
	MIR3648-2	ENSG00000264462	MI0031512	chr21(+)	N/A	Not conserved	N/A	Not conserved
	MIR3911	ENSG00000283874	MI0016415	chr9(-)	N/A	Not conserved	BLAST	chr15(+)
	MIR3916	ENSG00000283881	MI0016422	chr1(-)	N/A	Not conserved	BLAST	chr1(+)
	MIR4435-2HG	ENSG00000172965	MI0016775	chr2(-)	N/A	Not conserved	BLAST	chr13(+)
	MIR4461	ENSG00000198868	MI0016807	chr5(+)	N/A	Not conserved	N/A	Not conserved
	MIR497HG	ENSG00000267532	MI0000489	chr17(-)	MI0000237	chr11(+)	MI0007658	chr16(-)
	MIR503HG	ENSG00000223749	MI0003188	chrX(-)	MI0000643	chrX(-)	MI0007777	chrX(-)
	MIR6080	ENSG00000278581	MI0020357	chr17(+)	N/A	Not conserved	BLAST	chr16(+)
	MIR7162	ENSG00000284277	MI0023623	chr10(-)	BLAST	chr2(+)	N/A	Not conserved
Downregulated	*MIR17HG*	ENSG00000215417	MI0000071	chr13(+)	MI0000687	chr14(+)	MI0003004	chr17(+)
	MIR22HG	ENSG00000186594	MI0000078	chr17(-)	MI0000570	chr11(+)	MI0002631	chr16(-)
	MIR3936	ENSG00000263597	MI0016592	chr5(-)	N/A	Not conserved	BLAST	chr6(-)
	MIR490	ENSG00000207597	MI0003125	chr7(+)	MI0005002	chr6(+)	MI0007764	chr3(+)
	MIR600HG	ENSG00000236901	MI0003613	chr9(-)	N/A	Not conserved	MI0007861	chr15(+)
	MIR635	ENSG00000207561	MI0003650	chr17(-)	N/A	Not conserved	BLAST	chr16(-)

Among the evolutionary conserved, some pri-miRs were barely expressed. Specifically, *MIR296* and *MIR503HG* in both species, *MIR1304*, *MIR497HG* and *MIR6080* in monkey and *MIR7162* in mouse **(Figure 10a and Table 4)**. Among the expressed, all the orthologous miR genes of upregulated human BIO-AGEmiRs were also upregulated in elder animals of both species. *MIR210HG*, *MIR3911*, *MIR3916*, and *MIR24-2* significantly and *MIR155HG* non-significantly increased with age in monkey's heart tissue with correlation coefficients from 0.43 to 0.56) **(Figure 10a and Table 4).** In mouse, *MIR210HG*, *MIR24-2*, *MIR155HG*, and *MIR497HG* increased as well with age, although non-significantly and with weaker correlation coefficients (R from 0.28 to 0.44) **(Figure 10a and Table 4)**. On the contrary, the orthologous miR genes of the

downregulated human BIO-AGEmiRs did not decrease in the naturally aged models. This indicates a poor maintenance of the expression profile of the human downregulated set in animal models and, therefore, limits their interest in the study. Exceptions were the murine *MIR490*, another human cardio-enriched BIO-AGEmiR (Chapter 1), which was significantly downregulated (R = -0.54), and the primate *MIR635*, which was significantly upregulated with high correlation coefficient (R = 0.57) **(Figure 10a and Table 4)**. Considering all three species, the pri-miRs of *MIR210HG*, *MIR24-2* and *MIR155HG*, were consistently upregulated with age, although the relation was more pronounced in monkey and mouse compared to humans and generally, in monkey compared to mouse.

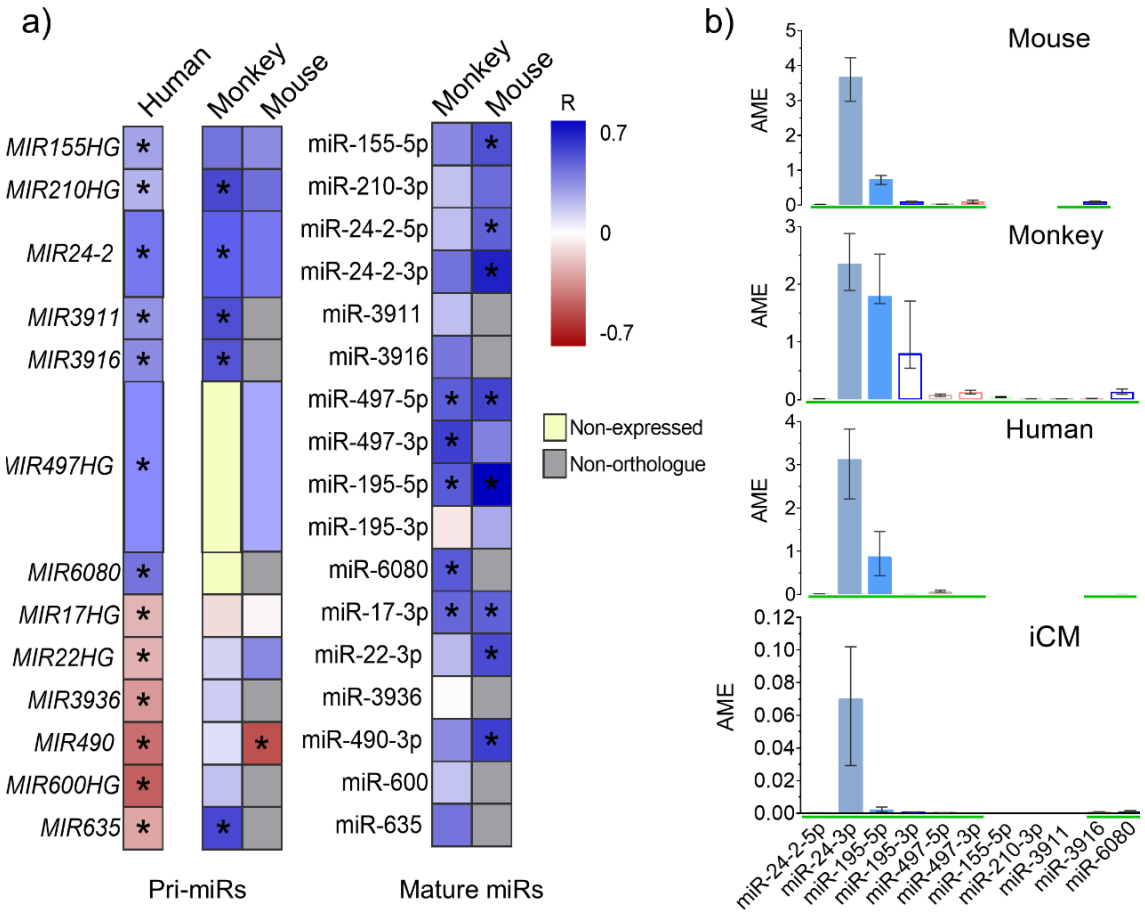


Figure 10. Analysis of the expression levels of BIO-AGEmiRs at the pri-miR and mature miR stages. a) Heatmap of the correlation coefficients between SenesAge and the levels of pri-miRs (left) and mature miRs (right) in all three species: humans, monkeys and mice (R: Spearman correlation coefficient). **b)** Expression profile of the mature miRs in LV tissue from animals, humans and human iCMs. The quantified miRs in each species are marked with a green line y the abscissa (AME: Absolute miR Expression).

Table 4. Association of BIO-AGEmiRs and mature miRs with SenesAge in animal models (mouse and monkey) and in humans. Statistical threshold was established at P ≤ 0.1 for mouse and monkey and P ≤ 0.05 for human. (R: Spearman´s correlation coefficient, P: p-value, NO: no orthologue (grey cells), NQ: no quantified for technical reasons (blue cells); NE, non-expressed (yellow cells).

BIO-AGEmiRs	RNA-seq data GTEX		qPCR data				Mature miRs	qPCR data			
	Human		Mouse		Monkey			Mouse		Monkey	
	R	P	R	P	R	P		R	P	R	P
MIR1304	0.26	0.002	NO		NE		miR-1304-5p	NO		NQ	
MIR155HG	0.28	<0.0001	0.357	0.256	0.433	0.124	miR-155-5p	0.550	0.067	0.367	0.197
MIR210HG	0.23	0.008	0.441	0.154	0.565	0.038	miR-210-3p	0.462	0.134	0.194	0.504
MIR24-2	0.37	<0.0001	0.410	0.186	0.499	0.072	miR-24-2-5p	0.497	0.104	0.202	0.485
							miR-24-2-3p	0.699	0.014	0.440	0.117
MIR296	0.24	0.006	NE		NE		miR-296-3p	NQ		NQ	
MIR3648	0.25	0.003	NO		NO		miR-3648	NO		NQ	
MIR3911	0.33	<0.0001	NO		0.544	0.047	miR-3911	NO		0.200	0.492
MIR3916	0.36	<0.0001	NO		0.530	0.054	miR-3916	NO		0.424	0.132
MIR4435-1HG	0.46	<0.0001	NO		NO		miR-4435	NO		NO	
MIR4461	0.20	0.024	NO		NO		miR-4461	NO		NO	
MIR497HG	0.37	<0.0001	0.28	0.38	NE		miR-497-5p	0.587	0.049	0.508	0.067
							miR-497-3p	0.392	0.206	0.601	0.026
							miR-195-5p	0.797	0.003	0.517	0.061
							miR-195-3p	0.266	0.400	-0.081	0.785
MIR503HG	0.34	<0.0001	NE		NE		miR-503-5p	NQ		NQ	
MIR6080	0.43	<0.0001	NO		NE		miR-6080	NO		0.517	0.061
MIR7162	0.21	0.014	NE		NO		miR-7162-3p	NQ		NO	
MIR17HG	-0.23	0.007	-0.032	0.93	-0.114	0.696	miR-17-3p	0.497	0.102	0.477	0.087
MIR22HG	-0.24	0.006	0.364	0.246	0.139	0.638	miR-22-3p	0.566	0.059	0.218	0.454
MIR3936	-0.32	0.0002	NO		0.156	0.594	miR-3936	NO		-0.018	0.955
MIR490	-0.45	<0.0001	-0.539	0.073	0.097	0.749	miR-490-3p	0.601	0.043	0.358	0.209
MIR600HG	-0.50	<0.0001	NO		0.191	0.512	miR-600	NO		0.182	0.532
MIR635	-0.28	0.001	NO		0.569	0.037	miR-635	NO		0.433	0.124

Moving forward into the functional miR species, we evaluated the expression levels of the mature miR strands processed from conserved miR genes. Although low expression was detected for *MIR497HG* and for *MIR6080* in monkey, they were also quantified at the mature level because their pri-miRs were among the most highly correlated human BIO-AGEmiRs **(Table 4)**. The results showed that all the mouse and 77% of monkey mature miRs increased with age as their increasing precursors **(Figure 10a and Table 4)**, suggesting that the observed change in the mature BIO-AGEmiR profile may primarily arise at the transcriptional level, not during their maturation. In contrast, for the non-expressed monkey *MIR497HG*, significant upregulation of the mature strands was detected, with exception of miR-195-3p, indicating that this miR cluster may control its mature levels during biogenesis. The mature miRs concomitantly upregulated with age

in both animal species and that presented higher association with age in increasing order were miR-24-3p (R > 0.44), miR-497-5p (R > 0.51) and miR-195-5p (R > 0.52) **(Figure 10a and Table 4)**. Interestingly, the human downregulated BIO-AGEmiRs were, as their mouse and monkey precursors, generally upregulated at the mature level with age. In contrast, the mouse miR-490-3p, which was significantly downregulated at the pri-miR level, significantly increased its expression. Like for the MIR497HG miRs, this suggests a strong control of the miR-490-3p expression levels during biogenesis.

As previously mentioned, those miRs highly expressed in a tissue are supposed to exert the gene expression regulation in this particular context. Among all the human orthologues of upregulated BIO-AGEmiRs, miR-24-3p was the most highly expressed miR in mouse and monkey cardiac tissue **(Figure 10b)**. From those with higher age association in monkey (R > 0.44), also miR-24-3p showed the highest expression levels in human cardiac tissue, followed by quite some distance by miR-195-5p, in agreement with previous data [131]. CMs are the primary functional cell type of the heart, thus, we quantified the expression levels of the mature miRs in them, verifying that the tissue miR profile is also maintained at the cellular level. MiR-24-2-3p was the most highly expressed in iCMs in agreement with the human, mouse, and monkey profiles **(Figure 10b)**.

2.3.3 Mir-24-2 upregulation perturbs the proteome affecting metabolism, cardiac function and development and aging hallmarks

Given the consistent age-related profile of mir-24-2 in cardiac tissue across species, including human, its preservation at the mature level in mouse and monkey hearts, and its dominant expression levels over other mature miRs in hearts of all three species and in human iCMs, mir-24-2 was chosen for gain-of-function studies to dissect its downstream regulatory role in human iCMs. This overexpression system was chosen to mimic the observed age-related increase in all three species for this miR. Mir-24-2^{+} and mir-24-2^{-} hiPSC lines were generated, differentiated to iCMs and induced for 14 days to overexpress tdT-mir-24-2 or only tdT, respectively **(Figure 7).** The transgene induction levels were comparable between lines and the mir-24-2 was strongly upregulated in the mir-24-2^{+} line as compared to the mir-24-2^{-} line (~ 220-fold increase) **(Figure 11).**

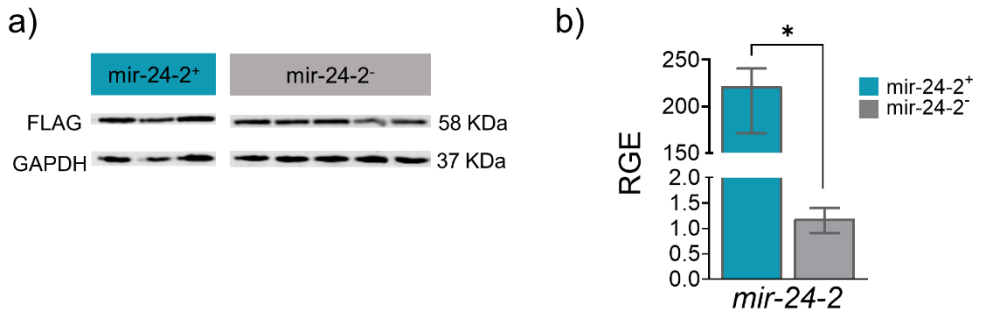


Figure 11. Assessment of the mir-24-2 induction levels. a) Western Blot of 3FLAG and GAPDH. **b)** Relative mir-24-2 expression levels assessed by qPCR.

Proteomics resulted in the identification of nearly 2000 proteins per sample (~ 13% of the identified coding transcriptome in section 2.3.4). Differential global proteomics revealed modest proteome changes induced by the mir-24-2 overexpression**.** Only 161 proteins were dysregulated (P ≤ 0.05) **(Figure 12a),** of which 47 were differentially expressed proteins (DEPs) (FDR ≤ 0.1) in miR-24-2^{+} induced iCMs compared to their miR-24-2^{-} counterparts **(Figure 12b)**. Overall, the downregulated proteins predominated, representing 66% of the DEPs.

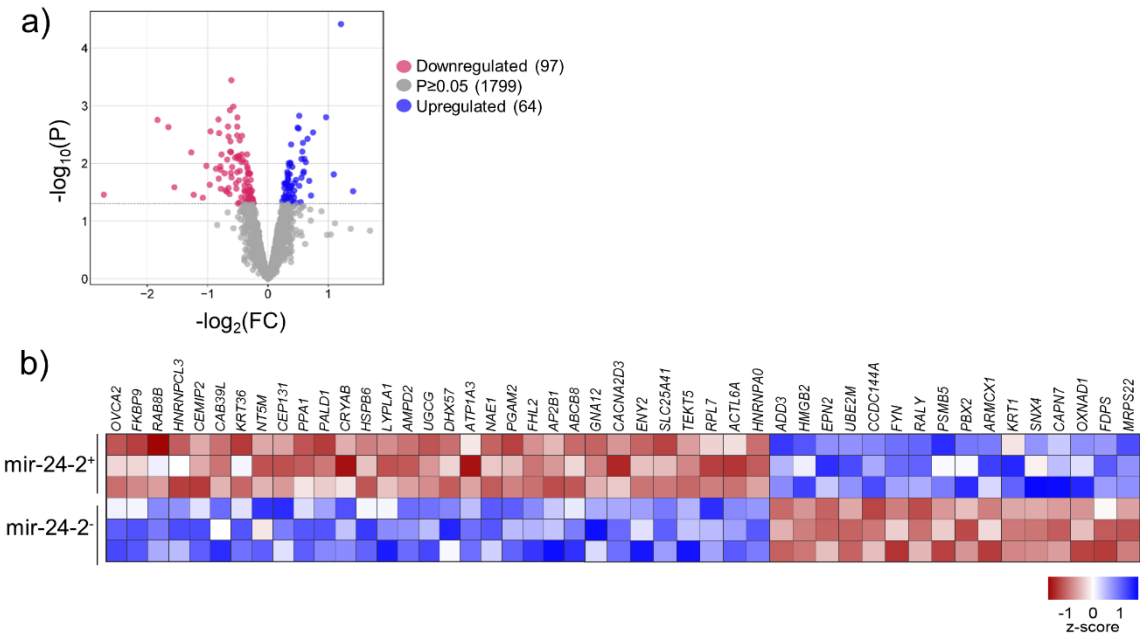


Figure 12. Profiling of the proteomic changes in response to mir-24-2 overexpression in iCMs. a) Volcano plot representing all the identified proteins. Red and blue points indicate proteins with P ≤ 0.05 in mir-24-2^{+} induced iCMs compared to the mir-24-2^{-} induced iCMs. Retrieved from SRplot. **b)** Heatmap representing z-score of DEPs (FDR ≤ 0.1) in mir-24-2^{+} and mir-24-2^{-} induced iCMs.

The functional annotation of the complete proteome retrieved 693 significantly dysregulated biological processes (FDR ≤ 0.05). The top 25 were mainly related to metabolism of proteins (including trafficking), nucleotides and nucleosides, and energy derivation, respiration and oxidative phosphorylation **(Figure 13a).** A classification of the individual GO biological processes grouped in broader functional categories, confirmed the metabolism as an important regulated process by mir-24-2, mainly the one of proteins and nucleotides/nucleosides, but also of RNA, energy, carbohydrates, DNA and lipids. However, proteostasis, considered an aging hallmark, also appeared among the most affected categories. This was accompanied by other proportionally less affected aging hallmarks, such as telomere maintenance, mitochondrial function, oxidative stress or apoptosis. Cellular and subcellular structural and functional processes were also perturbed, including the cytoskeletal function, closely related to intercellular communication (another aging hallmark), vesicular transport or the biogenesis of cellular components. Last, cardiac-specific functions were also affected by miR-24-2 overexpression. In particular, cardiac contraction and electrophysiology, involving calcium handling, were perturbed, but also cardiac tissue development, which could in turn be related to other developmental-related functions (i.e., tissue or cell development-related GOs) **(Figure 13b)**.

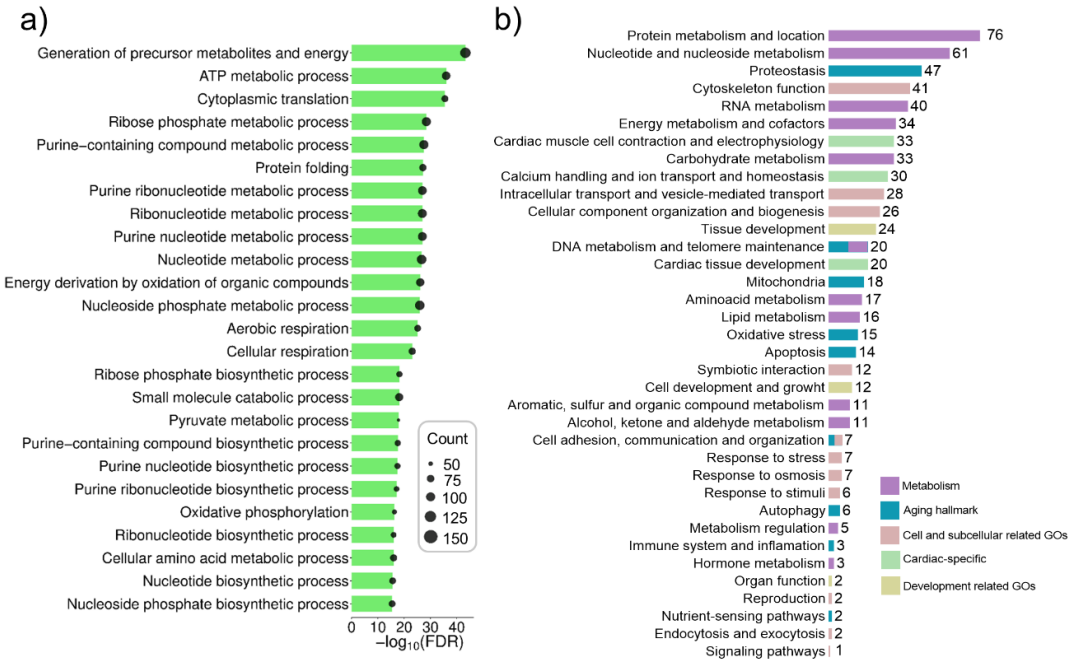


Figure 13. Functional annotation of the total proteome with the overexpression of mir-24-2. a) Top 25 dysregulated GO biological processes by FDR (Count indicates the number of proteins in each GO biological process). Retrieved from SRplot. **b)** Manual classification of GO biological processes in broader categories (Numbers next to the bars indicate the number of GO biological processes in each category).

Within the identified proteins, direct targets of miR-24-2 were predicted **(Figure 14)**. The genome-wide targetome of miR-24-2 obtained *in silico* with multiMiR yielded 6910 validated and predicted genes, 953 and 6525 for the 5p and 3p strands, respectively. Cross-comparison of these lists with the human LV transcriptome, which consisted of 28033 genes (obtained as the top 50% expressed genes in [12]), yielded a predicted cardiac targetome of miR-24-2 of 6446 genes, 896 and 6099 genes for the 5p and 3p strands, respectively. The predicted cardiac targetome was 93% of the genome-wide one, reinforcing the relevance of miR-24-2 for the maintenance of the cardiac tissue homeostasis. The predicted cardiac targetome was then intersected with the list of the top 10% downregulated proteins from the proteomic data to finally identify 80 and 13 putative targets for the miR-24-2-3p and -5p strands, respectively. Some of the proteins were common for both strands, leading to a total of 83 putative cardiac targets of mir-24-2, being 12 of which DEPs (FDR ≤ 0.1) **(Table 5)**. The number of putative targets for the miR-24-3p strand was considerably higher as expected according to its higher expression levels **(Figure 14).**

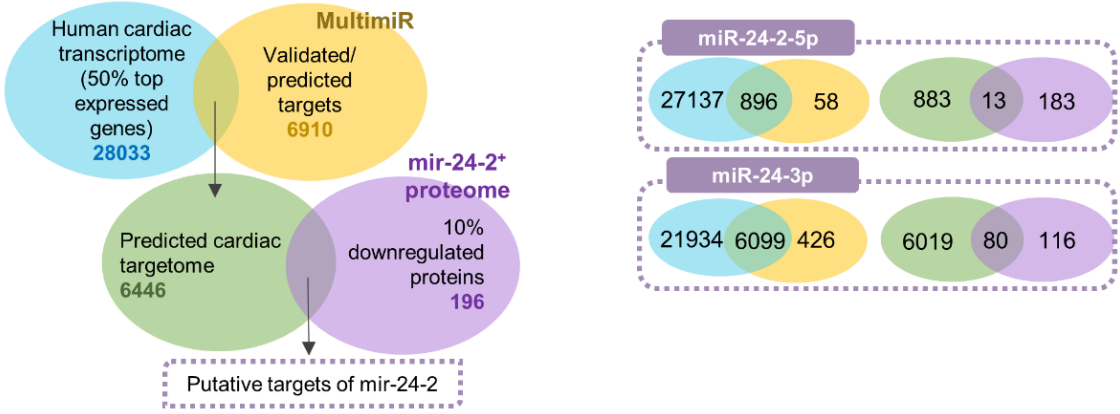


Figure 14. Workflow of the identification of putative targets of mir-24-2.

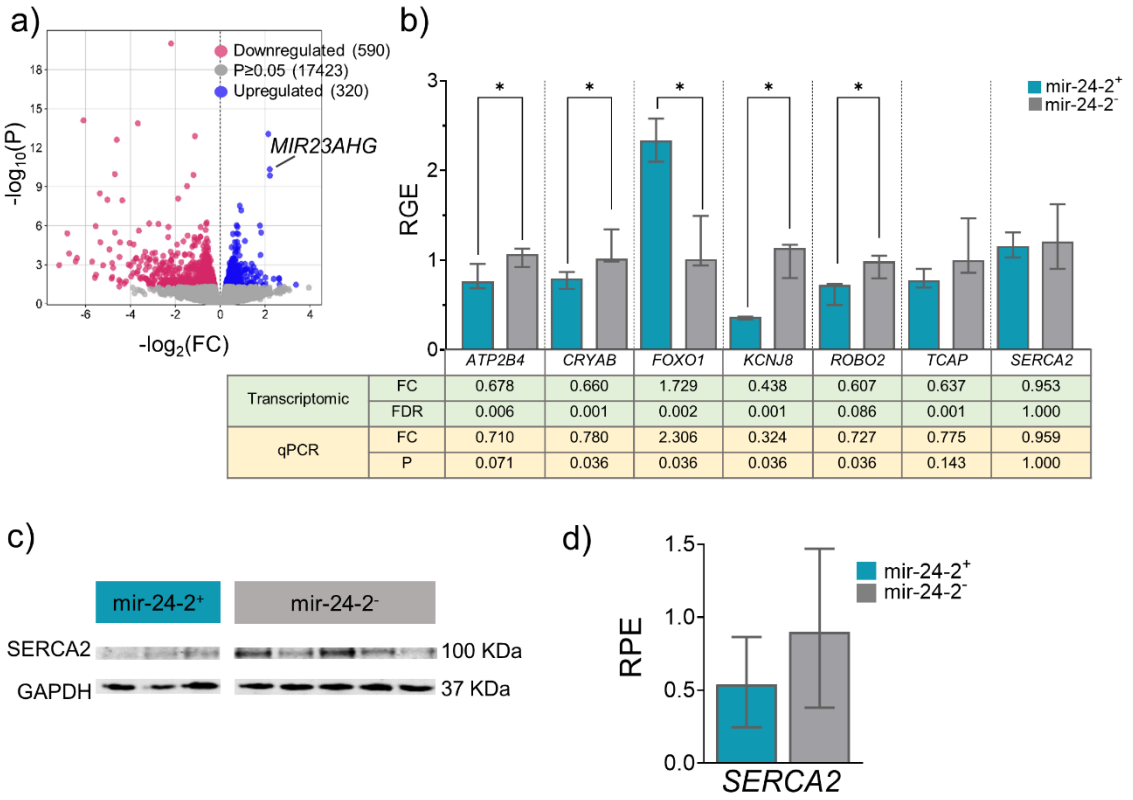
Table 5. Putative cardiac targets of mir-24-2 downregulated at the protein level: differential expression at the RNA and protein levels (FC: Fold change, FDR: adjusted p-value, P: p-value, FDR ≤ 0.1 and P ≤ 0.05 marked as blue cells) and predicted or validated interactions from multiMiR for miR-24-2-5p and miR-24-3p strands (marked as green cells).

Gene name	Transcriptome			Proteome			miR-24-2-5p		miR-24-3p	
	Log_2FC	FDR	P	Log_2FC	FDR	P	Predicted	Validated	Predicted	Validated
CRYAB	-0.599	0.001	0.000	-0.626	0.050	0.006				
ATP2B4	-0.560	0.006	0.000	-0.288	0.622	0.100				
ROBO2	-0.712	0.086	0.001	-0.45	0.778	0.192				
LRIG1	-0.383	0.242	0.004	-0.391	0.281	0.029				
ATP2B1	-0.479	0.790	0.032	-0.32	0.321	0.034				
PALD1	-0.461	0.791	0.033	-0.63	0.003	0.001				
CAMK2B	0.297	1.000	0.063	-0.387	0.236	0.024				
GBF1	0.225	1.000	0.064	-0.378	0.359	0.039				
PLN	-0.216	1.000	0.071	-0.369	0.550	0.079				
HADH	-0.250	1.000	0.077	-0.414	0.744	0.162				
PRKAR1B	-0.281	1.000	0.092	-0.262	0.856	0.320				
TFRC	0.310	1.000	0.108	-0.337	0.117	0.012				
PITPNA	0.237	1.000	0.111	-0.254	0.755	0.171				
MT-ATP8	0.336	1.000	0.133	-0.402	0.517	0.071				
RAB8B	-0.336	1.000	0.138	-1.27	0.053	0.006				
POPDC2	0.167	1.000	0.157	-0.271	0.873	0.371				
MTAP	-0.294	1.000	0.199	-0.465	0.127	0.013				
GSS	0.177	1.000	0.216	-0.353	0.862	0.336				
CLIP2	-0.329	1.000	0.246	-0.324	0.433	0.051				
PSMD5	-0.176	1.000	0.278	-0.296	0.541	0.077				
UGCG	-0.725	1.000	0.284	-0.574	0.002	0.001				
LONP1	-0.140	1.000	0.291	-0.367	0.748	0.165				
GRIP1	-0.254	1.000	0.304	-0.252	0.370	0.041				
DYNLL2	-0.140	1.000	0.318	-0.388	0.626	0.101				
EEA1	0.225	1.000	0.320	-0.263	0.813	0.234				
AP2B1	0.137	1.000	0.325	-0.496	0.074	0.008				
DCTN1	0.129	1.000	0.348	-0.28	0.758	0.173				
HNRNPA0	-0.115	1.000	0.352	-0.346	0.059	0.007				
EPHB1	-0.244	1.000	0.377	-1.55	0.253	0.026				
HDLBP	0.127	1.000	0.386	-0.342	0.641	0.106				
AIMP2	0.165	1.000	0.392	-0.306	0.807	0.226				
SPINK5	-0.616	1.000	0.405	-0.783	0.122	0.013				
DES	-0.619	1.000	0.435	-0.389	0.428	0.050				
MAPK6	-0.157	1.000	0.437	-0.654	0.260	0.027				
BLVRB	0.126	1.000	0.453	-0.301	0.809	0.229				
VAPB	0.096	1.000	0.468	-0.524	0.265	0.027				
ABCB8	-0.136	1.000	0.476	-0.481	0.069	0.008				
GMPS	-0.118	1.000	0.491	-0.325	0.135	0.014				
PRKAR2A	0.088	1.000	0.509	-0.285	0.189	0.019				
SMUG1	-0.123	1.000	0.536	-0.248	0.383	0.043				
SPHKAP	-0.093	1.000	0.538	-0.362	0.406	0.046				
PARVA	0.118	1.000	0.540	-0.279	0.450	0.055				
MDH1	-0.082	1.000	0.561	-0.266	0.442	0.053				
CEP170B	0.095	1.000	0.565	-0.571	0.699	0.133				
ACTL6A	-0.102	1.000	0.572	-0.369	0.089	0.010				
RPL7	-0.076	1.000	0.576	-0.413	0.078	0.009				
GNB2	0.074	1.000	0.578	-0.376	0.813	0.235				
PGAM4	0.186	1.000	0.608	-0.433	0.700	0.133				
KDM2B	-0.091	1.000	0.609	-0.351	0.443	0.053				
IFT172	-0.078	1.000	0.615	-0.377	0.411	0.047				
IDI1	0.081	1.000	0.623	-0.293	0.273	0.028				
DNAJB11	-0.081	1.000	0.626	-0.341	0.720	0.145				
LDHA	-0.088	1.000	0.640	-0.265	0.283	0.030				
COX6B1	-0.061	1.000	0.646	-0.35	0.408	0.047				
MTA2	-0.068	1.000	0.648	-0.329	0.370	0.041				
NAE1	-0.072	1.000	0.652	-0.51	0.015	0.003				
PUF60	0.059	1.000	0.654	-0.34	0.910	0.551				
INTS3	-0.061	1.000	0.671	-0.391	0.743	0.161				
SNAP23	0.077	1.000	0.681	-0.453	0.508	0.068				
CNNM4	-0.101	1.000	0.683	-0.377	0.570	0.084				
UBQLN2	0.052	1.000	0.698	-0.781	0.266	0.027				
CNDP2	0.050	1.000	0.722	-0.354	0.790	0.205				
CYCS	-0.062	1.000	0.725	-0.288	0.579	0.086				
GNA12	-0.060	1.000	0.727	-0.479	0.064	0.007				
HNRNPUL2	-0.054	1.000	0.740	-0.452	0.603	0.094				
BICD1	0.080	1.000	0.763	-0.338	0.456	0.056				
RAB2A	0.046	1.000	0.768	-0.386	0.421	0.049				
TBC1D1	0.035	1.000	0.797	-0.531	0.219	0.022				
SSU72	0.035	1.000	0.801	-0.289	0.636	0.105				
MAT2B	-0.040	1.000	0.804	-0.707	0.278	0.029				
PEX19	0.035	1.000	0.807	-0.317	0.820	0.245				
ATP1A2	0.135	1.000	0.841	-0.252	0.662	0.115				
CCT6A	-0.024	1.000	0.852	-0.252	0.601	0.093				
RANBP3	-0.027	1.000	0.859	-0.265	0.646	0.109				
GOT1	0.026	1.000	0.866	-0.345	0.106	0.011				
ARCN1	-0.019	1.000	0.909	-0.393	0.894	0.459				
TXNDC12	-0.030	1.000	0.912	-0.248	0.926	0.697				
RPL5	-0.013	1.000	0.930	-0.262	0.532	0.074				
TXNL1	-0.007	1.000	0.957	-0.274	0.666	0.117				
DHX57	0.008	1.000	0.963	-0.544	0.071	0.008				
STAM	0.008	1.000	0.963	-1.23	0.328	0.035				
PRPS1	0.002	1.000	0.991	-0.349	0.400	0.045				
ATP6V1B2	0.001	1.000	0.996	-0.32	0.686	0.126				

2.3.4 Transcriptome profiling identifies cardiac contractility and tissue structure and development regulated by mir-24-2 in human iCMs

As global proteomics only identifies a limited fraction of the proteome and the miR regulatory effects are expected to be reflected as well in the transcriptome, we complemented the characterization of the mir-24-2-induced molecular perturbations by profiling the transcriptome changes in iCMs. MiR-24-2 overexpression resulted in the dysregulation of 1002 RNAs (197 of them non-coding RNAs) ($P \leq 0.05$), 4.5% of the identified transcriptome, of which the majority (60.2%) were downregulated **(Figure 15a).** Of these, only 100 were differentially expressed genes (DEGs) (FDR ≤ 0.05), 26% upregulated, including *MIR23AHG* (miR gene cluster that harbors *MIR24-2*), and 74% downregulated**.** As for proteins, downregulated DEGs predominated over those upregulated. The obtained profile was validated in a broader set of samples using a subset of genes **(Figure 15b and Table 9)**. Interestingly, a validated target of miR-24-2 in our previous studies, *SERCA2* [12], that was downregulated in human, monkey and mouse tissue at the mRNA levels **(Figure 9)**, was not downregulated in the proteomic and transcriptomic analysis in iCMs. However, the downregulation was apparent even if not significant when assessed by Western blot **(Figure 15c-d).** This suggests a modest mir-24-2-mediated post-transcriptional inhibition of SERCA2 in human iCMs and/or that in the tissue, additional *SERCA2* mRNA inhibitory mechanisms may contribute to its global tissue downregulation.

The functional annotation of the mir-24-2-dysregulated RNAs ($P \leq 0.05$) retrieved 619 altered biological processes (FDR ≤ 0.05). The top 25 were mainly related to cardiac muscle contraction, cardiac tissue development and cell adhesion and organization including tissue remodeling processes **(Figure 16a)**, revealing the important contribution of mir-24-2 to maintain the cardiac contractility and tissue structure**.** The classification of the individual GO of biological processes into broader functional categories, confirmed cell and tissue development and organization as important dysregulated processes by mir-24-2, proportionally mainly related to cardiac tissue development, but also related to other systems such as musculoskeletal, nervous, urinary, renal, vascular or respiratory system and to embryonic development and morphogenesis. Molecular signaling represented also a prominent dysregulated category, including, for example, signaling pathways related to development and morphogenetic control and cellular stress and growth regulation.



		ATP2B4	CRYAB	FOXO1	KCNJ8	ROBO2	TCAP	SERCA2
Transcriptomic	FC	0.678	0.660	1.729	0.438	0.607	0.637	0.953
	FDR	0.006	0.001	0.002	0.001	0.086	0.001	1.000
qPCR	FC	0.710	0.780	2.306	0.324	0.727	0.775	0.959
	P	0.071	0.036	0.036	0.036	0.036	0.143	1.000

Figure 15. Profiling of the transcriptomic changes in response to mir-24-2 overexpression in iCMs. **a)** Volcano plot representing all the identified RNAs. Red and blue points indicate RNAs with P ≤ 0.05 in mir-24-2$^+$ induced iCMs (n=2) compared to mir-24-2$^-$ induced iCMs (n=2). Retrieved from SRplot. **b)** Relative gene expression -RGE- to an arbitrary mir-24-2$^-$ sample of a subset of genes obtained by qPCR. The numeric value of the FC is indicated below for both the qPCR (yellow cells) and the transcriptomic data (green cells). **c-d)** SERCA2 expression levels in mir-24-2$^+$ and mir-24-2$^-$ induced iCMs assessed by Western blot represented as relative protein expression -RPE- to an arbitrary mir-24-2$^-$ sample.

Related to intercellular communication, an aging hallmark, cell adhesion, communication, organization, and cytoskeleton function were dysregulated by mir-24-2 overexpression, but also processes related to cell and tissue migration. Organ and system function mainly related to nervous system and to CV system, including cardiac contraction and electrophysiology accompanied with calcium handling and ion transport appeared affected. Metabolism is a broad category perturbed, especially the one of proteins (including trafficking), but also lipids, hormones, energy metabolism or carbohydrates. Immunity and inflammation are also represented, along with other age-related hallmarks that are under-represented, such as apoptosis, nutrient sensing or proteostasis **(Figure 16b)**.

In combination with the proteomic data, the perturbation profile shows coherence for some age-related functions or aging hallmarks such as those related to cellular component organization and biogenesis, intercellular communication (cytoskeleton

function) and metabolism (proteins and carbohydrates). The combined analysis also revealed coherence in some cardiac-specific categories related to calcium handling and cardiac muscle contraction, and electrophysiology.

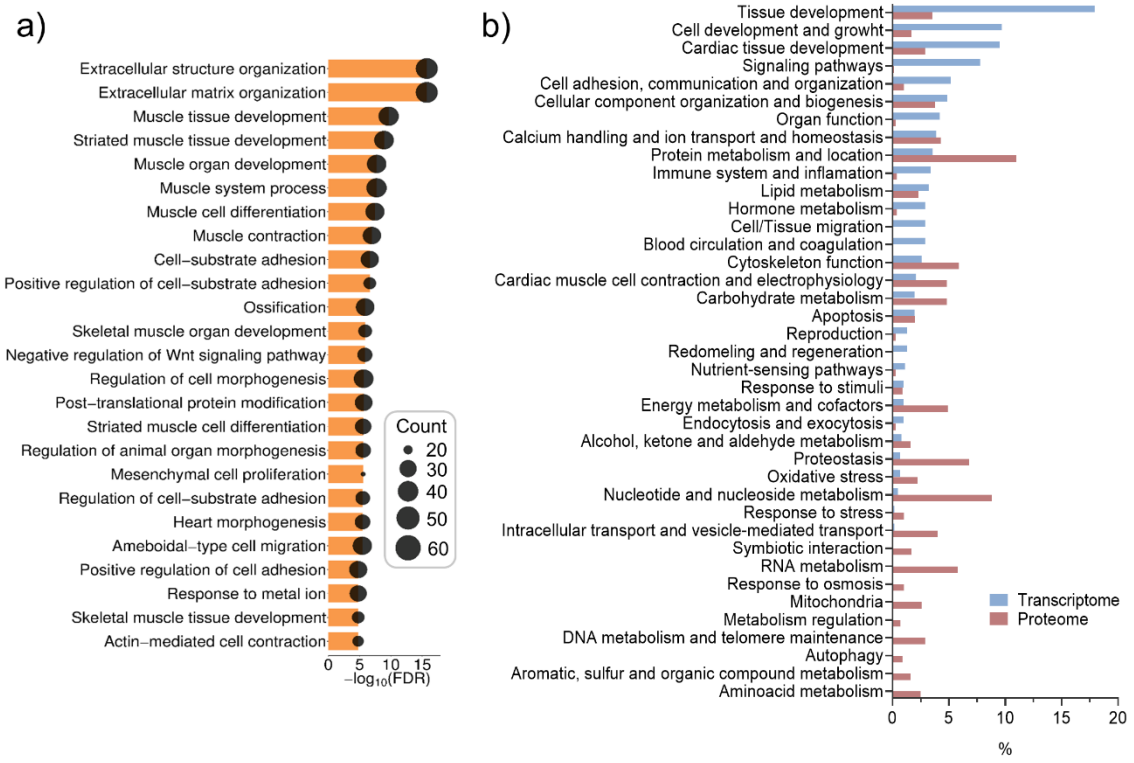


Figure 16. Functional annotation of the transcriptome with the overexpression of mir-24-2. **a)** Top 25 dysregulated GO biological processes, classified by FDR ("Count" indicates the number of RNAs in each GO biological process). Retrieved by SRplot. **b)** Classification of GO biological processes in broader categories in transcriptomic and proteomic analyses (Bars indicate the percentage (%) of GO terms in each category relative to all GO identified in the transcriptomic and proteomic datasets, separately).

Understanding the mechanism of action of miR-24-2 at the individual gene level in CMs could help to interpret the effects of its therapeutic modulation in preclinical research. Specifically, looking at miR-24-2 target genes downregulated at the mRNA level could facilitate monitoring changes of therapeutic approaches at this level (Chapter 4). In agreement with the canonical post-transcriptional regulatory mechanism of miRs, the coherence between the downregulation of the 83 predicted protein targets of miR-24-2 and their coding mRNAs was low, but statistically significant (R = 0.213, P= 0.053) **(Figure 17a).** Among the downregulated pairs, a number of mRNAs were strongly and significantly downregulated (FDR ≤ 0.1), namely *ATP2B4*, *CRYAB* and *ROBO2* **(Table 5)**. *ATP2B4* is a validated target of miR-24-2-5p [132], and *CRYAB* and *ROBO2* are validated targets of miR-24-3p [133,134]. These genes were involved in relevant functional processes mainly related to heart morphogenesis and cardiac muscle

development and contraction **(Figure 17b)**. These three genes are mir-24-2 candidate targets regulated through mRNA degradation that could have application in the characterization of the effect of mir-24-2 modulatory treatments in iCMs.

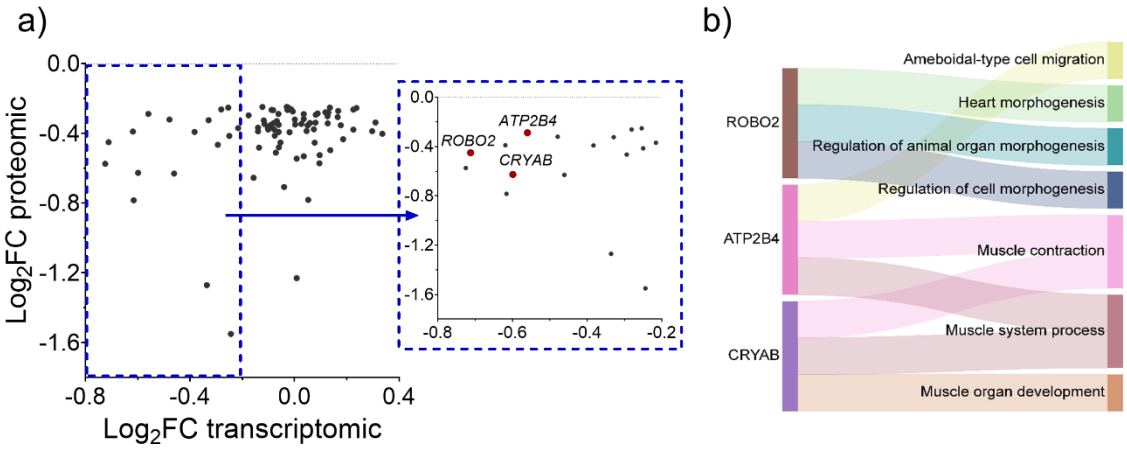


Figure 17. **Analysis of the protein and mRNA perturbation coherence in response to mir-24-2 overexpression. a)** Log_2FC of transcript expression from the putative targets of mir-24-2 compared to the corresponding log_2FC observed at the protein level. An inset shows the selection of candidates with significant mRNA downregulation. **b)** Functional role of the selected putative targets. Retrieved from SRplot.

2.4 Discussion

MiRs have been set in the spotlight of advanced medicine, including the promotion of healthy cardiac aging. However, their role in this process is still not well understood. In this study, we used an evolutionary approach to identify key miRs consistently dysregulated in the aged heart of mice, monkey and human during natural aging and from a biological perspective, to minimize the interindividual variability introduced by the aging rate. For this purpose, SenesAge has been confirmed to perform as a cardiac BA indicator in heart tissue of both animal models of natural aging similarly to how it does in humans, but with a stronger relationship in monkeys than in mice. Also, the high level of preservation of the gene expression profile agrees with the known conserved character of age-related mechanisms across species, even at the molecular level [1,115,135,136], thereby, substantiating the evolutionary approach utilized.

Using this strategy, the high degree of genetic conservation of human BIO-AGEmiRs in the monkey and mouse genomes and the marked preservation of the pri-miR expression profile of the upregulated set of human BIO-AGEmiRs in the animal models, suggests that the upregulated set contributes more significantly to cardiac aging. This relegates the set of downregulated human BIO-AGEmiRs to a secondary role and we did not

pursue their study further as key regulators of cardiac aging. However, we characterized all of them at the mature level to gain fundamental knowledge of their biology in these species with age. The pri-miR profile of the upregulated set was mainly maintained at the mature level in the animal models. This supports an inference from the animal data to humans at the mature level for those pri-miRs consistently upregulated across species, namely *MIR155HG*, *MIR210HG*, *MIR24-2*, *MIR3911* and *MIR3916*. In the downregulated set, this tendency was maintained, globally indicating that mostly the transcriptional level defines the mature levels of cardiac miRs. But exceptions such as the monkey *MIR497HG* and *MIR6080* or the murine *MIR490*, confirm that tight regulation during miR biogenesis exists [42,43]. Therefore, from pri-miR and mature miR expression data across species, mir-24-2 is identified as one with consistent strong association with age between species. Also, it is the most highly expressed mature upregulated BIO-AGEmiR in animal and human LV tissue and specifically, in iCMs, in agreement with previous data [131]. Altogether, starting from pri-miR human data, miR-24-2 ranks among the most relevant miRs involved in regulating the cardiac aging process. Furthermore, our data rule out the utility as circulating indicators of cardiac BA of the human cardiac-enriched BIO-AGEmiR miR-4461, which is not genetically conserved, and questions the capacity of miR-490-3p, whose expression profile is not preserved in animal species. However, exploring miR-490-3p is worth given the opportunities it could offer in cardiac BA monitoring (Chapter 5).

The limited coherence between dysregulated proteins and their coding transcripts underscored the need to profile miR-regulated molecular networks and to assess their global impact on multiple targets, an approach that has demonstrated their potential utility in advanced medicine by revealing miR-mediated molecular signatures with diagnostic, prognostic and therapeutic relevance (i.e., for neurodegenerative disorders [137,138]). Profiling the regulatory effects of mir-24-2 in human iCMs revealed modest perturbations to the proteome and transcriptome at the individual protein or gene level, respectively. Future research could further clarify the underlying mechanisms by employing high-throughput RNA–protein interaction techniques, such as eCLIP or similar approaches, which have recently proven effective in mapping context-specific miR targetomes [139]. However, a large number of biological processes were altered. This is in line with previous findings that suggest that the impact of miR regulation results in a small number of significant changes in individual targets, but to collective small changes that shift molecular networks [140,141]. The functional annotation of these changes at the proteome and transcriptome level reveal discrepancies and similarities between data. However the inherent limitations and benefits of each technique, on one hand,

proteomics detects only around the 13% of the expressed protein-coding transcriptome, but delivering the outcome at the molecular level from the main regulatory mechanism of action of miRs (post-transcriptional), and, on the other hand, transcriptomic, relatively insensitive to the main effect of miRs on their targets (post-transcriptional regulation), but sensitive enough to gather the whole cellular biology, makes it worthwhile to consider both outputs, the individual and the complementary. Individually, proteomics finds metabolism (mostly of protein, nucleic acids and RNA) and proteostasis, one of the aging hallmarks, predominantly altered in response to mir-24-2. Transcriptomic analysis reports cell and tissue development, including cardiac development, as the functional categories most dysregulated, possibly indicating cell state transitions of iCMs as part of a tissue remodeling process triggered by the mir-24-2 (identified among the top 25 altered processes) and molecular signaling. These are followed by alterations in calcium handling, determinant of cardiac contractility and electromechanical coupling, which is also a well-known factor altered with age [142]. The complementary analysis confirmed the relevance of disturbances of the protein metabolism caused by mir-24-2 expression, but also of cardiac development and function, including contraction and electrophysiology and calcium handling, or cytoskeletal function, also a key player of the aging hallmark of intercellular communication**.** At lower levels, other aging hallmarks are detected by these analyses, such as telomere maintenance, mitochondrial function, oxidative stress or nutrient sensing, further supporting the age-related molecular response displayed.

Interestingly, a considerable number of ncRNAs were found among the dysregulated RNAs. This observation agrees with previous findings indicating that miRs can act not only upon protein-coding RNAs but also ncRNAs at the transcriptional and post-transcriptional levels [50]. In addition, exploring the regulatory capacity of mir-24-2 in human iCMs, provide valuable insights into its potential therapeutic modulation in this species. For example, *ATP2B4*, *CRYAB* and *ROBO2* were identified as candidate targets regulated via mRNA degradation, which may mediate some of its age-associated effects in the heart. However, further experimental validation will be required to confirm these individual interactions and fully characterize the therapeutic potential of mir-24-2 in modulating cardiac aging phenotypes *in vivo*. Also, although less relevant, this study could help determine the human-specific downstream regulatory mechanisms as compared to animal models.

2.5 Conclusions

Through a cross-species approach, miR-24-2 has been identified as a key miR involved in cardiac BA. The comprehensive analysis of its regulatory action in human CMs highlights its relevance in cardiac functions that are known to decline with age and in several hallmarks of aging. Collectively, these findings establish miR-24-2 as a promising therapeutic target for the development of strategies aimed at preserving cardiac function and promoting healthy aging. Beyond its specific implications for CV research, this work underscores the importance of understanding the molecular mechanisms of ageing as a cornerstone for designing future translational interventions that may alleviate the clinical and socioeconomic impacts of age-related disease.

Chapter 3

Cardiac miRNA therapies: challenges and opportunities

Based on:

"Nanotechnology-driven heart targeting to fulfil the potential of cardiac miR therapies"
Hernández-Bellido N.✉, Hernández-Ainsa S., Köhler R., Ordovás L.✉
International Journal of Pharmaceutics. https://doi.org/10.1016/j.ijpharm.2026.126643
(✉Corresponding author)

3.1 Introduction

As described in Chapters 1 and 2, there is a growing interest in the therapeutic potential of miRs to treat cardiac disease and dysfunction. However, despite this potential, cardiac miR therapies are still in their infancy. To better understand this scenario, it is important to comprehend the main bottlenecks in their development **(Figure 18)**.

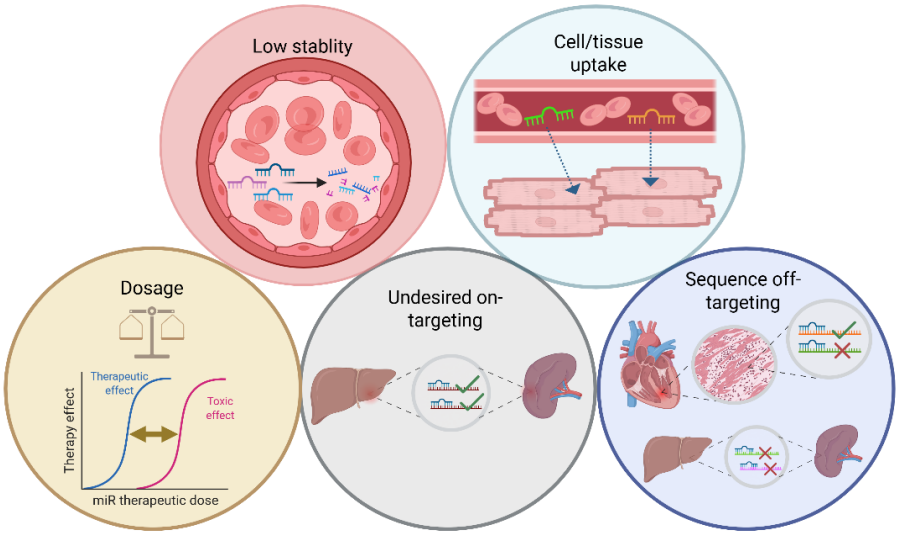


Figure 18. Challenges of cardiac miR therapies. On-targeting and off-targeting are represented with a green tick and red cross, respectively.

To be effective, miR therapies must overcome a number of biological barriers. They must resist nuclease degradation in the blood and extracellular media, avoid rapid renal clearance and immune elimination, be able to cross the capillary endothelium of the target organ, and finally cross the plasma membrane of the target cell to reach the cytoplasm, where they must be present in sufficient amount to specifically exert their regulatory function. The intrinsic physicochemical and biological properties of miRs pose difficulties throughout these processes, leading to defective intracellular delivery and thus lack of efficacy, the most common cause of clinical trial termination of RNA therapies [18].

The persistence of miR therapies in the organism is determined by their stability and rate of clearance. Their negative charge and hydrophilicity limit the efficiency of the vascular extravasation and cellular uptake at the anionic phospholipid bilayer of the cell membrane. Taken together, the cellular uptake ratio of miR therapies is low and the circulating half-life is short. Thus, systemic delivery of miR therapies faces a major obstacle in tissue penetration and achieving a sufficient on-target dose. In addition, the

continuous vasculature of the heart makes the efficiency of cardiac uptake lower than in other organs with fenestrated or discontinuous vessels, such as the kidney, liver, or spleen. These hurdles cannot simply be overcome by using higher doses of miR, as this could lead to renal or hepatic toxicity [143] or other so far unknown side effects.

Side effects could be triggered by (i) saturation of the endogenous RNA interference (RNAi) processing machinery, altering the normal function of endogenous miRs [144,145]; (ii) off-target activity and/or (iii) on-target activity in undesired organs. The intracellular dose of the miR therapy may be critical to avoid undesired perturbations of its natural targetome. Preclinical studies to assess the optimal effective doses without undesired alterations of the miR targetome seem to be fundamental to ensure future clinical translation. Sequence-mediated off-targeting, the ability of miRs to simultaneously regulate hundreds to thousands of genes, has been suggested as a possible cause of side effects observed in clinical trials of discontinued miR therapeutics [146]. However, miR therapies are particularly interesting for those conditions with complex mechanisms where exploiting the miR pleiotropy may offer an advantage over conventional drugs with a single molecular target. Specifically, a given miR can regulate multiple genes and thus potentially control multiple functional processes. For example, it has been reported that the miR-15a-16-1 cluster, directly or indirectly, can regulate approximately 14% of the total transcriptome in leukemic cells [25]. Therefore, leveraging their ability to regulate entire pathways and a variety of processes with a single intervention is highly valuable for treating intricate pathological processes. Undesired on-targeting occurs when a miR-based treatment simultaneously acts through its specific targets in unwanted organs or in non-target cell types within the desired organ. For example, a liposomal miR-34a mimic for cancer therapy (MRX34) showed undesired on-target effects in immune cells. It led to severe immune-related adverse effects and to the termination of clinical trials [147]. In the heart, miRs can also have cell type-specific effects and responses [148,149]. For instance, miR-29 has been described as anti-fibrotic in cardiac fibroblasts [150], but pro-hypertrophic and pro-fibrotic in CMs [151]. To split hairs, even the 5p and 3p strands of a given miR can have opposite effects, one being associated with therapeutic effects and the other with pathological effects (i.e., miR-199a discussed in section 3.2.1).

To diminish the potential side effects and enhance efficacy, local delivery of miR therapies has been applied successfully compared to systemic injection [152]. This holds true also for the heart via intramyocardial (IM) or intracoronary (IC) administration [153]. However, local administration did not prevent the miR therapies from being effective in extracardiac organs [154]. In view of all the hurdles identified, strategies aimed at

optimizing the delivery of the therapeutic miR in the heart/cell type of interest, combined with strategies to improve their specificity (i.e., by promoting RISC loading of the guide strand or applying chemical modifications to minimize sequence-mediated off-targeting [155]), are currently in development. In this review, we focus in the challenge of delivery and the progresses made to overcome it, including the encapsulation of miR therapies in NCs and developing strategies promoting targeted delivery to the heart.

3.2 Current development status of cardiac miR therapies

Since the first reports in the first decade of the 2000s investigating the role of miRs in HD (i.e., HF [156,157]), their potential as therapeutic targets has been attractive [158]. After 20 years of research, the body of evidence is large enough to warrant recognition of their active contribution to HD, but the translation of this knowledge into clinical applications has yet to occur **(Figure 19)**. The aforementioned challenges together with interspecies differences most likely explain why the percentage of miR drugs reaching clinical trials is minimal compared to those that have shown therapeutic effects in preclinical studies. In fact, none have reached phase III clinical trials [146]. Currently, miR therapies are mainly at the discovery or preclinical testing phases, with most studies conducted so far in small animal models. Relatively few are evaluating their therapeutic efficacy in large animal models and, to date, only two miR therapies have entered clinical trials for the treatment of HD (CDR132L and MRG-110).

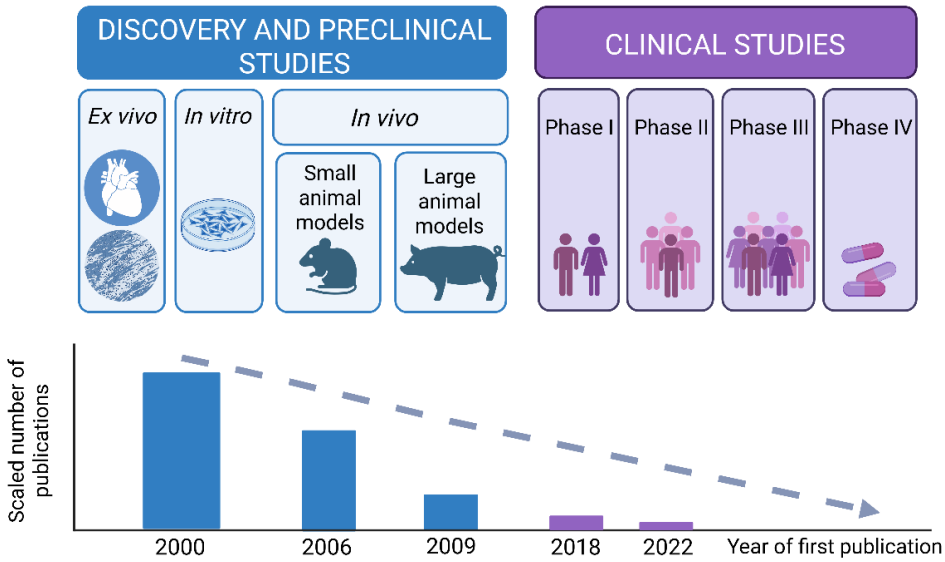


Figure 19. Representation of the course of miR-related research in HD and its progress into clinical investigations. The bar graph represents a figurative scaled number of publications and the year of the first publication on each phase.

Next, we describe key miRs involved in HD and summarize their specific stages of development. The focus is set on those with a higher preclinical level of development (efficacy assessed in large animals), highlighting important aspects related to the faced challenges **(Table 6, section 3.2.1)**. In addition, we review the miR therapies that have entered clinical trials for HD, but also those for non-cardiac pathologies with potential application in HD **(Table 7, section 3.2.2)**.

3.2.1 Effective miR therapies in late preclinical research

Just a reduced number of miR therapies have reached late preclinical trials. Those are gathered in **Table 6** and the most significant are described next.

The miR-92a, a member of the mir-17-92 cluster, is upregulated in ischemic mouse heart tissue. Its inhibition demonstrated its capacity to regulate the ischemia-induced angiogenesis *in vivo* in mice [159]. However, the cell compartment involved in this effect is unclear since, in agreement with its cell-type specific effect [160], the inhibition of miR-92a was not only detected in endothelial cells [159]. In large animal models of cardiac ischemia, miR-92a inhibition promoted neovascularization through its proangiogenic effect leading to cardiac functional and structural improvements [153,161]. Locked nucleic acid (LNA)-anti-miR-92a administered intravenously (IV) or IC showed efficacy only with IC [153], providing the first evidence of the higher miR therapeutic efficacy of local over systemic administration. However, undesired on-targeting in extracardiac organs was still present in both administration routes. Instead, a single IC injection of the anti-miR-92a encapsulated in albumin-polylactic-co-glycolic acid (PLGA) microspheres in ischemic pigs avoided the organ off-targeting while it maintained efficacy by restoring the LV ejection fraction (LVEF) up to 51.4% compared to 36.7% in untreated animals [161].

The miR-21 pathological effect is complex due to its cell-type and CVD-dependent effect [149,162]. miR-21 is described as pro-fibrotic and pro-hypertrophic in CVD [163] and to be upregulated in the LV myocardium in patients of HF [164] or myocardial infarction (MI) [150]. However, it has also been reported to exert cardioprotective effects in ischemia by enhancing angiogenesis and myocardial remodeling [163,165,166]. Repeated IC infusion of LNA-anti-miR-21 in pig models of ischemic HF was anti-fibrotic and anti-hypertrophic and improved the cardiac function by enhancing the LVEF up to ~ 35% compared to untreated animals (~ 25%) [154]. However, there was also downregulation of miR-21 in kidney and lung, raising safety concerns related to organ off-targeting even with local administration. In mimic approaches, ultrasound-targeted microbubble

destruction (UTMD) with pre-mir-21-loaded microbubbles in pig models of coronary microembolization (CME)-induced inflammation, showed functional improvement without structural recovery with systemic treatment [167]. IM-injected hydrogels harboring miR-21-loaded mesoporous silica NCs (MSN) in ischemic pigs demonstrated the cardioregenerative and cardioprotective role of the miR by increasing the LVEF up to ~ 50% compared to untreated MI animals (~ 40%) [168]. Therefore, the dual role of miR-21 in cardiac pathophysiology demands a careful therapeutic use of its related therapies in very well-defined pathological conditions.

HF patients presented upregulated myocardial expression of miR-132 [60]. The role of miR-132 in cardiac hypertrophy and adverse myocardial remodeling along with its therapeutic potential was then demonstrated in mouse models of MI and HF [169–171]. In pig models of ischemia, the anti-miR-132 treatment led to tolerability and safety as well as to cardiac functional and structural improvements up to 43.8% of LVEF (over 35% in untreated animals) after IV or IC followed by IV administrations using different dosing regimens of up to 5 months [171,172]. In this case, the administration pathway resulted in comparable therapeutic effect, validating the IV administration scheme. No therapy-related adverse effects were reported, but the expression levels of miR-132 were not investigated in other tissues despite of miR-132 having a well-known role in neurological disorders (i.e., Alzheimer disease [141] or cancer [173]. Comparable therapeutic effects were observed in a porcine model of LV pressure overload-induced HF after 8 weeks, where the anti-miR CDR132L was administered twice IC with 4-weeks interval between administrations, achieving 48.9% LVEF over 36.1% in untreated HF animals [174]. Despite of the promising beneficial effects, and the lack of apparent side effects, full recovery was not achieved (52% LVEF in sham-operated animals) independently of the administration route or dosing program, suggesting that prolonged treatments may be needed.

Following a high-throughput functional screen, miR-199a-3p was found to promote murine CM proliferation *in vitro* and to induce cardiac regeneration with functional and structural improvement after infarction in mice [58]. Similar therapeutic outcomes were reported in infarcted rats and pigs with miR-199a-3p treatment [175,176] holding promise for the cardiac regeneration in humans. In pigs, LVEF was restored up to ~ 65%, closer to untreated healthy animals (~ 72%) after single IM injection of an adenoassociated virus (AAV6)-delivered pri-miR-199a-1 gene. However, these results must be taken with caution, as the persistent expression of the pre-miR led to arrhythmic events and sudden cardiac death in pigs [176]. Whether this lethal outcome is explained by the persistent expression of the pre-miR-199a and/or the co-expression of the miR-199a-5p strand

remains unknown. In support of the temporal hypothesis and the potentially safer profile of transient miR-based regenerative treatments, a methodologically comparable study with miR-125-5p mimic [64] obtained similar beneficial effects without therapy-related arrhythmogenic events [177]. On the other hand, the effect of the miR-199a-5p passenger strand in the heart is unclear. It has been associated with pathological processes where it is both upregulated, i.e., in murine models of cardiac hypertrophy and fibrosis and MI [178–181], and downregulated, in murine models of MI and patients of DCM and other cardiac pathologies [182]. Indeed, anti-miR-199a-5p hard decoys revealed its important role in cardiac hypertrophy in mice [183], while IM supplementation with miR-199a-5p mimic promoted cardiac regeneration in infarcted rats [182]. In any case, these studies highlight the relevance of transient and strand-specific delivery of miR mimic therapies to minimize potential side effects due to persistent exposure to the therapy and/or active passenger strands.

All these studies, mostly focusing on cardiac regeneration, provide robust evidence for the efficacy of the miR therapies in translational models of cardiac disease. However, they also highlight the potential disadvantages of miR therapies and the remaining challenges to overcome, mainly those related to safety, controlled and targeted delivery and dosage. Despite the apparent superiority of IC infusion or IM injection in terms of efficacy and reduced adverse effects when compared with systemic administration, these routes are limited in their clinical applicability since multiple administrations to achieve sustained therapeutic effects and full recovery may be needed. The serious adverse effects observed for the AAV-delivered miR-199a-3p suggest that the therapeutic potential of miRs will require meticulous regulation of the local dose and duration of the treatment, as well as the provision of only the therapeutic strand of the miR, ideally with a cell-type-specific delivery strategy. However, the delivery of miRs in a heart-, cell-, transient- and/or strand-specific manner is beyond the capabilities of naked or viral delivery. As outlined in section 3.3, recent advancements in targeted drug delivery employing non-viral vectors hold great potential for the advancement of miR therapies into clinical phases, with the prospect of achieving efficacy and safety.

Table 6. Preclinical efficacy evaluation of miR therapies in large animal models (Sp.: Specie, Ref.: Reference).

miR	Sp.	Disease model	Therapeutic molecule	Vehicle	Administration route/time course	Main findings	Undesired side effects	Ref.
miR-92a	Pig	Ischemia (LAD occlusion 60 min)	LNA-anti-miR-92a	Naked	IV, IC, 5 min before reperfusion	Structural and functional improvement only with IC	miR-92a expression decreased in liver, spleen and kidney (lower by IC administration)	[153]
	Pig	Ischemia (LAD occlusion 49 and 60 min)	Anti-miR-92a	Albumin-PLGA microspheres	IC, 5 min after reperfusion in 2 injections	Structural and functional improvement	Microspheres not present in spleen, lung and liver, no suppression of miR-92 in remote organs No proarrhythmic effect	[161]
miR-21	Pig	Ischemia (LAD occlusion, 60 min)	LNA anti-miR-21	Naked	IC, d5 and d19 after reperfusion	Structural and functional improvement	Downregulation of miR-21 in kidney and lung	[154]
	Pig	CME model	Pre-miR-21 plasmid	Microbubbles for UTMD	IV, d4 before CME treatment	Functional improvement Size of CME-induced infarct not greatly reduced	Not assessed	[167]
	Pig	Ischemia (OM1 and OM2 of the circumflex artery ligation)	miR-21 mimic	MSN and injectable hydrogel matrix	IM, immediately post-MI in 6 injection sites	Local, controlled and long half-time delivery (28 d) Long-term safety risk Structural and functional improvement	Not assessed	[168]
miR-132	Pig	Ischemia (LAD occlusion 90 min)	CDR132L	Naked	IV, monthly during 3 or 5 months starting 1 month after ischemia	Safe and well-tolerated and structural and functional improvement	No therapy-related adverse events (body weight, electrocardiographic or hematology or laboratory chemistry parameters)	[172]
	Pig	Ischemia (LAD occlusion 90 min)	Anti-miR-132	Naked	IC or IV d3 post-MI and IV d28	Safe, well-tolerated and favorable PK Dose-dependent PK/PD relationships Structural and functional improvement	No therapy-related adverse effects (hematology or laboratory chemistry parameters and myocardial damage)	[171]
	Pig	HF (pTAC stent model, LV pressure overload)	Anti-miR-132	Naked	IC, d0 and d28 after aortic stent implantation	Structural and functional improvement	Not assessed	[174]
miR-199a-3p	Pig	Ischemia (LAD occlusion 90 min)	pri-mir-199a-1 gene	AAV	IM, 10 min after reperfusion	Structural and functional improvement	Not assessed	[176]
miR-125a-5p	Pig	Ischemia (LAD occlusion 60 min)	miR-125a-5p mimic	Naked	IM, at the onset of reperfusion	Persistence of miR-125a-5p for up to 28 days after cardiac I/R Structural and functional improvement	No hepatic, renal or cardiac toxicity (blood chemistry indicators) Not increase the burden of arrhythmia	[177]
miR-19a/b	Pig	Ischemia (LAD occlusion, 10 min)	miR-19a/b mimic	ROS-scavenging hydrogel	IM, immediately post-MI in 9 injection sites	Structural and functional improvement	Not assessed	[184]
miR-146b-5p	Pig	Ischemia (left circumflex artery ligation, time not specified)	Anti-miR-146b-5p	Naked	IM, after ligation	Functional improvement Short term inhibition of targets	Not assessed	[185]
miR-328	Dog	AF (right A-TP during 8 weeks)	Anti-miR-328	AAV	Intramuscular, after A-TP in 10 injection sites	Structural and functional improvement	Not assessed	[186]
miR-206	Dog	AF (right A-TP during 4 weeks)	Anti-miR-206	Lentivirus	Intramuscular after A-TP in 8 injection sites	Structural and functional improvement	Not assessed	[187]

3.2.2 MiR therapies in clinical trials suitable for cardiac therapy

The development status of cardiac miR therapies is still concentrated in the preclinical phase, but a few miR therapies for cardiac and non-cardiac diseases have entered clinical trials **(Table 7)**. Next, we will describe them, also including those for non-cardiac diseases that may be applicable to HD upon adequate cardiac delivery, namely miR-92, miR-21, miR-17-5p and miR-155.

One of the miR therapies developed for the treatment of HD that entered clinical trials is CDR132L, an anti-miR-132 that was developed for the treatment of ischemic HF [172]. CDR132L has completed a phase I clinical trial (NCT04045405) with patients of ischemic HF and its systemic administration has shown good tolerability and safety, favorable pharmacokinetics and preliminary evidence of therapeutic efficacy [188]. A Phase II trial evaluating efficacy and safety in HF with reduced LVEF after MI (NCT05350969, HF-REVERT) is currently active, but not recruiting [189]. Another Phase II trial evaluating the efficacy and safety of CDR132L in patients with HF with mildly reduced or preserved LVEF and cardiac hypertrophy (NCT05953831, REMOD-REVERT) has been withdrawn due to transfer of study responsibility and planning.

miR-92 has a role in promoting wound healing [190,191] and in endothelial dysfunction and atherosclerosis [192], suggesting that its inhibition may promote angiogenesis/revascularization in the CV system and skin [190]. Other miR therapy developed for HD treatment that entered in clinical trials is MRG-110 or S95010. Two Phase I clinical trials in healthy volunteers (NCT03494712 and NCT03603431) were designed to test the safety and efficacy of this LNA-anti-miR-92a for the treatment of ischemic conditions such as HF and skin wound healing, respectively. In NCT03494712, MRG-110 was administered IV in healthy volunteers in single ascending doses, demonstrating safety and tolerability [193]. For its potential application in skin wound healing, NCT03603431 was also carried out in healthy volunteers but administered by intradermal injection at the site of small skin wounds for 3 weeks. The treatment was safe and preliminary evidence of therapeutic effects related to the promotion of angiogenesis and improvement of wound healing were obtained [194]. Altogether, MRG-110, due to its systemic safety (NCT03494712) and pro-angiogenic effect (NCT03603431) in humans demonstrated by preclinical evidence demonstrated by anti-miR-92 efficacy in small and large animal models of MI [153,159,161], could be further considered a candidate for the regeneration of the ischemic heart.

The miR-21 is pro-fibrotic in lung [195], kidney [196–198] and in liver diseases [199], has a pro-inflammatory role in immune-related diseases [200] and a pro-proliferative and anti-apoptotic role in cancer (onco-miR) [201]. An anti-miR-21 modified with sugar moieties and phosphorotioate (RG-012, Lademirsen or SAR339375) that showed preclinical efficacy in Alport nephropathy models [197], entered Phase I (NCT03373786) and Phase II (NCT02855268) clinical trials in patients with Alport syndrome. Phase I results were not reported, but subcutaneous administration in Phase II showed an acceptable safety profile with no significant improvement in renal function [202]. Whether the reported plasma concentrations of RG-012, which accumulated less than 2-fold over the duration of the trial, were insufficient to achieve therapeutic effects remains unknown. However, based on the safety profile in NCT02855268, the preclinical efficacy results in large animals [154] and, supposing that the functional role of miR-21 in HD is properly elucidated, RG-012 could be a candidate to treat ischemic HF [154,164], MI [150,168] or myocarditis [203].

The miR-29 is downregulated during lung, liver and kidney fibrosis [204]. A cholesterol conjugated miR-29 mimic (MRG-201, Remlarsen) effective in preclinical trials [205,206], completed a Phase I clinical trial (NCT02603224). Single or multiple ascending doses of miR-29 mimic were injected intradermally into healthy volunteers with and without skin incisions, demonstrating safety and tolerability [206]. A subsequent Phase II study in patients with a history of keloid (NCT03601052) showed fibroplasia reduction compared to placebo, but no effect on normal wound healing [207]. In the context of HD, miR-29 has been described as an anti-fibrotic miR that is downregulated after MI due to cardiac injury, particularly in the region adjacent to the infarct zone in human LV myocardial samples [150]. Therefore, miR-29 supplementation therapy could be a candidate miR therapy with application in the treatment of MI-related cardiac fibrosis. However, as for miR-92 and miR-21 [149,160,162], its application requires thorough evaluation considering the cell-specific effects described in preclinical [150,151].

The miR-17-5p was upregulated in renal cysts of both mice and humans with autosomal dominant polycystic kidney disease (ADPKD) [208]. A LNA-anti-miR-17-5p (RGLS4326 or RG4326) evaluated preclinically in ADPKD models, completed a Phase I clinical trial (NCT04536688) with ADPKD patients. The trial provided clinical proof of functionality, but also of toxicity to the central nervous system at higher doses [209]. Subsequently, a second-generation LNA-anti-miR-17-5p (Farabursen or RGLS8429) also showed efficacy, but without neurological adverse effects [210] and Phase I (NCT054269073) or Ib (NCT05521191) trials in healthy volunteers or ADPKD patients, respectively, started. The company announced that preliminary results found RGLS8429 efficient in

NCT05521191 [211]. In the context of HD, miR-17-5p is upregulated in mouse models of ischemia/reperfusion (I/R)-induced cardiac injury [212], MI [213] and HCM [214], and its downregulation has demonstrated therapeutic effects in both ischemia models. Thus, RGLS8429 could potentially be a candidate treatment for these cardiac pathologies [212,214].

The miR-155 is involved in the pathogenesis of many types of hematological malignancies, but it has a strong causative role in the development of diffuse large B-cell lymphoma [215]. A LNA-anti-miR-155, (Cobomarsen or MRG-106) [216] safe and effective in preclinical models of lymphoma [217], completed a Phase I trial with lymphoma and leukemia patients (NCT02580552). The subcutaneous or systemic injection of the LNA-anti-miR-155 showed therapeutic efficacy without serious adverse effects [218,219]. Subsequently, two Phase II clinical trials in cutaneous T-cell lymphoma/mycosis fungoides subtype were terminated: The SOLAR trial (NCT03713320) because of business reasons although the results showed safety and low efficacy, and the PRISM trial (NCT03837457) because of a crossover with an arm of the SOLAR clinical trial. Noteworthy, the miR-155 has been described to be upregulated during inflammation, atherosclerosis and AF in animal models (reviewed in [220]) and in the atria of AF patients [221]**.** Therefore, clinical advancements in the development of Cobomarsen could potentially have an application in the treatment of these CV pathologies.

To sum up, if compared to the extensive preclinical research *in vivo*, only a limited number of miR-based clinical trials have been conducted for cardiac and non-cardiac diseases. Consistent with the preclinical research in large animals **(Table 6)**, but even more pronounced, anti-miR therapies predominate over the miR mimic-based therapies in the clinical phase of development **(Table 7)**, which in turn indicates that the miR supplementation therapies are lagging behind. Overall, all but one of the clinical trials demonstrate safety and tolerability of miR therapies. However, they also show limited therapeutic effect. It remains to be investigated whether the intracellular dose in target organs explains this general outcome, and how the route of administration and/or the delivery method (all treatments using naked miR/anti-miR molecules in humans) may influence this. Nevertheless, as suggested by the efficacy improvements of local and/or encapsulated delivery in large animal models **(Table 6)**, the advances of targeted miR delivery are likely to have a positive impact on the clinical outcome of cardiac repair and regeneration miR therapies.

Table 7. miR therapies in clinical trials with potential application in cardiac pathologies (Admin.: administration route, Ref.: Reference).

	PRECLINICAL PHASE			CLINICAL PHASE					
	Specie	**Indication**	**Ref.**	**Therapeutic molecule**	**Sponsor**	**Admin./ Vehicle**	**Trial phase, subjects and NCT number**	**Status and main reported results**	**Cardiac indication**
miR-92	Mouse Pig	Cardiac ischemia	[153, 159,161]	LNA-anti-miR-92a (MRG-110, S95010)	miRagen Therapeutics and Servier	IV, naked	Phase I, healthy volunteers (NCT03494712)	Completed: safe, tolerable and molecularly effective [193]	Cardiac ischemia [153,161]
	Mouse Pig	Skin wound healing	[190, 191]	LNA-anti-miR-92a (MRG-110, S95010)	miRagen Therapeutics and Servier	ID, naked	Phase I, healthy volunteers (NCT03603431)	Completed: safe, promoted skin angiogenesis and wound healing [194]	
miR-21	Mouse	Alport nephropathy	[196–198]	Anti-miR-21 modified with sugar moieties and phosphorothioate (RG012, Lademirsen, SAR339375)	Genzyme, a Sanofi Company	SC, naked	Phase I, Alport syndrome patients (NCT03373786)	Completed: without results	Ischemic HF [154,164] MI [150,168] and myocarditis [203]
							Phase II, Alport syndrome patients (NCT02855268)	Terminated [202]	
miR-132	Pig	HF	[171, 172,174]	LNA-anti-miR-132 (CDR132L)	Cardior Pharmaceuticals GmbH	IV, naked	Phase I, ischemic HF patients with reduced LVEF (NCT04045405)	Completed: safe, tolerable, favourable pharmacokinetic and moderate effect [222]	HF [60,154,171,172]
							Phase II, HF patients with preserved LVEF (NCT05350969)	Active (not recruiting)	
							Phase II, HF patients with mild reduced/preserved LVEF (NCT05953831)	Withdrawn	
miR-29	Mouse Rat Rabbit	Fibrotic scar (keloid)	[206]	Cholesterol-conjugated miR-29 mimic (MRG-201, Remlarsen)	miRagen Therapeutics	ID, naked	Phase I, healthy volunteers (NCT02603224)	Completed: safe and tolerable [206]	MI [150]
	Mouse	Pulmonary fibrosis	[205]				Phase II, keloid patients (NCT03601052)	Completed: reduced fibroplasia with normal wound healing [207]	
miR-17-5p	Mouse	ADPKD	[208]	LNA-anti-miR-17-5p (RGLS4326)	Regulus Therapeutics	SC, naked	Phase Ib, APKD patients (NCT04536688)	Completed: clinical proof of mechanism, but neurological toxicity	I/R [212], MI [213] and HCM [214]
				LNA-anti-miR-17-5p (RGLS8429, Farabuantirsen)		SC, naked	Phase I, healthy volunteers (NCT05429073)	Completed: without results	
							Phase Ib, ADPKD patients (NCT05521191)	Recruiting, preliminary results announce therapeutic effect [211]	
miR-155	Mouse	DLBCL	[217]	LNA-ant-miR-155 (MRG-106, Cobomarsen)	miRagen therapeutics	SC and IV, naked	Phase I, lymphoma and leukemia patients (NCT02580552)	Completed: safe, therapeutic effect [218,219]	HF [220], AF [220,221] and HCM [214]
						IV, naked	Phase II, cutaneous T-cell Lymphoma/mycosis fungoides patients (NCT03713320)	Terminated	
						IV, naked	Phase II, cutaneous T-cell Lymphoma/mycosis fungoides patients (NCT03837457)	Terminated	

3.3 The challenge of *in vivo* miR delivery

The *in vivo* delivery method most commonly used so far in late preclinical or clinical stages of miR therapeutics is naked delivery; with some studies using viral vectors **(Tables 6 and 8)**. Drug encapsulation in nanostructures emerged as a promising approach to overcome most of the limitations of conventional gene therapies and their side effects caused by unfavorable systemic distribution and toxicity. Particularly, NCs using engineered macromolecules and biomaterials have advanced drug delivery by leveraging a combination of capabilities (i.e., biocompatibility, tunable in size/shape/surface properties). This improves circulation and retention time of the drug by protecting it from degradation and inactivation, controllable drug release profiles, low immunogenicity or amenability to targeted delivery with appropriate functionalization. Thanks to these properties, many lipophilic and biological drugs such as proteins or peptides can be delivered avoiding solubility limitations, enhancing their efficacy and promoting their prolonged and sustained release at the desired site of action [223,224]. miR therapies can also leverage these properties for restoring impaired cardiac function and promote cardiac regeneration. Next, we will comprehensively review the different materials used as NCs for the delivery of cardiac miR therapies **(Table 8)**.

3.3.1 Polymeric NCs

Natural polymers such as heparin [147,225] or semi-synthetic, such as hyaluronan sulfate [166], have been used to deliver cardiac miR therapies. Among biopolymers, nucleic acids have also been used as scaffolds to construct emerging nanomaterials with unique properties, particularly in terms of programmability and biodegradability [226,227]. In addition, their preparation reproducibility, design versatility and suitability for functionalization make them amenable vehicles for gene therapy based on nucleic acid base complementarity [228,229]. However, nucleic acid nanotechnology is nearly unexplored to develop cardiac therapies. Chapter 4 of this thesis describes the development of an anti-mir-24-2 therapy based on DNA nanotechnology.

So far, most of the used polymeric NCs are based on synthetic polymers, such as ethanolamine-aminated polyglycidyl methacrylate (PGEA), PLGA, dendrigraft poly-L-lysine (DGL), polyethylene imine (PEI), polyethylene glycol (PEG)-polylactic acid (PLA) and PEG-DGL derivatives [147,161,203,225,230–232].

Compared to naked delivery, polymeric NCs significantly accumulated the miR therapeutics in the heart after systemic administration in murine models of MI

[147,225,230] (i.e., ~ 2.3-fold increase of cardiac content [230]). Also, NC-based delivery led to improved therapeutic effect over naked delivery, i.e., shorter ST segment in the ECG or restoring the LVEF [232]. All miRs packaged in polymeric NCs, mostly administered systemically for MI treatment, exhibited therapeutic effect.

When assessed, functionalized polymeric NCs with non-cardiac specific ligands such as the arginine-glycine-aspartic acid (RGD) penetrating peptide [232] or angiotensin II type 1 (AT_1) peptide [231] demonstrated higher cardiac accumulation and heart therapy retention *in vivo* compared to non-functionalized NCs [231,232] with no significant toxic effects in off-target organs and high effects in hypoxic cells [231]. Thus, functionalization of the polymeric NCs administered systemically for MI treatment led to superior therapeutic efficacy compared to their non-functionalized counterparts [231,232].

3.3.2 Lipid-based NCs

Different lipid-based NCs (LNCs) have been developed for drug delivery, including nanoemulsions, liposomes, solid lipid nanoparticles, nanostructured lipid carriers or lipid-polymer hybrid NCs. The first LNCs-based drug, Doxil, was approved by FDA more than a decade ago [233]. LNCs have been widely used for nucleic acid delivery *in vivo* due to their easy adaptability and their efficient cellular delivery [234]. In particular cationic and ionizable LNCs, have received much attention due to the strong electrostatic interactions between negatively charged miR and positive lipids, resulting in an efficient complexation that protects miR from rapid degradation and inactivation while enhancing their cellular uptake by improved interaction with the cell membrane [235]. In addition, their popularity increased in the last years during the development of the mRNA COVID-19 vaccine [236,237].

In MI, modified cationic LNCs have been used to deliver miR therapies in murine models of MI [238–241]. Compared to naked delivery, one study shows that repeated dosing of miR-21-loaded LNCs restored miR-21 expression levels in the infarcted myocardium of mice, even beyond those found in healthy controls, while with the naked therapy remained unchanged [241]. MiR therapeutics-loaded LNCs showed efficacy in terms of improved cardiac remodeling and function (e.g., with improvements in the percentage of LVEF) over untreated MI animals up to 4 weeks using a single-dose IM administration of miR-153-3p-loaded liposomes [239], after repeated IV doses of miR-21-loaded liposomes [241] or after a single-dose IV injection of miR-21-loaded LNCs [238]. Single-dose IV injection of AMO-1 also improved cardiac function with shorter ST segment in the ECG over naked delivery up to 3 days [240]. This suggests that, even if LNC

encapsulation improves delivery, the therapy efficacy may still depend on any of these other factors, such as the dosing scheme, administration pathway or the miR-specific activity.

Functionalization with either cell camouflage (coating approaches to evade immune recognition), with hyaluronic acid, or with cardiac-specific targeting molecules such as anti-cardiac troponin I (cTnI) antibodies, increased the accumulation of LNCs in the heart after systemic administration over their non-functionalized configurations [238–241] improving the therapeutic effects [238,241] irrespective of the evaluation at short [238] or long [241] time points. For example, treatment with miR-21-loaded anti-cTnI antibody-functionalized LNCs restored the LVEF from ~ 45% in untreated MI animals up to ~ 75% (~ 65% without functionalization), which is near the ~ 80% value at baseline in untreated healthy controls [241].

3.3.3 Inorganic NCs

Among all the inorganic materials proposed as NCs for the delivery of miR therapies, MSN have received attention for clinical applications due to their large surface area, high pore volume, tunable structure, high biocompatibility, and thermal stability [242,243].

In relation to HD, MSNs have been used for miR delivery via systemic administration in murine models of MI and have clearly contributed to both functional and morphological recovery compared to untreated animals [182,244,245]. In agreement with polymeric or LNCs particles, encapsulation outperformed naked delivery as proven by superior therapeutic effect, i.e., improved cardiac function, reduction of myocardial apoptosis, and increased CM proliferation [245].

Cellular camouflage [245], cardiac-specific peptides [182,246], or even the combination of both functionalization approaches [244,247], were applied to successfully increase cardiac targeting, which improved functional and structural recovery mediated by the cargo over their non-functionalized versions.

3.3.4 Hydrogels

Hydrogels have emerged as versatile delivery systems for the local controlled and sustained release of therapeutic agents or drugs, including miRs [248], thanks to their tunable physicochemical properties, controlled degradation, biocompatibility and ability to prevent degradation of labile drugs [249].

In HD, therapeutic miR-loaded hydrogels, alone or in combination with NCs, acting as scaffolds, have demonstrated, along with the aforementioned properties, efficacy when applied locally in murine and porcine models of MI or I/R [168,175,184,250,251]. In addition, in pigs, hydrogel-encapsulation of miR-21 mimic has demonstrated advantages over naked delivery [168] accomplishing increased myocardial levels of the miR, improved LVEF and reduced scar size in infarcted pigs [168].

Functionalization with non-cardiac specific ligands, such as trans-activating transcriptional activator (TAT) peptide [175], or the use of bioactive hydrogels, such as ROS-scavenging materials [184], have been used with success to enhance miR delivery and therapeutic effect in both small and large animal models of MI, with sustained therapeutic effects observed up to three months after a single administration [175].

3.3.5 EVs

EVs, small membrane vesicles enriched in a variety of biomolecules including miRs, have been explored to deliver miR therapies due to their circulatory stability, biological barrier permeability, low immunogenicity and high delivery efficiency, among other properties [252]. EVs from different biological origins have been engineered to enrich their content in specific miR mimics to treat HD observing therapeutic effects [253–255].

Current EVs engineering efforts are mainly focused on strategies to enhance site-directed delivery [256,257]. These include the functionalization of EVs and/or surface modification [253,254] to improve targeting regardless of the administration route and to overcome the limitation of exosome intracellular recruitment to RNA substrates for degradation. MiR-loaded EVs functionalized with cardiac-specific peptides were reported to improve their accumulation in the heart and therapeutic effect over non-functionalized EVs or naked miR following multiple doses of systemic administration [253,254].

In summary, several types of NCs have demonstrated their ability to deliver miR therapeutics to the heart and promote therapeutic effects in preclinical studies, mainly cardiac regeneration in small animal models of MI, but also in large animal models **(Tables 6 and 8).** Even if only a limited number of studies have compared the performance of naked and encapsulated delivery of miR therapies, all, regardless of the nature of the used NC material and mostly using systemic administration, have demonstrated improved stability and/or therapeutic efficacy over naked delivery. This is remarkable as most of the studies in large animal models and clinical trials rely on naked miR therapeutics, which according to preclinical data limits their therapeutic potential. Systematic comparisons of the therapy effect depending on the administration route of NC-based formulations are lacking. Thus, it remains unclear whether the advantages offered by the systemic administration of NCs over the naked delivery exceeds the benefits of naked/encapsulated local administration. However, the clinical applicability of the systemic pathway remains convenient for those pathologies where repeated therapy administrations may be needed. In addition, functionalization of NCs to enhance cardiac tissue retention has consistently been shown to improve the therapeutic efficacy of miR therapeutics in terms of cardiac function repair and regeneration.

Table 8. NCs for miR delivery for cardiac therapeutic purposes (NC: Nanocarrier, HD: Heart disease, F: Functionalized nanocarrier, NF: Non-functionalized nanocarrier, ND: Naked delivery, Ref.: reference).

NC type	Material	Specie	HD	Administration route and time course	Cargo	*In vivo* targeted delivery		*In vivo* therapeutic effect		Ref.
						Functionalization or targeting ligand	Targeting efficacy of F vs NF or ND	General outcome	Effect of F over NF and/or over ND delivery	
Polymeric NCs	Heparin-PGEA	Mouse	MI	IV, daily during 3d pre and post MI	miR-499 mimic	Heparin	Cardiac accumulation of F over ND	Improved cardiac function and tissue remodeling 2w post-MI	Not assessed	[225]
	Hyaluronan-sulfate – Ca^{2+}	Mouse	MI	IV, daily during 3d post-MI, starting 24h post-MI	miR-21 mimic	N/A	N/A	Improved cardiac function and tissue remodeling 30d post-MI	Not assessed	[166]
	Cholesterol-PGEA	Mouse	CH	IV, from 3rd to 9th week post-TAC, one time during 3d	Anti-miR-182	Cholesterol	Cardiac accumulation of F over ND	Improved cardiac function 9w post-TAC	Not assessed	[230]
	PLGA microspheres	Pig	MI	IC, 5 min post-MI, single dose	Anti-miR-92	N/A	N/A	Improved cardiac tissue remodeling 30d post-MI	Not assessed	[161]
	LMW Heparin-DGL	Rat	MI	IV, 2 h post-MI, single dose	Anti-miR-1 (AMO-1)	LMW Heparin	Cardiac accumulation of F over ND and NF	Improved cardiac function 3w post-MI	Not assessed	[147]
	PEI F25-LMW	Mouse	EAM	IV+IP 1d pre-EAM and IP 6d post-EAM	Anti-miR-21a-5p	N/A	N/A	Improved cardiac remodeling 7w post-EAM	Not assessed	[203]
	RGD-PEG-PLA	Rat	MI	IV, post-MI, single	miR-133 mimic	RGD tripeptide [258]	Cardiac accumulation of F over NF	Improved cardiac function and tissue remodeling 1w post-MI	▪ Improved electrophysiological (ST segment) and functional parameters with F (i.e., LVEF ~ 55%), NF (i.e., LVEF ~ 47%), and ND (i.e., LVEF ~ 37%) vs untreated MI animals (i.e., LVEF ~ 29%) ▪ Improved serum levels of cardiac damage markers and inflammatory profile markers, mitochondrial oxidative stress markers, vascular endothelial cell damage markers in F and NF vs ND ▪ Improving myocardial remodeling (improved cellular organization and reduced fibrosis) and reduced apoptosis in F and NF vs ND	[232]
	PEG-DGL	Mouse	MI	IV, 24h post-MI, single	Anti-miR-1 (AMO-1)	AT_1	Cardiac accumulation of F over NF	Improved cardiac function and tissue remodeling 48h post-MI	▪ Reduced miR-1 with F (0.7-fold) vs NF (1.9-fold) and untreated (2.3-fold) relative to sham (1-fold). ▪ Improved functional parameters with F (i.e., LVEF = 35.9%), NF (i.e., LVEF = 30%) vs untreated MI animals (i.e., LVEF = 13.9%) ▪ Reduced infarct size with F (16.6%), NF (28.9%) vs untreated (46.2%) ▪ Improving myocardial remodeling (reduced fibrosis) and reduced apoptosis (2-fold) with F vs NF	[231]

NC type	Material	Specie	HD	Administration route and time course	Cargo	*In vivo* targeted delivery			*In vivo* therapeutic effect		Ref.
						Functionalization or targeting ligand	Targeting efficacy of F vs NF or ND	General outcome	Effect of F over NF and/or over ND delivery		
Lipid NCs	Hyaluronic-cationic liposomes	Rat	MI	IM, 3d pre-MI, single	miR-153-3p mimic	Hyaluronic acid	Cardiac accumulation of F over NF	Improved cardiac tissue remodeling (not specified day of measurement)	Not assessed	▪ Promoted reparative polarization of inflamed macrophages with F vs NF ▪ Improved inflammatory cytokines profile in heart in F vs NF ▪ Improved function with F (i.e., LVEF ~ 38%) vs NF (i.e., LVEF ~ 32%) and untreated MI (i.e., LVEF ~ 32%) ▪ Improving myocardial remodeling (increased left ventricular anterior wall (LVAW) thickness, reduced fibrosis and promoted angiogenesis) with F vs NF	[239]
	Platelet like-fusogenic liposomes	Mouse	I/R	IV, 3d post-MI, single	miR-21 mimic	Platelet membranes camouflage	Cardiac accumulation of F over NF	Improved cardiac function 4w post-MI and cardiac tissue remodeling 5d post-MI			[238]
	Liposomes (DSPE-PEG-Maleimide)	Rat	MI	IV, post-MI, single	Anti-miR-1 (AMO-1)	Anti-cTnI antibody	Cardiac accumulation of F over NF	Improved cardiac function 3d post-MI	▪ Reduced miR-1 with F (~ 0.5-fold) vs NF (~ 3.2-fold), untreated MI (~ 1.7-fold) relative to untreated healthy animals (1-fold) ▪ Improved ECG parameters (ST segment) with F vs ND		[240]
	Liposomes (DSPE-PEG-Maleinide)	Rat	AMI	IV, 12h, 3d and 7d post-MI	miR-21 mimic	Anti-cTnI antibody	Cardiac accumulation of F over NF	Improved cardiac function and tissue remodeling 15d post-MI	▪ Increased miR-21 with F (3.48-fold) vs NF (2.15-fold), ND (~ 0.5-fold) and untreated MI (0.53-fold) relative to untreated healthy animals (1-fold) ▪ Reduced expression of pro-apoptotic factors in F and NF vs ND. ▪ Improved function with F (i.e., LVEF ~ 75%) and NF (i.e., LVEF ~ 65%) vs untreated MI animals (i.e., LVEF ~ 45%) ▪ Reduced infarct size with F (16.4%), NF (27.9%) vs untreated MI (38.9%) relative to untreated healthy animals		[241]

NC type	Material	Specie	HD	Administration route and time course	Cargo	*In vivo* targeted delivery		*In vivo* therapeutic effect		Ref.
						Functionalization or targeting ligand	Targeting efficacy of F vs NF or ND	General outcome	Effect of F over NF and/or over ND delivery	
Inorganic NCs	MSN	Mouse	MI	IV, 24h post-MI, single	miR-1, miR-133, miR-208 and miR-499 mimic	FH peptide [247] and neutrophil membrane camouflage	Ligand and cell camouflage favor F accumulation over NF	Improved cardiac function and tissue remodeling 4w post-MI	▪ Increased miR combo with F (> ~ 7.5-fold) vs NF (~ 1-fold) relative to untreated MI ▪ Functional test in F and no detected in NF ▪ Improved function with F (i.e., LVEF ~ 70%) vs NF (i.e., LVEF ~ 47%) and untreated MI (i.e., LEVF ~ 27%) ▪ Reduced infarct size with F (~ 21%), NF (~ 47%) vs untreated MI (~ 60%)	[244]
	MS membranes-PEI	Rat	MI	IV, following MI, single	miR-199a-5p mimic	IMTP [259]	Cardiac accumulation of F over NF	Improved cardiac function and tissue remodeling 4w post-MI	▪ Improved function with F (i.e., LVEF ~ 24.5%), NF (i.e., LVEF ~ 22.3%) vs untreated (i.e., LVEF ~ 14.0%) ▪ Reduced infarct size with F (~ 11 %), NF (~ 25%) vs untreated MI (~ 43%)	[182]
	MSN	Rat	MI	IV, daily during 3d, starting 24h post-MI	miR-21 mimic	MSC membrane camouflage	Cardiac accumulation of F over N and ND	Improved cardiac function and tissue remodeling 4w post-MI	▪ Improved function with F (i.e., LVEF = 63.2%), NF (i.e., LVEF = 54.9%) vs ND (i.e., LVEF = 31.6%) and untreated MI (i.e., LVEF = 28.0%) ▪ Improving myocardial remodeling (reduced CM apoptosis and enhanced CM proliferation) with F vs NF and both vs ND	[245]
Hydrogels	Hyaluronic acid hydrogel	Mouse	MI	IM, post-MI, single	miR-302 mimic	N/A	N/A	Improved cardiac function and tissue remodeling 4w post-MI	Not assessed	[260]
	PFBT-DSPE-PEG injected with elastin-like protein-hyaluronic acid hydrogel	Rat	MI	IM, post-MI in 3 injection sites	miR-199a-3p mimic	TAT	Not assessed	Improved cardiac function 1- and 3-months post-MI and tissue remodeling 28d post-MI	▪ Improved function at 3 months with F-hydrogel (i.e., LVEF = 64%) vs NF (i.e., LVEF ~ 45%) and untreated MI (i.e., LVEF = 45%)	[175]
	MSN loaded in hydrogel (Ciclodextrin-PEG)	Pig	MI	IM, following MI in 6 injection sites	miR-21-5p mimic	N/A	N/A	Improved cardiac function 2w and 4w post-MI and tissue remodeling 4w post-MI	▪ Increased miR-21 with NF-hydrogel (~ 2.5-fold) vs ND (~ 1.2-fold) and untreated MI (~1-fold) relative to sham (1-fold) ▪ Improved function at 4w with NF-hydrogel (i.e., LVEF ~ 50%), ND (i.e., LVEF ~ 42%) vs untreated MI (i.e., LVEF ~ 40%) and sham (i.e., LVEF ~ 65%) ▪ Reduced infarct size with NF-hydrogel (~ 15 %), ND (~ 27%) vs untreated MI (~ 35%) relative to sham ▪ Improving myocardial remodelling (reduced fibrosis, promoted angiogenesis and reduced inflammation mediators expression) in NF-hydrogel compared to ND	[168]
	ROS-scavenging hydrogel	Rat Pig	MI	IM, 10 min post-MI, single	miR-19a/b mimic	N/A	N/A	Improved cardiac function 4w post-MI and tissue remodeling 50d post-MI	Not assessed	[184]

NC type	Material	Specie	HD	Administration route and time course	Cargo	*In vivo* targeted delivery			*In vivo* therapeutic effect		Ref.
						Functionalization or targeting ligand	Targeting efficacy of F vs NF or ND	General outcome	Effect of F over NF and/or over ND delivery		
EVs	Engineered exosomes derived from bone marrow mesenchymal stem cells	Mouse	I/R	IV, every 2d for 4w, post-I/R	miR-302 mimic	Modified PCM peptide [261]	Not assessed	Improved cardiac function and tissue remodeling 4w post-MI	▪ Increased miR-302 with F (~ 1.6-fold), ND (~ 1.1-fold) vs untreated I/R (0.75-fold) relative to sham (1-fold) ▪ Decreased necrosis and apoptosis markers, myocardial injury markers, proinflammatory factors with F vs ND ▪ Improved function with F (i.e., LVEF ~ 43%), ND (i.e., LVEF ~ 39%) vs untreated I/R (i.e., LVEF ~ 32%) and sham (i.e., LVEF ~ 48%)	[253]
	Milk-derived EVs	Mouse	Hyper-trophic HF	IV, 3 times per week for 4w	miR-30d mimic	IMTP [259]	Cardiac accumulation of F over NF	Improved cardiac function and tissue remodeling 4w post-MI	▪ Improved cardiac remodeling (reduced cardiac hypertrophy and fibrosis) with F vs NF ▪ Improved cardiac function with F (i.e., LVEF ~ 65%) vs NF (i.e., LVEF ~ 50%), untreated hypertrophic mouse (i.e., LVEF ~ 50%) and healthy animals (i.e., LVEF ~ 65%)	[254]
	HEK293-derived EVs	Mouse	MI	IM, following IM, single	miR-21 mimic	N/A	N/A	Improved cardiac function and tissue remodeling 4w post-MI	Not assessed		[255]

3.4 The challenge of targeted delivery to the heart

Targeting a specific organ, tissue and/or cell remains an independent hurdle of utmost relevance in terms of reducing off-tissue/cell toxicity and increasing on-tissue/cell drug availability. Different approaches or even their combination are available to achieve targeted drug delivery such as UTMD, which efficiently delivered both conventional [262–264] and cardiac miR therapeutics *in vivo* [165,167] as well as cellular camouflage, that has been explored for cardiac targeting delivery [238,244]. Another strategy consists in targeting LNCs with modified lipids [265], which however remains unexplored for cardiac targeting.

However, most frequent targeting strategy of NCs rely on the use of targeting moieties. These are natural, rationally designed or functionally-selected ligands that aim to achieve specific interactions between NCs and target cells via cell surface molecules. Next, we will describe here the kind of targeting strategies used to address the challenge of targeted delivery to the heart, including those used for miR therapies **(Table 8)**.

3.4.1 Non-cardiac specific targeting

Non-cardiac cell-specific surface molecules include those that are upregulated in response to disease. For example, functionalization with ligands of AT_1 receptor (AT_1R), which is upregulated in the CM of the infarcted myocardium [231,266], increased the accumulation of NCs in the infarcted heart compared to non-functionalized NCs [231,266]. However, AT_1R is also expressed in other organs [267], such as the liver [266], although no liver side effects have been reported [231]. Ligands of adhesion molecules, such as P-selectin, ICAM-1 or E-selectin, which are upregulated on the endothelium in response to ischemia or inflammation [268], have been also used [269,270]. However, differences in the temporal expression of the disease-response specific molecules [269,270] as well as changes related to inflammation, perfusion, and vascularization in the affected area [266] require fine-tuning of the injection time to ensure effective targeting and retention in the infarcted myocardium. In addition, the use of disease-response-specific molecules for targeting may limit their applicability to acute conditions.

Cell-penetrating peptides (CPPs), short peptides with amphipathic helixes or arginine-rich sequences, are often used to increase the cellular permeability of NCs, and so the cargo delivery, although without cellular selectivity [271]. For example, the TAT peptide [272,273] has been used to deliver miR to infarcted mouse tissue demonstrating its beneficial effect on promoting the therapeutic effect of the miR over the non-

functionalized configuration [175]. The RGD tripeptide [232] or FH peptide [244] enhanced the cardiac accumulation and therapeutic effects of miR-loaded NCs.

3.4.2 Cardiac specific targeting

Among the different molecules used as ligands to target the heart with NCs, cardiac cell-specific antibodies have been used. Remarkably, and in contrast to the traditional approach of targeting cell-surface molecules, NCs decorated with intracellular antibodies such as anti-myosin- and anti-cTnI- have successfully targeted the myocardium in small animal models [274–277]. Functionalization of LNCs with Anti-cTnI antibodies improved cardiac accumulation and the functional effect of cardiac miR therapeutics over their non-functionalized versions [240,241]. Whether this increased delivery results from intracellular targeting alone or from a combination with the lipophilic properties of LNCs remains unclear. However, this strategy is rarely used these days.

Cardiac cell-specific penetrating peptides (cardiac CPPs) have been identified through *in vitro* [261] and *in vivo* [246,278,279] affinity screens (phage display biopanning). They have been used to specifically deliver miR therapies to CMs and other cardiac cells (endothelial cells, cardiac fibroblasts, c-Kit+ cells) *in vivo* **(Table 3)**. The primary-CM (PCM) peptide, selected *in vitro* to bind to CM [261], demonstrated CM targeting *in vitro* and heart targeting *in vivo* in a variety of NCs loaded with different kinds of cargoes [280–284], including miR-302 enriched EVs [253]. *In vivo* PCM-based targeting showed limited presence of NCs in other organs and consequently absence of side effects [280–282]. The cardiac targeting peptide (CTP) [278] (US9249184B2), selected *in vivo* to bind to CM, demonstrated *in vivo* CM targeting of NCs [285]. The CTP linked to a naked miR also demonstrated specific delivery *in vitro* to human CMs compared to other cardiac (cardiac fibroblasts or endothelial cells) and non-cardiac cells (HEK293) [286]. This peptide has been also used for the NC-based delivery of drugs showing the cardiac-specific delivery to cardiac cells *in vitro* and to the heart *in vivo* [287]. NCs' functionalization with the *in vivo*-identified ischemic myocardial targeting peptide (IMTP) [246], selected for its binding capacity to ischemic LV and that showed higher targeting capacity in ischemic heart than in normal heart [246,288] or in other organs, enhanced the therapeutic efficacy of the cargo over non-functionalized NCs [289,290]. IMTP-functionalized NCs have been used to deliver miR therapeutics improving cardiac function and remodeling over non-decorated NCs [182,254]. Finally, other cardiac cell-specific peptides for CM, endothelial cells, cardiac fibroblasts and c-Kit+ cells in the infarcted/border zones were identified *in vivo* [279]. They were validated for targeted

delivery with NCs *in vivo* and also the therapeutic efficacy was assessed *in vivo* for the specific targeting of CM with the I-1 peptide [279]. Although the capabilities of CPPs for *in vivo* heart targeted delivery of NCs have been explored, the cell-type specific targeting of PCM and CTP remains unreported.

Aptamers are synthetic short DNA or RNA sequences selected by *in vitro* or *in vivo* affinity screens, namely Systematic Evolution of Ligands by Exponential Enrichment (SELEX). They are ligands with high specificity and affinity for a given target molecule that have low molecular weight, leading to enhanced and rapid tissue penetration, high chemical and thermal stability, low or non-immunogenicity and toxicity, high biodegradability and biocompatibility and low-cost production [291]. Specific aptamer-based functionalization of NCs for target delivery has been explored, even to promote their active transport across the blood-brain barrier, which acts as a bottleneck in the treatment of brain diseases [292,293]. Aptamers have been used to decorate NCs for the targeted delivery of miR or short interference RNA (siRNA) therapies in tumoral and non-tumoral tissues, demonstrating high cell and/or tissue specificity and significant therapeutic efficacy *in vitro* and *in vivo* [294,295]. For example, osteoblast-specific aptamer-functionalized LNCs harboring a bone anabolic siRNA targeted rat osteoblasts over 20-fold more efficiently than the non-functionalized NC *in vitro,* which was translated in the targeted therapy promoting bone formation in osteopenic and healthy rodents [295]. Aptamers recognizing cardiac cells have been identified by SELEX for phospholamban (PLN)-binding [296,297] that were later found to have theragnostic purposes [298,299]. More recently, CM-specific binding [300] and internalizing [301] RNA aptamers have been obtained by *in vivo* SELEX. However, their capabilities for *in vivo* heart targeting of NCs remains to be explored.

In general, the different targeting strategies increased the cardiac accumulation of NCs and the effect of their cargo. This holds true for the miR targeted delivery to the heart with non-cardiac- [175,231,232,244] and cardiac-specific ligands [182,240,241,254] as compared to non-functionalized NCs, highlighting the therapeutic improvement achieved with functionalization. However, the gain in cellular selectivity in the delivery of NCs provided by the cardio-specific ligands, which is fundamental for the cell-type specific targeted delivery, has been mostly demonstrated *in vitro.* More importantly, different studies evidence how the ligand-mediated targeted delivery, either in heart [254,279,280,282,290] or other tissues [295], leads to active liver (and other organs) detargeting, measured between 4 to 24 h post-NC systemic administration. This proves the active contribution of the tissue/cell-specific ligands to reduce extrahepatic delivery, one of the major hurdles of drug delivery. It is likely that increased drug safety and

compatibility of the systemic administration of cardiac (miR) therapies (important for repeated dosing regimens) benefits from this effect.

Considering the relevance of targeting ligands to unlock miR therapeutic potential in combination with NCs, identifying ligands that recognize human cardiac cells seems fundamental for the progress of miR therapies into clinical applications. For that, it is interesting to highlight the contrast between the intraspecies translational value for targeted drug delivery of *in vitro*-selected ligands and the lack of studies that select ligands specific of human cardiac cells (i.e., derived from hiPSC). The intraspecies translational value refers in particular to ligands selected *in vitro* [261,295] that are specific in the same species *in vivo* and enable targeted drug delivery with NCs [253,280–284,302–305]. It is also remarkable the limited number of studies that assess the specificity of murine-raised cardiac-specific ligands in human cardiac cells [254,306]. Therefore, translationally relevant cardiac-specific ligands are very limited and have not been tested in clinically relevant species.

3.5 Conclusions

MiRs emerged as key regulators in cardiac pathophysiology, converting them in a new class of attractive therapeutics to treat HD and dysfunction. While preclinical research in small animals confirms this potential, their development has reached a bottleneck in late preclinical phases primarily due to delivery limitations. This review highlights how most of the studies in large animal models and clinical trials are conducted with naked miR therapeutics, while their encapsulation in NCs followed by functionalization for cardiac-targeted delivery improves the miRs' beneficial effects on the heart. Importantly, it also underscores how this is accompanied by an improvement of non-cardiac detargeting, which can enhance safety. In combination, this work provides future directions for the development of translational targeting strategies for cardiac miR therapy. Overall, while substantial technical and biological hurdles remain, progress in miR biology and delivery with nanotechnology suggests that miR-based therapies could realistically form part of future cardiac treatments.

Chapter 4

Development of anti-miRNA nanotherapies to modulate miR-24-2

Based on:

“DNA-based nanocarriers to sequester altered microRNAs in cardiac dysfunction”

Postigo A.*, Hernández-Bellido N.*, Sánchez-Barat M., García-Mendívil L., Pueyo E., del Barrio J., Hernández-Ainsa S.✉, Ordovás L.✉ (2024).
Advanced Therapeutics. https://doi: 10.1002/adtp.202400247
(*Equal contribution, ✉Corresponding author)

Declaration of own contribution:

N H-B. contributed equally to the experimental design of the study, data interpretation and manuscript writing and carried out the characterization of the nanotherapy bioactivity *in vitro.*

4.1 Introduction

The development of novel therapeutic approaches for the treatment of CVD is lagging behind, hampered by a lack of an in-depth understanding of the molecular pathways governing cardiac dysfunction. At the same time, the modulation of cardiac miRs has demonstrated reparative and regenerative potential in the heart, extensively reviewed in Chapter 3. In Chapter 2, we identify miR-24-2 as a key dysregulated miR in cardiac aging, which could be a lever to promote healthy cardiac aging and thus, transversally reduce the burden of CVD. In addition, miR-24-2 is also upregulated in heart tissue of HF [156] and AF [63] patients and is implicated in the regulation of post-MI cardiac fibrosis [307,308], further confirming its significance in cardiac pathogenesis and its interest as therapeutic target. Molecularly, it is known that the strand 5p of miR-24-2 interacts with SERCA2 [12], a fundamental pump located in the sarcoplasmic reticulum of CMs and whose activity is critical for controlling cardiac contractility and relaxation. Opposite to the miR profile, *SERCA2* levels decrease in human heart tissue with age and in HF [10,12,309]. Restoring SERCA2 levels currently represents a key pathway in gene therapy to address failing hearts [310] with several completed or ongoing *SERCA2* supplementation trials (i.e., CUPID, MUSIC-HFrEF or MUSIC-HFpEF). All of these trials are based on *SERCA2* delivery with AAV1, however, the existence of AAV1 neutralizing antibodies in humans could compromise their success [311].

In addition, miR-24-2 *in silico*-identified targets, namely *ATP2B4*, *CRYAB* and *ROBO2,* downregulated in human iCMs at the protein and mRNA levels in response to the miR overexpression, are also downregulated mRNAs in the aged human heart [10,12]. These genes contribute to cardiac muscle contraction and development and heart morphogenesis, which are relevant for cardiac function **(Figure 17b)**. Therefore, restoring the perturbation generated by miR-24 in the cardiac tissue is a promising strategy for the treatment of age and disease-related cardiac dysfunction.

Developing non-viral methods based on NCs can overcome important limitations of miR therapies, as discussed in Chapter 3. DNCs have emerged as promising candidates for efficient delivery of miRs *in vivo*. Constructed using a bottom-up approach that relies on highly specific and programmable self-assembly of individual DNA oligonucleotides, DNCs have exhibited biocompatibility at the cellular level as well as in animal models [311], with no systemic toxicity and low immunogenic response [312]. These favourable properties, combined with their straightforward and reproducible preparation, versatile design, functionality and facile adaptability for targeted delivery, make DNCs suitable vehicles for therapeutic delivery in various applications, including chemotherapy [313],

gene therapy [228,229] or immunotherapy [314], among others. The chemical backbone of DNCs makes them particularly suited for gene delivery, as it can be tailored to harbour therapeutic sequences, such as antisense oligonucleotides (ASOs), mRNAs, miR mimics, anti-miRs and siRNAs [228].

In the context of miR-related therapy, DNA nanocages with truncated octahedral shapes, [315], RCA-based DNA nanosponges [316], branched DNA nanostructures [317–319] and a DNA tetrahedron [320] have successfully inhibited oncogenic miRs within cells. *In vivo* efficacy has been also provided by 3-way junction RNA nanoparticles that efficiently reduce the activity of oncogenic miR-21 and miR-17 in mice [321,322], by DNA tetrahedron loaded with miR inhibitors for skin anti-aging properties [323] and for miR-22-3p carriers to address a depressive disorder [324]. Additionally, hybrid miR-containing DNA tetrahedron and hydrogel systems have shown *in vivo* effect in tackling osteonecrosis through combined therapy [325]. While these examples highlight the potential of DNCs for miR-based therapies in cancer, it is noteworthy that their use in treating cardiac diseases remains unexplored.

Here, we present DNCs tailored to address cardiac dysfunction with miR therapies, in particular with application to mitigate the deleterious effects of miR-24-2-induced cardiac aging or other pathological processes. Specifically, the DNCs are designed to modulate the intracellular levels of miR-24-2 using an anti-miR approach and consequently, the levels of experimentally verified (SERCA2) or *in silico*-identified (*ATP2B4*, *CRYAB* and *ROBO2*) targets. Collectively, these structures show proper assembly, specific capture of the target miR, stability in biological conditions *in vitro* and adequate internalization capacity in a cellular model and in human iCMs, among other features. Interestingly, only one of the two configurations developed is able to rescue the intracellular levels of SERCA2 in a cellular model. This configuration is also able to restore the mRNA expression levels of *ROBO2* in human iCMs demonstrating its efficacy also in a translational *in vitro* model.

4.2 Materials and methods

4.2.1 DNCs development and structural characterization

4.2.1.1 Design and assembly

The design of DNCs was conducted based on an adaptation from previous reports [326]. Prior to assembly, all DNA sequences underwent analysis using Nupack [327] and BLAST software. The sequences of all used oligonucleotides can be found in **Table A3**.

DNCs are composed of three building units: monomer (M), linker (L) and stopper (S). M, S and L were assembled at equimolar oligonucleotide concentration in PBS solution. DNCs were assembled by mixing M, S and L following the ratio 64:1 (M:S), 1:1.5 (M:L) and 2:1 (S:L). These ratios correspond to molar concentrations of 4 µM of M, 62.5 nM of S and 6.031 µM of L. The assembly of DNA nanostructures (M, S, L and the DNCs) was carried out in a thermocycler with a thermal-annealing protocol from 95 to 25 °C in 140 steps (0.5 °C per step, 30 seconds (s) each step). Samples were stored at 4 ºC until use.

In Cy3-labeled DNCs, 40% of Cy3-labeled M was added to samples for DNCs assembly. Specifically, 40% of M is labeled with one strand fluorescently functionalized with the Cy3 fluorophore **Table A3** and 60% of M is added unlabeled.

DNCs with a fluorescence reporter system ($DNCs_{LU}$) were developed to track ssDNA/ssRNA-mediated disassembly process and to monitor the intracellular stability of DNCs. To this end, 20% of M_{LU} was Cy3 labeled (present in one of the 3 strands) and 100% of L_{LU} were labeled with BMNQ535 quenchers (present in the two strands composing L_{LU}). Note that M_{LU} contains a single Cy3 label, whereas L_{LU} is labeled with two BMNQ535 quenchers, one per overhang, to ensure complete fluorescence quenching upon assembly.

4.2.1.2 Electrophoretic mobility shift assay

Electrophoretic mobility shift assay (EMSA) was performed using either PAGE or AGE. For PAGE and AGE, 20 ng and 50 ng, respectively, of each DNA sample were loaded and run in an 8% polyacrylamide and 3% agarose gel, respectively, immersed in a solution containing 11 mM $MgCl_2$ buffered with 1x TAE (pH=8.3) (Thermo Fisher). For subsequent visualization, the gels were stained with GelRed (Biotium) and imaged under ultraviolet light transillumination.

4.2.1.3 Dynamic light Scattering

The hydrodynamic sizes of M, DNC_A (N_A) and DNC_B (N_B) were measured by dynamic light scattering (DLS). N_A and N_B were folded in PBS at a concentration of 200 ng/µL and M was folded at a higher concentration of 800 ng/µL (20 µM) due to its smaller size. Samples were analyzed at 25 ºC using the Malvern analytical Zetasizer Nano ZS instrument. The reported values represent the average of 5 independent studies of 10 measurements each, consisting of 5 reads per run. Values in intensity are provided.

4.2.1.4 Atomic Force Microscopy

For atomic force microscopy (AFM) studies, 4 µL of either M, N_A or N_B at a concentration of 50 ng/µL were spotted onto freshly exfoliated mica and left to adsorb to the surface for 5 min. Then, sample was washed thrice with filtered Milli-Q water followed by soaking up of excess water using a tissue and slow drying under a soft air nitrogen steam for 3 min. Samples were analyzed using a Veeco-Bruker Multimode 8 instrument with NGS30 tips in tapping mode in air. Images were analyzed using Gwyddion 2.60 Software. The diameters of DNA nanostructures were estimated extracting profiles of individual motifs in the two different axes. The value per particle is the average of the profiles of the two different axes. 50 motifs were analyzed to provide the averaged value.

Further methodological details of the structural characterization of the DNCs can be found in the original article [328].

4.2.2 Characterization of DNCs bioactivity

4.2.2.1 MiR capturing study

DNCs with the same M concentration (1 µM) were incubated with the ssRNA, ssDNA or $ssDNA_{mock}$ during 1h at 37 ºC at various molar ratios (bait fragment: anti-miR target sequence). Samples were then analyzed by PAGE and fluorescence spectrophotometry. PAGE was performed as described above. $DNCs_{LU}$ samples were assembled as described for DNCs. Samples were diluted 1:5 in PBS (final M concentration of 800 nM) and sequences (ssDNA, ssRNA, $ssDNA_{mock}$) were added to a final concentration of 2.4 µM to match the concentration of bait overhangs. Fluorescence was recorded in a ClarioStar plate reader setting the excitation at 540 nm and the emission window from 556 to 696 nm. Fluorescent measurements were recorded at 37 ºC. Fluorescence curves data were processed with Origin software. Fluorescence maxima was fixed at 565 nm.

4.2.2.2 DNCs stability assays

Nuclease degradation of M, N_A and N_B was studied through incubation with either DNase I or DMEM (Thermo Fisher) supplemented with 10% FBS (Sigma Aldrich) (DMEMc). Regarding DNase I degradation study, samples were incubated at a DNA concentration of 50 ng/µL with 4.0 U/mL, 2.0 U/mL, 1.0 U/mL, 0.5 U/mL, 0.25 U/mL, 0.125 U/mL and 0 U/mL of DNase I (New England Biolabs, M0303) along with 1x DNase I buffer at 37 ºC for 1 h. For the DMEMc degradation study, 50 ng/µL of M, N_A and N_B were incubated with this media at 37 ºC during different times: 0, 1, 3, 6 and 24 h. All samples were analyzed using PAGE. The degree of stability was quantified by measuring the decrease in the intensity of the main band corresponding to the non-degraded DNC and the emergence of a smear resulting from degradation compared to time 0 h, using image J. Specifically, the percentage of non-degraded structure (NDS) was calculated using the following two equations:

$$\mathrm{F} = \frac{\mathrm{I}}{\mathrm{I+S}} \qquad \text{Eq 1.}$$

$$\%\ \mathrm{NDS} = \frac{Fi}{F0}\mathrm{x}\ 100 \qquad \text{Eq 2.}$$

Where F is the fraction of the main band; I, is the intensity of the main band; S, is the intensity of the slurry; % NDS, is the percentage of non-degraded structure; F_i, is the fraction of the main band at every time point *I* and F_0, is the fraction of the main band at the initial time point.

4.2.2.3 Cell culture and viability assay

HEK293 cells were maintained in MEM (Biowest) supplemented with 10% FBS (Thermo Fisher) and 1% Penicillin/Streptomycin (Thermo Fisher), according to manufacturer's recommendations and passaged regularly when reaching confluence using EDTA 0.5 mM.

hiPSC culture and iCM differentiation was conducted following the methods described in Chapter 2, section 2.2.3. For each experiment, iCMs in expansion were detached using TrypLE Select (10x) (Thermo Fisher), seeded at 4-6x10^5 cells/cm^2 and the culture was checked for purity by estimating the proportion of $TNNT2^+/MYL2^+$ iCMs by flow cytometry (see Chapter 2, section 2.2.6). Cultures with more than 95% of $TNNT2^+/MYL2^+$ were only used. The iCMs were expanded in CEM for 3 more days (until reaching 85-90% confluence) and transferred to CMM for 4 days before DNCs addition to gain maturity before DNCs addition.

For viability assays, HEK293 were seeded in a 96-well plate at a density 6x10^5 cells/cm^2 cells/cm^2 and, after 24 h, M, N_A and N_B were added at final concentration of 100 ng/µL of DNA. Immediately, three phase contrast images per well were acquired every 2 h during 48 h at 10x magnification in the Incucyte® SX5 platform (Sartorius). Image analysis was done in the Incucyte 2021C software by determining the percentage of confluence per well normalized to untreated cells (without DNCs) and normalized to 0 h.

4.2.2.4 Flow cytometry

The internalization and intracellular stability of DNCs (N_A and N_B) were evaluated in HEK293 cells with the addition of 50 ng/µL of Cy3-labeled DNCs or 50 ng/µL $DNCs_{LU}$, respectively. HEK293 were seeded in a 96-well plate at a density of 6x10^4 cells/cm^2 and after 24 h, DNCs were added and incubated for 0.5, 7, 24 and 48 h and after this time detached with EDTA 0.5 mM and washed with PBS.

Uptake capacity was evaluated in HEK293 and iCMs with 100 ng/µL of Cy3-labeled DNCs after 24 and 48 h of treatment (in CMs only after 24 h). HEK293 were prepared as for internalization/intracellular stability analysis. iCM were treated Cy3-labeled DNCs (N_B and N_{sc}) in CMM supplemented with 10% of FBS and after 24 h, detached with TrypLE Select (10x) and washed with PBS before analysis.

HEK293 and iCMs were analyzed in the Gallios 10 (Beckman Coulter) flow cytometer and data analysis was performed with FlowJo software. Internalization and intracellular stability were determined as the percentage of $Cy3^+$ cells and the Cy3 mean fluorescence intensity (MFI), respectively.

4.2.2.5 Confocal imaging

HEK293 and iCMs were prepared as for flow cytometry analysis but plated on 10 mm cover slip and incubated with 100 ng/µL DNCs (M, N_A and N_B) for 24 h before fixation with 4% PFA. HEK293 were permeabilized with 0.1% saponin and 1% BSA (Sigma-Aldrich) in DPBS, stained with 1:100 dilution of Phalloidin Alexa Fluor 488 (Thermo Fisher, A12379) in DPBS for 1 h at room temperature in darkness and finally counterstained with 3 µM DAPI for 20 min (Abcam, ab228549). DNCs treated-iCMs were permeabilized and blocked with 0.1% Triton X-100 during 15 min and with undiluted protein block (Agilent, X090930-2) during 25 min, respectively. After DPBS washing, cells were incubated with a 1:100 dilution of primary antibody rabbit anti-Cardiac Troponin I (Abcam, ab91605) overnight at 4 ºC. The secondary antibody, Alexa Fluor

488 goat anti-rabbit IgG (Invitrogen, A11034) diluted 1:1000, was incubated during 30 min in darkness followed by 3 µM DAPI counterstaining as indicated previously.

Images were acquired with a Carl Zeiss LSM 880 Confocal Microscope (Carl Zeiss, Germany) at 40x magnification. Image processing and analysis was performed with ZEN software.

4.2.2.6 Luciferase reporter assay

HEK293 cells were plated in 384-well plates at a density of $1x10^6$ cells/cm^2 and co-transfected with a SERCA2 luciferase vector [12] **(Figure 20)** and miR mimics using Lipofectamine 2000 Transfection Reagent (Invitrogen) according to manufacturer's instructions. Specifically, 45 ng of *pmiRGLO-SERCA2* reporter vector and 0.6 pmoles of miR mimic sequences, including hsa-miR-24-2-5p miR Mimic (Cohesion Bioscience) and miR Mimic Negative Control (miR_{mock}) (Cohesion Bioscience) were used. The media was changed after 24 h post-transfection, and, after another 24 h, cells were incubated with 100 ng/µl of N_A, N_B or M for 24 h. Also, 100 ng/µl of a DNC with a random bait sequence (N_{sc}) was used as negative control **(Table A3)**. Luciferase reporter assays were conducted using the Dual-Glo Luciferase Assay System (Promega), following manufacturer's instructions. Luminescence signal produced by the reporter and normalizer proteins, namely Firefly (*Fluc*) and Renilla luciferases, respectively, were measured on the Biotek Synergy HT.

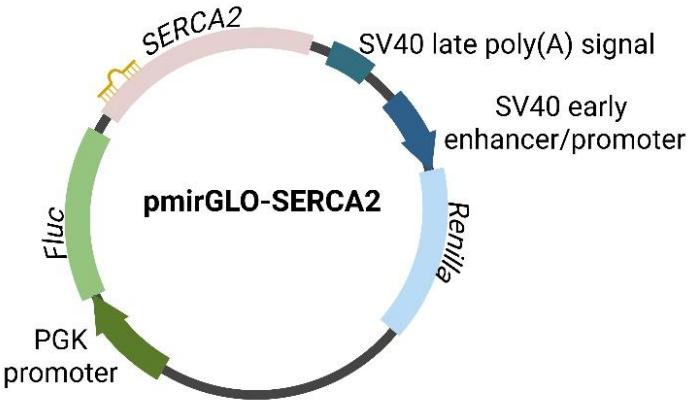


Figure 20. pmiRGLO-SERCA2 vector map. The expression of *Firefly* luciferase (*Fluc*) (light green), used as reporter gene, followed by the *SERCA2* gene sequence in a single polycistronic mRNA is governed by the PGK promoter (dark green). The expression of *Renilla* luciferase (light blue), is used as a control reporter for normalization, is governed by the SV40 enhancer/promoter (dark blue). Figure extracted from Ape software [329].

Relative luciferase activity (RLA) was calculated as the ratio of each experimental condition to the basal luciferase activity of the cellular model, namely the cells transfected with miR_{mock} and treated with N_{sc}. Luminescence values in each well were determined by normalizing the Fluc relative light units (RLUs) to Renilla RLUs.

4.2.2.7 Quantification of gene expression levels

Mir-24-2^{+} induced iCMs were treated with 100 ng/µl of N_B and N_{sc} in 10% FBS-supplemented CMM for 24 h before RNA extraction and processing for qPCR analysis. Cells were harvested using TrypLE Select (10x) (Thermo Fisher) and washed with PBS. RNA was extracted with Direct-zol™ RNA Miniprep and later retrotranscribed using PrimeScript RT Master Mix. Finally, qPCR was conducted by using NZYSupreme qPCR Probe Master Mix (2x) (and the primers listed in **Table A2**. Gene expression was normalized with *POLR2A* and expression calculated as relative ($2^{-\Delta\Delta Ct}$ method) to N_{sc}-treated iCMs.

4.2.3 Statistical Analysis

GraphPad Prism 8 was used for statistical analyses. One-way ANOVA test and t-test were used to compare independent groups. Data is reported as mean ± standard deviation (SD), unless specified otherwise in the figure captions. All experiments were carried out at least two independent times with at least with two technical replicates. The statistical threshold applied for each experiment is indicated in the figure captions.

4.3 Results

4.3.1 DNCs correctly self-assemble into stable biodegradable structures carrying anti-miR-24-2

DNCs were prepared through complementary hybridization of smaller building block units to render nanohydrogel-type nanostructures **(Figure 21)**.

Initially, two Y-shaped DNA constructs, M and S, each composed by three complementary strands, and one double-stranded DNA serving as L, were assembled in PBS using a thermal gradient. M comprises three dsDNA arms ending in 22-nucleotides long overhangs fully complementary to the target miR-24-2-5p, thereby acting as anti-miR-24-2. L hybridizes with 12- nucleotides of these overhangs to drive the assembly of

the entire DNC. The non-hybridized 10 nucleotides of M act as bait for miR capture. S contains a 12 nucleotides-long overhang in just one arm to block DNC growth. Two types of DNCs were prepared by modifying the position at which L bridges the monomers. Namely, N_A was assembled with L, hybridizing with the internal part of the M overhang, leaving a 10 nucleotides long external bait, and with S_A. Conversely, N_B was assembled with L hybridizing with the external part of the M overhang, leaving a 10 nucleotides long internal bait, and with S_B **(Figure 21 and Table A3)**.

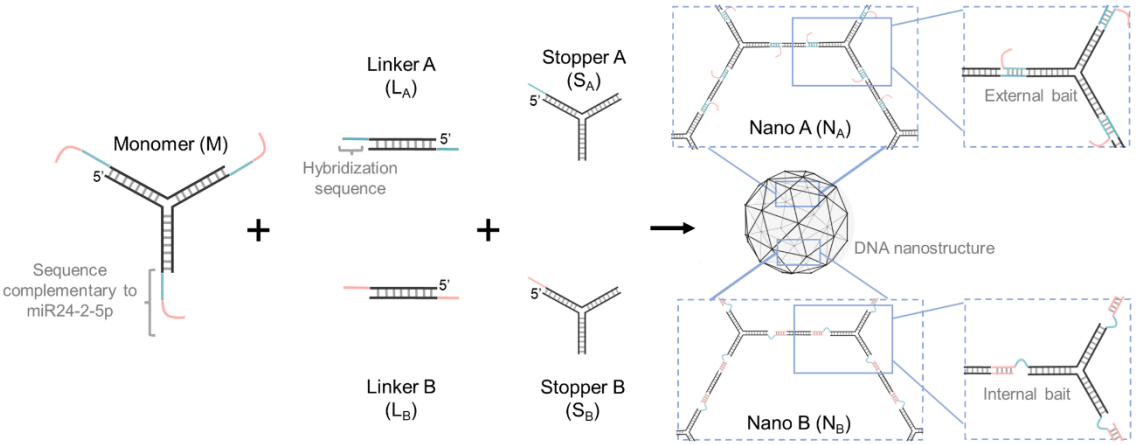


Figure 21. DNCs assembly in their two configurations (N_A and N_B). Complementary sequences between monomer, linker and stopper overhangs are shown in either blue (N_A) or red (N_B). DNCs were assembled by mixing M, S and L following the ratio 64:1 (M:S), 1:1.5 (M:L) and 2:1 (S:L).

To assess the proper assembly and the structural characterization of DNCs, PAGE, DLS and AFM were employed. In PAGE **(Figure 22a)**, distinct bands for M, S and L were observed and their mobility, following the order L>S>M, correlated with their respective structural sizes. For N_A and N_B lanes, DNA signals were visibly retained in the wells, smearing toward faster mobility species, indicating correct assembly of small components into larger structures.

DLS data **(Figure 22b)** and AFM images **(Figure 22c)** showed increased sizes for the DNCs compared to M. Specifically, average hydrodynamic diameters (Dh) of 81 ± 26 nm, 67 ± 15 nm and 12 ± 2 nm were obtained by DLS for N_A, N_B and M, respectively, with larger SD observed for N_A **(Figure 22b)**. The 10 nucleotides long internal bait present in N_B introduces larger flexibility and hence may facilitate the hybridization of the linker leading to a narrower size distribution. DNCs displayed a globular-like morphology in AFM images, which is consistent with the expected structural design for these nanostructures [326,330,331].

DNCs' biodegradability was confirmed by evaluating their susceptibility to nuclease-mediated degradation by DNase I, a major nuclease presents in serum. PAGE analysis showed that N_A, N_B and M are all degraded by DNase I **(Figure 22d)**, confirming their optimal degradation in biological conditions and supporting their potential as safe, biodegradable NCs.

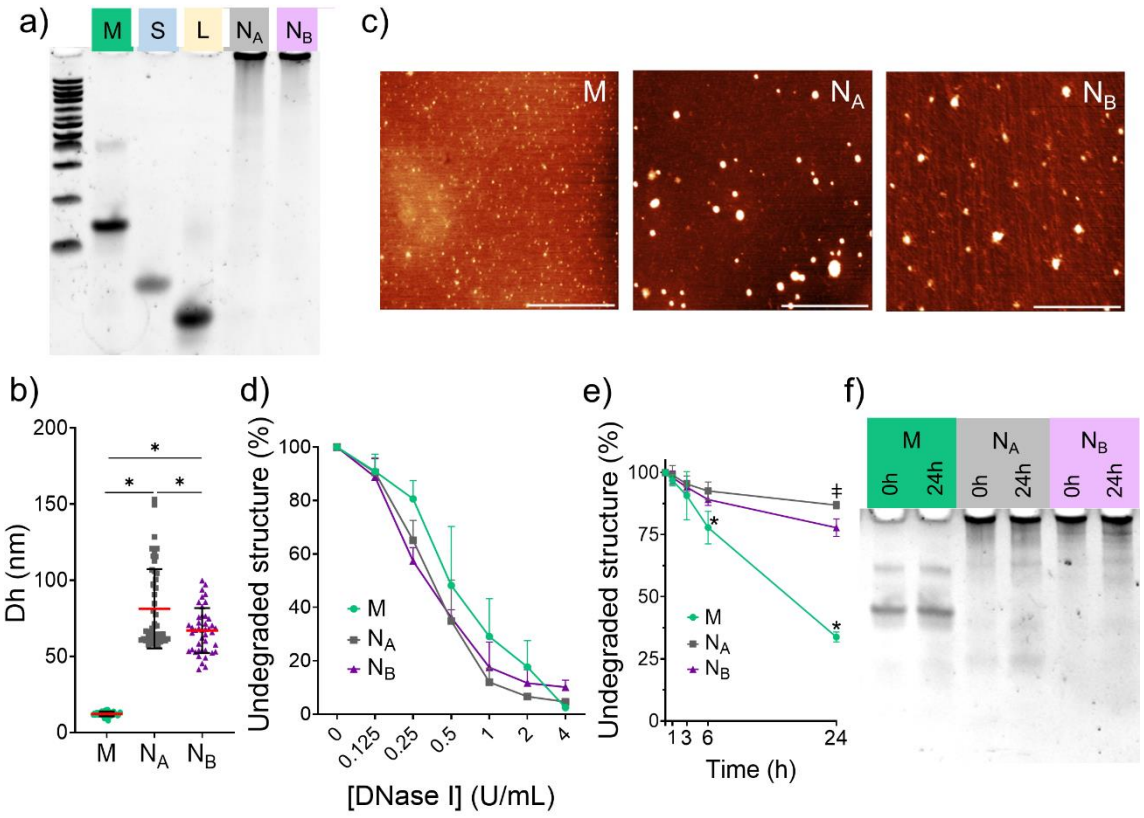


Figure 22. Characterization of the DNCs. a) PAGE showing retarded mobility of the assembled N_A and N_B compared to M, S and L. 100 bp DNA ladder is included at the most left lane. **b)** Distribution of the hydrodynamic diameter (Dh) values (in intensity) obtained by DLS of M, N_A and N_B. **c)** AFM images (topography) of M, N_A and N_B (Scale bar = 500 nm). **d-e)** Percentage (%) of undegraded DNA nanostructures incubated in with DNase I (d) and in cell culture media with serum over time in hours (h) (e). Statistical threshold (*/ǂ) was established at $P \leq 0.05$ (* for statistical comparison of M with both N_A and N_B; ǂ for statistical comparison of N_A with N_B). **f)** Representative PAGE images of DNCs incubated in PBS as a control of thermal stability.

Next, to assess whether the DNCs maintain their structural integrity under the chemical conditions relevant to subsequent investigations with cultured cells, we analyzed the stability of the DNCs in cell culture media DMEMc for different times up to 24 h at 37 ºC. A notable degradation of M in DMEMc at 24 h (only 34 ± 2% of intact structure remaining) indicated the vulnerability in serum of the building unit. Instead, N_A and N_B displayed good stability in DMEMc up to 24 h (87 ± 2% and 78 ± 4% of non-degraded structure, respectively), with N_A being significantly more stable than N_B at 24 h **(Figure 22e)**.

Stability controls were performed by incubating the structures in nuclease-free PBS for 24 h at 37 ºC **(Figure 22f)**, and all structures remained stable, confirming their robustness under nuclease-free physiological conditions. The higher stability of N_A and N_B compared to M in DMEMc highlights the enhanced protection of the anti-miR sequences by the assembled DNCs in biological media.

Therefore, the designed building units self-assemble into DNA nanohydrogel-type structures bearing anti-miR-24-2 sequences with Dh of around 75 nm. These DNCs are biodegradable but stable in cell culture conditions during 24 h.

4.3.2 DNCs specifically capture miR-24-2

Prior to the functional assessment in cells, the capability of the assembled DNCs to specifically sequester miR-24-2 was evaluated *in vitro* using PAGE and fluorescence spectroscopy. According to the DNCs design **(Figure 21),** in the presence of miR 24-2, L is expected to be displaced from M by the miR via toehold-mediated strand displacement, which results in DNCs disassembly. This design of miR-triggered disassembling nanostructures provides an intrinsic structural reporter to confirm successful miR capture. Furthermore, upon recognition of the target miR, the unoccupied anti-miR sequences of inner locations within the DNCs improve their exposure, subsequently potentially increasing the accessibility of the bait to the miR. Finally, this system is expected to facilitate RNase H-mediated degradation of the resulting DNA-RNA heteroduplex in the intracellular media. To probe this disassembly, N_A and N_B were incubated for 1 h at 37 ºC in PBS with the miR-24-2 target sequence as either single-stranded DNA (ssDNA) or RNA (ssRNA). Incubation of M with each target sequence in a molecular ratio anti-miR bait: target strand (both in ssDNA or in ssRNA) 1:2 resulted in gel migration retardation of M, supporting effective capture. In the case of N_A and N_B, the non-migrating band of the fully assembled DNCs nearly vanished upon incubation with the target strands at this ratio. Instead, a band corresponding to M with the captured ssDNA or ssRNA was observed, with just a few complexes of smaller size than the original fully assembled DNCs present, which supports successful disassembly of both DNCs. The specificity of the interaction was further validated for all M, N_A and N_B by using a single-stranded DNA sequence with a random sequence lacking homology to miR-24-2 ($ssDNA_{mock}$) **(Figure 23a)**.

Fluorescence spectroscopy was also employed to quantitatively assess the degree of target sequence capture and its selectivity under physiological temperature (37 ºC). To this end, DNCs with a fluorescent reporter system were designed ($DNCs_{LU}$). $DNCs_{LU}$

were designed to hold a Cy3 fluorophore quenched by BMN-Q535 in their assembled form (light down). Disassembly results in unquenching and Cy3 fluorescence emission (light up, LU) **(Figure 23b)**. These DNC_{LU}, were incubated for 1 h at 37 ºC with the miR-24-2 target sequence at 1:2 ratio of anti-miR bait: target strand sequences **(Figure 23c-d)**. Fluorescence intensity was significantly increased for both $DNCs_{LU}$ upon incubation with both ssDNA and ssRNA, whereas no substantial enhancement was observed in the case of the $ssDNA_{mock}$ control **(Figure 23c)**. This result confirmed the specific capability of both $DNCs_{LU}$ to capture the miR-24-2 target sequence. The increase in fluorescence signal for N_A in presence of ssRNA was significantly lower than for ssDNA, while fluorescence enhancement for N_B was equally substantial for both ssRNA and ssDNA **(Figure 23c-d)**. This data suggests a more efficient ssRNA-mediated disassembly in the case of N_B than N_A, and hence more efficient capture of the specific miR sequence by N_B than by N_A at physiological temperature.

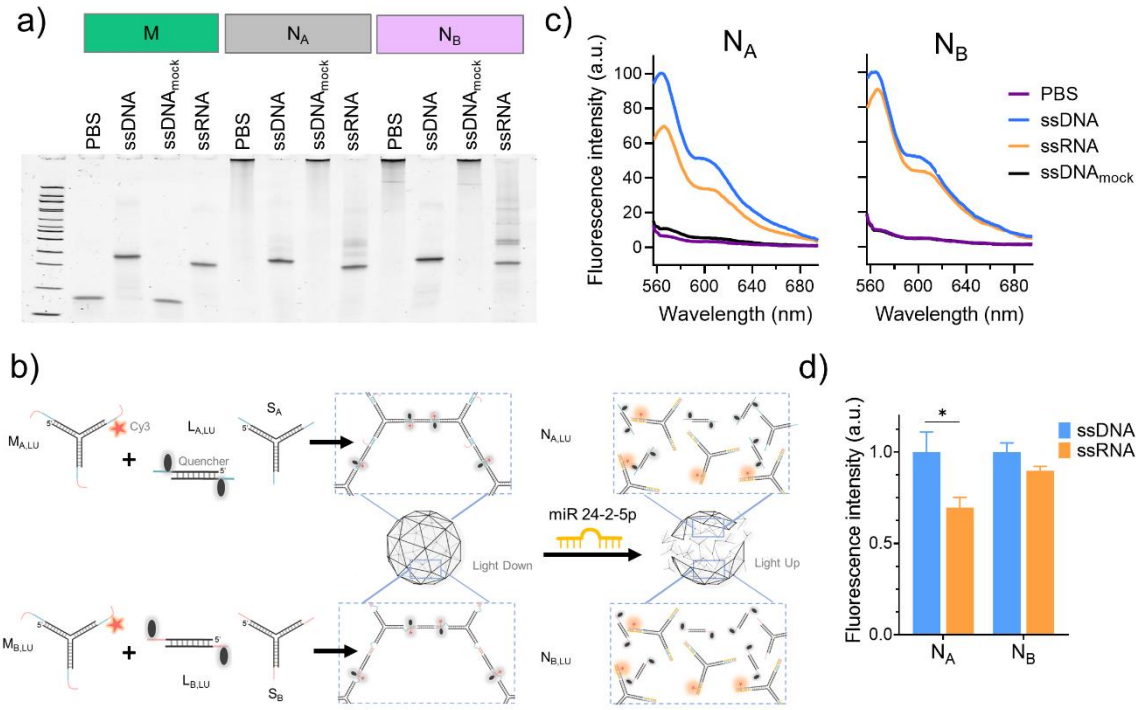


Figure 23. Assessment of capture capacity and specificity of miR-24-2 by DNCs. a) PAGE showing interaction of M with the target sequence (as ssDNA, ssRNA) and disassembly of N_A and N_B with the target sequence (as ssDNA and ssRNA) and random sequence ($ssDNA_{mock}$) at ratio 1:2 of anti-miR bait: ssDNA/ssRNA/$ssDNA_{mock}$). 100 bp DNA ladder is included at the most left lane. **b)** $DNCs_{LU}$ design with fluorescence up detection capacity for disassembly. **c)** Fluorescence spectra of $DNCs_{LU}$ upon incubation at 37 ºC for 1 h with ssRNA and ssDNA target sequences and $ssDNA_{mock}$ (ratio 1:2 anti-miR bait: target strand). **d)** Fluorescence fold enhancement of DNCs after incubation with the target ssDNA or ssRNA sequences at a ratio 1:2 anti-miR bait: target strand. Values are normalized by the enhancement observed for ssDNA for each DNC. Statistical threshold (*) was established at $P \leq 0.05$.

Overall, both DNCs demonstrated the capacity to specifically capture the miR target sequence *in vitro* at 37 ºC.

4.3.3 DNCs appropriately internalize in HEK293 cells showing biocompatibility

Next, we investigated the DNCs bioactivity *in vitro*. A routine cell line with no expression of miR-24-2, namely HEK293, was chosen as a model system to demonstrate the functionality of the customized DNCs. Cell proliferation of HEK293 treated with M, N_A and N_B in DMEMc for up to 24 h paralleled the one of untreated cells **(Figure 24a)**, confirming the lack of cytotoxicity of all the structures.

Regarding internalization, both Cy3-labeled DNCs, N_A and N_B, were avidly internalized after 7 h of incubation in HEK293, with more than 50% of $Cy3^+$ cells observed **(Figure 24b)**. They displayed though a low DNC load, as indicated by the nearly unnoticed increase in the Cy3 MFI **(Figure 24c)**. After 24 h of incubation, 100% of the cells had internalized Cy3-labeled DNCs and showed an average of more than 3-fold increase in the DNC load per cell compared to the initial time point. Beyond 24 h, the uptake persisted reaching more than 10-fold increase in load. Both N_A and N_B showed comparable internalization capabilities in the HEK293 cellular model **(Figure 24b-c)**.

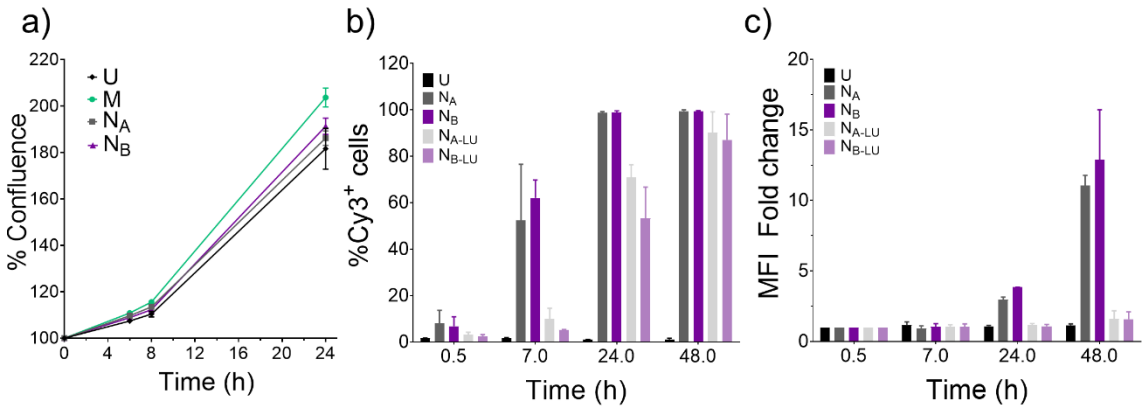


Figure 24. Cellular viability, kinetic of cellular uptake, intracellular stability of anti-miR fragments of DNCs in HEK293 cells. a) Cell viability assessment based in cell proliferation. Percentage (%) of confluence normalized to untreated condition (U) and to time 0 h. Each point represents mean ± standard error of each well. The mean corresponds to three wells with three images per well. **b)** Percentage (%) of $Cy3^+$ cells in the presence of Cy3-labeled DNCs or $DNCs_{LU}$ compared to untreated (U) cells reporting uptake or anti-miR trap degradation, respectively. **c)** Levels of average Cy3 fluorescence per cell (MFI) in the presence of Cy3-labeled DNCs or $DNCs_{LU}$ compared to untreated (U) cells reporting uptake or degradation, respectively. Data is normalized to the initial time point of each treatment.

The intracellular stability of DNCs was tracked using the $DNCs_{LU}$ system exploiting the lack of expression of miR-24-2 in HEK293 cells, which rules out the DNCs disassembly specifically triggered by the miR. In this system, the increase in fluorescence signal can be related to the intracellular degradation of the functional anti-miR fragments of $DNCs_{LU}$. As such, the proportion of cells with intracellular degradation of both $N_{A\text{-}LU}$ and $N_{B\text{-}LU}$ gradually rose over time following the uptake trend and reaching almost 100% of cells harboring degraded DNCs at 48 h **(Figure 24b)**. However, the amount of degraded DNCs per cell of both structures ($N_{A\text{-}LU}$ and $N_{B\text{-}LU}$) remained minimal compared to the initial time point and the total DNC load (Cy3-DNCs)**.** No significant differences in the intracellular stability were observed between $N_{A\text{-}LU}$ and $N_{B\text{-}LU}$ **(Figure 24c).** Single-plain confocal microscopy confirmed the intracellular location of Cy3-labeled M, N_A and N_B in HEK293 **(Figure 25)**. Altogether, this data indicates that DNCs are highly internalized in HEK293 cells, maintaining the stability of their functional anti-miR fragment for at least 48 h.

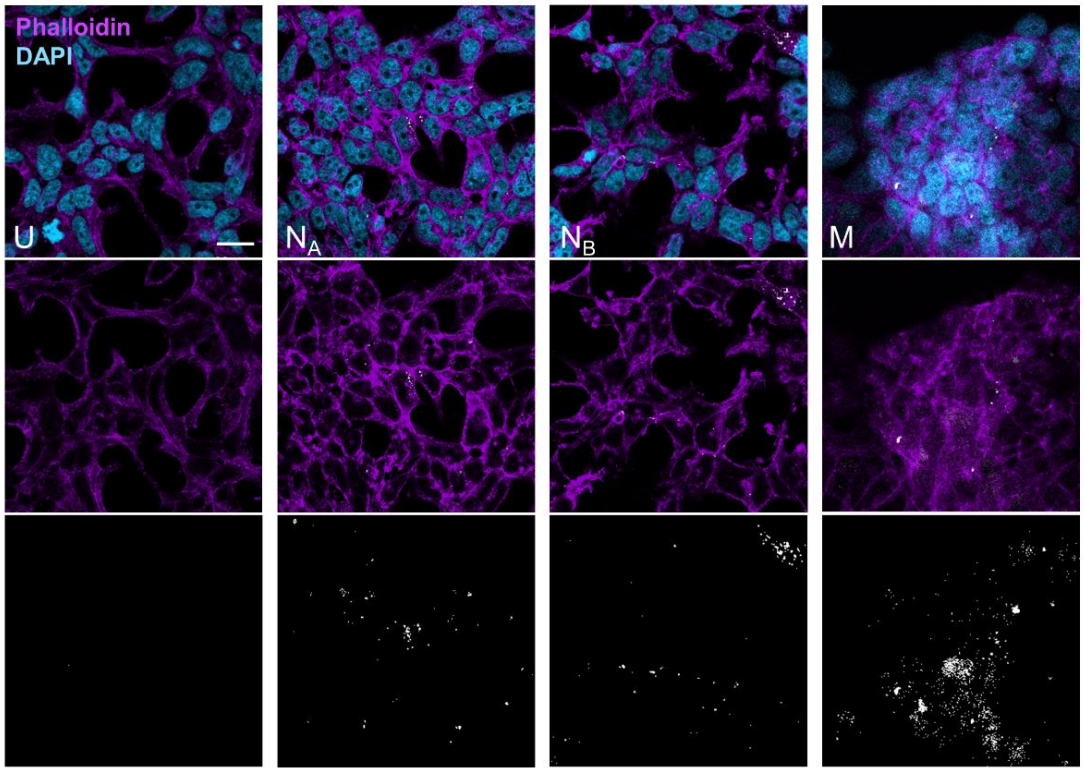


Figure 25. Subcellular location of DNCs in HEK293. Immunostaining with nuclear counterstain (DAPI) and Phalloidin (HEK293, top) of cells treated with Cy3-labeled N_B (An orthogonal projection is shown, Scale bar = 20 µm).

4.3.4 SERCA2 levels are effectively restored by N_B in a cellular model system

We firstly evaluated the functionality of the developed DNCs in a cellular model via luciferase reporter assay **(Figure 26a)**. Briefly, HEK293 were co-transfected with a luciferase reporter vector containing the *SERCA2* gene sequence and either miR-24-2 or a commercial miR mock (miR_{mock}, which does not interact with human mRNAs **(Figure 20)**. The luciferase activity of the vector co-transfected with the miR_{mock} represents the basal activity of the model, while with the miR-24-2 it represents the maximum degree of inhibition exerted by the miR on SERCA2 **(Figure 26a)**.

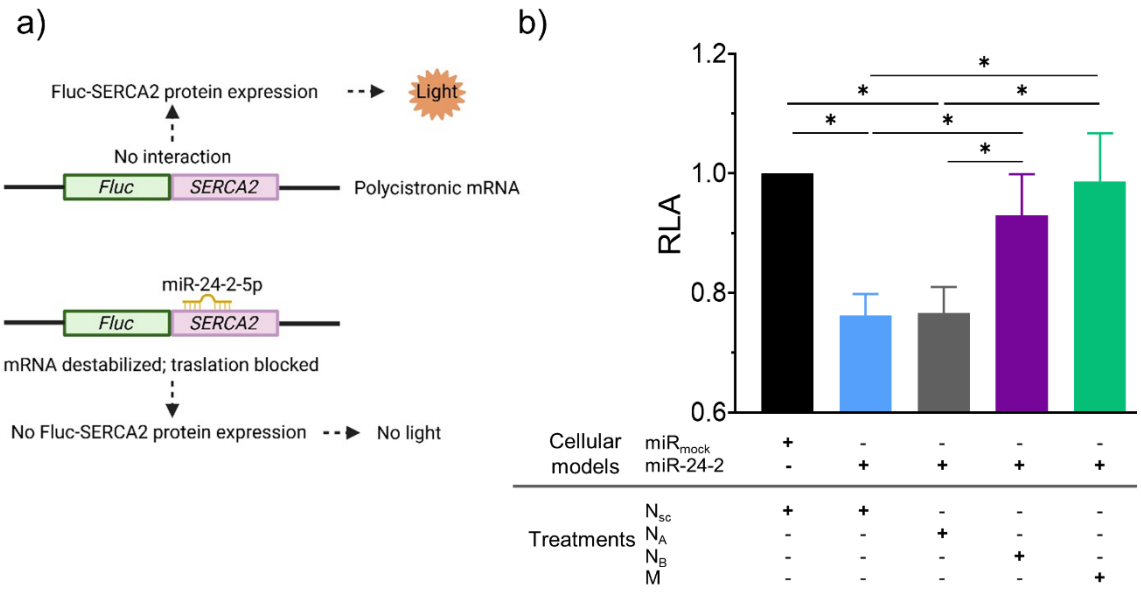


Figure 26. Functional assay of miR-24-2 inhibition by luciferase reporter assay. a) Descriptive figure of the luciferase reporter assays. HEK293 cells are co-transfected with the pmiRGLO-SERCA2 vector and miRs. If the miR does not interact with the target sequence, Fluc metabolizes its substrate producing light. If the miR interacts, the mRNA destabilizes or the translation is blocked, reducing the Fluc amount and so its activity. Created with BioRender.com. **b)** Luciferase reporter assay result for the functional assessment of DNCs in HEK293. Relative luciferase activity (RLA) of the pmiRGLO-SERCA2 vector reporter vector co-transfected with miR mimics (miR-24-2 or miR_{mock}) was determined after 24 h treatment with the different DNCs. Statistical threshold (*) was established at $P \leq 0.05$.

These cellular models were treated with N_A, N_B, M or N_{sc} **(Figure 26b)**. N_{sc} shares the configuration of N_A and the sequences of M, but with the exception that M_{sc} harbours a random anti-miR sequence that is not complementary to miR-24-2 or miR_{mock}. Therefore, N_{sc} is a negative control for the specificity of miR-24-2 capture. The combination of the miR_{mock} cells with the N_{sc} treatment gives the basal luciferase activity of the model treated with DNCs. With this set up, miR-24-2 transfected cells treated with N_{sc} maintained the

described level of miR-24-2-mediated SERCA2 inhibition [12] by 0.76 ± 0.03 fold. When assessing the anti-miR-24-2 treatments, N_B and M specifically and significantly restored the luciferase activity to levels not statistically different to the basal condition, with fold changes of 0.93 ± 0.06 and 0.94 ± 0.06, respectively. Therefore, N_B and M were able to rescue the miR-24-2-mediated inhibition. Instead, N_A did not have an effect, in agreement with the lower capturing capacity of $N_{A\text{-}LU}$ as compared to $N_{B\text{-}LU}$ by fluorometric analysis **(Figure 23c-d)**.

Overall, this result shows higher functional performance of N_B over the N_A in capturing the miR-24-2 intracellularly and validates the ability of N_B to modulate the effects of this age and pathology-related cardiac miR *in vitro* using biocompatible DNCs.

4.3.5 N_B functionality is verified in human iCMs

Next, the capacity of the functional N_B to modulate target genes in the cell type of interest for the application of the therapy, human iCMs, was evaluated. For that, we used the mir-24-2$^+$ line and a mRNA-based readout. Because *SERCA2* mRNA was not downregulated in induced miR-24-2$^+$ iCMs, the candidate targets *ROBO2*, *ATP2B4* and *CRYAB* were used.

N_B and N_{sc} internalized properly in iCMs observing that 100% of the cells marked Cy3$^+$ after 24 h of treatment **(Figure 27a)**, and localized intracellularly **(Figure 27a-b)**. Treatment with N_B for 24 h of mir-24-2$^+$ induced iCMs significantly reduced the levels of tdT and the mir-24-2 over the N_{sc} treated cells **(Figure 27c).** At the mRNA level, the treatment with N_B significantly released the inhibition of miR-24-2 only on *ROBO2*, while the inhibition on *CRYAB* kept increasing and the one on *ATP2B4* remained unchanged, both non-significantly **(Figure 27d)**. This suggests that miR-24-2 interacts only with *ROBO2* downregulating its mRNA, validating this gene as miR-24-2 target, but also that the functional N_B is able to modulate the miR-24-2 target gene expression in human CMs.

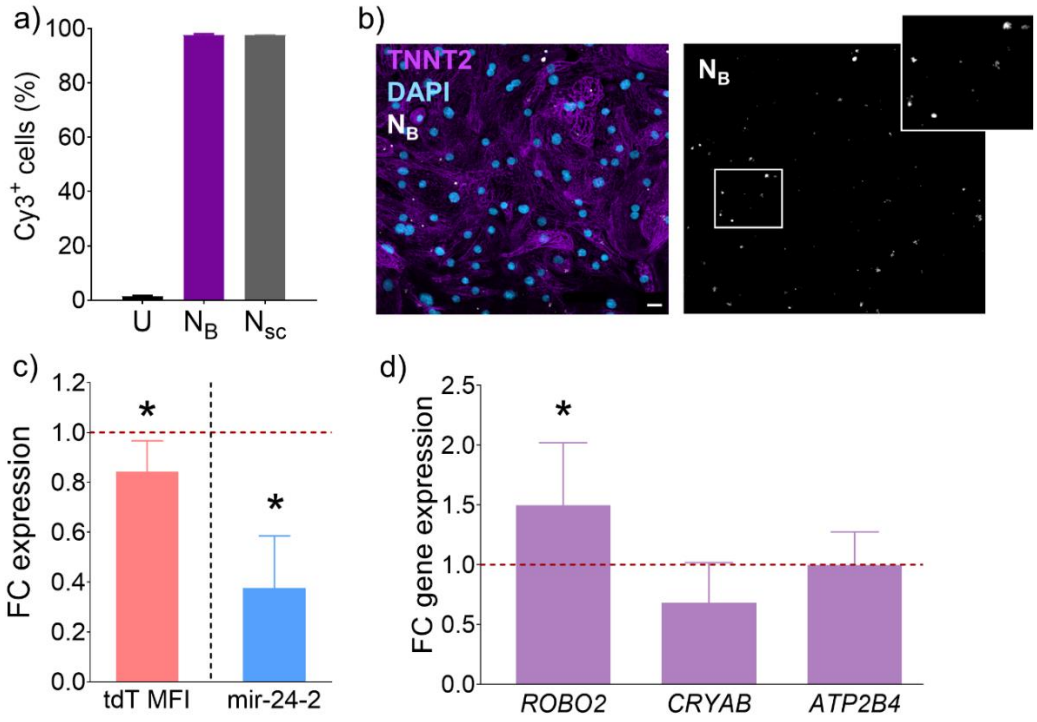


Figure 27. Functional evaluation of N_B in iCMs. a) Percentage (%) of $Cy3^+$ iCMs treated with DNCs for 24 h compared to untreated (U) cells. **b)** Orthogonal projection of TNNT2 immunostaining and nuclei counterstain (DAPI) of iCMs treated with Cy3-labeled N_B for 24 h (Scale bar = 20 µm). **c)** Quantification of the effect of 24 h treatment with N_B relative to N_{SC} represented as fold change (FC) in mir-24-2^+ induced iCMs in terms of tdT MFI (left) and mir-24-2 expression (right) **d)** Effect of the same treatment N_B relative to N_{SC} in terms of gene expression of the miR-24-2 putative targets represented as FC. Statistical threshold (*) was established at $P \leq 0.1$. The red line represents the outcome of mir-24-2^+ induced iCMs treated with N_{sc}.

4.4 Discussion

This work reports the successful development and characterization of biocompatible anti-miR-loaded DNCs that effectively and specifically capture the target miR-24-2 *in vitro*. The DNCs show stability against nuclease degradation in cell culture media up to 24 h and exhibit the capacity to be internalized by HEK293 cells with minimal intracellular degradation in a biocompatible manner. DNCs were properly internalized also in human iCMs, supporting their functional evaluation in this cell type.

DNCs, particularly N_B and M, show the ability to restore SERCA2 levels in a cellular model system, providing proof of concept of efficacy of a new system with therapeutic capacity to modulate miR-24-2. Interestingly, the hybridization strategy employed to form DNCs has a discernible impact on their ability to modulate the miR-24-2 effect. Namely, the internal miR bait structure N_B functionally outperforms the 3'-end bait N_A structure, highlighting the significance of DNC design in enhancing its performance capabilities. In addition to providing nuclease protection, the larger size exhibited by N_B compared to M,

should benefit retarding renal clearance in systemic delivery [332], making N_B interesting for future *in vivo* studies.

The functionality of the treatment is moreover verified in human iCMs, confirming this potential in a translationally relevant model and enhancing its therapeutic value to tackle age- or disease-related cardiac dysfunction mediated by miR-24-2. Specifically, a short-term treatment with N_B released the inhibitory effect of mir-24-2 on its verified target mRNA, *ROBO2* [134], which confirms ROBO2 as a mir-24-2 target in human iCMs. Since miR-24-2 overexpression also inhibited ROBO2 protein levels in iCMs (Chapter 2), the effect of N_B is expected to be evident at this level. Importantly, the functional *in vitro* data shows the capacity of the developed anti-miR DNCs to regulate the miR at different levels of its biogenesis from pri-miR (downregulation of tdT fluorescence and mir-24-2 expression) to mature miR (restoration of SERCA2 levels), highlighting its effectiveness as miR modulator and suggesting an RNA degradation mechanism triggered by the DNA anti-miR. Modulation of target gene levels through the sequestration of miR-24-2 together with the proteomic and RNA profiling of miR-24-2 overexpressing iCMs (Chapter 2), evidences the potential of the developed DNCs to effectively modulate age- and disease-related pathways that are central to cardiac function. These processes include, for example, calcium homeostasis and excitation–contraction coupling (*SERCA2)* or heart morphogenesis (*ROBO2)*. Finally, the light-up system integrated in the developed DNCs makes them potentially suitable, upon adequate cardiac-targeting engineering, for *in vivo* preclinical imaging of miR-24-2 present in cardiac tissue, and hence interesting for theragnostic purposes.

Whether the developed nanotherapy can benefit of functionalization strategies to promote efficient and specific uptake by the heart *in vivo, i.e.,* aptamers [300] or cardiac-specific peptides [261,282], remains future work.

4.5 Conclusions

This work reports the development and characterization of *in vitro* effective biocompatible anti-miR DNCs for the modulation of the age-related miR-24-2. The results indicate that DNCs hold promise as carriers for miR therapies in human cardiac cells by evidencing their capacity to modulate verified target genes of the miR, which are, in addition, functionally relevant. These findings not only open new avenues for non-viral cardiac miR therapies, but also provide a framework for developing next-generation nanostructured platforms capable of addressing and modulating the multifactorial nature of cardiac aging and disease.

Chapter 5

Definition of biomarkers descriptive of cardiovascular health-related biological age

Based on:

"A simple blood biomarker based on gene expression describes cardiovascular health-related biological age"
Hernández-Bellido N.✉, Hernández-Vicente A., García-Mendívil L., Ramos-Marquès E., Hernando D., Cebollada A., Köhler R., Garatachea N., Pueyo E., Ordovás L. ✉ (2025). *Geroscience*. https://doi.org/10.1007/s11357-025-01784-6
(✉Corresponding author)

This work has been done in collaboration with Dr. Nuria Garatachea from Faculty of Health and Sport Sciences (University of Zaragoza) and Agri-Food Institute of Aragon (IA2)-Agri-Food Research and Technology Centre of Aragon (CITA) and Dr. Esther Pueyo from the Aragon Engineering Research Institute (I3A).

5.1 Introduction

As described in Chapter 1, predicting CV health in relation to the individual and/or heart BA rather than by CA could more efficiently help to manage the age-related associated risk of CVD and reduce its socioeconomic burden. Definition of BOAs with this capacity, imply the need to investigate their real-time relationship with parameters representative of the individual's CV health.

Autonomic nervous system (ANS) regulation and physical activity (PA) levels are significant independent predictors of CV health and mortality [333,334]. ANS regulation plays an important role during aging, leading to a gradual deterioration of body organs and functions, disrupting the homeostasis of the CV system and subsequently, affecting the level of CV health of individuals [335]. Heart rate variability (HRV) is recognized as a robust method to assess the status of the ANS [336,337], and is also an indicator of arrhythmic complications and a strong predictor of mortality and sudden death [338]. Indeed, there is a correlation of HRV markers with age, highlighting the intricate relationship between aging and the ANS [339]. In relation to PA, it is well known that PA declines with age, with older adults being the most physically inactive population group. PA levels are associated with the prevalence of risk factors that predispose individuals to the development of CV diseases [340] and with all-cause mortality [341]. Importantly, age modifies the relationship between PA and mortality, with its inverse association being stronger in the elderly [341]. In addition, Grässler and colleagues demonstrated the improvements in HRV markers, CV health and CV risk factors in response to different levels of PA by using data from 26 studies [337], linking exercise and ANS modulation to CV health. Overall, the evidence suggests that indices reporting the ANS function and PA levels of individuals are relevant age-related phenotypes and so, they are suitable for assessing the biological significance of novel BOAs in relation to CV health. Consequently, ANS- and/or PA-related BOAs can adequately monitor the current BA of individuals and, potentially, of their hearts.

Cardiac-enriched miRs are hypothetically suitable biomolecules for minimally invasive reporting of the biological status of the heart in body fluids. Although our cross-species approach does not identify *MIR490* as a key age-related miR, its release into the bloodstream could still be age-related and informative, as it is enriched in the human heart as compared to other tissues [12]. Theoretically, this relation with age would be stronger with the BA of the individual than with CA. Here, we aim at assessing this hypothesis and to develop novel tools for CV-health BA real-time monitoring. To do so, we create and characterize a novel and simple blood gene expression-based BOA

descriptor of the individual BA, the Gene expression-based Age Monitoring Clock (GamC), and evaluate the relation of miR-490-3p with CA and GamC. GamC demonstrates an association with CA in three independent cohorts supported by whole transcriptome changes, thus confirming its age-related nature. Consistently, GamC associates with synchronous indicators of CV health of individuals. It shows however differential sensitivity for variables related to the ANS activity and PA levels, which is indicative of the specific biological meaning of GamC. In addition, it shows a moderate sensitivity to an effective healthy-aging intervention in centenarians, collectively demonstrating its biological relevance as an aging clock. Instead, miR-490-3p is ruled out as an indicator of cardiac BA since it did not demonstrate association with CA nor with GamC. Overall, this study proposes a simple and affordable BOA that gathers information about the current CV health status of individuals.

5.2 Materials and methods

5.2.1 Identification of consistently dysregulated age-related genes in blood for GamC building

A literature search was conducted in PubMed to identify transcriptomic studies that have published lists of age-related differentially expressed genes in human blood. A cross-comparison of the lists resulted in the proposal of candidate genes for the construction of GamC **(Figure 28)**.

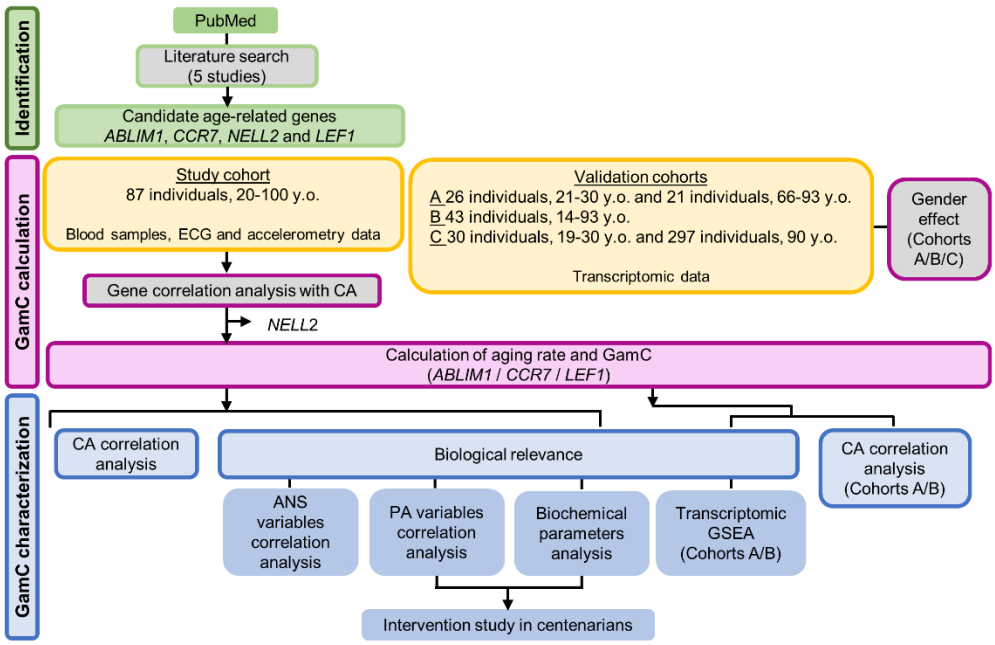


Figure 28. **Workflow for the description and characterization of GamC.** The study cohorts used for GamC calculation, validation and characterization are described in the yellow boxes.

5.2.2 Donors and samples of the study cohort

The study cohort is formed by a total of 87 Caucasian individuals from the region of Aragón (Spain) **(Table 9 and A4)**. The study was approved by the ethical committee for clinical research of Aragón (ID of the approval: PI17/0409 and PI18/381), and donors signed a written informed consent prior to enrolment. The study was conducted by adhering to the Declaration of Helsinki and in compliance with the European Union General Data Protection Regulation (EU 2016/679).

Table 9. Individuals in the study cohort: age range in years old (y.o.), total number of individuals, and percentage of males.

Group	Age range (y.o.)	Number (% male)
Young	20-30	22 (100)
Adult	40-50	22 (100)
Elder	60-70	21 (100)
Centenarian	>100	19 (26)

Subjects self-reported their date of birth and current medical conditions and medications. They were divided into four age groups **(Table 9)**. Young, adult and elderly individuals were excluded from the study if they suffered from acute illness, HD (such as HF or AF), were taking cardiac medication, or had any other clinical condition that contraindicated exercise. However, centenarians and donors who were overweight, sedentary, or had chronic diseases such as hypertension, diabetes, or hypercholesterolemia were included in the study, since they are representative of extreme longevity or have a high prevalence in society, respectively and thus contribute to the power of GamC. Further demographic, clinical, and biometric data are shown in **Table A4.**

Whole blood samples, electrocardiogram (ECG) recordings and PA data were synchronously collected from each individual along with their CA.

5.2.3 Gene and miR expression analysis by qPCR and generation of GamC

Whole blood samples were immediately processed to obtain plasma and peripheral blood mononuclear cells (PBMC) by using standard density gradient centrifugation procedures and stored at -80 ºC until use. Plasma samples were spiked-in with *Caenorhabditis elegans* cel-miR-39 for qPCR normalization purposes, RNA was extracted using the miRNeasymSerum/plasma (Quiagen) and retrotranscribed using the microScript microRNA cDNA Synthesis Kit (Norgen). RNA from PBMCs was extracted

using the All Prep DNA/RNA/miRNA Universal Kit (Quiagen) and next, RNA were reverse transcribed using the PrimeScript™ RT Reagent Kit (Takara). Later, qPCR was performed using the NZYSupreme qPCR Green Master Mix Kit (Nzytech) with gene- or miR-specific oligonucleotide pairs **(Table A2)** in a Viia7 instrument (Thermo Fisher). The absolute expression level of each gene (in PBMC) or miR (in plasma) was calculated as $2^{-\Delta Ct}$, where $\Delta Ct = Ct_{Gene}-Ct_{Reference}$, being Ct_{Gene} the expression value of the gene or miR and $Ct_{Reference}$ the expression value of the reference gene(s). Specifically, the mean Ct values of *UBE2D2* and *GUSB2* and the Ct values of *cel-miR-39* were used to normalize gene expression and the levels of the circulating miR, respectively.

The GamC of each individual was calculated as the sum of the aging rate and CA [12]. The aging rate was calculated according to previously described methods [342]. Briefly, the candidate genes with significant Pearson correlation coefficient between their expression level and CA were selected to construct GamC **(Figure 28)**. The aging rate of each individual (Δ_i) was obtained by linear regression of the expression levels ($2^{-\Delta Ct}$) of each gene G against CA. The regression analysis returned the residual expression level of gene G in each individual i ($\sigma_{G,i}$) and the regression factor associated to the gene G expression levels (a_G). The Δ_i is calculated as the integration of all (N) gene-specific $\Delta_{G,i}$ (which is in turn obtained as the ratio between $\sigma_{G,I}$ and a_G) **(Figure 28)** (Equation 3):

$$Aging\ rate(\Delta_i) = \frac{1}{N}\sum_{G=1}^{N}\Delta_{G,i} = \frac{1}{N}\sum_{G=1}^{N}\frac{\sigma_{G,i}}{a_G} \qquad \text{Eq. 3}$$

5.2.4 Validation cohorts and transcriptomic analysis

The literature search of section 5.2.1 and a search conducted in the GEO DataSets database were filtered to extract studies containing readily accessible bulk tissue transcriptomic datasets from PBMC (as the study cohort) from young to elder individuals. Three independent transcriptomic datasets were obtained for analysis: cohort A (study from USA, two age groups being 21-30 and >70 years old) [343], cohort B (study from Spain, continuous ages from 19 to 93 years old) [344] and cohort C (study from Finland, two age groups being 19-30 and 90 years old) [345] **(Figure 28 and Table 10)**. Data were retrieved using the GEOquery package in R software, and gene annotation was applied to assign biological identifiers and filter out unannotated genes. Expression values were normalized and standardized by quantile method for further analysis.

GamC was calculated as described above in cohorts A and B, but using the normalized and standardized expression values of the GamC-building genes. Cohort C was

excluded from this calculation due to the lack of age variability in the older group (all donors 90 years old).

Differential expression analysis was performed in cohorts A and B using the Limma package in R software. Individuals were ranked by chronological age and GamC values, then divided into quartiles (Q): young/first quartile (Q_1) and elderly/fourth quartile (Q_4) **(Table 10)**. A linear model was fitted to the normalized and standardized expression data, including contrast matrices to define age-based comparisons. Log_2FC values were estimated, and GSEA was performed using log_2FC values to identify enriched or depleted biological processes (GO terms) with a FDR ≤ 0.05. The top 50 GO terms with the highest absolute normalized enrichment score (NES) were manually classified into broader functional categories.

Table 10. Description of the validation cohorts A, B and C. Demographic data (purple background): study origin, age group, age range, number of individuals (% of males)). Age groups used in the differential expression analysis and GSEA of each cohort for both CA and GamC (green background): age and number of individuals (% of males).

			Demographic data				Analysis of enriched functions in elder at the transcriptomic level (GSEA)			
Transcriptomic study	**Simple type**	**GEO**	**Study origin**	**Group**	**Age range (y.o.)**	**Number (% male)**	**Individuals ranked by**	**Quartile**	**Age (y.o.)**	**Number (%male)**
Cohort A [343]	PBMC	GSE59635 GSE59654	USA	Young	21-30	27 (29.6)	CA	Young (Q_1)	≤ 27	15 (40)
				Elder	≥ 70	31 (38.7)		Elder (Q_4)	≥ 74	14 (35.7)
							GamC	Q_1	≤ 20.64	15 (20)
								Q_4	≥ 77.05	14 (57.1)
Cohort B [344]	PBMC	GSE69832	Spain	Young to elder	14-93	43 (51.2)	CA	Young (Q_1)	≤ 34	11 (45.5)
								Elder (Q_4)	≥ 62	10 (40)
							GamC	Q_1	≤ 11.92	11 (27.3)
								Q_4	≥ 82.03	10 (60)
Cohort C [345]	PBMC	GSE40366	Finland	Young	19-30	30 (30)	Not applicable			
				Elder	90	146 (29.5)				

5.2.5 ECG data recording and HRV analysis

ECG recordings were obtained for all individuals in the study cohort (**Figure 28**). A 12-lead high-resolution Holter ECG was acquired at rest with the 10 electrodes placed according to the manufacturer´s instructions (H12+, Mortara Instrument, Milwaukee, WI, USA) and digitized at a sampling rate of 1000 Hz.

From the ECG recording, the heart beats were detected and the RR interval time series were extracted using a multi-lead wavelet-based approach [346]. An operator manually verified each beat detection using a dedicated interface.

The 5-min RR interval series of each young, adult, and elderly subject were trimmed by removing 0.5 min from the beginning and the end, resulting in a final time series of 4 min. For the centenarian series, 4-min windows were defined within the 10-min recording in order to select the window with the lowest SD.

Linear and non-linear HRV indices were derived using algorithms developed and previously published in our research. These algorithms were implemented in MATLAB version R2021a (MATLAB, MathWorks Inc., Natick, MA, USA) [346–349]. The HRV markers extracted from the ECG are explained below.

5.2.5.1 Linear domain indices

5.2.5.1.1 Temporal domain indices

The time series of normal RR intervals after correction for ectopic beats [347] were denoted as NN and used for subsequent analyses. Several temporal HRV indices were derived from the NN interval series including mean heart rate (MHR) calculated as the inverse of the mean NN intervals, standard deviation of NN intervals (SDNN), standard deviation of the differences between adjacent NN intervals (SDSD), root mean square of consecutive differences of adjacent NN intervals (RMSSD), and percentage of consecutive NN intervals differing by more than 50 milliseconds (ms) divided by the total number of all NN intervals (pNN50). SDNN is considered a long-term variability measure of total HRV power, representing the variability of the ANS activity. RMSSD, SDSD and pNN50 are short-term variability measures of parasympathetic nervous system (PNS) activity.

5.2.5.1.2 Frequency domain indices

From the NN interval series, the instantaneous HR signal (dHR(n)), was derived using the integral pulse frequency modulation (IPFM) model, taking into account the presence of ectopic beats [347], and sampled at 4 Hz. This signal was high pass filtered (0.03 Hz) to remove the very low frequency components (dMHR(n)) and corrected as displayed in Equation 4 [348]. This modulating signal (m(n)) carries information about the ANS activity.

$$m(n) = \frac{dHR\,(n) - dMHR\,(n)}{dMHR\,(n)} \qquad \text{Eq.4}$$

To estimate the spectral properties of the HRV signal, the Welch period programme was applied to m(n) using a Hamming window of 60 s length with 30 s overlap. The power in the low frequency (LF) band, P_{LF}, and the power in the high frequency (HF) band, P_{HF}, were extracted by integrating the power in their respective bands: 0.04-0.15 Hz and 0.15-0.4 Hz, respectively. Normalized P_{LF} with the total power, named as P_{LFn} and the ratio P_{LF}/P_{HF}, as an indicator of the activity of both ANS branches, were also calculated.

5.2.5.2 Non-linear indices

Non-linear HRV indices, as non-stationary measures, were also derived from the RR interval series between the individual heart beats. Detrended fluctuation analysis (DFA) was performed by extracting the correlations between successive RR intervals at different time scales in order to measure fluctuations at different scales to detect short- and long-term correlations (α_1 and α_2, respectively) [350]. These markers are used to assess the complexity and adaptability of the ANS.

Finally, SD1 and SD2 were extracted from the Poincaré plot by plotting each RR interval against the previous interval to create a scatter plot. SD1 and SD2 measure the short-term and long-term beat-to-beat variability of the RR interval series, respectively. The ratio SD1/SD2 was also calculated, as the ratio between the two variabilities in the RR time series [350]. These measures are used to investigate the structure and complexity of the interbeat intervals.

5.2.6 Accelerometer data recording and analysis

Accelerometer data recordings were obtained for all individuals in the study cohort **(Figure 28)**. All individuals were asked to wear GENEActiv triaxial accelerometers (ActivInsights Ltd., Cambridgeshire, UK) for 24 h over seven consecutive days. These accelerometers were placed on the non-dominant wrist and programmed to record accelerations at 10 Hz, a frequency previously validated to classify daily activities [351]. Initialisation of the GENEActiv accelerometers and retrieval of data in binary format were performed using GENEActiv PC (version 3.2) (ActivInsights Ltd., Cambridgeshire, UK).

The GGIR 3.0-2 package of the statistical programming language R v.4.3.2. [352] was used to perform accelerometer data analysis. Non-wear time detection and minimum valid time requirements for each accelerometer register were evaluated using GGIR default settings to facilitate comparability with previous studies. The minimum valid hours per day were set to sixteen, while the minimum valid days per record were set to two.

Accelerometer variables were calculated [353], including the MX metrics, the average acceleration (AA), and the intensity gradient (IG). The MX metrics [354] assess the acceleration of the most active X min of a participant´s daily activity (e.g., M30 refers to the acceleration at which the most active 30 min were spent). These metrics can be used to describe the distribution of intensities over different time periods and allow for direct comparison with health-related PA guidelines. Intensity levels corresponding to the most active 1, 2, 5, 10, 15, 20, 30, 45, 60, 120, 240, 360, 480, 600, and 720 min were recorded. AA reflects the average acceleration throughout the entire measurement period and can be used as a proxy for total daily PA-related energy expenditure or PA volume [353,355]. IG, calculated as the slope (negative) of the linear regression between the natural logarithm of time and acceleration intensity, captures the distribution of PA intensity.

Despite knowing the limitations of traditional cut-points [356,357] due to their widespread use, the following indices were also calculated: Inactive time (IT: <30 mg), time spent in light intensity PA (LPA: 30–100 mg), moderate intensity PA (MPA: >100-400 mg), vigorous intensity PA (VPA: >400 mg), and moderate-vigorous intensity PA (MVPA: >100 mg) [358].

5.2.7 Exercise intervention

For the exercise intervention **(Figure 28)**, centenarians were randomly assigned to the control or intervention group using a computer-generated shuffle list. Participants in the control group maintained their usual PA. The intervention group performed twice per week, non-consecutive, resistance training sessions over 12 weeks (24 sessions in total). All the sessions were performed one-on-one in the gym of the geriatric nursing home and were supervised by an experienced (5 years) strength and conditioning trainer (MSc in Sports Science). After the initial assessment, participants were enrolled in a resistance exercise routine consisting of 8 different exercises according to their Functional Ambulation Classification level [359].

Each session lasted 40-60 min, including a 10 min warm-up and 30-50 min of resistance training. The warm-up consisted of one set of eight single-joint seated exercises without resistance, 10 repetitions, 30-s rest between exercises. Resistance training consisted of 1-3 sets of the 8 exercises routine adapted to Functional Ambulation Classification (8-10 repetitions as fast as possible, at 50-70% of the one-repetition maximum) with resting periods of 1 min between exercises and 3-5 min between sets [360]. Load, number of sets, and type of exercise routine were adjusted to the new level of physical capacity every 2 weeks.

Whole blood samples and accelerometer variables were obtained at the end of the 3 months' intervention for both control and intervention groups as described above. Biochemical analysis for total cholesterol, low-density lipoproteins (LDL), triglycerides, creatine kinase (CK) and glucose levels were conducted by Centro Inmunológico de la Comunidad Valenciana (CIALAB). The accelerometer variables were obtained as described before. For each PA variable, biochemical parameter and GamC, the change in the value of each parameter after the intervention period in each individual (P_i) was calculated as the difference between after (II) and before (I) the intervention (ΔP_i). Then, the median and IQR of ΔP_i for each PA variable, biochemical parameter and GamC were calculated for the control and intervention groups.

5.2.8 Statistical Analysis

All statistical analyses were performed using GraphPad Prism 8.0. Association analysis between two variables was performed using Pearson correlation analysis for the calculation of GamC [342], its association with CA and the association of AR with CA. Spearman correlation analysis was used for the assessment of the association between independent HRV markers, PA variables and miR-490-3p levels with CA or GamC and also between HRV markers with PA variables.

Comparisons between unpaired observations in two independent groups were assessed using the Mann-Whitney U test.

As normality could not be assumed in the intervention study due to the small group sizes, the Wilcoxon matched-pairs signed rank test was performed in values of control and intervention groups independently to examine differences on ΔP_i of PA variables, biochemical parameters and GamC. The magnitude of the effect size (|r|) was calculated as described in Equation 5, where Z represents the Z-score for the Wilcoxon matched-pairs signed rank test and n is the total number of observations [361].

$$|r| = \frac{Z}{\sqrt{n}} \qquad \text{Eq. 5}$$

The |r| was considered small if |r|=0.1, medium if |r|=0.3 and large if |r|=0.5 [362].

Data is represented as displayed in figure captions. Statistical threshold was established at $P \leq 0.05$ or, when adjusted for multiple-testing correction, at $FDR \leq 0.05$, as conveniently indicated in the text and figure legends. The numerical value of P or FDR of every statistical test can be found in the supplementary tables from the original article [363].

5.3 Results

5.3.1 GamC is associated with CA

The calculation of the individual BOA started by identifying genes whose expression was consistently and significantly dysregulated with CA across independent study cohorts in PBMC or whole blood **(Figure 28)**. We performed a literature search seeking bulk tissue transcriptomic studies from different geographic origins (in some cases of different ancestries), hypothesising that such genes, when combined in the BOA, would be able to account for genetic and environmental differences, including cultural and lifestyle, in relation to CA. A total of five independent studies were identified, which included variable geographic origins and age ranges from young to centenarians [89,345,364–366] **(Table 11)**. A manual cross-comparison of the published lists of age-related DEGs revealed four consistently dysregulated genes across all studies: *ABLIM1*, *CCR7*, *LEF1* and *NELL2*. These were selected as candidates for the construction of GamC.

Their potential to define a relevant BOA was evaluated in blood samples from a study cohort composed of 87 individuals with varying overall health and ages ranging from 20 to over 100 years old **(Figure 28 and Tables 9 and A4)**. In agreement with the studies of the identification section of the workflow **(Figure 28 and Table 11)** [89,345,364–366], *ABLIM1*, *CCR7*, and *LEF1* showed a significant negative correlation with CA in the study cohort ($R = -0.41, -0.33, -0.55$, respectively and all $P \leq 0.05$), confirming their association with age **(Figure 29a and Table A4)**. *NELL2* instead was not significantly correlated with CA ($R = -0.18$, $P = 0.1$) therefore, it was excluded from the following steps of the study.

Table 11. Studies reporting age-related changes in the blood transcriptome found in the identification phase of the workflow. List of published studies used for the identification of candidate age-related genes: sample type, dysregulated genes common across studies in this list, geographical origin, age group, age range, number of individuals (% of males) and reported CA-dysregulated processes (Ref.: reference).

Study [Ref.]	Sample type	DEGs	Geographical origin	Age group	Age range	Number (% males)	CA-downregulated processes	CA-upregulated processes
Petters et al. 2015 [89]	Whole blood	*ABLIM1 CCR7, LEF1 NELL2*	Multiple origins: European (5 cohorts: Estonia, Italy, Germany (x2), The Netherland) and European American (1 cohort:USA)	Young to centenarian	18-104	7092 (not specified)	RNA and purine metabolism and ribosome biogenesis and ribosomal genes Mitochondria and metabolism pathways DNA replication, elongation and mismatch repair	Innate and adaptive immunity, cytokine and chemokine signaling Regulation of actin cytoskeleton, focal adhesion Fatty acid metabolism, peroxisome activity Lysosome metabolism and glycosaminoglycan degradation
Harries et al. 2011 [364]	PBMC	*ABLIM1 CCR7 LEF1 NELL2*	Europe (Italy)	Young to centenarian	30-104	698 (44.8)	RNA binding and splicing mRNA metabolism and binding Ribonuleoprotein complex biogenesis and assembly Chromatin remodeling	Biological functions related to extracellular region genes and ion transport genes (although no significant)
Pastoors et al. 2012 [365]	Whole blood	*ABLIM1 CCR7 LEF1 NELL2*	Europe (The Netherland)	Middle-age Nonagenarian	43.7-78.8 89.3-102.2	50 (48) 50 (52)	Lymphocyte activation Anatomical structure development Response to stimuli (including immune response) Regulation of gene expression Regulation of signal transduction	
Zubakov et al. 2016 [366]	Whole blood	*ABLIM1 CCR7 NELL2*	Europe (The Netherland)	Young Elder	23-28 66-72	22 (100) 25 (100)	Not reported	Not reported
Marttila et al. 2013 [345]	PBMC	*ABLIM1 CCR7 LEF1 NELL2*	Europe (Finland)	Young Elder	19-30 90	30 (30) 146 (29.5)	T cell function and adaptive immunity	Inflammation Hormone-related pathways (males)

Next, *ABLIM1*, *CCR7*, and *LEF1* were used to construct the aging rate and GamC for each individual **(Figure 28)**. GamC was positively and significantly correlated with CA (R = 0.59). The degree of association exceeded that the observed for the individual genes **(Figue 29b)**, demonstrating an improved explanatory power of this gene combination to describe CA. Instead, the aging rate was not significantly correlated with CA **(Figure 29c)** consistent with its expected individual-dependent nature.

These results indicate that GamC is associated with CA and, consequently, that the molecular data used to construct it contributes to describe this association

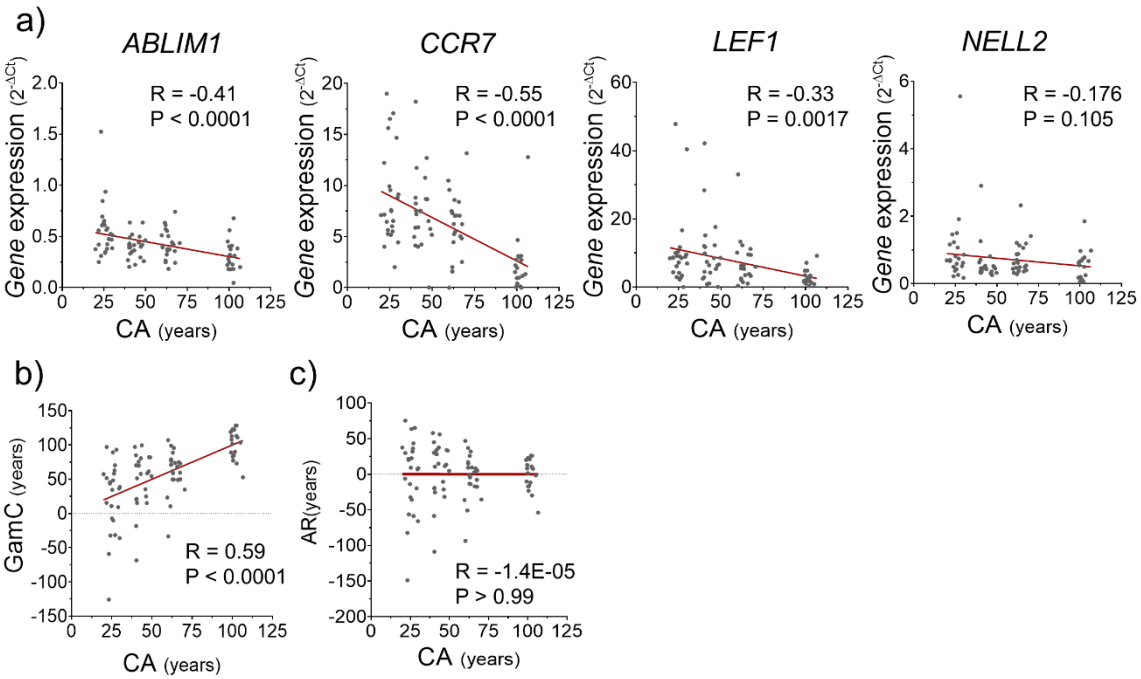


Figure 29. Evaluation of the relation with age of the candidate genes, GamC and AR. **a)** Pearson's correlation analysis of the gene expression levels in PBMC (obtained by qPCR) of the age-related candidate genes and CA in the study cohort. **b-c)** Pearson's correlation analysis of GamC (b) and aging rate (AR) (c) with CA (R: Correlation coefficient, P: p-value, linear regression shown as red line).

5.3.2 GamC association with age is maintained across independent study cohorts and at the transcriptome-wide level

The capacity to describe age of GamC was analyzed in independent validation cohorts **(Figure 28)**. As the study cohort was mainly composed of male donors **(Table A4)**, first the gender influence on this relationship was studied **(Figure 28)**. Using bulk PBMC transcriptomic data from three different cohorts of variable geographic origin (cohorts A – USA, 34% of males-, B – Spain, 51 % of males- and C – Finland, 29 % of males) **(Table 12)** [343–345], a general downregulation of *ABLIM1*, *CCR7* and *LEF1* with CA was observed in both genders in each dataset, but also globally. The association was significant in all cases except for *ABLIM1* and *CCR7* in the segregated groups of cohort B, for which only a moderate non-significant correlation was observed **(Figure 30 and Table 12)**. Thus, *ABLIM1*, *CCR7* and *LEF1* were generally associated with CA in a cohort- and gender-independent manner. Consequently, GamC was calculated without gender segregation for cohorts A and B **(Figure 28)**. Calculation of GamC for cohort C was not mathematically possible and was therefore excluded from further analysis.

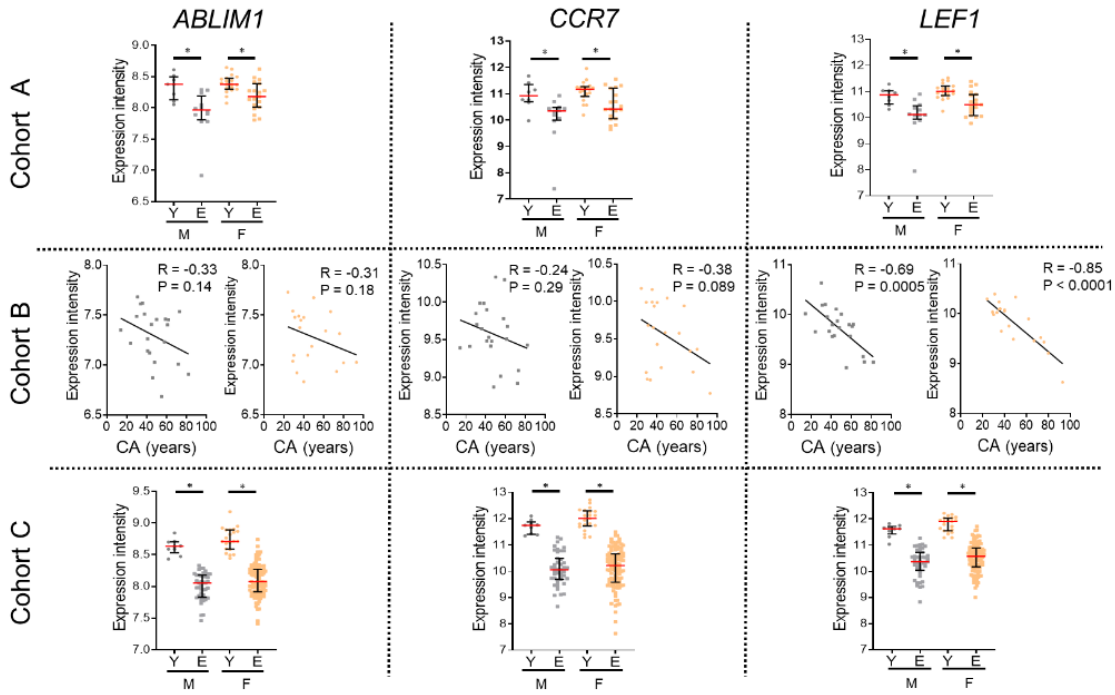


Figure 30. Normalized and standardized expression values of *ABLIM1*, *CCR7* and *LEF1* in blood samples of the individuals of the three independent validation cohorts. Cohorts A and C contain young (Y) and elder (E) age groups, while cohort B is constituted with individuals of continuous ages. Genders are colour coded: males (M) in grey and females (F) in orange. Mann-Whitney U test was used for cohorts A and C and Pearson correlation analysis for cohort B. Statistical threshold (*) was established at P ≤ 0.05 (R: Pearson's correlation coefficient, P: p-value, linear regression shown as black line).

Table 12. Analysis of the relationship of *ABLIM1*, *CCR7* and *LEF1* expression levels with CA and gender. Decreased expression in elderly compared to young individuals is represented as ↓ followed by the p-value of the Mann-Whitney U test (cohorts A and C). Pearson correlation coefficients with CA and p-value is shown for cohort B.

	Relationship with CA and gender			
Transcriptomic study	**Gene/GamC**	**Males**	**Females**	**Combined sexes**
Cohort A [343]	*ABLIM1*	↓ 0.0015	↓ 0.0038	↓ <0.0001
	CCR7	↓ 0.0055	↓ 0.0075	↓ <0.0001
	LEF1	↓ 0.0022	↓ 0.0011	↓ <0.0001
	GamC	-	-	0.55 / <0.0001
Cohort B [344]	*ABLIM1*	-0.33 / 0.14	-0.31 / 0.18	-0.31 / 0.04
	CCR7	-0.24 / 0.29	-0.38 / 0.089	-0.37 / 0.039
	LEF1	-0.69 / 0.0005	-0.85 / <0.0001	-0.76 / <0.0001
	GamC	-	-	0,45 / 0.0024
Cohort C [345]	*ABLIM1*	↓ <0.0001	↓ <0.0001	↓ <0.0001
	CCR7	↓ <0.0001	↓ <0.0001	↓ <0.0001
	LEF1	↓ <0.0001	↓ <0.0001	↓ <0.0001
	GamC	-	-	Not applicable

Consistent with the results observed in the study cohort, GamC maintained a significant positive correlation with CA in the validation cohorts A and B with R = 0.55 and R = 0.45, respectively, **(Figure 31a and Table 12)** that was independent of the aging rate **(Figure 31b)**, demonstrating its age-related relevance across populations.

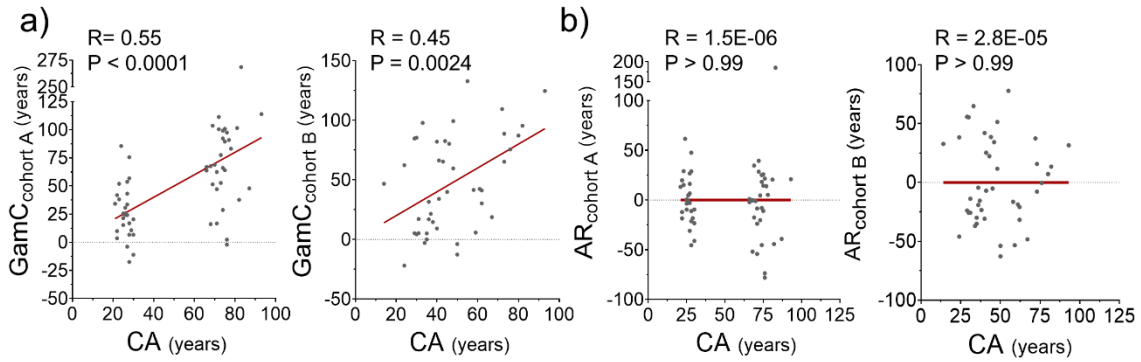


Figure 31. Validation of GamC and aging rate in independent cohorts. Evaluation of the association of **a)** GamC and **b)** aging rate (AR) (constructed from transcriptomic data) with CA in the validation cohorts A (left) and B (right) (R: Pearson's correlation coefficient, P: p-value, linear regression shown as red line). Data of individuals from cohorts A, B and C can be found in Table S6 from original publication [363].

Then, the biological significance of GamC was examined by analysing its ability to capture age-related transcriptomic changes **(Figure 28)**. GSEA revealed that, in general, there was a high degree of overlap of functional processes dysregulated with CA and GamC between cohorts. Only the depleted processes of cohort B seemed differential, but those of GamC mostly matched the depleted ones of cohort A, suggesting that GamC in cohort B may better describe the age-related changes in gene expression than CA itself **(Figure 32)**. Overall, both cohorts retrieved processes previously reported to be altered with aging [1] and/or found dysregulated in the studies of the identification section of the workflow **(Table 11)**. Enriched processes included, for example, defense and response to stimuli, immune response, inflammation or metabolism and molecule transport, whereas depleted processes included, for example mitochondrial function, RNA metabolism and transcription, translation and proteostasis or epigenetics. Therefore, GamC is able to capture the transcriptomic changes that occur with CA, confirming its age-related nature in different cohorts also at the molecular level.

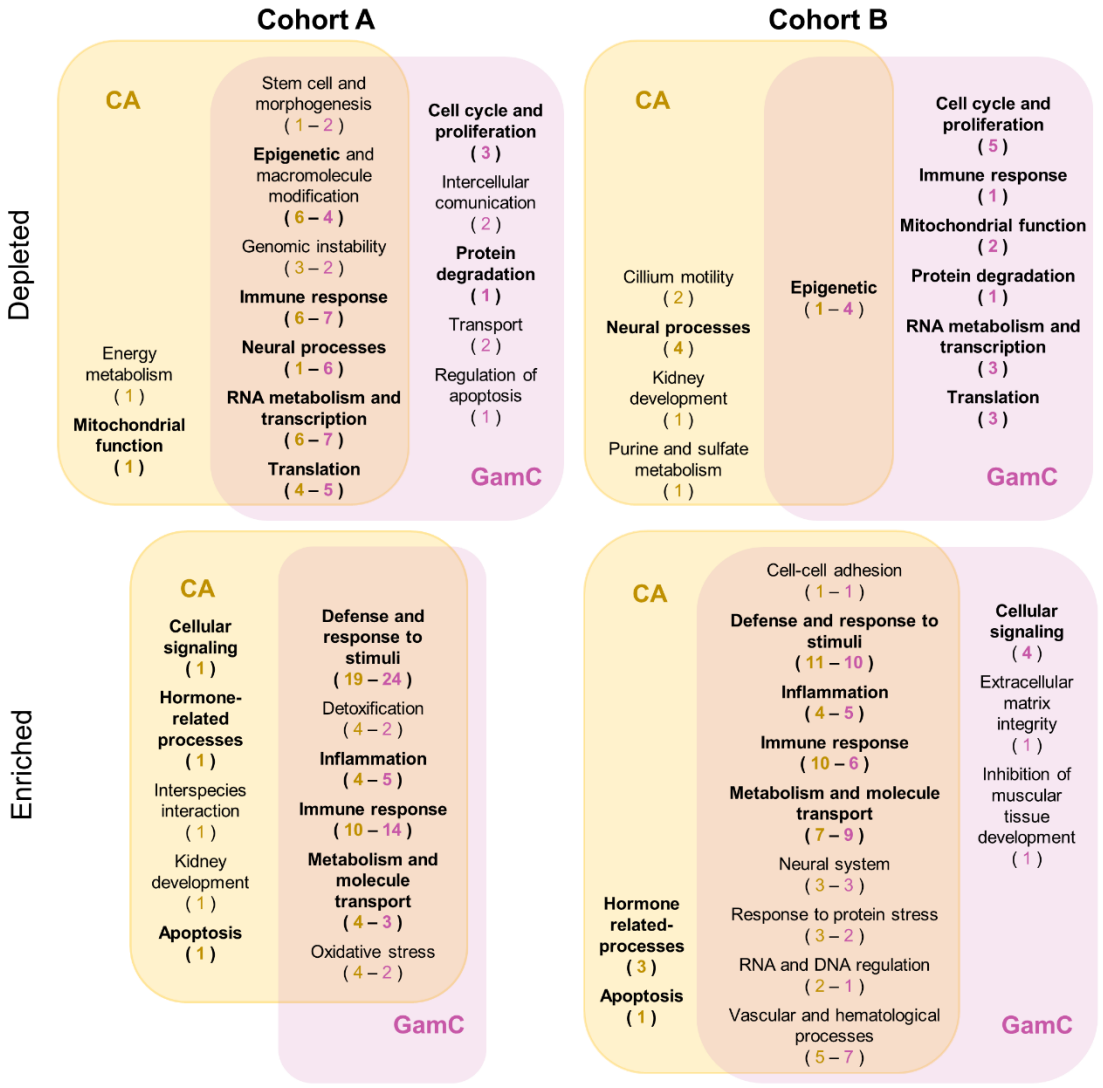


Figure 32. Evaluation of Gamc biological relevance at the molecular level in independent cohorts. GSEA in the transcriptomic datasets of the validation cohorts A and B. Enriched and depleted functional categories in the elderly classified by CA or GamC are shown (bold letters are used for categories common between CA and GamC and/or cohorts A and B). The number of gene ontologies belonging to each functional category is indicated in brackets and color coded (CA in yellow or GamC in pink). GSEA complete results and classification in broader categories can be found in Tables S7 and S8, respectively, of the original publication [363].

Thus, the relationship between GamC and age is robust across independent cohorts of different geographic origin and is supported by a molecular basis. Of note, GamC can also be calculated from different sources of gene expression data, namely qPCR and transcriptomic.

5.3.3 GamC marginally describes age-related changes in the ANS function

To further study the biological relevance of GamC, we observed the ability to predict the current CV health of individuals in terms of ANS function and PA levels **(Figure 28)**. Because of the established relationship between ANS and PA with age and, in turn, in defining CV health, we analyzed the general relationship between HRV and PA markers hypothesising that those correlated would be stronger age-related functional indicators. Accelerometer and HRV markers were only partially significantly associated (116 out of 308 tested correlations were statistically significant (FDR ≤ 0.05)). In particular, some frequency domain (PLFn, P_{LF}/ P_{HF}) and non-linear domain indices (α_1, α_2 or SD1 and SD2) had no relationship with virtually any of the PA markers **(Figure 33)**.

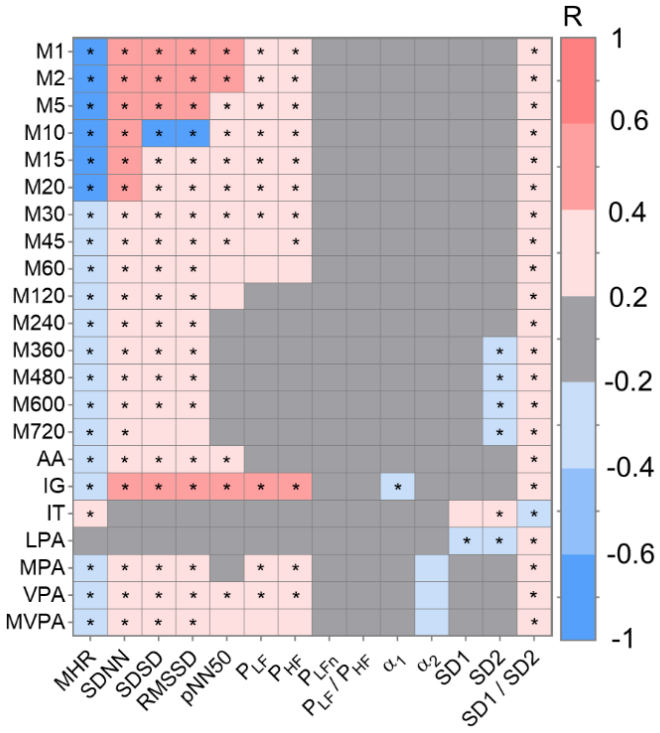


Figure 33. Independent association analysis between accelerometer metrics and HRV parameters in the study cohort. Spearman's correlation coefficients (R) are colour coded according to the scale and significant correlations (FDR ≤ 0.05) are marked with an asterisk (*). The numeric data of this figure can be found in Table S9 of the original publication [363].

Consistent with this observation and the established hypothesis, CA was only significantly associated with PA-related HRV markers, especially linear temporal and absolute frequency domain markers, including SDNN, SDSD, RMSSD, pNN50, PLF, PHF and SD1/SD2 (R around -0.6 and FDR ≤ 0.05) **(Figure 34)**. This suggests that CA can moderately explain HRV data in the study cohort, which are influenced by the

individuals' PA levels. GamC largely replicated these findings, but with even weaker power than CA (R between -0.2 and -0.4) **(Figure 34)**, indicating that GamC marginally described the ANS function.

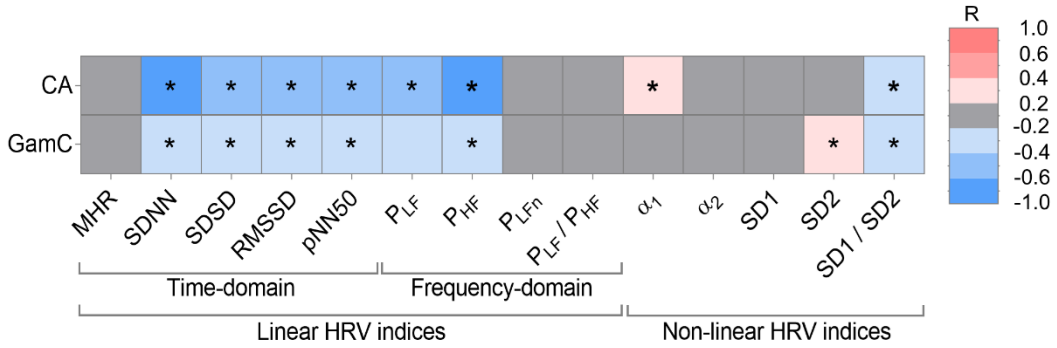


Figure 34. Evaluation of the association of age with HRV parameters. Spearman's correlation coefficients (R) of HRV parameters with CA or GamC are colour coded according to the scale and significant correlations (FDR ≤ 0.05) are marked by an asterisk (*). The groups of HRV parameters are delimited below as linear (time domain or frequency domain) and non-linear. The numeric data of this figure can be found in Table S10-S11 of the original publication [363].

5.3.4 GamC is associated with PA levels and responds modestly to a healthy-aging exercise intervention in centenarians

The relationship of GamC with accelerometer variables, as a direct measure of PA levels and of CV health was then analyzed **(Figure 28)**. CA was significantly correlated with all PA markers (FDR ≤ 0.05 and with R < -0.4 for most markers) except for IT (R = 0.20). GamC largely replicated this relationship, with an even stronger significant association with IT (R = 0.39) **(Figure 35)**. CA and GamC showed comparable sensitivity with respect to short-term metrics (from M1 to M240). However, GamC was more sensitive than CA to long-duration MX metrics (from M360 to M720), demonstrating a better description of the acceleration at longer active periods. AA and IG, as standardized variables to describe the volume and intensity of PA, also showed their moderately negative and significant association with GamC (R = -0.44 and -0.52, respectively). In terms of PA intensities, GamC showed a weaker correlation with LPA (R = -0.33) than with MPA, VPA and MVPA (R = -0.47, -0.46 and -0.46, respectively), suggesting that GamC may reflect PA of higher intensities with greater precision. This fact is also observed in the associations with CA, which shows stronger associations with MPA, VPA and MVPA (R = -0.49, -0.51 and -0.48, respectively) than with LPA (R = -0.29). Therefore, GamC is able to describe individual PA levels in terms of MX metrics, AA, IG, and IT to the same

extent as CA, but with improved sensitivity in some aspects over CA. In addition, the biological nature of GamC is better at describing activities of longer duration and higher intensity than those of shorter duration and lower intensity.

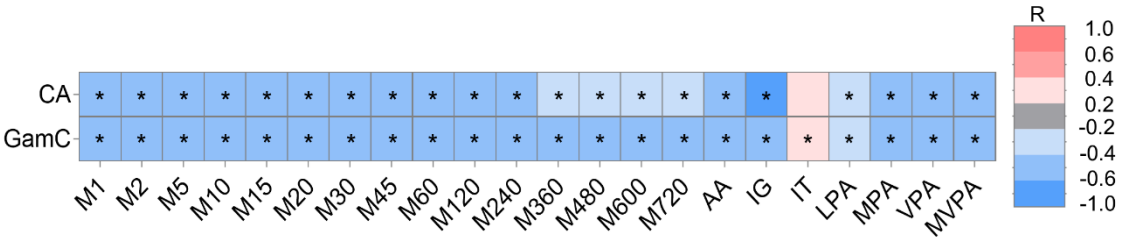


Figure 35. Evaluation of the association of age with parameters of PA. Evaluation of the association between accelerometer-derived variables indicative of PA levels with CA and GamC by Spearman correlation analysis. Correlation coefficients (R) are colour coded according to the scale and significant independent associations (FDR ≤ 0.05) are marked with an asterisk (*). The numeric data of this figure can be found in Table S12-S13 of the original publication [363].

We then examined the potential of GamC to monitor the effect of a healthy-aging intervention in centenarians **(Figure 28)**, since the significance of the findings in this age group is potentially higher than in younger ones [367]. Individuals in the centenarian group were randomized to follow (intervention group) or not follow (control group) a 3 month of strength exercise training. The intervention was based on the fact that exercise, including strength training [368], promotes CV health and is associated with a lower risk of all-cause mortality [369], but also that the effects of aging are modifiable [73,370].

The intervention showed a global beneficial effect in the trained group **(Figure 36a)**. As expected for the age-related physical decline, the PA variables mostly worsened after the intervention in the control group with a general decrease of the median ΔP_i of PA variables (some of them being significant) with large average effect sizes ($|\bar{r}|$ = 0.6) **(Figure 36a)**. However, the intervention group seemed able to buffer and moderately counteract this decline after the exercise-training period. Namely, an opposite trend of the median ΔP_i of the PA variables was observed (general increased values) that was accompanied by medium average effect sizes ($|\bar{r}|$ = 0.3) **(Figure 36a)**. In addition, well established biochemical parameters associated with increased risk of CVD, including cholesterol, LDL, CK and glucose, also worsened after the intervention in the control group showing moderate average effect sizes ($|\bar{r}|$ = 0.4) **(Figure 36b)**, but generally improved in the intervention group. Decreased median ΔP_i values of cholesterol, LDL, CK and glucose with large average effect sizes ($|\bar{r}|$ = 0.5) were observed in the intervened group **(Figure 36b)**. Interestingly, the levels of triglycerides decreased in both the control and intervention groups, which requires further investigation.

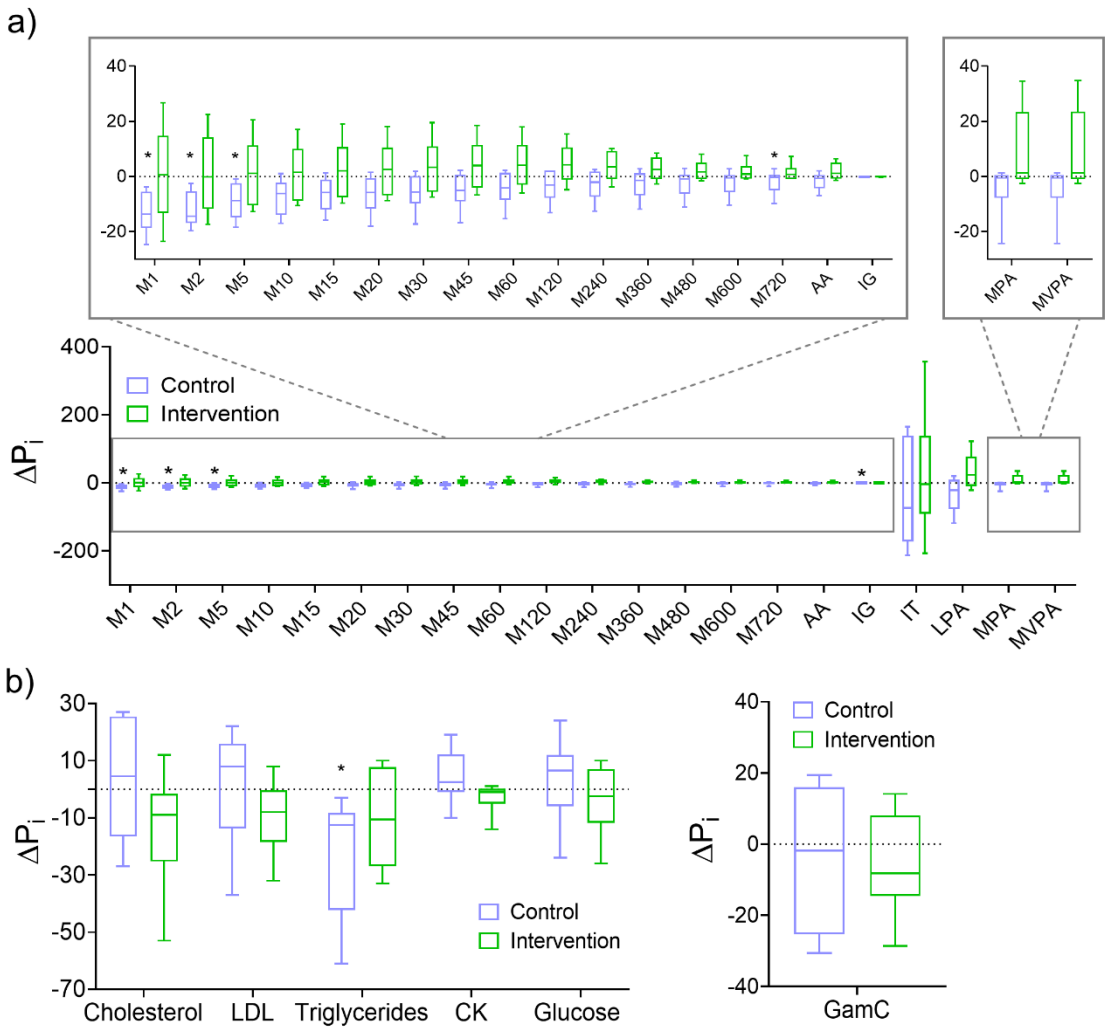


Figure 36. Evaluation of healthy-aging intervention study in centenarians. Effect of the healthy-aging intervention (strength exercise training for 3 months) in centenarians on the **a)** PA levels, **b)** biochemical parameters related to CV health and **c)** GamC in each control and intervention group. Box plots and whiskers represent the median and 2.5–97.5 percentiles of the differences after (II)-before (I) intervention (ΔP_i) (Significance results from Wilcoxon paired test ($P \leq 0.05$) for each control and intervention groups are marked with an asterisk (*). The numeric data of this figure can be found in Table S14-S15 of the original publication [363].

The improvement in the PA metrics and biochemical parameters in the intervention group was translated into an apparent decrease of the GamC ΔP_i median value (median (IQR) = -8.2 (12.8) years) with a medium effect size ($|r| = 0.4$), that was greater and less disperse than the differences observed in the control group (median (IQR) = -1.8 (31.3) years) with a small effect size ($|r| = 0.2$) **(Figure 36c)**.

Overall, GamC describes the current PA levels of individuals, with some improvements over CA, and shows a capacity to respond to an effective healthy-aging intervention in centenarians, highlighting its biological relevance.

5.3.5 Cardiac-enriched miR-490-3p is not suitable for cardiac BA monitoring in human plasma

The plasma levels of circulating miR-490-3p in the study cohort increase with CA, but do not correlate with GamC **(Figure 37)**. However, the plasmatic levels of the miR were too low challenging a reliable quantification. Therefore, the results rule out the value of miR-490-3p as circulating cardiac BA indicator.

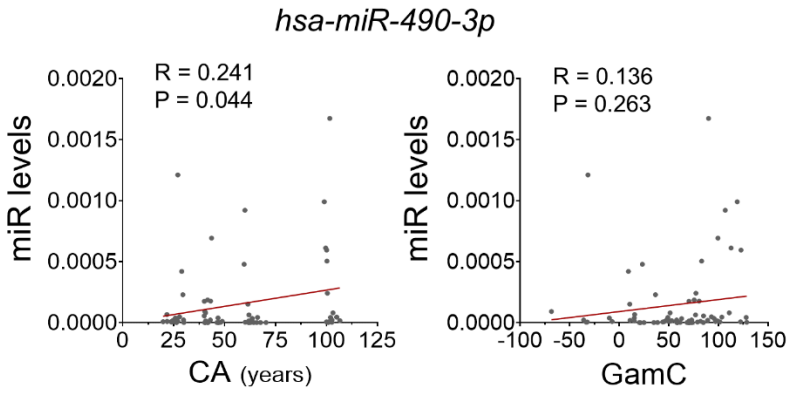


Figure 37. Evaluation of the relation with age and with GamC of the cardiac-enriched miR. Pearson correlation analysis between the absolute miR levels in human plasma (obtained by qPCR) of the cardiac-enriched miR-490-3p and CA (left) and GamC (right) in the study cohort (R: Pearson´s correlation coefficient, P: p-value, linear regression shown as red line).

5.4 Discussion

In our aging societies, the need to promote healthy aging claims for objective biomarkers that monitor the aging process beyond the simple recognition of age as indicated by the date of birth. This need is underpinned by the individual aging rate, which our work confirms is consistently unassociated with CA.

In this study, we report GamC, a simple blood-based BOA that describes the current BA of individuals in terms of CV health-related markers, specifically those that report the PA levels of individuals.

The age-related mechanisms observed in different populations may vary considerably [93,94]. However, the association between GamC and CA remains consistent across

study populations of different geographic origins. This is important because reliable BOAs with potential broad translational application are expected to demonstrate such consistency [371].

The observed association between GamC and CA is not as high as other established age predictors (e.g., PhenoAge, GrimAge [71,78]). However, a partial correlation with CA is consistent with an important consideration in the development of BOAs. They should be strongly, but not perfectly, related to CA in order to represent the age-related physiological variability of each individual [70]. However, the cut-off point for this distinction is unknown. Our group previously reported AppAge, a cardiac transcriptomic BOA constructed similarly to as GamC, but using almost 3,000 age-related genes [12]. AppAge had a correlation coefficient value with CA similar to that of GamC in the cohorts used in that study, namely R = 0.47, but described age-related cardiac transcriptomic changes and an aging phenotype better than CA. Similar but less sensitive results were obtained for a single gene (SenesAge)-based BOA (R = 0.24 with CA), suggesting that even a single functionally relevant age-related gene can describe molecular changes of cardiac aging. In other words, a high correlation of BOAs with CA does not necessarily imply a better ability to explain the biology of aging. Conversely, a less than perfect association may actually leave room for a biology-based personalized description of an individual's aging status. In this regard, GamC, which has correlation coefficients with CA ranging from 0.45 to 0.59 in the studied cohorts, but which describes both changes in biological processes at the transcriptomic level and phenotypes related to the CV health of individuals (specifically PA levels), is calculated based on the expression levels of only three age-related genes (*ABLIM1*, *CCR7* and *LEF1*). These genes are consistently dysregulated in CA in all the independent cohorts considered in this work [89,343–345,364–366]. In addition, our data shows that they contribute synergistically to the meaning of GamC, as their independent association with CA is improved by their combination in the BOA. GamC, in turn, demonstrates a differential nature, since it does not equally describe all age-related functional data of the study cohort. It describes the PA levels even better than CA for some PA-related variables, but is only marginally sensitive for ANS functional markers. This can most likely be explained by the age-related gene-specific contribution of *ABLIM1*, *CCR7* and *LEF1* to the biological meaning of GamC. Whether GamC can describe other age-related functional data requires further investigation. But indeed, our results support the idea that based on the biological data used to construct BOAs, each BOA is expected to describe different and/or complementary aspects of aging [70]. Taken together, our data suggest that *ABLIM1*, *CCR7* and *LEF1* are functionally relevant age-related genes able to capture different

aspects of an individual's aging biology in GamC, specifically PA-related, and, consequently, GamC is able to describe synchronous functional aspects of individuals regardless of (or perhaps exploiting) its partial correlation with CA. GamC is therefore able to estimate the CV-related BA of individuals in real time in terms of their PA levels.

Instead, we rule out miR-490-3p as potential indicator of heart-specific BA due to its poor presence in human plasma. This underscores the limited BOA capacity of the so far identified cardiac-enriched miRs to minimally invasively monitor human cardiac aging in comparison to other heart-specific BOAs such as those based on epigenetics or imaging [86,87]. Other cardiac BIO-AGEmiRs [12] could be evaluated for this purpose, however the tissue specificity would most likely be diminished in comparison to miR-490-3p.

Overall, this study proposes a simple and affordable BOA that gathers information about the current CV health status of individuals. Although the significance of the outcome of our intervention study in centenarians is limited by the small size of the study groups, it encourages further research into the ability of GamC to monitor BA in response to healthy-aging interventions. This is supported by the non-significant decrease of the median difference of GamC in the intervention group after the intervention, which accompanies the overall beneficial effect of exercise observed in their PA-related variables and biochemical parameters. Therefore, GamC's sensitivity to exercise training seems remarkable considering that the size of the effect of the intervention on the PA levels and in biochemical indicators is mostly medium too. Whether an intervention with a greater effect size (perhaps a longer training) would translate in greater changes in GamC in centenarians and whether the findings in centenarians hold true for other age groups remains to be explored.

For such purpose and beyond, the simplicity and consequent affordability of GamC (a blood sample and PCR test accessible to any basic molecular laboratory), together with the fact that its biological relevance is determined in relation to synchronous functional data rather than with mortality risk or disease outcome, makes GamC a valuable translational tool with potential application in real-time clinical decision-making and intervention monitoring.

5.5 Conclusions

We develop and characterize a simple and cost-effective BOA based on gene expression in blood, GamC, which meets capabilities of an aging clock. Unfortunately, heart-specific BOAs based on miRs could not be developed and the potential of cardiac miRs as biomarkers of heart age remains to be determined. We propose GamC as a suitable candidate BOA for future research to determine the real-time CV health risk in relation to BA, as well as to monitor the effect of healthy-aging interventions, which is beyond the capabilities of CA. Its simplicity enhances its clinical translational value to large populations. In conclusion, GamC is a relevant candidate BOA for promoting healthy-aging in relation to CV health, the leading cause of death worldwide.

General conclusions

Conclusiones generales

General conclusions

This thesis investigates the contribution of miRNAs to human cardiac aging as one of the underlying molecular mechanisms active during this process, gathers the state-of-the-art of miRNA-based therapies and their associated challenges and future opportunities, and explores their therapeutic value in combination with cutting-edge nanocarriers and their potential as biomarkers of aging. This integrative approach not only improves the understanding of miRNA-controlled molecular mechanisms underlying the process of cardiac aging but also strengthens the foundation for future biotechnology-based interventions aimed at promoting cardiac healthy aging and reducing the socioeconomic burden of cardiovascular diseases.

Identifying miR-24-2 as a key regulator of cardiac BA highlights its potential as therapeutic target for preserving cardiac function and development and mitigating age-related decline (Chapter 2). Chapter 3 shows how the success of translating miRNA-based therapies into clinical practices hinges on overcoming delivery limitations, particularly by combining nanotechnology and cardiac-targeting moieties for targeted delivery. Chapter 3 also underscores the lack of therapies for mir-24-2 in late preclinical phases of development, despite its implication in important cardiac pathologies such as heart failure, myocardial infarction or atrial fibrillation and being identified now as a key regulator of cardiac BA. These observations substantiate the development and characterization of anti-miR-24-2 treatments in Chapter 4.

Leveraging DNA nanotechnology, this chapter demonstrates the utility of biocompatible nanocarriers to deliver *in vitro* functional miR-24-2-sponging elements. These show regulatory capacity of miR-24-2 target genes in non-cardiac and, importantly, in cardiac cells. Together, the comprehensive profiling of the molecular perturbations induced by miR-24-2 overexpression in human cardiomyocytes (Chapter 2) and the proof of modulation of target genes through the sequestration of miR-24-2 (Chapter 4), provide evidence for the potential of the developed DNA nanocarriers to effectively modulate multiple age- and disease-related pathways that are central to cardiac function by manipulating this miR. Specifically, the modulation of the levels of miR-24-2 could translate into the synchronous manipulation of cardiomyocyte metabolism, intercellular communication, proteostasis or cardiac contraction and electrophysiology, among other relevant pathways, through its pleiotropic effect. To increase safety *in vivo*, the developed therapies could benefit from the targeting strategies described in Chapter 3. Finally, the creation of the GamC blood-based biomarker of aging in Chapter 5 demonstrates that simple systemic molecular signatures can predict cardiovascular health-related biological age, underscoring the translational potential of aging clocks in

clinical and preventive cardiology. Subsequently, the cardiac-enriched and genetically conserved miR-490-3p (Chapter 2), is discarded as heart-specific-biomarker of aging due to its low presence in plasma. However, other cardiac-conserved miRNAs, such as mir-24-2 (Chapter 2) or myomiRs (such as miR-1, miR-133a/b, miR-208a/b or miR-499), could still be evaluated despite of not being fully cardiac-specific, which theoretically reduces their capacity to specifically report on the biological state of the heart. Notwithstanding this, GamC may be a novel tool that can be used to monitor the effect of new therapies that promote age-related cardiovascular health, such as the one developed in Chapter 4. Definitely, GamC could contribute to fulfil the is increasing interest in understanding how biomarkers can guide interventions and improve our knowledge of aging biology by characterizing interventional outcomes.

In conclusion, this thesis advances the translation of miRNA research from molecular discovery to preclinical assessment of therapeutic applications for human cardiac aging. The thesis bridges fundamental insights into miRNA regulation and practical applications for age-related cardiac decline and dysfunction, paving the way for future interventions that promote healthy cardiac aging along with monitoring tools.

The following specific conclusions can be drawn from each chapter:

Chapter 2. Uncovering miR-24-2 key role in human cardiac biological aging.

- Through a cross-species approach, the genetically conserved miR-24-2 was identified as a key miR involved in human cardiac biological aging.
- Profiling the molecular miR-24-2 regulatory effect in human cardiomyocytes confirms its relation to aging via implication in several hallmarks of aging, both general and cardiac-related, and underscores the perturbation of other biological processes relevant for human cardiac function.
- Collectively, miR-24-2 positions as a promising therapeutic target for strategies aimed at preserving cardiac function while promoting healthy aging.

Chapter 3. Cardiac miRNA therapies: challenges and opportunities

- miRNAs constitute a new class of therapeutic molecules with proven preclinical efficacy for heart disease, and therefore, are capable of fulfilling unmet medical needs related to cardiovascular health, the first global cause of death.
- The development of miRNA therapeutics has stalled in the final preclinical phases due to challenges in heart delivery.

- Encapsulating miRNA therapeutics in nanocarriers and targeting them to the heart significantly enhances efficacy and reduces non-cardiac targeting, thereby enhancing safety over the typical naked delivery.
- Advances in miRNA biology and nanotechnology are paving the way for effective translational strategies in cardiac miRNA therapy. Despite remaining technical and biological hurdles, miRNA-based therapeutics show realistic potential to become future cardiac treatments.

Chapter 4. Development of anti-miRNA therapies to modulate miR-24-2

- Biocompatible anti-miR-24-2 DNA nanocarriers have been developed and characterized *in vitro*.
- Anti-miR-24-2 DNA nanocarriers hold promise as carriers for miRNA-based therapies in human cardiac cells, as shown by their ability to modulate miR-24-2 target genes relevant for cardiac function.
- These findings open new avenues for non-viral cardiac miRNA therapies, offering a biocompatible and controllable alternative to viral delivery systems.
- This study establishes a conceptual framework for next-generation nanostructured platforms that can address and modulate the multifactorial nature of cardiac aging and disease.

Chapter 5. Definition of biomarkers descriptive of cardiovascular health-related biological age

- A simple, cost-effective, blood-based biomarker of aging named GamC demonstrates functional capabilities of an aging clock in multiple independent cohorts supported by transcriptomic data.
- GamC can describe aspects of the current cardiovascular health of individuals, such as physical activity levels, and displays moderate responsiveness to a healthy-aging intervention in centenarians.
- The cardiac-enriched miR-490-3p is ruled out as heart-specific plasmatic biomarker of aging. Therefore, the potential of cardiac-enriched miRNAs as aging biomarkers remains to be determined.
- GamC presents as a candidate for the real-time assessment of cardiovascular health-related risks in relation to biological age and for monitoring the effects of healthy-aging interventions.

Conclusiones generales

Esta tesis investiga la contribución de los microARNs al envejecimiento cardíaco humano como uno de los mecanismos moleculares que subyacen este proceso, recopila el estado del arte de las terapias basadas en microARNs, sus desafíos asociados y oportunidades futuras, y explora su valor terapéutico en combinación con nanotransportadores de última generación y su potencial como biomarcadores del envejecimiento. Este enfoque integrador no solo mejora la comprensión de los mecanismos moleculares controlados por miARNs subyacentes al envejecimiento cardíaco, sino que también fortalece la base para futuras intervenciones biotecnológicas destinadas a promover un envejecimiento cardíaco saludable y reducir la carga socioeconómica de las enfermedades cardiovasculares.

La identificación de miR-24-2 como regulador clave de la edad biológica cardíaca resalta su potencial como diana terapéutica para preservar la función y el desarrollo cardíacos y mitigar el deterioro relacionado con la edad (Capítulo 2). El Capítulo 3 muestra cómo el éxito de la traducción de las terapias basadas en miARNs a la práctica clínica depende de superar las limitaciones de administración, especialmente mediante la combinación de nanotecnología y ligandos de direccionamiento cardíaco para una entrega específica. Este capítulo también subraya la falta de terapias para miR-24-2 en fases preclínicas tardías, a pesar de su implicación en patologías cardíacas importantes como insuficiencia cardíaca, infarto de miocardio o fibrilación auricular, y de haber sido identificado recientemente como regulador clave de la edad biológica cardíaca. Estas observaciones justifican el desarrollo y la caracterización de tratamientos anti-miR-24-2 en el Capítulo 4.

Aprovechando la nanotecnología de ADN, este capítulo demuestra la utilidad de nanotransportadores biocompatibles para entregar elementos funcionales que secuestran miR-24-2 *in vitro*. Estos muestran capacidad reguladora sobre los genes diana de miR-24-2 en células no cardíacas y, de manera importante, en células cardíacas. En conjunto, el perfil exhaustivo de las perturbaciones moleculares inducidas por la sobreexpresión de miR-24-2 en cardiomiocitos humanos (Capítulo 2) y la prueba de la modulación de genes diana mediante el secuestro de miR-24-2 (Capítulo 4), proporcionan evidencia del potencial de los nanotransportadores de ADN desarrollados para modular efectivamente múltiples vías relacionadas con la edad y la enfermedad que son centrales para la función cardíaca manipulando este miARN.

Específicamente, la modulación de los niveles de miR-24-2 podría traducirse en la manipulación sincrónica del metabolismo de los cardiomiocitos, la comunicación

intercelular, la proteostasis o la contracción y la electrofisiología cardíaca, entre otras vías relevantes, a través de su efecto pleiotrópico. Para aumentar la seguridad *in vivo*, las terapias desarrolladas podrían beneficiarse de las estrategias de direccionamiento descritas en el Capítulo 3. Finalmente, la creación del biomarcador sanguíneo GamC en el Capítulo 5 demuestra que patrones moleculares sistémicos simples pueden predecir la edad biológica relacionada con la salud cardiovascular, resaltando el potencial traslacional de los "relojes de envejecimiento" en cardiología clínica y preventiva. Posteriormente, el miR-490-3p, enriquecido en el corazón y conservado genéticamente (Capítulo 2), es descartado como biomarcador cardíaco específico de envejecimiento debido a su baja presencia en plasma. Sin embargo, otros miARNs cardíacos conservados, como mir-24-2 (Capítulo 2) o los myomiRs (miR-1, miR-133a/b, miR-208a/b o miR-499), podrían seguir evaluándose a pesar de no que no sean completamente específicos del corazón, lo que teóricamente limita su capacidad para reflejar específicamente el estado biológico del órgano.

No obstante, GamC podría ser una herramienta novedosa para monitorear el efecto de nuevas terapias que promuevan la salud cardiovascular relacionada con la edad, como la desarrollada en el Capítulo 4. Definitivamente, GamC podría contribuir a satisfacer el creciente interés en comprender cómo los biomarcadores pueden guiar intervenciones y mejorar el conocimiento de la biología del envejecimiento mediante la caracterización de los resultados de las intervenciones.

En conclusión, esta tesis avanza en la traducción de la investigación sobre miARNs desde el descubrimiento molecular hasta la evaluación preclínica de aplicaciones terapéuticas para el envejecimiento cardíaco humano. La tesis conecta conocimientos fundamentales sobre la regulación de los miARNs con aplicaciones prácticas para el deterioro y la disfunción cardíaca relacionados con la edad, allanando el camino para futuras intervenciones que promuevan un envejecimiento cardíaco saludable junto con herramientas de monitoreo.

De cada capítulo se pueden extraer las siguientes conclusiones específicas:

Capítulo 2. Descubrimiento del papel clave de miR-24-2 en el envejecimiento biológico cardíaco humano

- A través de un enfoque inter-especies, se identificó el miR-24-2, conservado genéticamente, como un miARN clave involucrado en el envejecimiento biológico cardíaco humano.
- El perfil del efecto regulador molecular de miR-24-2 en cardiomiocitos humanos confirma su relación con el envejecimiento mediante su implicación en varios pilares del envejecimiento, tanto generales como específicos del corazón, y subraya la perturbación de otros procesos biológicos relevantes en la función cardíaca humana.
- Colectivamente, miR-24-2 se posiciona como una diana terapéutica prometedora para estrategias dirigidas a preservar la función cardíaca al mismo tiempo que promueve un envejecimiento saludable.

Capítulo 3. Terapias cardíacas basadas en miARNs: desafíos y oportunidades

- Los miARNs constituyen una nueva clase de moléculas terapéuticas con eficacia preclínica probada para las enfermedades cardíacas y, por lo tanto, son capaces de satisfacer necesidades médicas no cubiertas relacionadas con la salud cardiovascular, la primera causa de muerte a nivel mundial.
- El desarrollo de terapias con miARN se ha estancado en las fases preclínicas finales debido a los retos que plantea su administración al corazón.
- La encapsulación de terapias basadas en miARNs en nanotransportadores y su direccionamiento al corazón aumenta significativamente la eficacia y reduce la entrega no cardíaca, mejorando así la seguridad respecto a la típica entrega sin encapsulación.
- Los avances en biología de miARNs y nanotecnología están allanando el camino para estrategias traslacionales efectivas en terapias cardíacas con miARNs. A pesar de los obstáculos técnicos y biológicos restantes, las terapias basadas en miARNs muestran un potencial realista de convertirse en futuros tratamientos cardíacos.

Capítulo 4. Desarrollo de terapias anti-miARN para modular miR-24-2

- Se desarrollaron y caracterizaron *in vitro* nanotransportadores de ADN anti-miR-24-2 biocompatibles.
- Estos nanotransportadores muestran capacidad para modular genes diana relevantes para la función cardíaca en células cardíacas humanas.
- Los hallazgos abren nuevas vías para terapias cardíacas con miARNs no virales, ofreciendo una alternativa biocompatible y controlable a los sistemas de entrega viral.
- Este estudio establece un marco conceptual para plataformas nanostructuradas de próxima generación capaces de abordar y modular la naturaleza multifactorial del envejecimiento y la enfermedad cardíaca.

Capítulo 5. Definición de biomarcadores descriptivos de la edad biológica relacionada con la salud cardiovascular

- A simple, económico y biomarcador de edad basado en sangre llamado GamC demuestra capacidades funcionales como reloj de envejecimiento en múltiples cohortes independientes respaldadas por datos transcriptómicos.
- GamC puede describir aspectos de la salud cardiovascular actual de los individuos, como niveles de actividad física, y muestra una respuesta moderada a intervenciones de envejecimiento saludable en centenarios.
- El miR-490-3p, enriquecido en el corazón, queda descartado como biomarcador plasmático cardíaco específico del envejecimiento. Por lo tanto, el potencial de los miARNs enriquecidos en corazón como biomarcadores de envejecimiento aún debe determinarse.
- GamC se presenta como un candidato para la evaluación en tiempo real de riesgos relacionados con la salud cardiovascular en relación con la edad biológica y para el monitoreo de los efectos de intervenciones de envejecimiento saludable.

Study limitations, future work, scientific production and academic activities

Study limitations and future work

In *Chapter 2*, we show the subtle but broad regulatory role of miR-24-2 at the protein and RNA level in CMs, although the number of identified proteins in the proteomic analysis limits our conclusions. However, this is an inherent limitation of the technique which remains to be addressed only by advances in proteomic analysis. Future work will focus on the generation of hiPSC lines to overexpress other conserved human upregulated BIO-AGEmiRs such as mir-195 or mir-497, although less expressed in animal and human LV and in iCMs, to further decipher their role during cardiac BA.

In *Chapter 4*, we validate the functional effect of anti-mir-24-2 DNCs in iCMs only at the RNA level and in a short treatment period. Future work will focus on the validation of anti-mir-24-2 DNCs efficacy at the protein level and at different time points. In addition, it will focus on developing strategies of cardiac targeted delivery, such as those described in Chapter 3, with application in *in vivo* assays.

In *Chapter 5*, we show that *ABLIM1*, *CCR7* and *LEF1* expression are related with age in a gender-independent manner; however, the low presence of females in the study cohort may limit our conclusions. The small number of centenarians in the study also limits the conclusions of the healthy-aging intervention, which was performed only in this age group. GamC shows potential as a BOA related to PA levels and biochemical parameters, but future work will focus on studying its association in independent and larger populations, and with different healthy-aging interventions, such as diet-related or long-term exercise applicated at different age groups. Future work also will study the use of BIO-AGEmiRs such as mir-24-2 or myomiRs as cardiac biomarkers of BA, although not heart-specific.

Scientific production and academic activities

▪ Publications in peer-reviewed journals derived from the thesis

Postigo A*., **Hernández-Bellido N***., Sánchez-Barat M., García-Mendívil L., Pueyo E., del Barrio J., Hernández-Ainsa S. ✉, Ordovás L. ✉ (2024). DNA-Based Nanocarriers to Sequester Altered microRNAs in Cardiac Dysfunction. *Advanced Therapeutics, 2400247.* https://doi: 10.1002/adtp.202400247 (*Equal contribution, ✉Corresponding author)

Hernández-Bellido N. ✉, Hernández-Vicente A., García-Mendívil L., Ramos-Marquès E., Hernando D., Cebollada A., Köhler R., Garatachea N., Pueyo E., Ordovás L. ✉ (2025). A simple blood biomarker based on gene expression describes cardiovascular health-related biological age. *Geroscience.* https://doi.org/10.1007/s11357-025-01784-6 (✉Corresponding author)

Hernández-Bellido, N.✉, Hernández-Ainsa S, Köhler R, Ordovás L.✉ (2025) "Nanotechnology-driven heart targeting to fulfil the potential of cardiac miR therapies". (2025). *International Journal of Pharmaceutics*. https://doi.org/10.1016/j.ijpharm.2026.126643. (✉Corresponding author)

▪ Conference proceedings derived from collaborations during the thesis

Sánchez-Barat M., **Hérnandez-Bellido N.,** Postigo A., Ripalda-Paredes M., Hernández-Ainsa S., Ordovás L. (2024). Desarrollo de nanotransportadores de DNA de vanguardia con capacidad cardioregenerativa utilizando el potencial terapéutico de los microRNAs. *Jornada De Jóvenes Investigadores Del I3A, 12.* https://doi.org/10.26754/jjii3a.202410625

Gómez C., **Hernández-Bellido N**., García-Mendívil L., Sánchez-Barat M., Paz-Artigas L., Ciriza J., Ordovás L. (2024). Exploring shRNA-based therapy to prevent chemotherapy-induced cardiotoxicity. *Jornada De Jóvenes Investigadores Del I3A, 12.* https://doi.org/10.26754/jjii3a.202410644

Garrido-Huéscar E., Vandeweyer L, García-Mendívil L., **Hernández-Bellido N**., Pueyo E., de Vos W. H., Ordovás L. (2023). Cardiomiocitos derivados de células pluripotentes inducidas (hiPSC-CM) con progerina inducible para estudiar envejecimiento cardiaco. *Jornada De Jóvenes Investigadores Del I3A, 11.* https://doi.org/10.26754/jjii3a.20239068

▪ Congresses and conferences derived from collaborations during the thesis

Ordovás L., **Hernández-Bellido N.**, Postigo A., Sánchez-Barat M., Ripalda-Paredes M., Usón S., Ruíz-Araca JJ., Candeal E., Ramírez J., Ranera B., Valius M., Gorospe M., del Barrio J., Hernández-Ainsa S. "miR-24-2 modulation in cardiac dysfunction through DNA nanotechnology". NanoBio&Med2025, Barcelona (Spain). 2025. Poster.

Sánchez-Barat M., **Hernández-Bellido N.**, Postigo A., Ripalda-Paredes M., Hernández-Ainsa S, Ordovás L. "DNA nanoparticles for cardiac regeneration with miR-199a-3p". NanoBio&Med2025, Barcelona (Spain). 2025. Poster.

Sánchez-Barat M., **Hernández-Bellido N.**, Postigo A., Ripalda-Paredes M., Ordovás L., Hernández-Ainsa S. "Leveraging nucleic acid nanotechnology to boost the therapeutic potential and cardiac accumulation of regenerative miRNAs". Conexión Nanomedicina CSIC, Madrid (Spain). 2024. Poster.

Hernández-Ainsa S., Postigo A., **Hernández-Bellido N.**, Sánchez Barat M., Ripalda-Paredes M., del Barrio J., Ordovás L. "Nucleic acid-based nanostructures against cardiac dysfunction". Conexión Nanomedicina CSIC, Madrid (Spain). 2024. Oral communication.

Sánchez-Barat M., **Hernández-Bellido N.**, Postigo A., Ripalda-Paredes M., del Barrio J., Ordovás L., Hernández-Ainsa S. "Nanotecnología de ácidos nucleicos para la entrega de microRNA con potencial cardio-regenerativo". VI QuimBioQuim: Congreso de Jóvenes Químicos y Bioquímicos Terapéuticos, Jaén (Spain). 2024. Poster.

Ripalda-Paredes M., Sánchez Barat M., Postigo A., **Hernández-Bellido N.**, del Barrio J., Ordovás L., Hernández-Ainsa S. "Exploiting the therapeutic potential of microRNAs and DNA nanotechnology to address cardiac disease". XIII Reunión de Ácidos Nucleicos y Nucleósidos, Alcalá de Henares (Spain). 2024. Oral communication.

Sánchez-Barat M., **Hernández-Bellido N.**, Postigo A., Ripalda-Paredes M., Hernández-Ainsa S., Ordovás L. "Desarrollo de nanotransportadores de DNA de vanguardia con capacidad cardioregenerativa utilizando el potencial terapéutico de los microRNAs". V Jornada del I3A - XIII Jornada de Jóvenes Investigadores/as, Zaragoza (Spain). 2024. https://doi.org/10.26754/jjii3a.202410625. Poster and congress proceeding.

Sánchez-Barat M., **Hernández-Bellido N.**, Postigo A., Hernández-Ainsa S., Ordovás L. "Exploiting the therapeutic potential of microRNAs and DNA nanotechnology to create novel cardioregenerative treatments ". Cellular Biology of the Heart & Myocardial Function (CBFH) Biennial meeting, Naples (Italy). 2023. Poster.

Sánchez Barat M., **Hernández-Bellido N.,** Postigo A., Ordovás L., Hernández-Ainsa S. "Development of customised DNA-based nanostructures to treat heart disease by gene therapy". XXXIX Reunión Bienal de Química, Zaragoza (Spain). 2023. Poster.

Hernández-Ainsa S., Postigo A., **Hernández-Bellido N.**, Sánchez Barat M., Sarasa L., Ordovás L., del Barrio J. "Tailoring DNA-based nanostructures for the delivery of therapeutic agents", XXXIX Reunión Bienal de Química, Zaragoza (Spain). 2023. Oral communication.

Sánchez-Barat M., **Hernández-Bellido N.**, Postigo A., Ordovás L., Hernández-Ainsa S. "Towards post-ischemic cardiac regeneration with microRNA therapy and customized

DNA-based nanostructures". 12th Biennial Congress of the Spanish Society in Gene and Cellular Therapy (SETGYC), Pamplona (Spain). 2023. Poster.

Postigo A., **Hernández-Bellido N.**, Ordovás L., del Barrio J., Hernández-Ainsa S. "DNA nanostructures customized for therapeutic delivery". 5th Spanish Conference on Biomedical Applications of Nanomaterials SBAN, Madrid (Spain). 2022. Oral communication.

Postigo A., Marín P., **Hernández-Bellido N.**, Ordovás L., del Barrio J., Hernández-Ainsa S. "Development of tailored DNA nanostructures for anticancer drug delivery". XXXVIII Reunión Bienal RSEQ", Granada (Spain). 2022. Poster.

Gómez-Moreno G., **Hernández-Bellido N.**, García-Mendívil L., Sánchez-Barat M., Paz-Artigas L., Ciriza L., Ordovás L. "Exploring shRNA-based therapy to prevent chemotherapy-induced cardiotoxicity", "XIII Jornada de Jóvenes Investigadores/as", Zaragoza (Spain). 2024. Poster

Gómez-Moreno G., **Hernández-Bellido N.,** García-Mendívil L., Sánchez-Barat M., Paz-Artigas L., Ciriza L., Ordovás L. "Towards advanced therapies for chemotherapy-induced cardiotoxicity prevention", "III Encuentro de investigadores predoctorales en investigaciones biomédicas de Aragón (ipIBA)", Zaragoza (Spain). 2024. Poster

García-Mendívil L., **Hernández-Bellido N.**, Sánchez-Barat M., Pérez-Zabalza M., Garrido-Huéscar E., Vallejo-Gil JM., Matamala-Adell M., Sorribas-Berjón JF., Bellido-Morales JA., Vaca-Núñez AS., Ballester-Cuenca C., Verfaillie CM., Pueyo E., Ordovás L. "Progerin is an unlikely contributor to natural cardiac aging, but promotes age-related phenotypes *in vitro* ", "Cellular Biology of the Heart & Myocardial Function (CBFH) Biennial meeting 2023", Naples (Italy). 2023. Poster.

Garrido-Huéscar E., Vandeweyer L., García-Mendívil L., **Hernández-Bellido N.**, Pueyo E., De Vos WH., Ordovás L. "Induced pluripotent stem cell-derived cardiomyocytes (hiPSC-CM) with inducible progerin to study cardiac aging". "XII Jornada de Jóvenes Investigadores", Instituto de Investigación en Ingeniería de Aragón (I3A), Zaragoza (Spain). 2023. Poster.

Garrido-Huéscar E., Vandeweyer L., García-Mendívil L., **Hernández-Bellido N.**, Pueyo E., De Vos WH., Ordovás L. "Induced pluripotent stem cell-derived cardiomyocytes (hiPSC-CM) with inducible progerin to study cardiac aging", "Seminarios iPIBA day", Zaragoza (Spain). 2023. Poster.

Garrido-Huéscar E., Vandeweyer L., García-Mendívil L., **Hernández-Bellido N.**, Pueyo E., De Vos WH., Ordovás L. "A progerin-inducible human Induced Pluripotent Stem Cell line to study cardiac cell aging". "4th International Meeting on Laminopathies", Madrid (Spain). 2023. Poster.

Garrido-Huéscar E., García-Mendívil L., **Hernández-Bellido N.**, Sánchez-Barat M., Pérez-Zabalza M., Pueyo E., Ordovás L. "Development of new human models to determine age related cardiotoxicity of drugs". "Stem cells and stem cell models in disease & health (SCMiDH) symposium", Hasselt (Belgium). 2022. Poster.

García-Mendívil L., **Hernández-Bellido N.**, Sánchez-Barat M., Pérez-Zabalza M., Garrido-Huéscar E., Oliveros JC., Torres-Pérez R., Ramos-Marquès E., Pueyo E., Ordovás L. "Envejecimiento cardiaco humano: transcriptómica y desarrollo de modelos

celulares". "II Congreso Anual de Estudiantes de Doctorado (CAED)", Elche (Spain). 2022. Oral communication.

García-Mendívil L., **Hernández-Bellido N.**, Sánchez-Barat M., Pérez-Zabalza M., Garrido-Huéscar E., Oliveros JC., Torres-Pérez R., Ramos-Marquès E., Pueyo E., Ordovás L. "Envejecimiento cardiaco humano: transcriptómica y desarrollo de modelos celulares de envejecimiento". "X Jornadas de jóvenes investigadores del I3A", Zaragoza (Spain). 2021. Oral communication.

García-Mendívil L., **Hernández-Bellido N.**, Sánchez-Barat M., Pérez-Zabalza M., Garrido-Huéscar E., Oliveros JC., Torres-Pérez R., Ramos-Marquès E., Pueyo E., Ordovás L. "*In vivo* and *in vitro* cardiac aging: developing of cellular aging models". "XIX Congress of the Spanish Society of Cellular Biology", Boadilla del Monte (Spain). 2021. Poster.

▪ Teaching collaboration and bachelor thesis supervision

─ Co-Supervisor of Biotechnology Bachelor´s thesis entitle "Study of microRNAs related to cardiac aging". Course 2023/2024. University of Zaragoza (Spain).

─ Co-Supervisor of Biotechnology laboratory summer internship. 2023. University of Zaragoza (Spain)

─ Co-Supervisor of Biotechnology Bachelor´s thesis entitle "Analysis of interaction of microRNAs related to cardiac aging and their target genes". Course 2022/2023. University of Zaragoza (Spain).

─ Co-Supervisor of laboratory practices of Biochemistry of Chemistry Bachelor. Course 2023/2024. University of Zaragoza (Spain).

─ Co-Supervisor of laboratory practices of Clinical Biotechnology of Biotechnology Bachelor. Course 2022/2023 and 2023/2024. University of Zaragoza (Spain)

▪ Courses

─ Introduction to programming in MATLAB. Escuela de Doctorado, University of Zaragoza (Spain). 2024.

─ Editing and processing of texts in LaTex. Grupo G9 Universidades, University of Oviedo (Spain). 2024.

Annexes

Figure A1. Vector sequence used for hiPSC recombinant line to overexpress mir-24-2-tdT. Brown letters indicate the tetracycline operator and CMV minimal promoter (bold), green the 3Flag, red letters the tdT, blue the pri-miR, dark blue the 5p and 3p strands of miR-24-2 and grey the polyadenylation signal.

CGAGTTTACTCCCTATCAGTGATAGAGAACGATGTCGAGTTTACTCCCTATCAGTGATAGAGAACGTATGTCGAGTT
TACTCCCTATCAGTGATAGAGAACGTATGTCGAGTTTACTCCCTATCAGTGATAGAGAACGTATGTCGAGTTTATCC
CTATCAGTGATAGAGAACGTATGTCGAGTTTACTCCCTATCAGTGATAGAGAACGTATGTCGAGGT**AGGCGTGTAC**
GGTGGGAGGCCTATATAAGCAGAGCTCGTTTAGTGAACCGTCAGATCGCTTAAGGCCACCATGGACTACAAAGAC
CATGACGGTGATTATAAAGATCATGATATTGATTACAAGGATGACGATGACGACCGGTGGAGATATCCATATGCCAC
CATGGTGAGCAAGGGCGAGGAGGTCATCAAAGAGTTCATGCGCTTCAAGGTGCGCATGGAGGGCTCCATGAACG
GCCACGAGTTCGAGATCGAGGGCGAGGGCGAGGGCCGCCCCTACGAGGGCACCCAGACCGCCAAGCTGAAGGT
GACCAAGGGCGGCCCCCTGCCCTTCGCCTGGGACATCCTGTCCCCCCAGTTCATGTACGGCTCCAAGGCGTACGT
GAAGCACCCCGCCGACATCCCCGATTACAAGAAGCTGTCCTTCCCCGAGGGCTTCAAGTGGGAGCGCGTGATGAA
CTTCGAGGACGGCGGTCTGGTGACCGTGACCCAGGACTCCTCCCTGCAGGACGGCACGCTGATCTACAAGGTGA
AGATGCGCGGCACCAACTTCCCCCCCGACGGCCCCGTAATGCAGAAGAAGACCATGGGCTGGGAGGCCTCCACC
GAGCGCCTGTACCCCCGCGACGGCGTGCTGAAGGGCGAGATCCACCAGGCCCTGAAGCTGAAGGACGGCGGCC
ACTACCTGGTGGAGTTCAAGACCATCTACATGGCCAAGAAGCCCGTGCAACTGCCCGGCTACTACTACGTGGACA
CCAAGCTGGACATCACCTCCCACAACGAGGACTACACCATCGTGGAACAGTACGAGCGCTCCGAGGGCCGCCAC
CACCTGTTCCTGGGGCATGGCACCGGCAGCACCGGCAGCGGCAGCTCCGGCACCGCCTCCTCCGAGGACAACAA
CATGGCCGTCATCAAAGAGTTCATGCGCTTCAAGGTGCGCATGGAGGGCTCCATGAACGGCCACGAGTTCGAGAT
CGAGGGCGAGGGCGAGGGCCGCCCCTACGAGGGCACCCAGACCGCCAAGCTGAAGGTGACCAAGGGCGGCCC
CCTGCCCTTCGCCTGGGACATCCTGTCCCCCCAGTTCATGTACGGCTCCAAGGCGTACGTGAAGCACCCCGCCGA
CATCCCCGATTACAAGAAGCTGTCCTTCCCCGAGGGCTTCAAGTGGGAGCGCGTGATGAACTTCGAGGACGGCGG
TCTGGTGACCGTGACCCAGGACTCCTCCCTGCAGGACGGCACGCTGATCTACAAGGTGAAGATGCGCGGCACCAA
CTTCCCCCCCGACGGCCCCGTAATGCAGAAGAAGACCATGGGCTGGGAGGCCTCCACCGAGCGCCTGTACCCCC
GCGACGGCGTGCTGAAGGGCGAGATCCACCAGGCCCTGAAGCTGAAGGACGGCGGCCACTACCTGGTGGAGTTC
AAGACCATCTACATGGCCAAGAAGCCCGTGCAACTGCCCGGCTACTACTACGTGGACACCAAGCTGGACATCACC
TCCCACAACGAGGACTACACCATCGTGGAACAGTACGAGCGCTCCGAGGGCCGCCACCACCTGTTCCTGTACGGC
ATGGACGAGCTGTACAAGTAAACGCGTGGCGCGCCGCTGCTTGTGAGCAGGGTCCACACCAAGTCGTGTTCACAG
TGGCTAAGTTCCGCCCCCCAGGCCCTCACCTCCTCTGGCCTTGCCGCCTGTCCCCTGCTGCCGCCTGTCTGCCTG
CCATCCTGCTGCCTGGCCTCCCTGGGCTCTGCCTCCCGTGCCTACTGAGCTGAAACACAGTTGGTTTGTGTACACT
GGCTCAGTTCAGCAGGAACAGGGTCAAGCCCCCTTGGAGCCTGCAGCCCCTGCCTTCCCTGGGTGGGCTGATGC
TTGGAGCAGAGATGAGGACTCAGAATCAGACCTGTGTCTGGAGGAGGGATGTGGTGGGTGGGGTTGGCTGGGCC
CAAATGTGTGCTGCAGGCCCTGATCCCCAACTCTGCAACTGGGGACCCCTGCATGGCCACAGCTCAGGCTGGGCT
GTGGTGCCAGCATAGATAGGTGGGTGAGTGGGTGGCCCTTCCATTAAAAGGGAAGCCAGCTGTGTCCTTTCCGGG
CCTGGAGGCTTTTAATTAAACGCGTGGGGGAGGCTAACTGAAACACGGAAGGAGACAATACCGGAAGGAACCCGC
GCTATGACGGCAATAAAAAGACAGAATAAAACGCACGGTGTTGGGTCGTTTGTTCATAAACGCGGGGTTCGGTCCC
AGGGCTGGCACTCTGTCGATACCCCACCGAGACCCCATTGGGGCCAATACGCCCGCGTTTCTTCCTTTTCCCCAC
CCCACCCCCCAAGTTCGGGTGAAGGCCCAGGGCTCGCAGCCAACGTCGGGGCGGCAGGCCCTGCCATAG

Table A1. Method details for RNA processing and gene expression analysis.

Species	Tissue/ Cells	Assay	RNA processing		Gene expression analysis		
			Extraction	Retrotranscription	qPCR kit	Housekeeping genes	Calculation of gene expression
Mouse	LV	Gene profiling	TRI Reagent Solution (Thermo Fisher) and RNeasy Mini Kit (Quiagen)	Maxima Reverse Transcriptase (Thermo Fisher) + Random Hexamers (Thermo Fisher)	KAPA SYBR® FAST qPCR Master Mix (2X) Kit (KAPA Biosystems)	*GAPDH*, *IPO8* and *YWHAZ*	Relative to an arbiratry sample (RGE) or absolut miR expression (AME)
		pri-miR profiling		Maxima Reverse Transcriptase (Thermo Fisher) + Oligo (dT)20 (Thermo Fisher)	KAPA SYBR® FAST qPCR Master Mix (2X) Kit (KAPA Biosystems)	*GAPDH*, *IPO8* and *YWHAZ*	
		miR profiling		miR-X miRNA First Strand Synthesis (Takara)	KAPA SYBR® FAST qPCR Master Mix (2X) Kit (KAPA Biosystems)	*RNU6*	
Monkey	LV	Gene profiling	TRI Reagent Solution (Thermo Fisher) and RNeasy Mini Kit (Quiagen)	Maxima Reverse Transcriptase (Thermo Fisher) + Random Hexamers (Thermo Fisher)	KAPA SYBR® FAST qPCR Master Mix (2X) Kit (KAPA Biosystems)	*GAPDH*, *IPO8* and *YWHAZ*	
		pri-miR profiling		Maxima Reverse Transcriptase (Thermo Fisher) + Oligo (dT)20 (Thermo Fisher)	KAPA SYBR® FAST qPCR Master Mix (2X) Kit (KAPA Biosystems)	*GAPDH*, *IPO8* and *YWHAZ*	
		miR profiling		miR-X miRNA First Strand Synthesis (Takara)	KAPA SYBR® FAST qPCR Master Mix (2X) Kit (KAPA Biosystems)	*RNU6*	
Human	LV	miR profiling	All Prep DNA/RNA/miRNA Universal Kit (Quiagen)	microScript cDNA Synthesis Kit (Norgen)	NZYSupreme qPCR Probe Master Mix (2x) (Nzytech)	*RNU6*	Absolute miR expression (AME)
	iCM	miR profiling					
		Transcriptomic and qPCR validation (gene and pre-miR profiling)	Direct-zol™ RNA Miniprep (Zymo Research)	PrimeScript RT Master Mix (Takara)	NZYSupreme qPCR Probe Master Mix (2x) (Nzytech)	*POLR2A*	Relative to induced iCMs of the mir-24-2^{-} line

Table A2. PCR primers used in the thesis (F: Forward, R: Reverse).

Chapter	*Gene/MIR/mir/miR*		Specie	Sense	Sequence
	Name	ID			
5	*ABLIM1*	3983	H	F	GAGATTACCAGACACTCCCAG
5	*ABLIM1*	3983	H	R	CCAACATGTTGGGCATAGAC
2/4	*ATP2B4*	493	H	F	GCCCAAGTCAAATACGGTG
2/4	*ATP2B4*	493	H	R	GGACTTCTTGACATGGTCAGAT
5	*CCR7*	1236	H	F	TGGCTCTCCTTGTCATTTTCC
5	*CCR7*	1236	H	R	TTAAAGTTCCGCACGTCCTT
5	*Cel-miR-39-3p*	MIMAT0000010	H	F	CACCGGGTGTAAATCAGCTTG
2/4	*CRYAB*	1410	H	F	AAGAGCGCCAGGATGAAC
2/4	*CRYAB*	1410	H	R	GGTGAGAGGGTCTACATCAG
2	*FOXO1*	2308	H	F	GAGGGTTAGTGAGCAGGTT
2	*FOXO1*	2308	H	R	AGGGAGTTGGTGAAAGACATC
5	*GUSB*	2990	H	F	GCCCATTATTCAGAGCGAGTA
5	*GUSB*	2990	H	R	GTTTTTGATCCAGACCCAGATG
2	*KCNJ8*	3764	H	F	ATGTCAGGTCTTTCACTTCTGCT
2	*KCNJ8*	3764	H	R	TCATCCTCCCTCCAAACCCA
5	*LEF1*	51176	H	F	CGATGACGGAAAGCATCCAG
5	*LEF1*	51176	H	R	TGTACCCGGAATAACTCGAGTA
2	*miR-195-3p*	MIMAT0004615	H	F	TGGCTGTGCTGCTCCAA
2	*miR-195-5p*	MIMAT0000461	H	F	GCTAGCAGCACAGAAATATTGG
2/4	*mir-24-2*	MI0000081	H	F	CCTGTTCCTGCTGAACTGAG
2/4	*mir-24-2*	MI0000081	H	R	TGCCTACTGAGCTGAAACAC
2	*miR-24-2-5p*	MIMAT0004497	H	F	CCTACTGAGCTGAAACACAGA
2	*miR-24-3p*	MIMAT0000080	H	F	GGCTCAGTTCAGCAGGA
2	*miR-3916*	MIMAT0018190	H	F	AAGAGGAAGAAATGGCTGGT
5	*miR-4461*	MIMAT0018983	H	F	GATTGAGACTAGTAGGGCTAGG
5	*miR-490-3p*	MIMAT0002806	H	F	CCTGGAGGACTCCATGCT
2	*miR-497-3p*	MIMAT0004768	H	F	AAACCACACTGTGGTGTTAGA
2	*miR-497-5p*	MIMAT0002820	H	F	GCAGCACACTGTGGTTTG
2	*miR-6080*	MIMAT0023705	H	F	TCTAGTGCGGGCGTTCC
5	*NELL2*	4753	H	F	CCACCTACCGAGAATTTGAGTC
5	*NELL2*	4753	H	R	TGGGCAGATTAGAGTTTCACAC
2/4	*POLR2A*	5430	H	F	CTCCCTCATCATACCTGGTCA
2/4	*POLR2A*	5430	H	R	CATTCTCCACCACCACCTTG
2	*RNU6-1*	26827	H	F	CGCAAGGATGACACGCAAAT
2/4	*ROBO2*	6092	H	F	GGAAGTGGCATTGTTACGAG
2/4	*ROBO2*	6092	H	R	CAGCTGCCACTACAACATC
2	*TCAP*	8557	H	F	ATCTGACACTGTCCACACG
2	*TCAP*	8557	H	R	GGTGTCCTCCTCATGCAG
5	*UBE2D2*	7322	H	F	GTACTCTTGTCCATCTGTTCTCTG
5	*UBE2D2*	7322	H	R	CCATTCCCGAGCTATTCTGTT
2	*Actn2*	11472	M	F	GATTCTGGCTTCTGATAAGCCT
2	*Actn2*	11472	M	R	GAGAAGGCAGTGTAGTCCAG
2	*Adra1a*	11549	M	F	ATGCCCATTGGGTCCTTC
2	*Adra1a*	11549	M	R	GATGCAACTATTTAGGTACCCAAG
2	*Atp1a2*	98660	M	F	CCACCACTGCGGAAAATG
2	*Atp1a2*	98660	M	R	GCCCTTAGACAGATCCACTTG
2	*Atp1b1*	11931	M	F	CGTGCTAAACATCATCAGGTTC
2	*Atp1b1*	11931	M	R	GGAACATTGCCACAGTCCT
2	*Cacna1c*	12288	M	F	CTCCAACCTGGAACGAGT
2	*Cacna1c*	12288	M	R	AGAGAAGTCCGTAGGCAATTAC
2	*Camk2d*	108058	M	F	AGGCCGGAGCTTACGAT
2	*Camk2d*	108058	M	R	TGGCAGGGTTGATGGTC
2	*Casq2*	12373	M	F	ACCCACCCTACGTCGC
2	*Casq2*	12373	M	R	TTCTCCGCAAAGGCCAC
2	*Cdkn2a*	12578	M	F	CCAGGGCCCTGGAACTT
2	*Cdkn2a*	12578	M	R	CACGCTAGCATCGCTAGAAG
2	*Dmd*	13405	M	F	GGAAAGCAACACATAGACAACCT
2	*Dmd*	13405	M	R	GGGCATGAACTCTTGTAGATCC
2	*Dsp*	109620	M	F	TCATGCGAGATACATTGAACTG
2	*Dsp*	109620	M	R	TCAGCTTTAGATCTTCCAGACTC
2	*Gapdh*	14433	M	F	AGGTCGGTGTGAACGGATTTG
2	*Gapdh*	14433	M	R	TGTAGACCATGTAGTTGAGGTCA
2	*Gdf15* [372]	23886	M	F	CTGGCAATGCCTGAACAACG
2	*Gdf15* [372]	23886	M	R	GGTCGGGACTTGGTTCTGAG
2	*Gja1*	14609	M	F	TTCCAGCAGAGCCAGCA
2	*Gja1*	14609	M	R	AAATCTCCAGGTCATCAGGC
2	*Ipo8*	320727	M	F	GGAGCTTAACCAGTCCTACAAG
2	*Ipo8*	320727	M	R	CGCACAGGGAACTCCAC
2	*Kcnd3*	56543	M	R	TGGTGGAGGGGTAGTTCTG
2	*Kcnh2*	16511	M	F	GTGCTGCCTGAGTATAAGCTG
2	*Kcnh2*	16511	M	R	CCGAGTACGGTGTGAAGACT
2	*miR-155-5p*	MIMAT0000165	M	F	TTAATGCTAATTGTGATAGGGGT
2	*Mir155HG*	MI0000177	M	F	CCTTATCCTCTGGCTGCT
2	*Mir155HG*	MI0000177	M	R	AGTGCTAGTAACAGGCCTTG
2	*Mir17HG*	MI0000687	M	F	AAGTCTGTAGAGAAGTAAGGGA
2	*Mir17HG*	MI0000687	M	R	CACATCTTCTGGTCACAATCC

Chapter	Gene/MIR/mir/miR		Specie	Sense	Sequence
	Name	ID			
2	*Mir210HG*	MI0000286	M	F	GCCCAAGTTAGAGGAGATGAG
2	*Mir210HG*	MI0000286	M	R	GCCCAGACTCTGGTCAC
2	*Mir22HG*	MI0000570	M	F	GGAACCTGTGCCTCCCA
2	*Mir22HG*	MI0000570	M	R	TCTGTCACCTTCCGGATGATA
2	*Mir24-2*	MI0000572	M	F	CCCTGGACCCCATCTCCTC
2	*Mir24-2*	MI0000572	M	R	GTCTTGCTCACGGCAGACAT
2	*Mir490*	MI0005002	M	F	CTTTATGGAAGCCTGGCTGA
2	*Mir490*	MI0005002	M	R	GAAGTTCCGCTGCTTGTG
2	*Mir497HG*	MI0000237	M	F	GGAACCCTGGTAATGAGTTCT
2	*Mir497HG*	MI0000237	M	R	CTTGGCCCCTTCTCAGTAG
2	*Mybpc3*	17868	M	F	AAGTCCTGAAGGGTCAGTCTC
2	*Mybpc3*	17868	M	R	ACCATCCTGTGGTCGCAT
2	*p21* [372]	12575	M	F	TTGCCAGCAGAATAAAAGGTG
2	*p21* [372]	12575	M	R	TTTGCTCCTGTGCGGAAC
2	*Popdc2*	64082	M	F	TTCCAGGTGACGCTGAC
2	*Popdc2*	64082	M	R	GAGAAGAGGCGGGAGATG
2	*Serca2*	11938	M	F	ACAACCCGCAATACTGGAG
2	*Serca2*	11938	M	R	TGCAGAGGGCTGGTAGAT
2	*Tmod1*	21916	M	F	GCGAAGGAATTTAAGGACCGA
2	*Tmod1*	21916	M	R	ACCCAGACCTTTCCTCGT
2	*Tnnt2*	21956	M	F	CGTAGAAGAGGTTGGTCCTG
2	*Tnnt2*	21956	M	R	GGGTTTGGTGTCCTCTACTG
2	*Ywhaz*	22631	M	F	AGACAACTTAACATTGTGGACATC
2	*Ywhaz*	22631	M	R	GCAGACAAAGGTTGGAAGG
2	*ACTN2*	710012	RM	F	CATCAGAATCAGCTCCAGCA
2	*ACTN2*	710012	RM	R	CGAGTTGCTTCACCTTGTC
2	*ADRA1A*	712509	RM	F	GTGATGCCCATTGGGTCT
2	*ADRA1A*	712509	RM	R	GGGTTGATGCAGCTGTTTAG
2	*ATP1A2*	720191	RM	F	GGCACGGATATGGTTCCTG
2	*ATP1A2*	720191	RM	R	TTGTCTGTCTGGGAGTTTCG
2	*ATP1B1*	700443	RM	F	AACCATCCAAGTGATGCTGCTC
2	*ATP1B1*	700443	RM	R	TCTGGATCTGAGGAATCTGTGTT
2	*CACNA1C*	721721	RM	F	ACTAATTCCAACCTGGAACG
2	*CACNA1C*	721721	RM	R	GTGAAAGAGGAGTCCATAGGC
2	*CAMK2D*	702504	RM	F	AGGCTGGAGCTTATGATTTTCC
2	*CAMK2D*	702504	RM	R	TGGCAGGGTTGATAGTAAGCA
2	*CASQ2*	712373	RM	F	AAAGACCCACTCTACGTCGC
2	*CASQ2*	712373	RM	R	TCTTCTCTGCAAAGGCCACA
2	*CDKN2A*	BLAST	RM	F	GAAGGTCCCTCAGGCATC
2	*CDKN2A*	BLAST	RM	R	CCTTCGGTGATTGATGATCTAAG
2	*DMD*	708073	RM	F	CAGGTACAGGAGTCTAAAGCAC
2	*DMD*	708073	RM	R	TGCAATATTCCACCATGGGATAG
2	*DSP*	694860	RM	F	CGACCTGCGTGAGAAATCT
2	*DSP*	694860	RM	R	GTGATCCATCCTCTCAAAGGAC
2	*GAPDH*	574353	RM	F	GAGTCAACGGATTTGGTCGTA
2	*GAPDH*	574353	RM	R	ATGGCAACAATATCCACTTTACC
2	*GDF15*	719466	RM	F	CAACCAGAGCTGGGAAGATT
2	*GDF15*	719466	RM	R	ATCCCAGCCGCACTTCT
2	*GJA1*	714344	RM	F	CTTCAAGCAGAGCCAGCAG
2	*GJA1*	714344	RM	R	AGATCTCCAGGTCATCAGGC
2	*IPO8*	693514	RM	F	TGTTCAGTATGCATTGCCTCT
2	*IPO8*	693514	RM	R	TCATCAATGTGCAGAGTCTCAG
2	*KCND3*	641437	RM	R	TTGTGGATGGGTAGTTCTGC
2	*KCNH2*	714174	RM	F	GCCAGAGCCGTAAGTTCAT
2	*KCNH2*	714174	RM	R	AGCCGTCGTTGCAGTAGA
2	*miR-155-5p*	MIMAT0006216	RM	F	TTAATGCTAATCGTGATAGGGGT
2	*MIR155HG*	MI0007645	RM	F	TGCTGAAGGCTTGCTGTA
2	*MIR155HG*	MI0007645	RM	R	TGCTAGTAACAGGCATCATACC
2	*MIR17HG*	MI0003004	RM	F	GCCTGGTGTATCTGATGTGA
2	*MIR17HG*	MI0003004	RM	R	CAGTTTGATTGGGCGACAG
2	*MIR210HG*	MI0007670	RM	F	TGGGGTCGATCCCTCCG
2	*MIR210HG*	MI0007670	RM	R	TGTGGCCGGTCGCCTG
2	*MIR22HG*	MI0002631	RM	F	GAGCCTGTTCCTCTCACAC
2	*MIR22HG*	MI0002631	RM	R	CTTCTGTCACCTTCCAGATGAT
2	*MIR24-2*	MI0003053	RM	F	TCTGTCTGCCATCCTGCT
2	*MIR24-2*	MI0003053	RM	R	TCATCTCTGCTCCAAGCATC
2	*MIR3911*	BLAST	RM	F	AGTTTCTTCAGCGTGTCCAG
2	*MIR3911*	BLAST	RM	R	TTCCACTAGACCCAGACGAG
2	*miR-3911*	BLAST	RM	F	GCGTGGATCCTGGAGGAG
2	*MIR3916*	BLAST	RM	F	GCAGGTGTGATTTGTCCAGAT
2	*MIR3916*	BLAST	RM	R	GGCAGGTACATCAGAAGTACAG
2	*miR-3916*	BLAST	RM	F	AAGAGGAAGAAATGGCTGGT
2	*MIR3936*	BLAST	RM	F	GAAGGCACAAGCTTAGTCCA
2	*MIR3936*	BLAST	RM	R	AGGGTCATTCTTCAGGTATGC
2	*miR-3936*	BLAST	RM	F	AGAAGAGGTATGGCAGAAAC
2	*MIR490*	MI0007764	RM	F	GTGAAGAGGATCTCCCTTCAC
2	*MIR490*	MI0007764	RM	R	AGTTCTTGGGAAGATGGAGT
2	*MIR497HG*	MI0007658	RM	F	GGTCTTTGTTACCCACACC
2	*MIR497HG*	MI0007658	RM	R	AGAGGGCTGTTCCCTCTTC

Chapter	*Gene/MIR/mir/miR*		Specie	Sense	Sequence
	Name	ID			
2	*miR-600*	MIMAT0006457	RM	F	GTTACAGACAAGAGCCTTGC
2	*MIR600HG*	MI0007861	RM	F	CTGCAGTGCCAGGCGT
2	*MIR600HG*	MI0007861	RM	R	CAGGGCAGACGGCGAA
2	*MIR6080*	BLAST	RM	F	GATTTGCTGTCCCGGAGT
2	*MIR6080*	BLAST	RM	R	AGTGATTCAGGGTGCGAATA
2	*MIR635*	BLAST	RM	F	TGGAGCATCAACTCCTAGAAC
2	*MIR635*	BLAST	RM	R	GAAGCCAGACCTGCACT
2	*miR-635*	BLAST	RM	F	CGGGCACTGAAGCAATG
2	*MYBPC3*	712093	RM	F	GTCAAGGTCATCGACGTGC
2	*MYBPC3*	712093	RM	R	CTCCAGGATGTAGCCCAGG
2	*P21*	719199	RM	F	CAGGCGCCATGTCAGAA
2	*P21*	719199	RM	R	CCATTAGCGCATCACAGTC
2	*POPDC2*	712853	RM	F	CATCCTGGCTTCTAGAATTCCT
2	*POPDC2*	712853	RM	R	CAGTCCAATGATCCTTAAAGTTCAG
2	*SERCA2*	710702	RM	F	GGAACCTGCAATACTGGAGTAAC
2	*SERCA2*	710702	RM	R	AGAGGGTTGGTAGATGTGTTG
2	*TMOD1*	715838	RM	F	GCAAAGGAGTTTAAGGACCGA
2	*TMOD1*	715838	RM	R	AACCCAGACCTTTCCTCGT
2	*TNNT2*	709882	RM	F	TGCAGGAGAAGTTCAAGCAG
2	*TNNT2*	709882	RM	R	GCGGGTCTTGGAGACTTTC
2	*YWHAZ*	717666	RM	F	GGACACAGAACATCCAGTCA
2	*YWHAZ*	717666	RM	R	CTCAGTTACAGACTTCATGCAG
2	*KCND3/Kcnd3*	641437/56543	RM/M	F	CCCTGTTATCTGTACGAACCTC
2	*KCNN2/Kcnn2*	695374/100492	RM/M	F	GGTCTGATCATCGTGTACCA
2	*KCNN2/Kcnn2*	695374/100492	RM/M	R	GCTATTCTCCAGTCATCTGCTC
2	*miR-17-3p*	MIMAT0002701/MIMAT0000650	RM/M	F	GCAGTGAGGGCACTTGTA
2	*miR-195-3p*	MIMAT0026838/MIMAT0017000	RM/M	F	CCAATATTGGCTGTGCTG
2	*miR-195-5p*	MIMAT0006228/ MIMAT0000225	RM/M	F	AGCAGCACAGAAATATTGG
2	*miR-210-3p*	MIMAT0006240/MIMAT0000658	RM/M	F	GTGTGACAGCGGCTGA
2	*miR-22-3p*	MIMAT0002330/MIMAT0000531	RM/M	F	CTGCCAGTTGAAGAACTGT
2	*miR-24-2-5p*	MIMAT0002336/MIMAT0005440	RM/M	F	CCTACTGAGCTGAAACACAGA
2	*miR-24-3p*	MIMAT0002337/MIMAT0000219	RM/M	F	GGCTCAGTTCAGCAGGA
2	*miR-490-3p*	MIMAT0006351/MIMAT0003780	RM/M	F	CCTGGAGGACTCCATGCT
2	*miR-497-3p*	MIMAT0026887/MIMAT0017247	RM/M	F	CAAACCACACTGTGGTGTTAG
2	*miR-497-5p*	MIMAT0006359/MIMAT0003453	RM/M	F	GCAGCACACTGTGGTTTG
2	*miR-6080*	BLAST	RM	F	TCTCGTGCGGGCGTTC
2	*RNU6/Rnu6*	BLAST/19862	RM/M	F	TGACACGCAAATTCGTGAAG

Table A3. Sequences of DNA oligonucleotides used to prepare DNCs. Note that Cy3 and BMNQ535 are marked in red and green, respectively. All strands were analyzed by BLAST against the human genome to corroborate their lack of substantial sequence homology and, thus, rule out potential undesired functional effects.

M1	CCAGGCTAGCTACATATTCCAGACGACTCCTGTGTTTCAGCTCAGTAGGCA
M2	GAGTCGTCTGGAATTGTCTGGACTAACGACTGTGTTTCAGCTCAGTAGGCA
M3	TCGTTAGTCCAGACTTGTAGCTAGCCTGGCTGTGTTTCAGCTCAGTAGGCA
M_A1_{LU}	CCAGGCTAGCTACATATTCCAGACGACTCCTGTGTT/Cy3/TCAGCTCAGTAGGCA
M_B1_{LU}	CCAGGCTAGCTACATATTCCAGACGACTCCTGTGTTTCAGC/Cy3/TCAGTAGGCA
M3cy3	Cy3/TCGTTAGTCCAGACTTGTAGCTAGCCTGGCTGTGTTTCAGCTCAGTAGGCA
$M_{mock}1$	CCAGGCTAGCTACATATTCCAGACGACTCCATGTTGTCGTAGACAATCAGT
$M_{mock}2$	TCGTTAGTCCAGACTTGTAGCTAGCCTGGCATGTTGTCGTAGACAATCAGT
$M_{mock}3$	GAGTCGTCTGGAATTGTCTGGACTAACGACATGTTGTCGTAGACAATCAGT
L_A1	ACTAAGACTGGACTACCTGAAGAGACTACTGGGCTGAAACACAG
L_A2	CCAGTAGTCTCTTCAGGTAGTCCAGTCTTAGTGCTGAAACACAG
L_A1_{LU}	ACTAAGACTGGACTACCTGAAGAGACTACTGGGCTG/BMNQ535/AAACACAG
L_A2_{LU}	CCAGTAGTCTCTTCAGGTAGTCCAGTCTTAGTGCTG/BMNQ535/AAACACAG
L_B1	ACTAAGACTGGACTACCTGAAGAGACTACTGGTGCCTACTGAGC
L_B2	CCAGTAGTCTCTTCAGGTAGTCCAGTCTTAGTTGCCTACTGAGC
L_B1_{LU}	ACTAAGACTGGACTACCTGAAGAGACTACTGGTGCCTACTG/BMNQ535/AGC
L_B2_{LU}	CCAGTAGTCTCTTCAGGTAGTCCAGTCTTAGTTGCCTACTG/BMNQ535/AGC
$L_{mock}1$	ACTAAGACTGGACTACCTGAAGAGACTACTGGTACGACAACATG
$L_{mock}2$	CCAGTAGTCTCTTCAGGTAGTCCAGTCTTAGTTACGACAACATG
S1	CTAACCAGCTACTCAGGTCATCACTAGA
S2	TCTAGTGATGACCTGTGGGACAGAGCGT
S_A3	ACGCTCTGTCCCACGAGTAGCTGGTTAGCTGTGTTTCAGC
S_B3	ACGCTCTGTCCCACGAGTAGCTGGTTAGGCTCAGTAGGCA
$S_{mock}3$	ACGCTCTGTCCCACGAGTAGCTGGTTAGCATGTTGTCGTA
ssDNA miR-24-2-5p	TGCCTACTGAGCTGAAACACAG
ssRNA miR-24-2-5p	UGCCUACUGAGCUGAAACACAG
$ssDNA_{mock}$	CGAGCTTTACGTTACCTCATAT

Table A4. Data related to the study cohort: Demographic data, anthropometric measures, gene expression data and age biomarkers in the study cohort (GamC and AR).

	Demographic data			Gene expression data			Age Biomarkers	
Individual ID	**CA**	**Ethnicity**	**Sex**	***ABLIM1***	***CCR7***	***LEF1***	**GamC**	**AR**
J01	25.33	Caucasian	Male	0.61	9.55	4.18	34.56	9.23
J02	24.80	Caucasian	Male	0.63	9.93	10.36	10.89	-13.91
J03	23.86	Caucasian	Male	0.61	5.64	6.12	43.89	20.03
J04	28.98	Caucasian	Male	0.52	14.68	8.9	9.22	-19.76
J05	26.75	Caucasian	Male	0.38	5.52	8.52	62.94	36.19
J06	21.84	Caucasian	Male	0.25	4.01	4.33	97.13	75.29
J07	29.91	Caucasian	Male	0.39	4.44	40.41	-35.94	-65.85
J08	25.78	Caucasian	Male	0.35	7.61	11.7	48.24	22.46
J09	27.08	Caucasian	Male	0.58	17.08	16.66	-31.55	-58.63
J10	19.88	Caucasian	Male	0.38	7.11	8.45	57.44	37.55
J11	23.22	Caucasian	Male	0.31	6.45	47.82	-59.02	-82.24
J12	21.82	Caucasian	Male	0.42	7.16	8.58	51.66	29.84
J13	21.75	Caucasian	Male	0.56	12.23	8.71	15.51	-6.24
J14	30.06	Caucasian	Male	0.51	9.13	6.91	38.64	8.58
J15	29.57	Caucasian	Male	0.47	8.82	9.54	36.54	6.98
J16	25.89	Caucasian	Male	0.94	7.5	8.92	-9.99	-35.87
J17	23.19	Caucasian	Male	1.52	19	9.99	-125.66	-148.85
J18	24.12	Caucasian	Male	0.85	15.64	9.16	-32.27	-56.39
J19	23.90	Caucasian	Male	0.70	5.27	2.94	45.65	21.75
J20	25.14	Caucasian	Male	0.65	16.53	7.21	-7.21	-32.35
J21	26.99	Caucasian	Male	0.42	6.54	3.35	70.36	43.37
J22	26.39	Caucasian	Male	0.56	6.01	2.79	58.34	31.95
J24	27.91	Caucasian	Male	0.47	2.02	0.03	93.02	65.10
J25	25.67	Caucasian	Male	0.34	5.16	2.21	89.22	63.55
A01	47.05	Caucasian	Male	0.40	8.66	5.33	58.55	11.50
A02	40.70	Caucasian	Male	0.33	7.19	11.76	51.33	10.63
A03	40.12	Caucasian	Male	0.20	5.87	12.05	70.33	30.21
A04	41.71	Caucasian	Male	0.35	4.01	7.41	75.59	33.89
A05	48.89	Caucasian	Male	0.26	5.75	6.64	82.00	33.11
A06	40.06	Caucasian	Male	0.39	4.13	2.87	85.04	44.97
A07	47.92	Caucasian	Male	0.42	6.53	6.36	61.40	13.49
A08	49.75	Caucasian	Male	0.46	5.18	8.58	54.53	4.78
A09	43.67	Caucasian	Male	0.22	4.23	4.25	99.58	55.91
A10	40.36	Caucasian	Male	0.49	8.24	42.17	-68.41	-108.77
A11	43.16	Caucasian	Male	0.36	7.54	1.09	80.60	37.44
A12	46.33	Caucasian	Male	0.50	8.68	12.25	24.97	-21.37
A13	40.76	Caucasian	Male	0.40	11.73	15.16	15.25	-25.50
A15	39.38	Caucasian	Male	0.27	4.98	2.48	97.19	57.82
A16	48.19	Caucasian	Male	0.64	0.02	0.07	82.18	33.99
A17	41.81	Caucasian	Male	0.52	5.92	0.85	69.88	28.06
A20	40.29	Caucasian	Male	0.43	18.22	4.48	20.28	-20.01
A21	40.17	Caucasian	Male	0.42	8.81	28.38	-18.28	-58.45
A22	40.48	Caucasian	Male	0.64	7.54	9.88	21.28	-19.20
A23	46.80	Caucasian	Male	0.30	12.7	17.63	15.21	-31.59
A24	45.90	Caucasian	Male	0.44	10.76	8.5	35.38	-10.52
A25	43.04	Caucasian	Male	0.42	7.49	6.4	57.86	14.82
M01	61.88	Caucasian	Male	0.26	7.3	5.47	71.12	9.25
M02	61.88	Caucasian	Male	0.61	1.57	2.51	79.00	17.12
M03	64.31	Caucasian	Male	0.37	7.07	3.5	73.68	9.37
M05	62.63	Caucasian	Male	0.32	4.45	12.25	61.63	-1.00
M06	63.16	Caucasian	Male	0.38	8.59	6.17	58.78	-4.39
M07	60.17	Caucasian	Male	0.39	9.58	33.05	-33.32	-93.49
M09	66.20	Caucasian	Male	0.42	7.05	9.57	49.02	-17.18
M10	67.66	Caucasian	Male	0.24	6.22	9.45	72.90	5.25
M11	60.05	Caucasian	Male	0.41	0	0.38	106.95	46.90

	Demographic data			Gene expression data			Age Biomarkers	
Individual ID	**CA**	**Ethnicity**	**Sex**	***ABLIM1***	***CCR7***	***LEF1***	**GamC**	**AR**
M12	65.79	Caucasian	Male	0.44	8.4	1.06	68.44	2.64
M13	62.98	Caucasian	Male	0.36	5.26	1.47	88.81	25.83
M14	67.47	Caucasian	Male	0.36	4.82	11.19	59.60	-7.87
M15	61.95	Caucasian	Male	0.25	2.02	6.27	98.90	36.95
M16	59.61	Caucasian	Male	0.51	10.49	10.09	23.33	-36.28
M17	62.81	Caucasian	Male	0.56	6.23	5.53	49.60	-13.20
M18	67.62	Caucasian	Male	0.74	2.52	3.3	50.03	-17.59
M19	63.54	Caucasian	Male	0.50	7.04	6.43	49.56	-13.98
M20	63.65	Caucasian	Male	0.18	5.49	5.35	95.68	32.03
M21	70.38	Caucasian	Male	0.44	13.17	5.95	34.87	-35.52
M22	61.49	Caucasian	Male	0.63	7.5	13.33	10.60	-50.88
M23	62.00	Caucasian	Male	0.57	1.61	2.09	77.00	15.00
M25	66.68	Caucasian	Male	0.42	5.03	3.84	75.01	8.33
C01	106.62	Caucasian	Female	0.20	12.79	9.17	52.82	-53.80
C02	102.74	Caucasian	Female	0.68	0	1.52	73.00	-29.74
C03	100.05	Caucasian	Female	0.40	0.94	1.27	101.52	1.47
C04	100.53	Caucasian	Female	0.32	4.67	7.13	77.32	-23.21
C05	100.92	Caucasian	Male	0.37	3.1	4.84	84.84	-16.09
C06	102.53	Caucasian	Female	0.18	3.12	2.82	113.25	10.72
C07	101.69	Caucasian	Female	0.41	3.01	2.05	90.13	-11.56
C08	100.29	Caucasian	Female	0.56	0.42	2.01	83.15	-17.15
C09	98.99	Caucasian	Male	0.22	1.53	1.56	119.05	20.06
C10	99.56	Caucasian	Female	0.28	0.06	4.8	107.74	8.17
C11	102.70	Caucasian	Female	0.05	2.71	3.38	128.58	25.89
C12	99.68	Caucasian	Female	0.18	2.74	3.45	112.86	13.18
C13	102.06	Caucasian	Female	0.23	0.12	0.29	128.11	26.05
C14	100.13	Caucasian	Male	0.25	0.22	1.02	122.81	22.68
C15	103.25	Caucasian	Male	0.31	1.15	1.29	110.93	7.68
C16	101.22	Caucasian	Male	0.18	0.97	2.68	122.38	21.16
C18	105.06	Caucasian	Female	0.38	1.33	0.87	103.50	-1.56
C19	100.21	Caucasian	Female	0.18	1.93	1.66	122.03	21.82
C20	99.20	Caucasian	Female	0.45	2.19	1.87	89.12	-10.07

Bibliography

[1] López-Otín C, Blasco MA, Partridge L, Serrano M, Kroemer G. Hallmarks of aging: An expanding universe. Cell 2023;186:243–78. https://doi.org/10.1016/J.CELL.2022.11.001.

[2] World Health Organization (WHO). Cardiovascular diseases 2024. https://www.who.int/health-topics/cardiovascular-diseases.

[3] Varghese LN, Schwenke DO, Katare R. Role of noncoding RNAs in cardiac ageing. Front Cardiovasc Med 2023;10. https://doi.org/10.3389/fcvm.2023.1142575.

[4] World Health Organization (WHO). Cardiovascular diseases 2021. https://www.who.int/health-topics/cardiovascular-diseases.

[5] Rudnicka E, Napierała P, Podfigurna A, Męczekalski B, Smolarczyk R, Grymowicz M. The World Health Organization (WHO) approach to healthy ageing. Maturitas 2020;139:6–11. https://doi.org/10.1016/j.maturitas.2020.05.018.

[6] Zhou M, Zhao G, Zeng Y, Zhu J, Cheng F, Liang W. Aging and Cardiovascular Disease : Current Status and Challenges. Rev Cardiovasc Med 2022;23:135. https://doi.org/10.31083/j.rcm2304135.

[7] Rodgers JL, Jones J, Bolleddu SI, Vanthenapalli S, Rodgers LE, Shah K, et al. Cardiovascular Risks Associated with Gender and Aging. J Cardiovasc Dev Dis 2019;6:19. https://doi.org/10.3390/jcdd6020019.

[8] Hastings MH, Zhou Q, Wu C, Shabani P, Huang S, Yu X, et al. Cardiac ageing: from hallmarks to therapeutic opportunities. Cardiovasc Res 2025;121:1474–88. https://doi.org/10.1093/CVR/CVAE124.

[9] Li X, Pang X, Sun H, Zhang B, Wang H, Wu N, et al. Cardiac aging: Molecular mechanisms and therapeutic interventions. Pharmacol Res 2025;221:107954. https://doi.org/10.1016/J.PHRS.2025.107954.

[10] Malecki C, Guglielmi G, Hunter B, Harney D, Koay YC, Don AS, et al. The Human Cardiac “Age-OME”: Age-Specific Changes in Myocardial Molecular Expression. Aging Cell 2025:e70219. https://doi.org/10.1111/ACEL.70219.

[11] Raisi-Estabragh Z, Szabo L, Schuermans A, Salih AM, Chin CWL, Vágó H, et al. Noninvasive Techniques for Tracking Biological Aging of the Cardiovascular System: JACC Family Series. JACC Cardiovasc Imaging 2024;17:533–51. https://doi.org/10.1016/J.JCMG.2024.03.001.

[12] Ramos-Marquès E, García-Mendívil L, Pérez-Zabalza M, Santander-Badules H, Srinivasan S, Oliveros JC, et al. Chronological and biological aging of the human left ventricular myocardium: Analysis of microRNAs contribution. Aging Cell 2021;20:e13383. https://doi.org/10.1111/ACEL.13383.

[13] Varghese LN, Schwenke DO, Katare R. Role of noncoding RNAs in cardiac ageing. Front Cardiovasc Med 2023;10:1142575. https://doi.org/10.3389/fcvm.2023.1142575.

[14] Roselli C, Chaffin MD, Weng LC, Aeschbacher S, Ahlberg G, Albert CM, et al. Multi-ethnic genome-wide association study for atrial fibrillation. Nat Genet 2018;50:1225–33. https://doi.org/10.1038/S41588-018-0133-9.

[15] Nielsen JB, Thorolfsdottir RB, Fritsche LG, Zhou W, Skov MW, Graham SE, et al. Biobank-driven genomic discovery yields new insight into atrial fibrillation biology. Nat Genet 2018;50:1234–9. https://doi.org/10.1038/S41588-018-0171-3.

[16] Decoding noncoding RNAs. Nat Methods 2022;19:1147–8. https://doi.org/10.1038/S41592-022-01654-5.

[17] Samra M, Srivastava K. Non-coding RNA and their potential role in cardiovascular diseases. Gene 2023;851:147011. https://doi.org/10.1016/j.gene.2022.147011.

[18] Winkle M, El-Daly SM, Fabbri M, Calin GA. Noncoding RNA therapeutics — challenges and potential solutions. Nat Rev Drug Discov 2021 208 2021;20:629–51. https://doi.org/10.1038/s41573-021-00219-z.

[19] De Goede OM, Nachun DC, Ferraro NM, Gloudemans MJ, Rao AS, Smail C, et al. Population-scale tissue transcriptomics maps long non-coding RNAs to complex disease. Cell 2021;184:2633–48. https://doi.org/10.1016/j.cell.2021.03.050.

[20] Cech TR, Steitz JA. The Noncoding RNA Revolution—Trashing Old Rules to Forge New Ones. Cell 2014;157:77–94. https://doi.org/10.1016/j.cell.2014.03.008.

[21] Zhang Y, Fan M, Zhang X, Huang F, Wu K, Zhang J, et al. Cellular microRNAs up-regulate transcription via interaction with promoter TATA-box motifs. RNA 2014;20:1878. https://doi.org/10.1261/RNA.045633.114.

[22] Xiao M, Li J, Li W, Wang Y, Wu F, Xi Y, et al. MicroRNAs activate gene transcription epigenetically as an enhancer trigger. RNA Biol 2016;14:1326. https://doi.org/10.1080/15476286.2015.1112487.

[23] Friedman RC, Farh KKH, Burge CB, Bartel DP. Most mammalian mRNAs are conserved targets of microRNAs. Genome Res 2009;19:92–105. https://doi.org/10.1101/gr.082701.108.

[24] Salmena L, Poliseno L, Tay Y, Kats L, Pandolfi PP. A ceRNA Hypothesis: The Rosetta Stone of a Hidden RNA Language? Cell 2011;146:353–8. https://doi.org/10.1016/J.CELL.2011.07.014.

[25] Calin GA, Cimmino A, Fabbri M, Ferracin M, Wojcik SE, Shimizu M, et al. MiR-15a and miR-16-1 cluster functions in human leukemia. Proc Natl Acad Sci U S A 2008;105:5166. https://doi.org/10.1073/PNAS.0800121105.

[26] Diener C, Keller A, Meese E. Emerging concepts of miRNA therapeutics: from cells to clinic. Trends Genet 2022;38:613–26. https://doi.org/10.1016/J.TIG.2022.02.006.

[27] Viereck J, Thum T. Development of a Mechanism-Based Next-Generation Therapeutic for Heart Failure Derived From the Dark Genome. JACC Basic to Transl Sci 2023;8:1595–8. https://doi.org/10.1016/j.jacbts.2023.09.006.

[28] Mori MA, Ludwig RG, Garcia-Martin R, Brandão BB, Kahn CR. Extracellular miRNAs: From Biomarkers to Mediators of Physiology and Disease. Cell Metab 2019;30:656–73. https://doi.org/10.1016/j.cmet.2019.07.011.

[29] Wu Q, Li L, Jia Y, Xu T, Zhou X. Advances in studies of circulating microRNAs: origination, transportation, and distal target regulation. J Cell Commun Signal 2022;17:445. https://doi.org/10.1007/S12079-022-00705-Y.

[30] Chang C, Wang Y, Wang R, Bao X. Considering Context-Specific microRNAs in Ischemic Stroke with Three “W”: Where, When, and What. Mol Neurobiol 2024;61:7335–53. https://doi.org/10.1007/S12035-024-04051-5.

[31] Iftikhar H, Carney GE. Evidence and potential in vivo functions for biofluid miRNAs: From expression profiling to functional testing. BioEssays 2016;38:367–78. https://doi.org/10.1002/BIES.201500130.

[32] Condrat CE, Thompson DC, Barbu MG, Bugnar OL, Boboc A, Cretoiu D, et al. miRNAs as Biomarkers in Disease: Latest Findings Regarding Their Role in Diagnosis and Prognosis. Cells 2020;9:276. https://doi.org/10.3390/CELLS9020276.

[33] Stavast CJ, Erkeland SJ. The Non-Canonical Aspects of MicroRNAs: Many Roads to Gene Regulation. Cells 2019;8. https://doi.org/10.3390/cells8111465.

[34] Rodriguez A, Griffiths-Jones S, Ashurst JL, Bradley A. Identification of mammalian microRNA host genes and transcription units. Genome Res 2004;14:1902–10. https://doi.org/10.1101/GR.2722704.

[35] Vienberg S, Geiger J, Madsen S, Dalgaard LT. MicroRNAs in metabolism. Acta Physiol 2017;219:346–61. https://doi.org/10.1111/apha.12681.

[36] Bang C, Batkai S, Dangwal S, Gupta SK, Foinquinos A, Holzmann A, et al. Cardiac fibroblast-derived microRNA passenger strand-enriched exosomes mediate cardiomyocyte hypertrophy. J Clin Invest 2014;124:2136–46. https://doi.org/10.1172/JCI70577.

[37] Liu N, Okamura K, Tyler DM, Phillips MD, Chung WJ, Lai EC. The evolution and functional diversification of animal microRNA genes. Cell Res 2008 1810 2008;18:985–96. https://doi.org/10.1038/cr.2008.278.

[38] Medley JC, Panzade G, Zinovyeva AY. microRNA strand selection: Unwinding the rules. Wiley Interdiscip Rev RNA 2021;12:e1627. https://doi.org/10.1002/WRNA.1627.

[39] Tsai KW, Leung CM, Lo YH, Chen TW, Chan WC, Yu SY, et al. Arm Selection Preference of MicroRNA-193a Varies in Breast Cancer. Sci Reports 2016 61 2016;6:1–13. https://doi.org/10.1038/srep28176.

[40] Ro S, Park C, Young D, Sanders KM, Yan W. Tissue-dependent paired expression of miRNAs. Nucleic Acids Res 2007;35:5944–53. https://doi.org/10.1093/NAR/GKM641.

[41] Seal RL, Chen L, Griffiths-Jones S, Lowe TM, Mathews MB, O'Reilly D, et al. A guide to naming human non-coding RNA genes. EMBO J 2020;39. https://doi.org/10.15252/EMBJ.2019103777.

[42] Conrad T, Marsico A, Gehre M, Ørom UA. Microprocessor activity controls differential miRNA biogenesis in vivo. Cell Rep 2014;9:542–54. https://doi.org/10.1016/J.CELREP.2014.09.007.

[43] Michlewski G, Guil S, Semple CA, Cáceres JF. Posttranscriptional Regulation of miRNAs Harboring Conserved Terminal Loops. Mol Cell 2008;32:383. https://doi.org/10.1016/J.MOLCEL.2008.10.013.

[44] Donayo AO, Johnson RM, Tseng HW, Izreig S, Gariepy A, Mayya VK, et al. Oncogenic Biogenesis of pri-miR-17∼92 Reveals Hierarchy and Competition among Polycistronic MicroRNAs. Mol Cell 2019;75:340–56. https://doi.org/10.1016/J.MOLCEL.2019.05.033.

[45] Broughton JP, Lovci MT, Huang JL, Yeo GW, Pasquinelli AE. Pairing beyond the Seed Supports MicroRNA Targeting Specificity. Mol Cell 2016;64:320–33. https://doi.org/10.1016/J.MOLCEL.2016.09.004.

[46] Liu Z, Sall A, Yang D. MicroRNA: an Emerging Therapeutic Target and Intervention Tool. Int J Mol Sci 2008;9:978–99. https://doi.org/10.3390/ijms9060978.

[47] O'Brien J, Hayder H, Zayed Y, Peng C. Overview of microRNA biogenesis, mechanisms of actions, and circulation. Front Endocrinol (Lausanne) 2018;9:402. https://doi.org/10.3389/fendo.2018.00402.

[48] Ha M, Kim VN. Regulation of microRNA biogenesis. Nat Rev Mol Cell Biol 2014;15:509–24. https://doi.org/10.1038/nrm3838.

[49] Ni W-J, Leng X-M. miRNA-Dependent Activation of mRNA Translation. MicroRNA 2016;5:83–6. https://doi.org/10.2174/2211536605666160825151201.

[50] Pu M, Chen J, Tao Z, Miao L, Qi X, Wang Y, et al. Regulatory network of miRNA on its target: coordination between transcriptional and post-transcriptional regulation of gene expression. Cell Mol Life Sci C 2018;76:441–51. https://doi.org/10.1007/S00018-018-2940-7.

[51] Maes OC, An J, Sarojini H, Wang E. Murine microRNAs implicated in liver functions and aging process. Mech Ageing Dev 2008;129:534–41. https://doi.org/10.1016/j.mad.2008.05.004.

[52] Smith-Vikos T, Slack FJ. MicroRNAs and their roles in aging. J Cell Sci 2012;125:7–17. https://doi.org/10.1242/jcs.099200.

[53] Mercken EM, Majounie E, Ding J, Guo R, Kim J, Bernier M, et al. Age-associated miRNA alterations in skeletal muscle from rhesus monkeys reversed by caloric restriction. Aging (Albany NY) 2013;5:692–703. https://doi.org/10.18632/AGING.100598.

[54] Persengiev S, Kondova I, Otting N, Koeppen AH, Bontrop RE. Genome-wide analysis of miRNA expression reveals a potential role for miR-144 in brain aging and spinocerebellar ataxia pathogenesis. Neurobiol Aging 2011;32:2316.e17-2316.e27. https://doi.org/10.1016/J.NEUROBIOLAGING.2010.03.014.

[55] Holzenberger M, Dupont J, Ducos B, Leneuve P, Géloën A, Even PC, et al. IGF-1 receptor regulates lifespan and resistance to oxidative stress in mice. Nature 2003;421:182–7. https://doi.org/10.1038/nature01298.

[56] Oh HS-H, Rutledge J, Nachun D, Pálovics R, Abiose O, Moran-Losada P, et al. Organ aging signatures in the plasma proteome track health and disease. Nature 2023;624:164–72. https://doi.org/10.1038/s41586-023-06802-1.

[57] Sheikh MSA, Salma U. Impact of microRNAs on cardiovascular diseases and aging. J Int Med Res 2024;52:3000605241279190. https://doi.org/10.1177/03000605241279190.

[58] Eulalio A, Mano M, Ferro MD, Zentilin L, Sinagra G, Zacchigna S, et al. Functional screening identifies miRNAs inducing cardiac regeneration. Nat 2012 4927429 2012;492:376–81. https://doi.org/10.1038/nature11739.

[59] Boon RA, Iekushi K, Lechner S, Seeger T, Fischer A, Heydt S, et al. MicroRNA-34a regulates cardiac ageing and function. Nature 2013;495:107–10. https://doi.org/10.1038/nature11919.

[60] Thum T, Galuppo P, Wolf C, Fiedler J, Kneitz S, Van Laake LW, et al. MicroRNAs in the human heart: A clue to fetal gene reprogramming in heart failure. Circulation 2007;116:258–67. https://doi.org/10.1161/CIRCULATIONAHA.107.687947.

[61] Lu Y, Zhang Y, Wang N, Pan Z, Gao X, Zhang F, et al. MicroRNA-328 Contributes to Adverse Electrical Remodeling in Atrial Fibrillation. Circulation 2010;122:2378–87. https://doi.org/10.1161/CIRCULATIONAHA.110.958967.

[62] Van Den Berg NWE, Kawasaki M, Nariswari FA, Fabrizi B, Neefs J, van der Made I, et al. MicroRNAs in atrial fibrillation target genes in structural remodelling. Cell Tissue Res 2023;394:497–514. https://doi.org/10.1007/S00441-023-03823-0.

[63] Wang L yuan, Shen H, Yang Q, Min J, Wang Q, Xi W, et al. LncRNA-LINC00472 contributes to the pathogenesis of atrial fibrillation (Af) by reducing expression of JP2 and RyR2 via miR-24. Biomed Pharmacother 2019;120:109364. https://doi.org/10.1016/J.BIOPHA.2019.109364.

[64] Boštjančič E, Zidar N, Glavač D. MicroRNAs and cardiac sarcoplasmic reticulum calcium ATPase-2 in human myocardial infarction: Expression and bioinformatic analysis. BMC Genomics 2012;13:1–14. https://doi.org/10.1186/1471-2164-13-552.

[65] Searles CD. MicroRNAs and Cardiovascular Disease Risk. Curr Cardiol Rep 2024;26:51–60. https://doi.org/10.1007/S11886-023-02014-1/METRICS.

[66] Zhou S, Jin J, Wang J, Zhang Z, Freedman JH, Zheng Y, et al. miRNAS in cardiovascular diseases: potential biomarkers, therapeutic targets and challenges. Acta Pharmacol Sin 2018;39:1073–84. https://doi.org/10.1038/aps.2018.30.

[67] Noren Hooten N, Fitzpatrick M, Wood WH, De S, Ejiogu N, Zhang Y, et al. Age-related changes in microRNA levels in serum. Aging (Albany NY) 2013;5:725. https://doi.org/10.18632/AGING.100603.

[68] Zhang H, Yang H, Zhang C, Jing Y, Wang C, Liu C, et al. Investigation of MicroRNA Expression in Human Serum During the Aging Process. Journals Gerontol Ser A 2015;70:102–9. https://doi.org/10.1093/GERONA/GLU145.

[69] Kumar S, Vijayan M, Bhatti JS, Reddy PH. MicroRNAs as Peripheral Biomarkers in Aging and Age-Related Diseases. Prog Mol Biol Transl Sci 2017;146:47–94. https://doi.org/10.1016/bs.pmbts.2016.12.013.

[70] Moqri M, Herzog C, Poganik JR, Justice J, Belsky DW, Higgins-Chen A, et al. Biomarkers of Aging for the Identification and Evaluation of Longevity Interventions. Cell 2023;186:3758. https://doi.org/10.1016/J.CELL.2023.08.003.

[71] Liu Z, Kuo PL, Horvath S, Crimmins E, Ferrucci L, Levine M. A new aging measure captures morbidity and mortality risk across diverse subpopulations from NHANES IV: A cohort study. PLOS Med 2018;15:e1002718. https://doi.org/10.1371/JOURNAL.PMED.1002718.

[72] Bland JS. Age as a Modifiable Risk Factor for Chronic Disease. Integr Med 2018;17:16–9.

[73] Vitetta L, Anton B. Lifestyle and nutrition, caloric restriction, mitochondrial health and hormones: Scientific interventions for anti-aging. Clin Interv Aging 2007;2:537. https://doi.org/10.2147/CIA.S866.

[74] Nie C, Li Y, Li R, Yan Y, Zhang D, Li T, et al. Distinct biological ages of organs and systems identified from a multi-omics study. Cell Rep 2022;38:110459. https://doi.org/10.1016/J.CELREP.2022.110459.

[75] Jia L, Zhang W, Chen X. Common methods of biological age estimation. Clin Interv Aging 2017;12:759. https://doi.org/10.2147/CIA.S134921.

[76] Galkin F, Mamoshina P, Aliper A, de Magalhães JP, Gladyshev VN, Zhavoronkov A. Biohorology and biomarkers of aging: Current state-of-the-art, challenges and opportunities. Ageing Res Rev 2020;60:101050. https://doi.org/10.1016/J.ARR.2020.101050.

[77] Levine ME, Lu AT, Quach A, Chen BH, Assimes TL, Bandinelli S, et al. An epigenetic biomarker of aging for lifespan and healthspan. Aging (Albany NY) 2018;10:573–91. https://doi.org/10.18632/AGING.101414.

[78] Lu AT, Quach A, Wilson JG, Reiner AP, Aviv A, Raj K, et al. DNA methylation GrimAge strongly predicts lifespan and healthspan. Aging (Albany NY) 2019;11:303–27. https://doi.org/10.18632/AGING.101684.

[79] Belur Nagaraj S, Kieneker LM, Pena MJ. Kidney Age Index (KAI): A novel age-related biomarker to estimate kidney function in patients with diabetic kidney disease using machine learning. Comput Methods Programs Biomed 2021;211:106434. https://doi.org/10.1016/j.cmpb.2021.106434.

[80] Morris JF, Temple W. Spirometric “lung age” estimation for motivating smoking cessation. Prev Med (Baltim) 1985;14:655–62. https://doi.org/10.1016/0091-7435(85)90085-4.

[81] Voisin S, Harvey NR, Haupt LM, Griffiths LR, Ashton KJ, Coffey VG, et al. An epigenetic clock for human skeletal muscle. J Cachexia Sarcopenia Muscle 2020;11:887–98. https://doi.org/10.1002/JCSM.12556.

[82] Muralidharan C, Zakar-Polyák E, Adami A, Abbas AA, Sharma Y, Garza R, et al. Human Brain Cell-Type-Specific Aging Clocks Based on Single-Nuclei Transcriptomics. Adv Sci 2025:e06109. https://doi.org/10.1002/ADVS.202506109.

[83] Horvath S, Oshima J, Martin GM, Lu AT, Quach A, Cohen H, et al. Epigenetic clock for skin and blood cells applied to Hutchinson Gilford Progeria Syndrome and ex vivo studies. Aging (Albany NY) 2018;10:1758–75. https://doi.org/10.18632/AGING.101508.

[84] Roig-Genoves JV, García-Giménez JL, Mena-Molla S. A miRNA-based epigenetic molecular clock for biological skin-age prediction. Arch Dermatol Res 2024;316:1–9. https://doi.org/10.1007/S00403-024-03129-3.

[85] Tong H, Guo X, Jacques M, Luo Q, Eynon N, Teschendorff AE. Cell-type specific epigenetic clocks to quantify biological age at cell-type resolution. Aging (Albany NY) 2024;16:13452–504. https://doi.org/10.18632/AGING.206184.

[86] Mongelli A, Panunzi S, Nesta M, Gottardi Zamperla M, Atlante S, Barbi V, et al. Distinguishable DNA methylation defines a cardiac-specific epigenetic clock. Clin Epigenetics 2023;15:1–15. https://doi.org/10.1186/S13148-023-01467-Z/FIGURES/5.

[87] Raisi-Estabragh Z, Salih A, Gkontra P, Atehortúa A, Radeva P, Boscolo Galazzo I, et al. Estimation of biological heart age using cardiovascular magnetic resonance radiomics. Sci Rep 2022;12:1–12. https://doi.org/10.1038/S41598-022-16639-9.

[88] Bortz J, Guariglia A, Klaric L, Tang D, Ward P, Geer M, et al. Biological age estimation using circulating blood biomarkers. Commun Biol 2023 61 2023;6:1–10. https://doi.org/10.1038/s42003-023-05456-z.

[89] Peters MJ, Joehanes R, Pilling LC, Schurmann C, Conneely KN, Powell J, et al. The transcriptional landscape of age in human peripheral blood. Nat Commun 2015;6:8570. https://doi.org/10.1038/NCOMMS9570.

[90] Jansen R, Han LKM, Verhoeven JE, Aberg KA, van den Oord ECGJ, Milaneschi Y, et al. An integrative study of five biological clocks in somatic and mental health. Elife 2021;10:1–20. https://doi.org/10.7554/ELIFE.59479.

[91] Macdonald-Dunlop E, Taba N, Klarić L, Frkatović A, Walker R, Hayward C, et al. A catalogue of omics biological ageing clocks reveals substantial commonality and associations with disease risk. Aging (Albany NY) 2022;14:623–59. https://doi.org/10.18632/AGING.203847.

[92] Belsky DW, Moffitt TE, Cohen AA, Corcoran DL, Levine ME, Prinz JA, et al. Eleven Telomere, Epigenetic Clock, and Biomarker-Composite Quantifications of Biological Aging: Do They Measure the Same Thing? Am J Epidemiol 2018;187:1220–30. https://doi.org/10.1093/AJE/KWX346.

[93] Cohen AA, Morissette-Thomas V, Ferrucci L, Fried LP. Deep biomarkers of aging are population-dependent. Aging (Albany NY) 2016;8:2253–5. https://doi.org/10.18632/AGING.101034.

[94] Cohen AA, Legault V, Fuellen G, Fülöp T, Fried LP, Ferrucci L. The risks of biomarker-based epidemiology: Associations of circulating calcium levels with age, mortality, and frailty vary substantially across populations. Exp Gerontol 2018;107:11. https://doi.org/10.1016/J.EXGER.2017.07.011.

[95] Vidal-Bralo L, Lopez-Golan Y, Gonzalez A. Simplified Assay for Epigenetic Age Estimation in Whole Blood of Adults. Front Genet 2016;7:126. https://doi.org/10.3389/FGENE.2016.00126.

[96] Wolinsky H. Testing time for telomeres. Telomere length can tell us something about disease susceptibility and ageing, but are commercial tests ready for prime time? EMBO Rep 2011;12:897–900. https://doi.org/10.1038/EMBOR.2011.166.

[97] Artzi S, Kiezun A, Shomron N. miRNAminer: A tool for homologous microRNA gene search. BMC Bioinformatics 2008;9:39. https://doi.org/10.1186/1471-2105-9-39.

[98] Li SC, Chan WC, Hu LY, Lai CH, Hsu CN, Lin W chang. Identification of homologous microRNAs in 56 animal genomes. Genomics 2010;96:1–9. https://doi.org/10.1016/J.YGENO.2010.03.009.

[99] Yue J, Sheng Y, Orwig KE. Identification of novel homologous microRNA genes in the rhesus macaque genome. BMC Genomics 2008;9:8. https://doi.org/10.1186/1471-2164-9-8.

[100] Paczynska P, Grzemski A, Szydlowski M. Distribution of miRNA genes in the pig genome. BMC Genet 2015;16. https://doi.org/10.1186/s12863-015-0166-3.

[101] De Rie D, Abugessaisa I, Alam T, Arner E, Arner P, Ashoor H, et al. An integrated expression atlas of miRNAs and their promoters in human and mouse. Nat Biotechnol 2017;35:872–8. https://doi.org/10.1038/NBT.3947.

[102] Xu J, Zhang R, Shen Y, Liu G, Lu X, Wu CI. The evolution of evolvability in microRNA target sites in vertebrates. Genome Res 2013;23:1810–6. https://doi.org/10.1101/GR.148916.112.

[103] Karagiannis P, Takahashi K, Saito M, Yoshida Y, Okita K, Watanabe A, et al. Induced pluripotent stem cells and their use in human models of disease and development. Physiol Rev 2019;99:79–114. https://doi.org/10.1152/physrev.00039.2017.

[104] Lin J, Xue A, Li L, Li B, Li Y, Shen Y, et al. MicroRNA-19b downregulates gap junction protein alpha1 and synergizes with MicroRNA-1 in viral myocarditis. Int J Mol Sci 2016;17:741. https://doi.org/10.3390/ijms17050741.

[105] Danielson LS, Park DS, Rotllan N, Chamorro-Jorganes A, Guijarro M V., Fernandez-Hernando C, et al. Cardiovascular dysregulation of miR-17-92 causes a lethal hypertrophic cardiomyopathy and arrhythmogenesis. FASEB J 2013;27:1460–7. https://doi.org/10.1096/fj.12-221994.

[106] Wang H, Cai J. The role of microRNAs in heart failure. Biochim Biophys Acta - Mol Basis Dis 2017;1863:2019–30. https://doi.org/10.1016/j.bbadis.2016.11.034.

[107] Lin Z, Murtaza I, Wang K, Jiao J, Gao J, Lia PF. miR-23a functions downstream of NFATc3 to regulate cardiac hypertrophy. Proc Natl Acad Sci U S A 2009;106:12103–8. https://doi.org/10.1073/pnas.0811371106.

[108] Tu Y, Wan L, Bu L, Zhao D, Dong D, Huang T, et al. MicroRNA-22 Downregulation by Atorvastatin in a Mouse Model of Cardiac Hypertrophy: a new Mechanism for Antihypertrophic Intervention. Cell Physiol Biochem 2013;31:997–1008. https://doi.org/10.1159/000350117.

[109] Huang ZP, Wang DZ. miR-22 in cardiac remodeling and disease. Trends Cardiovasc Med 2014;24:267. https://doi.org/10.1016/J.TCM.2014.07.005.

[110] Huang X, Li Z, Bai B, Li X, Li Z. High expression of microRNA-208 is associated with cardiac hypertrophy via the negative regulation of the sex-determining region Y-box 6 protein. Exp Ther Med 2015;10:921–6. https://doi.org/10.3892/etm.2015.2645.

[111] Aggarwal P, Turner A, Matter A, Kattman SJ, Stoddard A, Lorier R, et al. RNA expression profiling of human iPSC-derived cardiomyocytes in a cardiac hypertrophy model. PLoS One 2014;9:108051. https://doi.org/10.1371/journal.pone.0108051.

[112] Ikeda S, He A, Kong SW, Lu J, Bejar R, Bodyak N, et al. MicroRNA-1 Negatively Regulates Expression of the Hypertrophy-Associated Calmodulin and Mef2a Genes. Mol Cell Biol 2009;29:2193–204. https://doi.org/10.1128/mcb.01222-08.

[113] Van Doorn ECH, Amesz JH, Sadeghi AH, de Groot NMS, Manintveld OC, Taverne YJHJ. Preclinical Models of Cardiac Disease: A Comprehensive Overview for Clinical Scientists. Cardiovasc Eng Technol 2024;15:232–49. https://doi.org/10.1007/S13239-023-00707.

[114] Niederer SA, Lumens J, Trayanova NA. Computational models in cardiology. Nat Rev Cardiol 2018 162 2018;16:100–11. https://doi.org/10.1038/s41569-018-0104-y.

[115] Mercken EM, Capri M, Carboneau BA, Conte M, Heidler J, Santoro A, et al. Conserved and species-specific molecular denominators in mammalian skeletal muscle aging. NPJ Aging Mech Dis 2017;3:8. https://doi.org/10.1038/S41514-017-0009-8.

[116] Selbach M, Schwanhäusser B, Thierfelder N, Fang Z, Khanin R, Rajewsky N. Widespread changes in protein synthesis induced by microRNAs. Nat 2008 4557209 2008;455:58–63. https://doi.org/10.1038/nature07228.

[117] Guo H, Ingolia NT, Weissman JS, Bartel DP. Mammalian microRNAs predominantly act to decrease target mRNA levels. Nat 2010 4667308 2010;466:835–40. https://doi.org/10.1038/nature09267.

[118] Walgrave H, Balusu S, Snoeck S, Vanden Eynden E, Craessaerts K, Thrupp N, et al. Restoring miR-132 expression rescues adult hippocampal neurogenesis and memory deficits in Alzheimer's disease. Cell Stem Cell 2021;28:1805–21. https://doi.org/10.1016/j.stem.2021.05.001.

[119] El Fatimy R, Li S, Chen Z, Mushannen T, Gongala S, Wei Z, et al. MicroRNA-132 provides neuroprotection for tauopathies via multiple signaling pathways. Acta Neuropathol 2018;136:537–55. https://doi.org/10.1007/S00401-018-1880-5.

[120] Mullokandov G, Baccarini A, Ruzo A, Jayaprakash AD, Tung N, Israelow B, et al. High-throughput assessment of microRNA activity and function using microRNA sensor and decoy libraries. Nat Methods 2012;9:840–6. https://doi.org/10.1038/NMETH.2078.

[121] Ordovás L, Boon R, Pistoni M, Chen Y, Wolfs E, Guo W, et al. Efficient recombinase-mediated cassette exchange in hPSCs to study the hepatocyte lineage reveals AAVS1 locus-mediated transgene inhibition. Stem Cell Reports 2015;5:918–31. https://doi.org/10.1016/j.stemcr.2015.09.004.

[122] Suttiprapa S, Rinaldi G, Brindley PJ. Prototypic chromatin insulator cHS4 protects retroviral transgene from silencing in Schistosoma mansoni. Transgenic Res 2012;21:555–66. https://doi.org/10.1007/S11248-011-9556-0.

[123] Lian X, Hsiao C, Wilson G, Zhu K, Hazeltine LB, Azarin SM, et al. Robust cardiomyocyte differentiation from human pluripotent stem cells via temporal modulation of canonical Wnt signaling. Proc Natl Acad Sci U S A 2012;109:E1848-57. https://doi.org/10.1073/PNAS.1200250109.

[124] Maas RGC, Lee S, Harakalova M, Snijders Blok CJB, Goodyer WR, Hjortnaes J, et al. Massive expansion and cryopreservation of functional human induced pluripotent stem cell-derived cardiomyocytes. STAR Protoc 2021;2. https://doi.org/10.1016/J.XPRO.2021.100334.

[125] Buikema JW, Lee S, Goodyer WR, Maas RG, Chirikian O, Li G, et al. Wnt Activation and Reduced Cell-Cell Contact Synergistically Induce Massive Expansion of Functional Human iPSC-Derived Cardiomyocytes. Cell Stem Cell 2020;27:50-63.e5. https://doi.org/10.1016/J.STEM.2020.06.001.

[126] Wiśniewski JR, Zougman A, Nagaraj N, Mann M. Universal sample preparation method for proteome analysis. Nat Methods 2009 65 2009;6:359–62. https://doi.org/10.1038/nmeth.1322.

[127] Distler U, Kuharev J, Navarro P, Levin Y, Schild H, Tenzer S. Drift time-specific collision energies enable deep-coverage data-independent acquisition proteomics. Nat Methods 2013 112 2013;11:167–70. https://doi.org/10.1038/nmeth.2767.

[128] Zhang X, Smits AH, Van Tilburg GBA, Ovaa H, Huber W, Vermeulen M. Proteome-wide identification of ubiquitin interactions using UbIA-MS. Nat Protoc 2018;13:530–50. https://doi.org/10.1038/NPROT.2017.147.

[129] Tang D, Chen M, Huang X, Zhang G, Zeng L, Zhang G, et al. SRplot: A free online platform for data visualization and graphing. PLoS One 2023;18:e0294236. https://doi.org/10.1371/JOURNAL.PONE.0294236.

[130] Ru Y, Kechris KJ, Tabakoff B, Hoffman P, Radcliffe RA, Bowler R, et al. The multiMiR R package and database: integration of microRNA-target interactions along with their disease and drug associations. Nucleic Acids Res 2014;42:e133. https://doi.org/10.1093/NAR/GKU631.

[131] Leptidis S, el Azzouzi H, Lok SI, de Weger R, Olieslagers S, Kisters N, et al. A deep sequencing approach to uncover the miRNOME in the human heart. PLoS One 2013;8:e57800. https://doi.org/10.1371/JOURNAL.PONE.0057800.

[132] Gillen AE, Yamamoto TM, Kline E, Hesselberth JR, Kabos P. Improvements to the HITS-CLIP protocol eliminate widespread mispriming artifacts. BMC Genomics 2016;17:338. https://doi.org/10.1186/S12864-016-2675-5.

[133] Boudreau RL, Jiang P, Gilmore BL, Spengler RM, Tirabassi R, Nelson JA, et al. Transcriptome-wide discovery of microRNA binding sites in Human Brain. Neuron 2014;81:294–305. https://doi.org/10.1016/j.neuron.2013.10.062.

[134] Nowakowski TJ, Rani N, Golkaram M, Zhou HR, Alvarado B, Huch K, et al. Regulation of cell-type-specific transcriptomes by microRNA networks during human brain development. Nat Neurosci 2018;21:1784–92. https://doi.org/10.1038/S41593-018-0265-3.

[135] Tyshkovskiy A, Ma S, Shindyapina A V., Tikhonov S, Lee SG, Bozaykut P, et al. Distinct longevity mechanisms across and within species and their association with aging. Cell 2023;186:2929–49. https://doi.org/10.1016/J.CELL.2023.05.002.

[136] Bhadra M, Howell P, Dutta S, Heintz C, Mair WB. Alternative splicing in aging and longevity. Hum Genet 2020;139:357–69. https://doi.org/10.1007/S00439-019-02094-6.

[137] Swarup V, Hinz FI, Rexach JE, Noguchi K ichi, Toyoshiba H, Oda A, et al. Identification of evolutionarily conserved gene networks mediating neurodegenerative dementia. Nat Med 2019;25:152–64. https://doi.org/10.1038/S41591-018-0223-3;SUBJMETA.

[138] Kaurani L, Pradhan R, Schröder S, Burkhardt S, Schuetz AL, Krüger DM, et al. A role for astrocytic miR-129-5p in frontotemporal dementia. Transl Psychiatry 2025;15:1–14. https://doi.org/10.1038/S41398-025-03338.

[139] Pozzo E, Yedigaryan L, Giarratana N, Wang C chi, Garrido GM, Degreef E, et al. miR-449a/miR-340 reprogram cell identity and metabolism in fusion-negative rhabdomyosarcoma. Cell Rep 2025;44:115171. https://doi.org/10.1016/j.celrep.2024.115171.

[140] M'baya-Moutoula E, Louvet L, Molinié R, Guerrera IC, Cerutti C, Fourdinier O, et al. A multi-omics analysis of the regulatory changes induced by miR-223 in a

monocyte/macrophage cell line. Biochim Biophys Acta - Mol Basis Dis 2018;1864:2664–78. https://doi.org/10.1016/J.BBADIS.2018.05.010.

[141] Walgrave H, Penning A, Tosoni G, Snoeck S, Davie K, Davis E, et al. microRNA-132 regulates gene expression programs involved in microglial homeostasis. IScience 2023;26:106829. https://doi.org/10.1016/J.ISCI.2023.106829.

[142] Chiao YA, Rabinovitch PS. The Aging Heart. Cold Spring Harb Perspect Med 2015;5:a025148. https://doi.org/10.1101/CSHPERSPECT.A025148.

[143] Bernardo BC, Ooi JYY, Lin RCY, Mcmullen JR. miRNA therapeutics: A new class of drugs with potential therapeutic applications in the heart. Future Med Chem 2015;7:1771–92. https://doi.org/10.4155/fmc.15.107.

[144] Khan AA, Betel D, Miller ML, Sander C, Leslie CS, Marks DS. Transfection of small RNAs globally perturbs gene regulation by endogenous microRNAs. Nat Biotechnol 2009 276 2009;27:549–55. https://doi.org/10.1038/nbt.1543.

[145] Grimm D, Streetz KL, Jopling CL, Storm TA, Pandey K, Davis CR, et al. Fatality in mice due to oversaturation of cellular microRNA/short hairpin RNA pathways. Nat 2006 4417092 2006;441:537–41. https://doi.org/10.1038/nature04791.

[146] Zhang S, Cheng Z, Wang Y, Han T. The Risks of miRNA Therapeutics: In a Drug Target Perspective. Drug Des Devel Ther 2021;15:721–33. https://doi.org/10.2147/DDDT.S288859.

[147] Hong T, Wei Y, Xue X, Li Y, Dong H, Guo X, et al. A Novel Anti-Coagulative Nanocomplex in Delivering miRNA-1 Inhibitor Against Microvascular Obstruction of Myocardial Infarction. Adv Healthc Mater 2020;9:1901783. https://doi.org/10.1002/ADHM.201901783.

[148] Liu B, Wang B, Zhang X, Lock R, Nash T, Vunjak-Novakovic G. Cell type-specific microRNA therapies for myocardial infarction. Sci Transl Med 2021;13:eabd0914. https://doi.org/10.1126/SCITRANSLMED.ABD0914.

[149] Dai B, Wang F, Nie X, Du H, Zhao Y, Yin Z, et al. The Cell Type–Specific Functions of miR-21 in Cardiovascular Diseases. Front Genet 2020;11:563166. https://doi.org/10.3389/FGENE.2020.563166/BIBTEX.

[150] Van Rooij E, Sutherland LB, Thatcher JE, DiMaio JM, Naseem RH, Marshall WS, et al. Dysregulation of microRNAs after myocardial infarction reveals a role of miR-29 in cardiac fibrosis. Proc Natl Acad Sci U S A 2008;105:13027–32. https://doi.org/10.1073/PNAS.0805038105.

[151] Sassi Y, Avramopoulos P, Ramanujam D, Grüter L, Werfel S, Giosele S, et al. Cardiac myocyte miR-29 promotes pathological remodeling of the heart by activating Wnt signaling. Nat Commun 2017;8. https://doi.org/10.1038/S41467-017-01737-4.

[152] Chen Y, Gao DY, Huang L. In vivo delivery of miRNAs for cancer therapy: Challenges and strategies. Adv Drug Deliv Rev 2015;81:128–41. https://doi.org/10.1016/j.addr.2014.05.009.

[153] Hinkel R, Penzkofer D, Zühlke S, Fischer A, Husada W, Xu QF, et al. Inhibition of microRNA-92a protects against ischemia/reperfusion injury in a large-animal model. Circulation 2013;128:1066–75. https://doi.org/10.1161/CIRCULATIONAHA.113.001904.

[154] Hinkel R, Ramanujam D, Kaczmarek V, Howe A, Klett K, Beck C, et al. AntimiR-21 Prevents Myocardial Dysfunction in a Pig Model of Ischemia/Reperfusion Injury. J Am Coll Cardiol 2020;75:1788–800. https://doi.org/10.1016/j.jacc.2020.02.041.

[155] Bereczki Z, Benczik B, Balogh OM, Marton S, Puhl E, Pétervári M, et al. Mitigating off-target effects of small RNAs: conventional approaches, network theory and artificial intelligence. Br J Pharmacol 2025;182:340–79. https://doi.org/10.1111/BPH.17302.

[156] Van Rooij E, Sutherland LB, Liu N, Williams AH, McAnally J, Gerard RD, et al. A signature pattern of stress-responsive microRNAs that can evoke cardiac hypertrophy and heart failure. Proc Natl Acad Sci U S A 2006;103:18255–60. https://doi.org/10.1073/pnas.0608791103.

[157] Yang B, Lin H, Xiao J, Lu Y, Luo X, Li B, et al. The muscle-specific microRNA miR-1 regulates cardiac arrhythmogenic potential by targeting GJA1 and KCNJ2. Nat Med 2007;13:486–91. https://doi.org/10.1038/nm1569.

[158] Van Rooij E, Olson EN. MicroRNAs: powerful new regulators of heart disease and provocative therapeutic targets. J Clin Invest 2007;117:2369–76. https://doi.org/10.1172/JCI33099.

[159] Bonauer A, Carmona G, Iwasaki M, Mione M, Koyanagi M, Fischer A, et al. MicroRNA-92a controls angiogenesis and functional recovery of ischemic tissues in Mice. Science (80-) 2009;324:1710–3. https://doi.org/10.1126/science.1174381.

[160] Rogg EM, Abplanalp WT, Bischof C, John D, Schulz MH, Krishnan J, et al. Analysis of Cell Type-Specific Effects of MicroRNA-92a Provides Novel Insights into Target Regulation and Mechanism of Action. Circulation 2018;138:2545–58. https://doi.org/10.1161/CIRCULATIONAHA.118.034598/SUPPL_FILE/CIRCULATIONAHA.118.034598.

[161] Bellera N, Barba I, Rodriguez-Sinovas A, Ferret E, Asín MA, Gonzalez-Alujas MT, et al. Single intracoronary injection of encapsulated antagomir-92a promotes angiogenesis and prevents adverse infarct remodeling. J Am Heart Assoc 2014;3:e000946. https://doi.org/10.1161/JAHA.114.000946.

[162] Surina, Fontanella RA, Scisciola L, Marfella R, Paolisso G, Barbieri M. miR-21 in Human Cardiomyopathies. Front Cardiovasc Med 2021;8:767064. https://doi.org/10.3389/FCVM.2021.767064.

[163] Cheng Y, Zhang C. MicroRNA-21 in cardiovascular disease. J Cardiovasc Transl Res 2010;3:251–5. https://doi.org/10.1007/s12265-010-9169-7.

[164] Thum T, Gross C, Fiedler J, Fischer T, Kissler S, Bussen M, et al. MicroRNA-21 contributes to myocardial disease by stimulating MAP kinase signalling in fibroblasts. Nature 2008;456:980–4. https://doi.org/10.1038/nature07511.

[165] Liu Y, Li L, Su Q, Liu T, Ma Z, Yang H. Ultrasound-Targeted Microbubble Destruction Enhances Gene Expression of microRNA-21 in Swine Heart via Intracoronary Delivery. Echocardiography 2015;32:1407–16. https://doi.org/10.1111/ECHO.12876.

[166] Bejerano T, Etzion S, Elyagon S, Etzion Y, Cohen S. Nanoparticle Delivery of miRNA-21 Mimic to Cardiac Macrophages Improves Myocardial Remodeling after Myocardial Infarction. Nano Lett 2018;18:5885–91. https://doi.org/10.1021/acs.nanolett.8b02578.

[167] Su Q, Li L, Liu Y, Zhou Y, Wang J, Wen W. Ultrasound-targeted microbubble destruction-mediated microRNA-21 transfection regulated PDCD4/NF-κB/TNF-α pathway to prevent coronary microembolization-induced cardiac dysfunction. Gene Ther 2015 2212 2015;22:1000–6. https://doi.org/10.1038/gt.2015.59.

[168] Li Y, Chen X, Jin R, Chen L, Dang M, Cao H, et al. Injectable hydrogel with MSNs/microRNA-21-5p delivery enables both immunomodification and enhanced angiogenesis for myocardial infarction therapy in pigs. Sci Adv 2021;7:eabd6740. https://doi.org/10.1126/SCIADV.ABD6740.

[169] Chen L, Wang GY, Dong JH, Cheng XJ. MicroRNA-132 improves myocardial remodeling after myocardial infarction. Eur Rev Med Pharmacol Sci 2019;23:6299–306. https://doi.org/10.26355/eurrev_201907_18452.

[170] Ucar A, Gupta SK, Fiedler J, Erikci E, Kardasinski M, Batkai S, et al. The miRNA-212/132 family regulates both cardiac hypertrophy and cardiomyocyte autophagy. Nat Commun 2012;3:1–11. https://doi.org/10.1038/ncomms2090.

[171] Foinquinos A, Batkai S, Genschel C, Viereck J, Rump S, Gyöngyösi M, et al. Preclinical development of a miR-132 inhibitor for heart failure treatment. Nat Commun 2020;11:633. https://doi.org/10.1038/s41467-020-14349-2.

[172] Batkai S, Genschel C, Viereck J, Rump S, Bär C, Borchert T, et al. CDR132L improves systolic and diastolic function in a large animal model of chronic heart failure. Eur Heart J 2020;42:192–201. https://doi.org/10.1093/eurheartj/ehaa791.

[173] Rafat M, Moraghebi M, Afsa M, Malekzadeh K. The outstanding role of miR-132-3p in carcinogenesis of solid tumors. Hum Cell 2021;34:1051–65. https://doi.org/10.1007/S13577-021-00544-W,.

[174] Hinkel R, Batkai S, Bähr A, Bozoglu T, Straub S, Borchert T, et al. AntimiR-132 Attenuates Myocardial Hypertrophy in an Animal Model of Percutaneous Aortic Constriction. J Am Coll Cardiol 2021;77:2923–35. https://doi.org/10.1016/J.JACC.2021.04.028.

[175] Yang H, Qin X, Wang H, Zhao X, Liu Y, Wo HT, et al. An in Vivo miRNA Delivery System for Restoring Infarcted Myocardium. ACS Nano 2019;13:9880–94. https://doi.org/10.1021/acsnano.9b03343.

[176] Gabisonia K, Prosdocimo G, Aquaro GD, Carlucci L, Zentilin L, Secco I, et al. MicroRNA therapy stimulates uncontrolled cardiac repair after myocardial infarction in pigs. Nature 2019;569:418–22. https://doi.org/10.1038/s41586-019-1191-6.

[177] Gao L, Qiu F, Cao H, Li H, Dai G, Ma T, et al. Therapeutic delivery of microRNA-125a-5p oligonucleotides improves recovery from myocardial ischemia/reperfusion injury in mice and swine. Theranostics 2023;13:685–703. https://doi.org/10.7150/THNO.73568.

[178] Zeng N, Huang YQ, Yan YM, Hu ZQ, Zhang Z, Feng JX, et al. Diverging targets mediate the pathological role of miR-199a-5p and miR-199a-3p by promoting cardiac hypertrophy and fibrosis. Mol Ther - Nucleic Acids 2021;26:1035–50. https://doi.org/10.1016/J.OMTN.2021.10.013.

[179] Yan H, Li Y, Wang C, Zhang Y, Liu C, Zhou K, et al. Contrary microRNA Expression Pattern Between Fetal and Adult Cardiac Remodeling: Therapeutic Value for Heart Failure. Cardiovasc Toxicol 2017;17:267–76. https://doi.org/10.1007/S12012-016-9381-Z.

[180] Song XW, Li Q, Lin LI, Wang XC, Li DF, Wang GK, et al. MicroRNAs are dynamically regulated in hypertrophic hearts, and miR-199a is essential for the maintenance of cell size in cardiomyocytes. J Cell Physiol 2010;225:437–43. https://doi.org/10.1002/JCP.22217.

[181] Asensio-Lopez MC, Sassi Y, Soler F, Fernandez del Palacio MJ, Pascual-Figal D, Lax A. The miRNA199a/SIRT1/P300/Yy1/sST2 signaling axis regulates adverse cardiac remodeling following MI. Sci Rep 2021;11. https://doi.org/10.1038/S41598-021-82745-9.

[182] Chen Y, Liu S, Liang Y, He Y, Li Q, Zhan J, et al. Single dose of intravenous miR199a-5p delivery targeting ischemic heart for long-term repair of myocardial infarction. Nat Commun 2024;15:5565. https://doi.org/10.1038/S41467-024-49901-X.

[183] Yan H, Wang H, Zhu X, Huang J, Li Y, Zhou K, et al. Adeno-associated virus-mediated delivery of anti-miR-199a tough decoys attenuates cardiac hypertrophy by targeting PGC-1alpha. Mol Ther - Nucleic Acids 2021;23:406–17. https://doi.org/10.1016/J.OMTN.2020.11.007.

[184] Wang K, Wen J, Liang T, Hu H, Li S, Shen L, et al. Enhancing miR-19a/b induced cardiomyocyte proliferation in infarcted hearts by alleviating oxidant stress and controlling miR-19 release. Biomaterials 2025;312:122732. https://doi.org/10.1016/J.BIOMATERIALS.2024.122732.

[185] Liao Y, Li H, Cao H, Dong Y, Gao L, Liu Z, et al. Therapeutic silencing miR-146b-5p improves cardiac remodeling in a porcine model of myocardial infarction by modulating the wound reparative phenotype. Protein Cell 2021;12:194–212. https://doi.org/10.1007/S13238-020-00750-6.

[186] Lu Y, Zhang Y, Wang N, Pan Z, Gao X, Zhang F, et al. MicroRNA-328 contributes to adverse electrical remodeling in atrial fibrillation. Circulation 2010;122:2378–87. https://doi.org/10.1161/CIRCULATIONAHA.110.958967.

[187] Zhang Y, Zheng S, Geng Y, Xue J, Wang Z, Xie X, et al. MicroRNA profiling of atrial fibrillation in canines: MiR-206 modulates intrinsic cardiac autonomic nerve remodeling by regulating SOD1. PLoS One 2015;10:e0122674. https://doi.org/10.1371/journal.pone.0122674.

[188] Täubel J, Hauke W, Rump S, Viereck J, Batkai S, Poetzsch J, et al. Novel antisense therapy targeting microRNA-132 in patients with heart failure: results of a first-in-human Phase 1b randomized, double-blind, placebo-controlled study. Eur Heart J 2021;42:178–88. https://doi.org/10.1093/EURHEARTJ/EHAA898.

[189] Bauersachs J, Solomon SD, Anker SD, Antorrena-Miranda I, Batkai S, Viereck J, et al. Efficacy and safety of CDR132L in patients with reduced left ventricular ejection fraction after myocardial infarction: Rationale and design of the HF-REVERT trial. Eur J Heart Fail 2024;26:674–82. https://doi.org/10.1002/EJHF.3139.

[190] Gallant-Behm CL, Piper J, Dickinson BA, Dalby CM, Pestano LA, Jackson AL. A synthetic microRNA-92a inhibitor (MRG-110) accelerates angiogenesis and wound healing in diabetic and nondiabetic wounds. Wound Repair Regen 2018;26:311–23. https://doi.org/10.1111/wrr.12660.

[191] Lucas T, Schäfer F, Müller P, Eming SA, Heckel A, Dimmeler S. Light-inducible antimiR-92a as a therapeutic strategy to promote skin repair in healing-impaired diabetic mice. Nat Commun 2017;8:15162. https://doi.org/10.1038/NCOMMS15162.

[192] Loyer X, Potteaux S, Vion AC, Guérin CL, Boulkroun S, Rautou PE, et al. Inhibition of microRNA-92a prevents endothelial dysfunction and atherosclerosis in mice. Circ Res 2014;114:434–43. https://doi.org/10.1161/CIRCRESAHA.114.302213.

[193] Abplanalp WT, Fischer A, John D, Zeiher AM, Gosgnach W, Darville H, et al. Efficiency and Target Derepression of Anti-miR-92a: Results of a First in Human Study. Nucleic Acid Ther 2020;30:335–45. https://doi.org/10.1089/nat.2020.0871.

[194] Viridian Therapeutics Inc. miRagen Announces New Clinical Data Showing MRG-110 Positively Impacted Tissue Repair and New Blood Vessel Growth 2019. https://investors.viridiantherapeutics.com/news/news-details/2019/miRagen-Announces-New-Clinical-Data-Showing-MRG-110-Positively-Impacted-Tissue-Repair-and-New-Blood-Vessel-Growth-10-16-2019/default.aspx.

[195] Liu G, Friggeri A, Yang Y, Milosevic J, Ding Q, Thannickal VJ, et al. miR-21 mediates fibrogenic activation of pulmonary fibroblasts and lung fibrosis. J Exp Med 2010;207:1589–97. https://doi.org/10.1084/JEM.20100035.

[196] Chau BN, Xin C, Hartner J, Ren S, Castano AP, Linn G, et al. MicroRNA-21 promotes fibrosis of the kidney by silencing metabolic pathways. Sci Transl Med 2012;4:121ra18. https://doi.org/10.1126/scitranslmed.3003205.

[197] Gomez IG, MacKenna DA, Johnson BG, Kaimal V, Roach AM, Ren S, et al. Anti–microRNA-21 oligonucleotides prevent Alport nephropathy progression by stimulating metabolic pathways. J Clin Invest 2014;125:141. https://doi.org/10.1172/JCI75852.

[198] Rubel D, Boulanger J, Craciun F, Xu EY, Zhang Y, Phillips L, et al. Anti-microRNA-21 Therapy on Top of ACE Inhibition Delays Renal Failure in Alport Syndrome Mouse Models. Cells 2022;11:594. https://doi.org/10.3390/CELLS11040594/S1.

[199] Zhang T, Yang Z, Kusumanchi P, Han S, Liangpunsakul S. Critical Role of microRNA-21 in the Pathogenesis of Liver Diseases. Front Med 2020;7:7. https://doi.org/10.3389/FMED.2020.00007.

[200] Dong L, Wang X, Tan J, Li H, Qian W, Chen J, et al. Decreased expression of microRNA-21 correlates with the imbalance of Th17 and Treg cells in patients with rheumatoid arthritis. J Cell Mol Med 2014;18:2213. https://doi.org/10.1111/JCMM.12353.

[201] Iorio M V., Croce CM. MicroRNAs in cancer: small molecules with a huge impact. J Clin Oncol 2009;27:5848–56. https://doi.org/10.1200/JCO.2009.24.0317.

[202] Gale DP, Gross O, Wang F, Esteban De La Rosa RJ, Hall M, Sayer JA, et al. A Randomized Controlled Clinical Trial Testing Effects of Lademirsen on Kidney Function Decline in Adults with Alport Syndrome. Clin J Am Soc Nephrol 2024;19:995–1004. https://doi.org/10.2215/CJN.0000000000000458.

[203] Mirna M, Paar V, Topf A, Kraus T, Sotlar K, Aigner A, et al. A new player in the game: treatment with antagomiR-21a-5p significantly attenuates histological and echocardiographic effects of experimental autoimmune myocarditis. Cardiovasc Res 2022;118:556–72. https://doi.org/10.1093/CVR/CVAB015.

[204] Deng Z, He Y, Yang X, Shi H, Shi A, Lu L, et al. MicroRNA-29: A Crucial Player in Fibrotic Disease. Mol Diagn Ther 2017;21:285–94. https://doi.org/10.1007/S40291-016-0253-9.

[205] Montgomery RL, Yu G, Latimer PA, Stack C, Robinson K, Dalby CM, et al. Micro RNA mimicry blocks pulmonary fibrosis. EMBO Mol Med 2014;6:1347–56. https://doi.org/10.15252/EMMM.201303604.

[206] Gallant-Behm CL, Piper J, Lynch JM, Seto AG, Hong SJ, Mustoe TA, et al. A MicroRNA-29 Mimic (Remlarsen) Represses Extracellular Matrix Expression and Fibroplasia in the Skin. J Invest Dermatol 2019;139:1073–81. https://doi.org/10.1016/j.jid.2018.11.007.

[207] miRagen Therapeutics Inc. A Phase 2, Double-blind, Placebo-Controlled Study to Investigate the Efficacy, Safety and Tolerability of MRG-201 Following Intradermal Injection in Subjects with a History of Keloids 2018. https://investors.viridiantherapeutics.com/news/news-details/2018/miRagen-Therapeutics-Announces-Initiation-of-Phase-2-Clinical-Trial-of-MRG-201-07-10-2018/default.aspx.

[208] Hajarnis S, Lakhia R, Yheskel M, Williams D, Sorourian M, Liu X, et al. microRNA-17 family promotes polycystic kidney disease progression through modulation of mitochondrial metabolism. Nat Commun 2017;8:14395. https://doi.org/10.1038/NCOMMS14395.

[209] Xue C, Lv J, Yang B, Mei S, Xu J, Li X, et al. Gene therapy in polycystic kidney disease: A promising future. J Transl Intern Med 2025;12:543. https://doi.org/10.1515/JTIM-2024-0021.

[210] Regulus Therapeutics. Regulus Therapeutics Announces Strategic Prioritization of RGLS8429, its Next-Generation Candidate for the Treatment of Autosomal Dominant Polycystic Kidney Disease 2021. https://ir.regulusrx.com/2021-10-12-Regulus-Therapeutics-Announces-Strategic-Prioritization-of-RGLS8429,-its-Next-Generation-Candidate-for-the-Treatment-of-Autosomal-Dominant-Polycystic-Kidney-Disease.

[211] Regulus Therapeutics. Regulus Therapeutics Announces Positive Clinical and Regulatory Updates from its Autosomal Dominant Polycystic Kidney Disease (ADPKD) Program for Farabursen (RGLS8429) 2025. https://www.prnewswire.com/news-releases/regulus-therapeutics-announces-positive-clinical-and-regulatory-updates-from-its-autosomal-dominant-polycystic-kidney-disease-adpkd-program-for-farabursen-rgls8429-302362731.html.

[212] Du W, Pan Z, Chen X, Wang L, Zhang Y, Li S, et al. By targeting Stat3 microRNA-17-5p promotes cardiomyocyte apoptosis in response to ischemia followed by reperfusion. Cell Physiol Biochem 2014;34:955–65. https://doi.org/10.1159/000366312.

[213] Chen B, Yang Y, Wu J, Song J, Lu J. microRNA-17-5p downregulation inhibits autophagy and myocardial remodelling after myocardial infarction by targeting STAT3. Autoimmunity 2022;55:43–51. https://doi.org/10.1080/08916934.2021.1992754.

[214] Shi H, Li J, Song Q, Cheng L, Sun H, Fan W, et al. Systematic identification and analysis of dysregulated miRNA and transcription factor feed-forward loops in hypertrophic cardiomyopathy. J Cell Mol Med 2019;23:306–16. https://doi.org/10.1111/jcmm.13928.

[215] Ranganath P. MicroRNA-155 and its role in malignant hematopoiesis. Biomark Insights 2015;10:95–102. https://doi.org/10.4137/BMI.S27676.

[216] Seto AG, Beatty X, Lynch JM, Hermreck M, Tetzlaff M, Duvic M, et al. Cobomarsen, an oligonucleotide inhibitor of miR-155, co-ordinately regulates multiple survival pathways to reduce cellular proliferation and survival in cutaneous T-cell lymphoma. Br J Haematol 2018;183:428–44. https://doi.org/10.1111/BJH.15547.

[217] Anastasiadou E, Seto AG, Beatty X, Hermreck M, Gilles ME, Stroopinsky D, et al. Cobomarsen, an Oligonucleotide Inhibitor of miR-155, Slows DLBCL Tumor Cell Growth In Vitro and In Vivo. Clin Cancer Res 2021;27:1139–49. https://doi.org/10.1158/1078-0432.CCR-20-3139.

[218] Querfeld C, Foss FM, Kim YH, Pinter-Brown L, William BM, Porcu P, et al. Phase 1 Trial of Cobomarsen, an Inhibitor of Mir-155, in Cutaneous T Cell Lymphoma. Blood 2018;132:2903–2903. https://doi.org/10.1182/BLOOD-2018-99-119861.

[219] Foss FM, Querfeld C, Kim YH, Pinter-Brown LC, William BM, Porcu P, et al. Ph 1 study of MRG-106, an inhibitor of miR-155, in CTCL. J Clin Oncol 2018;36:2511–2511. https://doi.org/10.1200/JCO.2018.36.15.

[220] Zhang RL, Wang WM, Li JQ, Li RW, Zhang J, Wu Y, et al. The role of miR-155 in cardiovascular diseases: Potential diagnostic and therapeutic targets. Int J Cardiol Cardiovasc Risk Prev 2025;24:200355. https://doi.org/10.1016/J.IJCRP.2024.200355.

[221] Wang J, Song S, Xie C, Han J, Li Y, Shi J, et al. MicroRNA profiling in the left atrium in patients with non-valvular paroxysmal atrial fibrillation. BMC Cardiovasc Disord 2015;15:1–7. https://doi.org/10.1186/S12872-015-0085-2.

[222] Taubel J, Hauke W, Rump S, Viereck J, Batkai S, Poetzsch J, et al. Novel antisense therapy targeting microRNA-132 in patients with heart failure. Eur Heart J 2021;42:178–88. https://doi.org/10.1093/EURHEARTJ/EHAB724.0920.

[223] Kalepu S, Nekkanti V. Insoluble drug delivery strategies: Review of recent advances and business prospects. Acta Pharm Sin B 2015;5:442–53. https://doi.org/10.1016/j.apsb.2015.07.003.

[224] Din FU, Aman W, Ullah I, Qureshi OS, Mustapha O, Shafique S, et al. Effective use of nanocarriers as drug delivery systems for the treatment of selected tumors. Int J Nanomedicine 2017;12:7291–309. https://doi.org/10.2147/IJN.S146315.

[225] Nie JJ, Qiao B, Duan S, Xu C, Chen B, Hao W, et al. Unlockable Nanocomplexes with Self-Accelerating Nucleic Acid Release for Effective Staged Gene Therapy of Cardiovascular Diseases. Adv Mater 2018;30:1801570. https://doi.org/10.1002/ADMA.201801570.

[226] Mathur D, Medintz IL. The Growing Development of DNA Nanostructures for Potential Healthcare-Related Applications. Adv Healthc Mater 2019;8:1801546. https://doi.org/10.1002/adhm.201801546.

[227] Hu Q, Li H, Wang L, Gu H, Fan C. DNA Nanotechnology-Enabled Drug Delivery Systems. Chem Rev 2019;119:6459–506. https://doi.org/10.1021/ACS.CHEMREV.7B00663.

[228] Zhu L, Luo J, Ren K. Nucleic acid-based artificial nanocarriers for gene therapy. J Mater Chem B 2023;11:261–79. https://doi.org/10.1039/D2TB01179D.

[229] Huang J, Ma W, Sun H, Wang H, He X, Cheng H, et al. Self-Assembled DNA Nanostructures-Based Nanocarriers Enabled Functional Nucleic Acids Delivery. ACS Appl Bio Mater 2020;3:2779–95. https://doi.org/10.1021/ACSABM.9B01197.

[230] Zhi Y, Xu C, Sui D, Du J, Xu FJ, Li Y. Effective Delivery of Hypertrophic miRNA Inhibitor by Cholesterol-Containing Nanocarriers for Preventing Pressure Overload Induced Cardiac Hypertrophy. Adv Sci 2019;6:1900023. https://doi.org/10.1002/ADVS.201900023.

[231] Xue X, Shi X, Dong H, You S, Cao H, Wang K, et al. Delivery of microRNA-1 inhibitor by dendrimer-based nanovector: An early targeting therapy for myocardial infarction in mice. Nanomedicine Nanotechnology, Biol Med 2018;14:619–31. https://doi.org/10.1016/j.nano.2017.12.004.

[232] Sun B, Liu S, Hao R, Dong X, Fu L, Han B. RGD-PEG-PLA Delivers MiR-133 to Infarct Lesions of Acute Myocardial Infarction Model Rats for Cardiac Protection. Pharmaceutics 2020;12:1–28. https://doi.org/10.3390/PHARMACEUTICS12060575.

[233] Barenholz Y. Doxil®--the first FDA-approved nano-drug: lessons learned. J Control Release 2012;160:117–34. https://doi.org/10.1016/J.JCONREL.2012.03.020.

[234] Mehta M, Bui TA, Yang X, Aksoy Y, Goldys EM, Deng W. Lipid-Based Nanoparticles for Drug/Gene Delivery: An Overview of the Production Techniques and Difficulties Encountered in Their Industrial Development. ACS Mater Au 2023;3:600–19. https://doi.org/10.1021/ACSMATERIALSAU.3C00032.

[235] Zhao Y, Huang L. Lipid nanoparticles for gene delivery. Adv. Genet., vol. 88, Academic Press Inc.; 2014, p. 13–36. https://doi.org/10.1016/B978-0-12-800148-6.00002-X.

[236] Wang Z, Cui K, Costabel U, Zhang X. Nanotechnology-facilitated vaccine development during the coronavirus disease 2019 (COVID-19) pandemic. Exploration 2022;2:20210082. https://doi.org/10.1002/EXP.20210082.

[237] Warne N, Ruesch M, Siwik P, Mensah P, Ludwig J, Hripcsak M, et al. Delivering 3 billion doses of Comirnaty in 2021. Nat Biotechnol 2023 412 2023;41:183–8. https://doi.org/10.1038/s41587-022-01643-1.

[238] Tan H, Song Y, Chen J, Zhang N, Wang Q, Li Q, et al. Platelet-Like Fusogenic Liposome-Mediated Targeting Delivery of miR-21 Improves Myocardial Remodeling by Reprogramming Macrophages Post Myocardial Ischemia-Reperfusion Injury. Adv Sci 2021;8:e2100787. https://doi.org/10.1002/ADVS.202100787.

[239] Zhou G, Hu T, Du Q, Huang W, Yao C. Nanoparticle-Delivered microRNA-153-3p Alleviates Myocardial Infarction-Induced Myocardial Injury in a Rat Model. ACS Biomater Sci Eng 2022;8:1696–705. https://doi.org/10.1021/ACSBIOMATERIALS.1C01198.

[240] Liu M, Li M, Sun S, Li B, Du D, Sun J, et al. The use of antibody modified liposomes loaded with AMO-1 to deliver oligonucleotides to ischemic myocardium for arrhythmia therapy. Biomaterials 2014;35:3697–707. https://doi.org/10.1016/j.biomaterials.2013.12.099.

[241] Li M, Tang X, Liu X, Cui X, Lian M, Zhao M, et al. Targeted miR-21 loaded liposomes for acute myocardial infarction. J Mater Chem B 2020;8:10384–91. https://doi.org/10.1039/D0TB01821J.

[242] Cha W, Fan R, Miao Y, Zhou Y, Qin C, Shan X, et al. Mesoporous silica nanoparticles as carriers for intracellular delivery of nucleic acids and subsequent therapeutic applications. Molecules 2017;22:782. https://doi.org/10.3390/molecules22050782.

[243] Fu Y, Chen J, Huang Z. Recent progress in microRNA-based delivery systems for the treatment of human disease. ExRNA 2019;1:24. https://doi.org/10.1186/s41544-019-0024-y.

[244] Wang Q, Song Y, Chen J, Li Q, Gao J, Tan H, et al. Direct in vivo reprogramming with non-viral sequential targeting nanoparticles promotes cardiac regeneration. Biomaterials 2021;276:121028. https://doi.org/10.1016/J.BIOMATERIALS.2021.121028.

[245] Yao C, Wu W, Tang H, Jia X, Tang J, Ruan X, et al. Self-assembly of stem cell membrane-camouflaged nanocomplex for microRNA-mediated repair of myocardial infarction injury. Biomaterials 2020;257:120256. https://doi.org/10.1016/J.BIOMATERIALS.2020.120256.

[246] Kanki S, Jaalouk DE, Lee S, Yu AYC, Gannon J, Lee RT. Identification of targeting peptides for ischemic myocardium by in vivo phage display. J Mol Cell Cardiol 2011;50:841–8. https://doi.org/10.1016/j.yjmcc.2011.02.003.

[247] Kim MY, Kim OR, Choi YS, Lee H, Park K, Lee CT, et al. Selection and Characterization of Tenascin C Targeting Peptide. Mol Cells 2012;33:71–8. https://doi.org/10.1007/S10059-012-2214-4.

[248] Yang H, Wang W, Xiao J, Yang R, Feng L, Xu H, et al. ROS-responsive injectable hydrogels loaded with exosomes carrying miR-4500 reverse liver fibrosis. Biomaterials 2025;314:122887. https://doi.org/10.1016/J.BIOMATERIALS.2024.122887.

[249] Jindal S, Awasthi R, Goyal K, Kulkarni GT. Hydrogels for localized drug delivery: A special emphasis on dermatologic applications. Dermatol Ther 2022;35:e15830. https://doi.org/10.1111/DTH.15830.

[250] Wang LL, Liu Y, Chung JJ, Wang T, Gaffey AC, Lu M, et al. Sustained miRNA delivery from an injectable hydrogel promotes cardiomyocyte proliferation and functional regeneration after ischaemic injury. Nat Biomed Eng 2017;1:983–92. https://doi.org/10.1038/s41551-017-0157-y.

[251] Eding JEC, Vigil-Garcia M, Vink M, Demkes CJ, Versteeg D, Kooijman L, et al. Hydrogel-Based Delivery of antimiR-195 Improves Cardiac Efficacy after Ischemic Injury. Adv Ther 2024;7. https://doi.org/10.1002/ADTP.202300241.

[252] Henning RJ. Cardiovascular Exosomes and MicroRNAs in Cardiovascular Physiology and Pathophysiology. J Cardiovasc Transl Res 2020;14:195–212. https://doi.org/10.1007/s12265-020-10040-5.

[253] Gu J, You J, Liang H, Zhan J, Gu X, Zhu Y. Engineered bone marrow mesenchymal stem cell-derived exosomes loaded with miR302 through the cardiomyocyte specific peptide can reduce myocardial ischemia and reperfusion (I/R) injury. J Transl Med 2024;22:168. https://doi.org/10.1186/S12967-024-04981-7.

[254] Tong L, Wang Q, Zhang Y, Lai F, Xu J, Yin W, et al. Myocardial delivery of miR30d with peptide-functionalized milk-derived extracellular vesicles for targeted treatment of hypertrophic heart failure. Biomaterials 2025;316:122976. https://doi.org/10.1016/J.BIOMATERIALS.2024.122976.

[255] Song Y, Zhang C, Zhang J, Jiao Z, Dong N, Wang G, et al. Localized injection of miRNA-21-enriched extracellular vesicles effectively restores cardiac function after myocardial infarction. Theranostics 2019;9:2346–60. https://doi.org/10.7150/THNO.29945.

[256] Salunkhe S, Dheeraj, Basak M, Chitkara D, Mittal A. Surface functionalization of exosomes for target-specific delivery and in vivo imaging & tracking: Strategies and significance. J Control Release 2020;326:599–614. https://doi.org/10.1016/j.jconrel.2020.07.042.

[257] Liang Y, Duan L, Lu J, Xia J. Engineering exosomes for targeted drug delivery. Theranostics 2021;11:3183–95. https://doi.org/10.7150/THNO.52570.

[258] Wang S, Jiang J, Wang Y, Jia Q, Dai S, Wang Y, et al. rLj-RGD3, a novel recombinant toxin protein from Lampetra japonica, prevents coronary thrombosis-induced acute myocardial infarction by inhibiting platelet functions in rats. Biochem Biophys Res Commun 2018;498:240–5. https://doi.org/10.1016/J.BBRC.2018.02.021.

[259] Kanki S, Jaalouk DE, Lee S, Yu AYC, Gannon J, Lee RT. Identification of targeting peptides for ischemic myocardium by in vivo phage display. J Mol Cell Cardiol 2011;50:841–8. https://doi.org/10.1016/J.YJMCC.2011.02.003.

[260] Wang LL, Liu Y, Chung JJ, Wang T, Gaffey AC, Lu M, et al. Sustained miRNA delivery from an injectable hydrogel promotes cardiomyocyte proliferation and functional regeneration after ischaemic injury. Nat Biomed Eng 2017 112 2017;1:983–92. https://doi.org/10.1038/s41551-017-0157-y.

[261] McGuire MJ, Samli KN, Johnston SA, Brown KC. In vitro selection of a peptide with high selectivity for cardiomyocytes in vivo. J Mol Biol 2004;342:171–82. https://doi.org/10.1016/j.jmb.2004.06.029.

[262] Chen ZY, Liang K, Qiu RX, Luo LP. Ultrasound- and Liposome Microbubble-Mediated Targeted Gene Transfer to Cardiomyocytes In Vivo Accompanied by Polyethylenimine. J Ultrasound Med 2011;30:1247–58. https://doi.org/10.7863/JUM.2011.30.9.1247.

[263] Saliba Y, Mougenot N, Jacquet A, Atassi F, Hatem S, Farès N, et al. A new method of ultrasonic nonviral gene delivery to the adult myocardium. J Mol Cell Cardiol 2012;53:801–8. https://doi.org/10.1016/J.YJMCC.2012.07.016.

[264] Vancraeynest D, Havaux X, Pouleur AC, Pasquet A, Gerber B, Beauloye C, et al. Myocardial delivery of colloid nanoparticles using ultrasound-targeted microbubble destruction. Eur Heart J 2006;27:237–45. https://doi.org/10.1093/EURHEARTJ/EHI479.

[265] Vasileva O, Zaborova O, Shmykov B, Ivanov R, Reshetnikov V. Composition of lipid nanoparticles for targeted delivery: application to mRNA therapeutics. Front Pharmacol 2024;15:1466337. https://doi.org/10.3389/FPHAR.2024.1466337.

[266] Dvir T, Bauer M, Schroeder A, Tsui JH, Anderson DG, Langer R, et al. Nanoparticles targeting the infarcted heart. Nano Lett 2011;11:4411–4. https://doi.org/10.1021/nl2025882.

[267] Gasc JM, Shanmugam S, Sibony M, Corvol P. Tissue-specific expression of type 1 angiotensin II receptor subtypes. An in situ hybridization study. Hypertension 1994;24:531–7. https://doi.org/10.1161/01.HYP.24.5.531.

[268] Scott RC, Crabbe D, Krynska B, Ansari R, Kiani MF. Aiming for the heart: Targeted delivery of drugs to diseased cardiac tissue. Expert Opin Drug Deliv 2008;5:459–70. https://doi.org/10.1517/17425247.5.4.459.

[269] Scott RC, Wang B, Nallamothu R, Pattillo CB, Perez-Liz G, Issekutz A, et al. Targeted delivery of antibody conjugated liposomal drug carriers to rat myocardial infarction. Biotechnol Bioeng 2007;96:795–802. https://doi.org/10.1002/bit.21233.

[270] Scott RC, Rosano JM, Ivanov Z, Wang B, Chong PL-G, Issekutz AC, et al. Targeting VEGF-encapsulated immunoliposomes to MI heart improves vascularity and cardiac function. FASEB J 2009;23:3361–7. https://doi.org/10.1096/fj.08-127373.

[271] Dowaidar M. Cell-penetrating peptides with nanoparticles hybrid delivery vectors and their uptake pathways. Mitochondrion 2024;78:101906. https://doi.org/10.1016/J.MITO.2024.101906.

[272] Frankel AD, Pabo CO. Cellular uptake of the tat protein from human immunodeficiency virus. Cell 1988;55:1189–93. https://doi.org/10.1016/0092-8674(88)90263-2.

[273] Vivès E, Brodin P, Lebleu B. A truncated HIV-1 Tat protein basic domain rapidly translocates through the plasma membrane and accumulates in the cell nucleus. J Biol Chem 1997;272:16010–7. https://doi.org/10.1074/jbc.272.25.16010.

[274] Verma DD, Levchenko TS, Bernstein EA, Mongayt D, Torchilin VP. ATP-loaded immunoliposomes specific for cardiac myosin provide improved protection of the mechanical functions of myocardium from global ischemia in an isolated rat heart model. J Drug Target 2006;14:273–80. https://doi.org/10.1080/10611860600763103.

[275] Torchilin VP, Klibanov AL, Huang L, O'Donnell S, Nossiff ND, Khaw BA. Targeted accumulation of polyethylene glycol-coated immunoliposomes in infarcted rabbit myocardium. FASEB J 1992;6:2716–9. https://doi.org/10.1096/fasebj.6.9.1612296.

[276] Torchilin VP, Narula J, Halpern E, Khaw BA. Poly(ethylene glycol)-coated anti-cardiac myosin immunoliposomes: factors influencing targeted accumulation in the infarcted myocardium. Biochim Biophys Acta 1996;1279:75–83. https://doi.org/10.1016/0005-2736(95)00248-0.

[277] Ko YT, Hartner WC, Kale A, Torchilin VP. Gene delivery into ischemic myocardium by double-targeted lipoplexes with anti-myosin antibody and TAT peptide. Gene Ther 2009;16:52–9. https://doi.org/10.1038/GT.2008.135.

[278] Zahid M, Phillips BE, Albers SM, Giannoukakis N, Watkins SC, Robbins PD. Identification of a cardiac specific protein transduction domain by in Vivo biopanning using a M13 phage peptide display library in mice. PLoS One 2010;5:e12252. https://doi.org/10.1371/journal.pone.0012252.

[279] Dasa SSK, Suzuki R, Gutknecht M, Brinton LT, Tian Y, Michaelsson E, et al. Development of target-specific liposomes for delivering small molecule drugs after reperfused myocardial infarction. J Control Release 2015;220:556–67. https://doi.org/10.1016/j.jconrel.2015.06.017.

[280] Zhao M, Liu C, Liu Z, Zuo Y, Chen C, Shi S, et al. Myocardium-targeted liposomal delivery of the antioxidant peptide 8P against doxorubicin-induced myocardial injury. Int J Pharm 2024;663:124569. https://doi.org/10.1016/J.IJPHARM.2024.124569.

[281] Zhao X, Luo W, Hu J, Zuo L, Wang J, Hu R, et al. Cardiomyocyte-targeted and 17β-estradiol-loaded acoustic nanoprobes as a theranostic platform for cardiac hypertrophy. J Nanobiotechnology 2018;16:36. https://doi.org/10.1186/s12951-018-0360-3.

[282] Rana S, Datta K, Reddy TL, Chatterjee E, Sen P, Pal-Bhadra M, et al. A spatio-temporal cardiomyocyte targeted vector system for efficient delivery of therapeutic payloads to regress cardiac hypertrophy abating bystander effect. J Control Release 2015;200:167–78. https://doi.org/10.1016/j.jconrel.2015.01.008.

[283] Mentkowski KI, Lang JK. Exosomes Engineered to Express a Cardiomyocyte Binding Peptide Demonstrate Improved Cardiac Retention in Vivo. Sci Rep 2019;9. https://doi.org/10.1038/s41598-019-46407-1.

[284] Nam HY, Kim J, Kim SW, Bull DA. Cell Targeting Peptide Conjugation to siRNA Polyplexes for Effective Gene Silencing in Cardiomyocytes 2012. https://doi.org/10.1021/mp200589z.

[285] Zahid M, Weber B, Yurko R, Islam K, Agrawal V, Lopuszynski J, et al. Cardiomyocyte-Targeting Peptide to Deliver Amiodarone. Pharmaceutics 2023;15:2107. https://doi.org/10.3390/PHARMACEUTICS15082107.

[286] Gallicano GI, Fu J, Mahapatra S, Sharma MVR, Dillon C, Deng C, et al. Reversing Cardiac Hypertrophy at the Source Using a Cardiac Targeting Peptide Linked to miRNA106a: Targeting Genes That Cause Cardiac Hypertrophy. Pharmaceuticals 2022;15:871. https://doi.org/10.3390/PH15070871.

[287] Kim H, Yun N, Mun D, Kang JY, Lee SH, Park H, et al. Cardiac-specific delivery by cardiac tissue-targeting peptide-expressing exosomes. Biochem Biophys Res Commun 2018;499:803–8. https://doi.org/10.1016/j.bbrc.2018.03.227.

[288] Won YW, McGinn AN, Lee M, Bull DA, Kim SW. Targeted gene delivery to ischemic myocardium by homing peptide-guided polymeric carrier. Mol Pharm 2013;10:378–85. https://doi.org/10.1021/mp300500y.

[289] Wang X, Chen Y, Zhao Z, Meng Q, Yu Y, Sun J, et al. Engineered exosomes with ischemic myocardium-targeting peptide for targeted therapy in myocardial infarction. J Am Heart Assoc 2018;7:e008737. https://doi.org/10.1161/JAHA.118.008737.

[290] Vandergriff A, Huang K, Shen D, Hu S, Hensley MT, Caranasos TG, et al. Targeting regenerative exosomes to myocardial infarction using cardiac homing peptide. Theranostics 2018;8:1869–78. https://doi.org/10.7150/thno.20524.

[291] Tan KX, Pan S, Jeevanandam J, Danquah MK. Cardiovascular therapies utilizing targeted delivery of nanomedicines and aptamers. Int J Pharm 2019;558:413–25. https://doi.org/10.1016/j.ijpharm.2019.01.023.

[292] Su Y, Huang Y, Kou Q, Lu L, Jiang H, Li X, et al. Study on the Role of an Erythrocyte Membrane-Coated Nanotheranostic System in Targeted Immune Regulation of Alzheimer's Disease. Adv Sci 2023;10:2301361. https://doi.org/10.1002/ADVS.202301361.

[293] Lombardo SM, Schneider M, Türeli AE, Türeli NG. Key for crossing the BBB with nanoparticles: the rational design. Beilstein J Nanotechnol 1172 2020;11:866–83. https://doi.org/10.3762/BJNANO.11.72.

[294] Yin H, Xiong G, Guo S, Xu C, Xu R, Guo P, et al. Delivery of Anti-miRNA for Triple-Negative Breast Cancer Therapy Using RNA Nanoparticles Targeting Stem Cell Marker CD133. Mol Ther 2019;27:1252–61. https://doi.org/10.1016/j.ymthe.2019.04.018.

[295] Liang C, Guo B, Wu H, Shao N, Li D, Liu J, et al. Aptamer-functionalized lipid nanoparticles targeting osteoblasts as a novel RNA interference–based bone anabolic strategy. Nat Med 2015 213 2015;21:288–94. https://doi.org/10.1038/nm.3791.

[296] Tanaka Y, Honda T, Matsuura K, Kimura Y, Inui M. In vitro selection and characterization of DNA aptamers specific for phospholamban. J Pharmacol Exp Ther 2009;329:57–63. https://doi.org/10.1124/jpet.108.149526.

[297] Sakai H, Ikeda Y, Honda T, Tanaka Y, Shiraishi K, Inui M. A cell-penetrating phospholamban-specific RNA aptamer enhances Ca2+ transients and contractile function in cardiomyocytes. J Mol Cell Cardiol 2014;76:177–85. https://doi.org/10.1016/j.yjmcc.2014.09.006.

[298] Zhan R, Li X, Guo W, Liu X, Liu Z, Xu K, et al. An Aptamer-Based Near-Infrared Fluorescence Nanoprobe for Detecting and Imaging of Phospholamban Micropeptide in Cardiomyocytes. ACS Sensors 2019;4:733–9. https://doi.org/10.1021/acssensors.9b00026.

[299] Honda T, Sakai H, Inui M. Intracellular delivery of a phospholamban-targeting aptamer using cardiomyocyte-internalizing aptamers. Eur J Pharmacol 2024;985:177130. https://doi.org/10.1016/J.EJPHAR.2024.177130.

[300] Philippou S, Mastroyiannopoulos NP, Tomazou M, Oulas A, Ackers-Johnson M, Foo RS, et al. Selective Delivery to Cardiac Muscle Cells Using Cell-Specific Aptamers. Pharmaceuticals (Basel) 2023;16:1264. https://doi.org/10.3390/PH16091264.

[301] Narayan C, Lin L-H, Barros MN, Gilbert TC, Brown CR, Reddin D, et al. Identification of In Vivo Internalizing Cardiac-Specific RNA Aptamers. BioRxiv Prepr Serv Biol 2024. https://doi.org/10.1101/2024.08.13.607054.

[302] Hong S, Cui Y, He D, Wu H, Jiang W, Cao J, et al. GelMA Hydrogels Integrated With aptamer CH6-Functionalized Tetrahedral DNA Nanostructures for Osteoporotic Mandibular Regeneration. Macromol Biosci 2025;25:e1400471. https://doi.org/10.1002/MABI.202400471,.

[303] Xu L, Zhu J, Rong L, Yang H, Wang B, Lu S, et al. Osteoblast-specific down-regulation of NLRP3 inflammasome by aptamer-functionalized liposome nanoparticles improves bone quality in postmenopausal osteoporosis rats. Theranostics 2024;14:3945–62. https://doi.org/10.7150/THNO.95423,.

[304] Zheng G, Peng X, Zhang Y, Wang P, Xie Z, Li J, et al. A novel Anti-ROS osteoblast-specific delivery system for ankylosing spondylitis treatment via suppression of both inflammation and pathological new bone formation. J Nanobiotechnology 2023;21:168. https://doi.org/10.1186/S12951-023-01906-2,.

[305] Ren M, Li Y, Zhang H, Li L, He P, Ji P, et al. An oligopeptide/aptamer-conjugated dendrimer-based nanocarrier for dual-targeting delivery to bone. J Mater Chem B 2021;9:2831–44. https://doi.org/10.1039/D0TB02926B,.

[306] Zahid M, Feldman KS, Garcia-Borrero G, Feinstein TN, Pogodzinski N, Xu X, et al. Cardiac targeting peptide, a novel cardiac vector: Studies in bio-distribution, imaging application, and mechanism of transduction. Biomolecules 2018;8:147. https://doi.org/10.3390/biom8040147.

[307] Wang J, Huang W, Xu R, Nie Y, Cao X, Meng J, et al. MicroRNA-24 regulates cardiac fibrosis after myocardial infarction. J Cell Mol Med 2012;16:2150–60. https://doi.org/10.1111/J.1582-4934.2012.01523.X.

[308] Ma T, Qiu F, Gong Y, Cao H, Dai G, Sun D, et al. Therapeutic silencing of lncRNA RMST alleviates cardiac fibrosis and improves heart function after myocardial infarction in mice and swine. Theranostics 2023;13:3826–43. https://doi.org/10.7150/THNO.82543.

[309] Hasenfuss G, Reinecke H, Studer R, Meyer M, Pieske B, Holtz J, et al. Relation between myocardial function and expression of sarcoplasmic reticulum Ca(2+)-ATPase in failing and nonfailing human myocardium. Circ Res 1994;75:434–42. https://doi.org/10.1161/01.RES.75.3.434.

[310] Zhihao L, Jingyu N, Lan L, Michael S, Rui G, Xiyun B, et al. SERCA2a: a key protein in the Ca2+ cycle of the heart failure. Heart Fail Rev 2020;25:523–35. https://doi.org/10.1007/S10741-019-09873-3.

[311] Greenberg B, Butler J, Felker GM, Ponikowski P, Voors AA, Pogoda JM, et al. Prevalence of AAV1 neutralizing antibodies and consequences for a clinical trial of gene transfer for advanced heart failure. Gene Ther 2016;23:313–9. https://doi.org/10.1038/gt.2015.109.

[312] Lucas CR, Halley PD, Chowdury AA, Harrington BK, Beaver L, Lapalombella R, et al. DNA Origami Nanostructures Elicit Dose-Dependent Immunogenicity and Are Nontoxic up to High Doses In Vivo. Small 2022;18. https://doi.org/10.1002/smll.202108063.

[313] Madhanagopal BR, Zhang S, Demirel E, Wady H, Chandrasekaran AR. DNA Nanocarriers: Programmed to Deliver. Trends Biochem Sci 2018;43:997–1013. https://doi.org/10.1016/J.TIBS.2018.09.010.

[314] Chi Q, Yang Z, Xu K, Wang C, Liang H. DNA nanostructure as an efficient drug delivery platform for immunotherapy. Front Pharmacol 2020;10:500239. https://doi.org/10.3389/FPHAR.2019.01585.

[315] Raniolo S, Unida V, Vindigni G, Stolfi C, Iacovelli F, Desideri A, et al. Combined and selective miR-21 silencing and doxorubicin delivery in cancer cells using tailored DNA nanostructures. Cell Death Dis 2021 121 2021;12:1–9. https://doi.org/10.1038/s41419-020-03339-3.

[316] Zhang K, Liu J, Song Q, Yang X, Wang D, Liu W, et al. DNA Nanosponge for Adsorption and Clearance of Intracellular miR-21 and Enhanced Antitumor Chemotherapy. ACS Appl Mater Interfaces 2019;11:46604–13. https://doi.org/10.1021/ACSAMI.9B18282.

[317] Nahar S, Nayak AK, Ghosh A, Subudhi U, Maiti S. Enhanced and synergistic downregulation of oncogenic miRNAs by self-assembled branched DNA. Nanoscale 2017;10:195–202. https://doi.org/10.1039/C7NR06601E.

[318] Kumari K, Kar A, Nayak AK, Mishra SK, Subudhi U. miRNA-mediated alteration of sulfatase modifying factor 1 expression using self-assembled branched DNA nanostructures. RSC Adv 2021;11:10670–80. https://doi.org/10.1039/D0RA10733F.

[319] Kar A, Kumari K, Mishra SK, Subudhi U. Self-assembled DNA nanostructure containing oncogenic miRNA-mediated cell proliferation by downregulation of FOXO1 expression. BMC Cancer 2022;22:1–10. https://doi.org/10.1186/S12885-022-10423-8.

[320] Yu L, Yang S, Liu Z, Qiu X, Tang X, Zhao S, et al. Programming a DNA tetrahedral nanomachine as an integrative tool for intracellular microRNA biosensing and stimulus-unlocked target regulation. Mater Today Bio 2022;15:100276. https://doi.org/10.1016/J.MTBIO.2022.100276.

[321] Shu D, Li H, Shu Y, Xiong G, Carson WE, Haque F, et al. Systemic Delivery of Anti-miRNA for Suppression of Triple Negative Breast Cancer Utilizing RNA Nanotechnology. ACS Nano 2015;9:9731–40. https://doi.org/10.1021/ACSNANO.5B02471.

[322] Binzel DW, Shu Y, Li H, Sun M, Zhang Q, Shu D, et al. Specific Delivery of MiRNA for High Efficient Inhibition of Prostate Cancer by RNA Nanotechnology. Mol Ther 2016;24:1267–77. https://doi.org/10.1038/MT.2016.85.

[323] Li S, Liu Y, Zhang T, Lin S, Shi S, He J, et al. A Tetrahedral Framework DNA-Based Bioswitchable miRNA Inhibitor Delivery System: Application to Skin Anti-Aging. Adv Mater 2022;34:2204287. https://doi.org/10.1002/ADMA.202204287.

[324] Luo Y, Yang X, Du Y, Dou Y, Cui W, Li J, et al. DNA Tetrahedra-Based Delivery of MicroRNA-22 to Reduce Depressive Symptoms in Mice. ACS Appl Mater Interfaces 2023;15:29813–26. https://doi.org/10.1021/ACSAMI.3C03054.

[325] Osteonecrosis S, Li D, Yang Z, Luo Y, Zhao X, Tian M, et al. Delivery of MiR335-5p-Pendant Tetrahedron DNA Nanostructures Using an Injectable Heparin Lithium Hydrogel for Challenging Bone Defects in 2022;2101412:1–19. https://doi.org/10.1002/adhm.202101412.

[326] Li J, Zheng C, Cansiz S, Wu C, Xu J, Cui C, et al. Self-assembly of DNA nanohydrogels with controllable size and stimuli-responsive property for targeted gene regulation therapy. J Am Chem Soc 2015;137:1412–5. https://doi.org/10.1021/JA512293F.

[327] Zadeh JN, Steenberg CD, Bois JS, Wolfe BR, Pierce MB, Khan AR, et al. NUPACK: Analysis and design of nucleic acid systems. J Comput Chem 2011;32:170–3. https://doi.org/10.1002/JCC.21596.

[328] Postigo A, Hernández-Bellido N, Sánchez-Barat M, García-Mendívil L, Pueyo E, Del Barrio J, et al. DNA-Based Nanocarriers to Sequester Altered microRNAs in Cardiac Dysfunction. Adv Ther 2024;7:2400247. https://doi.org/10.1002/ADTP.202400247.

[329] Davis MW, Jorgensen EM. ApE, A Plasmid Editor: A Freely Available DNA Manipulation and Visualization Program. Front Bioinforma 2022;2:818619. https://doi.org/10.3389/fbinf.2022.818619.

[330] Hu Y, Gao S, Lu H, Tan S, Chen F, Ke Y, et al. A Self-Immolative DNA Nanogel Vaccine toward Cancer Immunotherapy. Nano Lett 2023;23:9778–87. https://doi.org/10.1021/acs.nanolett.3c02449.

[331] Xu C, Liu Q, Shi J, Liu Z, Lei Z, Dai C, et al. Multifunctional Self-Assembled DNA Nanospheres for Glioma Fluorescence/Magnetic Resonance Imaging and Therapy. ACS Appl Nano Mater 2024;7:19143–52. https://doi.org/10.1021/acsanm.4c03033.

[332] Di J, Gao X, Du Y, Zhang H, Gao J, Zheng A. Size, shape, charge and “stealthy” surface: Carrier properties affect the drug circulation time in vivo. Asian J Pharm Sci 2021;16:444–58. https://doi.org/10.1016/J.AJPS.2020.07.005.

[333] Thayer JF, Yamamoto SS, Brosschot JF. The relationship of autonomic imbalance, heart rate variability and cardiovascular disease risk factors. Int J Cardiol 2010;141:122–31. https://doi.org/10.1016/J.IJCARD.2009.09.543.

[334] Nocon M, Hiemann T, Müller-Riemenschneider F, Thalau F, Roll S, Willich SN. Association of physical activity with all-cause and cardiovascular mortality: a systematic review and meta-analysis. Eur J Cardiovasc Prev Rehabil 2008;15:239–46. https://doi.org/10.1097/HJR.0B013E3282F55E09.

[335] Oluwagbamigbe Fajemiroye J, Carlos da Cunha L, Saavedra-Rodríguez R, Lima Rodrigues K, Marques Naves L, Andrade Mourão A, et al. Aging-Induced Biological Changes and Cardiovascular Diseases. Biomed Res Int 2018;2018:7156435. https://doi.org/10.1155/2018/7156435.

[336] Russoniello C V., Zhirnov YN, Pougatchev VI, Gribkov EN. Heart Rate Variability and Biological Age: Implications for Health and Gaming. Https://HomeLiebertpubCom/Cyber 2013;16:302–8. https://doi.org/10.1089/CYBER.2013.1505.

[337] Grässler B, Thielmann B, Böckelmann I, Hökelmann A. Effects of Different Training Interventions on Heart Rate Variability and Cardiovascular Health and Risk Factors in Young and Middle-Aged Adults: A Systematic Review. Front Physiol 2021;12:657274. https://doi.org/10.3389/FPHYS.2021.657274.

[338] Bonnemeier H, Wiegand UKH, Brandes A, Kluge N, Katus HA, Richardt G, et al. Circadian Profile of Cardiac Autonomic Nervous Modulation in Healthy Subjects: J Cardiovasc Electrophysiol 2003;14:791–9. https://doi.org/10.1046/J.1540-8167.2003.03078.X.

[339] Reardon M, Malik M. Changes in Heart Rate Variability with Age. Pacing Clin Electrophysiol 1996;19:1863–6. https://doi.org/10.1111/J.1540-8159.1996.TB03241.X.

[340] Isath A, Koziol KJ, Martinez MW, Garber CE, Martinez MN, Emery MS, et al. Exercise and cardiovascular health: A state-of-the-art review. Prog Cardiovasc Dis 2023;79:44–52. https://doi.org/10.1016/J.PCAD.2023.04.008.

[341] Martinez-Gomez D, Luo M, Huang Y, Rodríguez-Artalejo F, Ekelund U, Sotos-Prieto M, et al. Physical Activity and All-Cause Mortality by Age in 4 Multinational Megacohorts. JAMA Netw Open 2024;7:e2446802. https://doi.org/10.1001/JAMANETWORKOPEN.2024.46802.

[342] Rhinn H, Abeliovich A. Differential Aging Analysis in Human Cerebral Cortex Identifies Variants in TMEM106B and GRN that Regulate Aging Phenotypes. Cell Syst 2017;4:404–15. https://doi.org/10.1016/j.cels.2017.02.009.

[343] Thakar J, Mohanty S, Phillip West A, Joshi SR, Ueda I, Wilson J, et al. Aging-dependent alterations in gene expression and a mitochondrial signature of responsiveness to human influenza vaccination. Aging (Albany NY) 2015;7:38–52. https://doi.org/10.18632/aging.100720.

[344] Irizar H, Goñi J, Alzualde A, Castillo-Triviño T, Olascoaga J, de Munain AL, et al. Age gene expression and coexpression progressive signatures in peripheral blood leukocytes. Exp Gerontol 2015;72:50–6. https://doi.org/10.1016/J.EXGER.2015.09.003.

[345] Marttila S, Jylhävä J, Nevalainen T, Nykter M, Jylhä M, Hervonen A, et al. Transcriptional analysis reveals gender-specific changes in the aging of the human immune system. PLoS One 2013;8:e66229. https://doi.org/10.1371/JOURNAL.PONE.0066229.

[346] Martínez JP, Almeida R, Olmos S, Rocha AP, Laguna P. A wavelet-based ECG delineator: evaluation on standard databases. IEEE Trans Biomed Eng 2004;51:570–81. https://doi.org/10.1109/TBME.2003.821031.

[347] Mateo J, Laguna P. Analysis of heart rate variability in the presence of ectopic beats using the heart timing signal. IEEE Trans Biomed Eng 2003;50:334–43. https://doi.org/10.1109/TBME.2003.808831.

[348] Bailón R, Laouini G, Grao C, Orini M, Laguna P, Meste O. The integral pulse frequency modulation model with time-varying threshold: application to heart rate variability analysis during exercise stress testing. IEEE Trans Biomed Eng 2011;58:642–52. https://doi.org/10.1109/TBME.2010.2095011.

[349] Hernando D, Bailón R, Almeida R, Hernández A. QRS detection optimization in stress test recordings using evolutionary algorithms. Comput Cardiol 2014;41:737–40. https://doi.org/10.26754/JJI-I3A.201401652.

[350] Dimitriev DA, Saperova E V, Dimitriev AD. State Anxiety and Nonlinear Dynamics of Heart Rate Variability in Students 2016;11:e0146131. https://doi.org/10.1371/journal.pone.0146131.

[351] Zhang S, Murray P, Zillmer R, Eston RG, Catt M, Rowlands A V. Activity classification using the GENEA: optimum sampling frequency and number of axes. Med Sci Sports Exerc 2012;44:2228–34. https://doi.org/10.1249/MSS.0B013E31825E19FD.

[352] Migueles JH, Rowlands A V., Huber F, Sabia S, Van Hees VT. GGIR: A Research Community–Driven Open Source R Package for Generating Physical Activity and Sleep Outcomes From Multi-Day Raw Accelerometer Data. J Meas Phys Behav 2019;2:188–96. https://doi.org/10.1123/JMPB.2018-0063.

[353] Migueles JH, Aadland E, Andersen LB, Brønd JC, Chastin SF, Hansen BH, et al. GRANADA consensus on analytical approaches to assess associations with accelerometer-determined physical behaviours (physical activity, sedentary behaviour and sleep) in epidemiological studies. Br J Sports Med 2022;56:376–84. https://doi.org/10.1136/BJSPORTS-2020-103604.

[354] Rowlands A V., Dawkins NP, Maylor B, Edwardson CL, Fairclough SJ, Davies MJ, et al. Enhancing the value of accelerometer-assessed physical activity: meaningful visual comparisons of data-driven translational accelerometer metrics. Sport Med - Open 2019;5:1–11. https://doi.org/10.1186/S40798-019-0225-9.

[355] Rowlands A V., Edwardson CL, Davies MJ, Khunti K, Harrington DM, Yates T. Beyond Cut Points: Accelerometer Metrics that Capture the Physical Activity Profile. Med Sci Sports Exerc 2018;50:1323–32. https://doi.org/10.1249/MSS.0000000000001561.

[356] Hernández-Vicente A, Marín-Puyalto J, Pueyo E, Vicente-Rodríguez G, Garatachea N. Physical Activity in Centenarians beyond Cut-Point-Based Accelerometer Metrics. Int J Environ Res Public Heal 2022, Vol 19, Page 11384 2022;19:11384. https://doi.org/10.3390/IJERPH191811384.

[357] Rowlands A V., Sherar LB, Fairclough SJ, Yates T, Edwardson CL, Harrington DM, et al. A data-driven, meaningful, easy to interpret, standardised accelerometer outcome variable for global surveillance. J Sci Med Sport 2019;22:1132–8. https://doi.org/10.1016/J.JSAMS.2019.06.016.

[358] Schwendinger F, Wagner J, Knaier R, Infanger D, Rowlands A V., Hinrichs T, et al. Accelerometer Metrics: Healthy Adult Reference Values, Associations with Cardiorespiratory Fitness, and Clinical Implications. Med Sci Sports Exerc 2024;56:170–80. https://doi.org/10.1249/MSS.0000000000003299.

[359] Serra-Rexach JA, Bustamante-Ara N, Hierro Villarán M, González Gil P, Sanz Ibáñez MJ, Blanco Sanz N, et al. Short-Term, Light- to Moderate-Intensity Exercise Training Improves Leg Muscle Strength in the Oldest Old: A Randomized Controlled Trial. J Am Geriatr Soc 2011;59:594–602. https://doi.org/10.1111/J.1532-5415.2011.03356.X.

[360] Fragala MS, Cadore EL, Dorgo S, Izquierdo M, Kraemer WJ, Peterson MD, et al. Resistance training for older adults: Position statement from the national strength and conditioning association. J Strength Cond Res 2019;33:2019–52. https://doi.org/10.1519/JSC.0000000000003230.

[361] Tomczak M, Tomczak E. The need to report effect size estimates revisited. An overview of some recommended measures of effect size. TRENDS Sport Sci 2014;1:19–25. https://doi.org/10.1186/s13054-016-1208-6.

[362] Cohen J. Statistical Power Analysis for the Behavioral Sciences. 2nd Edition. New York: Routledge; 2013. https://doi.org/10.4324/9780203771587.

[363] Hernández-Bellido N, Hernández-Vicente A, García-Mendívil L, Ramos-Marquès E, Hernando D, Cebollada A, et al. A simple blood biomarker based on gene expression describes cardiovascular health-related biological age. GeroScience 2025:1–17. https://doi.org/10.1007/S11357-025-01784-6.

[364] Harries LW, Hernandez D, Henley W, Wood AR, Holly AC, Bradley-Smith RM, et al. Human aging is characterized by focused changes in gene expression and deregulation of alternative splicing. Aging Cell 2011;10:868–78. https://doi.org/10.1111/J.1474-9726.2011.00726.X.

[365] Passtoors WM, Boer JM, Goeman JJ, van den Akker EB, Deelen J, Zwaan BJ, et al. Transcriptional Profiling of Human Familial Longevity Indicates a Role for ASF1A and IL7R. PLoS One 2012;7:e27759. https://doi.org/10.1371/JOURNAL.PONE.0027759.

[366] Zubakov D, Liu F, Kokmeijer I, Choi Y, van Meurs JBJ, van IJcken WFJ, et al. Human age estimation from blood using mRNA, DNA methylation, DNA rearrangement, and telomere length. Forensic Sci Int Genet 2016;24:33–43. https://doi.org/10.1016/J.FSIGEN.2016.05.014.

[367] Chaudhari PS, Ermolaeva MA. Too old for healthy aging? Exploring age limits of longevity treatments. Npj Metab Heal Dis 2024 21 2024;2:1–9. https://doi.org/10.1038/s44324-024-00040-3.

[368] Paluch AE, Boyer WR, Franklin BA, Laddu D, Lobelo F, Lee DC, et al. Resistance Exercise Training in Individuals With and Without Cardiovascular Disease: 2023 Update: A Scientific Statement From the American Heart Association. Circulation 2024;149:E217–31. https://doi.org/10.1161/CIR.0000000000001189.

[369] Shailendra P, Baldock KL, Li LSK, Gorzelitz J, Matthews CE, Trabert B, et al. Weight training and risk of all-cause, cardiovascular disease and cancer mortality among older adults. Int J Epidemiol 2024;53. https://doi.org/10.1093/IJE/DYAE074.

[370] Pálovics R, Keller A, Schaum N, Tan W, Fehlmann T, Borja M, et al. Molecular hallmarks of heterochronic parabiosis at single-cell resolution. Nat 2022 6037900 2022;603:309–14. https://doi.org/10.1038/s41586-022-04461-2.

[371] Herzog CMS, Goeminne LJE, Poganik JR, Barzilai N, Belsky DW, Betts-LaCroix J, et al. Challenges and recommendations for the translation of biomarkers of aging. Nat Aging 2024 410 2024;4:1372–83. https://doi.org/10.1038/s43587-024-00683-3.

[372] Anerillas C, Herman AB, Munk R, Garrido A, Lam KWG, Payea MJ, et al. A BDNF-TrkB autocrine loop enhances senescent cell viability. Nat Commun 2022;13:6228-. https://doi.org/10.1038/S41467-022-33709-8.